/
Article / Book Information

( )	f
Title(English)	Separation of trivalent f-elements by tertiary pyridine resin
( )	
Author(English)	Atsushi Ikeda
( )	: , : 6578 , :2006 3 26 , : , :
Citation(English)	Degree:Doctor of Philosophy, Conferring organization: Tokyo Institute of Technology, Report number: 6578 , Conferred date:2006/3/26, Degree Type:Course doctor, Examiner:
( )	
Type(English)	Doctoral Thesis

Separation of Trivalent *f*-Elements

by Tertiary Pyridine Resin

IKEDA Atsushi

池田　篤史

Table of Contents

6. Application of the Partitioning Technique Using Tertiary Pyridine Resin to Innovative Reprocessing

7. Conclusions

Acknowledgement

Research Achievements

1   Introduction

1.1   Electricity and Nuclear Power Generation

Since the establishment of electromagnetism in the middle of 19th century, the applications of electricity have tremendously expanded in our daily lives, and they still continue growing. The latest high-technology apparatuses are developed on the assumption that they are operated by using electricity as their power sources. Consequently, our daily lives supported by these high-technology apparatuses are getting more and more dependent on the electricity. In fact, the consumption of electricity in Japan keeps on increasing year-by-year (the red plots in **Fig. 1-1** [1]). Although it is expected that the consumption of electricity in Japan will gradually decrease in future due to the decrease in population and the development of energy-saving products, the importance of electricity for us remains unchanged as long as we continue to use electric appliances and apparatus.
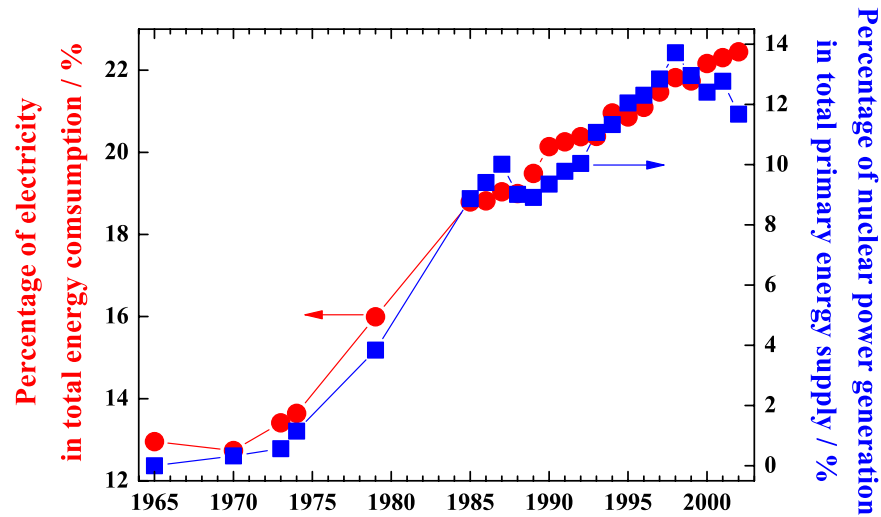
Figure 1-1. The change in the percentage of electricity in total energy consumption in Japan (red plots) [1], and the change in the percentage of nuclear power generation in total primary energy supply in Japan (blue plots) [2].

The present electricity in Japan is generated mainly by the following three ways; the thermal, hydroelectric, and nuclear power generations. **Fig. 1-2** shows a change of total electricity supply in Japan, along with the ratio of each component [3].
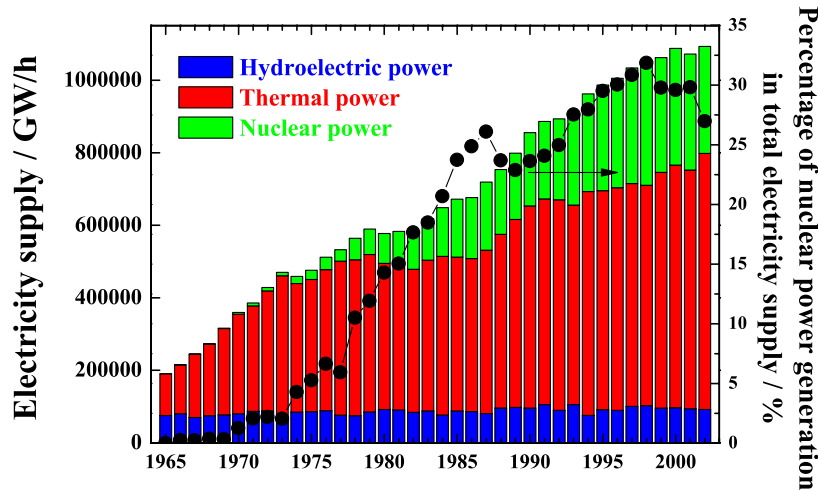
Figure 1-2. The change of electricity supply in Japan and the change of the percentage of nuclear power generation in total supply [3].

The thermal power generation is the largest source of electricity in Japan and it covers 65% of the total electric generation in 2002. The thermal power generation burns fossil fuels such as coal, petroleum (crude petroleum, heavy oil, and naphtha), liquefied natural gas (LNG), or liquefied petroleum gas (LPG), to take their thermal energy and to convert them into electricity. The thermal generation is a long-continued power generation system, and it still continues playing a very important roll in the present Japanese electric industry. However, it discharges a considerable amount of CO_2, which is known as the greenhouse gas, after generation. Moreover, we should not use too much limited petroleum for power generation because petroleum is a versatile fossil fuel and it is also used to make various essential materials such as plastics or synthetic fibers. Therefore, we should cut down on the consumption of petroleum for power generation to save limited petroleum from this time forward. The hydroelectric power generation is a very stable and clean source of electricity without any discharge of CO_2, supplying constant electricity every year.

From the point of view of domestic generation, the hydroelectric power generation is important in Japan, although it can not become the main power source in Japan due to its low generating capacity.

As compared with the thermal and hydroelectric power generations, the nuclear power generation is a relatively new source of electricity and its first commercial use in Japan was started in 1965 by Japan Atomic Power Company. The nuclear power generation can supply stable electricity with high energy output. Besides, it produces no CO_2 in its generation process and the cost of generation is the lowest for all the generation methods [4]. Due to these advantages, the percentage of nuclear power generation both in total primary energy supply (the blue plots in **Fig. 1-1**) and in total electricity supply (the plots in **Fig. 1-2**) increase drastically with an increase of the demand for electricity in Japan [2, 3]. As above-mentioned, it is expected that the consumption of electricity in Japan will slowly decrease in future. However, to the contrary, it is also expected that the demand of nuclear power generation will increase because the consumption of petroleum and LNG for electric power generation will be reduced [5]. Therefore, the nuclear power generation is expected to be more and more indispensable for us to sustain our daily electric lives in the next several decades.

1.2   Radioactive Waste Management

As mentioned in the previous section, the nuclear power generation is a very powerful and economical generation method without any discharge of CO_2. However, it has a fatal and inevitable problem, that is, the management of radioactive wastes. The radioactive wastes are defined as the wastes which include radioactive materials. These wastes are produced as a result of the operation of nuclear power plants, reprocessing plants, and the research activities concerning radioactivity and radioactive materials. As compared with other ordinary wastes, the production of radioactive wastes is far smaller (1/3333 for domestic waste and 1/26666 for industrial waste). However, we need to pay close attention to the management of radioactive wastes because their radioactivity is long-lasting, invisible, and, furthermore, the influence of radioactivity on the human body is still unclear.

In Japan, the radioactive wastes are classified under two categories: low-level radioactive wastes (LLW) and high-level radioactive wastes (HLW). The LLW are fur-

ther classified under four subcategories: the wastes from nuclear power plants, the wastes including a small quantity of transuranium (TRU) nuclides, the wastes including uranium, and the wastes from research facilities. The radioactivity of LLW is so low that they are buried in relatively shallow ground, expecting to handle as non-radioactive wastes in the near future. On the other hand, the management of HLW is not so easy. In Japan, the HLW are produced as a result of reprocessing of spent fuels, including high-level radioactive nuclides (*i.e.* actinoids (An) and fission products (FPs)). Due to their extraordinary long-lasting and high radioactivity, the HLW must be superintended for a long-long term in order to reduce their decay heat and to take their radioactivity away from human environment. Several important high-level radioactive nuclides in HLW are listed in **Table 1-1** [6]. The radioactivity of these nuclides lasts for a long-long term with high activity, while most of the nuclides in HLW decay within ten years and their radioactivity diminishes to the natural level.

Table 1-1. Important high-level radioactive nuclides in high-level radioactive wastes [6].

Nuclide	Half Life / y	Radioactivity / Bq/kg
^{99}Tc	2.11×10^5	6.3×10^{11}
^{129}I	1.57×10^7	6.5×10^9
^{135}Cs	2.30×10^6	4.2×10^{10}
^{233}U	1.59×10^5	3.6×10^{11}
^{237}Np	2.14×10^6	2.6×10^{10}
^{238}Pu	8.77×10^1	6.3×10^{14}
^{239}Pu	2.41×10^4	6.3×10^{12}
^{240}Pu	6.56×10^3	8.3×10^{12}
^{241}Pu	1.43×10^1	3.8×10^{15}
^{242}Pu	3.73×10^5	1.5×10^{11}
^{241}Am	4.33×10^2	1.3×10^{14}
^{243}Am	7.37×10^3	7.4×10^{12}
^{241}Cm	2.91×10^1	1.9×10^{15}
^{244}Cm	1.81×10^1	3.0×10^{15}
^{245}Cm	8.50×10^3	6.3×10^{12}

The present HLW are produced as liquid wastes of nitric acid solution containing non-radioactive metals in large quantities because the reprocessing of spent fuels is performed by cutting fuel assemblies together with covering materials (stainless steel) and dissolving them into nitric acid solution to separate burnable materials (*i.e.* U and Pu) from other An and FPs using PUREX process [7]. Typical compositions of HLW for several countries are listed in **Table 1-2** [8].

Table 1-2. Compositions of high-level radioactive liquid wastes for several countries [8].

Country	Japan	US	UK	France	France
Fuel Type	UO_2	UO_2, PuO_2	U metal	UO_2	MOX
Reactor Type	LWR	FBR	Gas	LWR	Gas
Burn-up / MWd/t	28,000	100,000	3,000	33,000	3,000~3,500
$[HNO_3]$ / mol/dm^3	2	0.5	-	1.5	0.7
Oxide Waste / g/L	100.57	294.77	241.18	75~160	17~190
Content of Oxide / g/L					
Na	30.37	3.1		7~30	7~11
Mg			60.25	-	3~7
Al	-	-	48.63	0~2	2~4
Cr	0.56	3.5	5.33	1.5~3	0~1.5
Fe	3.19	12.8	26.11	1~30	6~20
Ni	0.38	1.7	3.37	1.3~2.6	0~1.3
Zn			4.13	-	-
Mo				0~1	150
U	2.29	2.7	0.533	2.5	2.3
Np	1.8		0.045	0.45	0.11
Pu	0.15		0.0045	2	0.023
Am	0.32		0.165		
Cm	0.07		0.0045		
Total FP Oxides / g/L	61.32	268.7	92.38	63.3	30.42

At present, there is no trustworthy strategy for the treatment of HLW in the world. However, several countries are planning to treat the HLW by geological disposal. In

the geological disposal strategy, high-level liquid wastes are calcified as glass and packed in stainless steel canisters (in the case of once-through fuel cycle, spent fuels are directly packed in the canisters). Then the packed HLW are buried deeply (at several hundred meters underground) in solid rock layers with multiplex artificial barriers to isolate them from our human environment semipermanently. **Table 1-3** outlines the strategies of geological disposal for several countries. Basically, the packed HLW are supposed to be cooled off for several decades before burying in order to reduce their decay heat. After the cooling-off, the HLW must be reposited for at least ten thousand years until their radioactivity becomes weak enough to be negligible. Although the geological disposal is the only universal strategy for the treatment of HLW at the moment, there is still some doubt whether we can superinted them for such a extremely long term. Moreover, it is difficult to find appropriate sites for the geological disposal in Japan because many continental plates are intersected beneath the Japanese islands and, thus, the Japanese strata are very unstable. Due to these reasons, Japan has not been able to start any practical action for the HLW management, although we keep producing spent fuels at this moment.

1.3   Partitioning and Transmutation

Spent fuels contain a variety of elements as a result of fission of uranium. From the viewpoint of fuel reprocessing, only uranium (U) (and plutonium (Pu), depending on the fuel cycle strategy) is a matter of importance for recovering fissile materials from spent fuels and the rest is considered the HLW. However, only a few of the nuclides in HLW are really hazardous (the important hazardous high-level nuclides have been listed in **Table 1-1**). In other words, most of the nuclides in HLW are not so hazardous radioactively. Therefore, if we can separate (*i.e.* **partition**) the really hazardous nuclides from other nuclides, the volume of HLW becomes considerably small. Moreover, the present HLW contains a lot of valuable and useful elements. For example, spent fuels contain a considerable amount ($\sim$0.5wt%) of the platinum group elements (Ru, Rh, and Pd), whose demand continues increasing for various industrial applications although they are in danger of exhaustion due to their poor resources. If it is possible to separate these valuable elements from HLW, the HLW could turn into a precious resource of several useful elements.

Although the partitioning of nuclides in HLW according to their radioactivity or

Table 1-3. Outlines of geological disposal of high-level radioactive wastes for several countries.

Country	US [9]	Canada [10]	France [11]
Executive organization	DOE	AECL	ANDRA
Type of HLW	Spent fuels, Glass	Spent fuels	Spent fuels, Glass
Cooling-off term / y	-	∼50	over 30
Stratum	Tuff	Granite	Granite, Clay
Depth of reposition / m	350	500∼1000	400∼1000
Buffer material	-	Clay	Clay/Zeolite

Germany [12]	Switzerland [13]	Sweden [14]
BfS, DBE	NAGRA	SKB
Spent fuels, Glass	Spent fuels, Glass	Spent fuels
∼30	40	40
Rocksalt	Granite, Sedimentary rock	Granite
660∼900	800∼1000	500
Rocksalt	Bentonite	Bentonite

preciousness allows us to reduce the volume of HLW and to recycle valuable materials, the partitioning itself does not become the fundamental solution to the long-term radiotoxicity of HLW because the radioactivity of hazardous nuclides is unchanged. Hence, it follows that we need to change the nature of high-level radioactive nuclides in order to solve the problem of the radiotoxicity of HLW. At the moment, one and only possible solution to this problem is the **transmutation**. In the transmutation strategy, high-level radioactive nuclides are transmuted into other stable (or lower-level) nuclides by the irradiation of neutrons using normal light-water reactors (LWRs) or fast breeder reactors (FBRs) [15–17], or by the irradiation of charged particles (electrons, positrons, and ions) or γ-ray using accelerators [18–20]. **Table 1-4** shows a result of the test calculation for the transmutation of several nuclides. It is expected from the calculation that the half lives of target nuclides drastically decrease by the transmutation. If we can put this strategy into practice, we can achieve a breakthrough in the confounded nuisance of the HLW management.

The target nuclides for the transmutation are divided into two groups according to

Table 1-4. Test calculation of the transmutation of several high-level radioactive nuclides by different reactors (calculated by JAERI [21]).

Target nuclide	Spontaneous	LWR	Special reactor for TRU transmutation	FBR
		Half life / y		
			transmuted by	
^{237}Np	2.14×10^6	4	3.5	2
^{241}Am	4.33×10^2	0.9	2.9	1.8
^{243}Am	7.37×10^3	9	3.8	2.2
^{244}Cm	1.81×10^1	13	4.4	4.2

their atomic properties, which influence the irradiating condition of the transmutation, and the radiotoxicity, that is, the transuranium (or transuranic) elements (TRU) group and other lighter elements group. The nuclides in the TRU group, such as Np, Am, or Cm, are burdensome α-emitters with long half lives. Additionally, these nuclides are the main source of long-lasting decay heat of HLW. It has recently reported by Oigawa and his co-workers that removing the TRU nuclides from HLW brings the 60~80 vol% reduction of the storage space [22]. The transmutation of these nuclides requires the irradiation of neutrons. On the other hand, the nuisance of the nuclides in the lighter elements group, such as ^{90}Sr, ^{99}Tc, or ^{135}Cs, is mainly due to their decay heat or extremely long half lives, and they can be transmuted by irradiating charged particles or γ-ray. In addition to these nuclides, ^{129}I is also considered an important nuclide to be transmuted due to its volatile property and long-lasting radioactivity (over 10^7 years). The transmutation of these nuclides requires prior partitioning because the irradiating conditions of the transmutation for these nuclides are different from each other, and the irradiation with wrong condition may produce further hazardous nuclides. This means that the transmutation can not be realized without the development of partitioning technique and they are like two sides of the same coin. A typical flowchart of the partitioning and transmutation strategy for the reduction of HLW is given in **Fig. 1-3**. Among the above-mentioned radioactive nuclides, ^{90}Sr and ^{135}Cs do not require immediate transmutation because their half lives are only several decades or their decay heat can be utilized for a source of heat. Thus, the nuclides to be transmuted for the moment are ^{99}Tc, ^{129}I, and TRU, in particular, TRPu (they are also called minor actinides (MA)) nuclides [23].
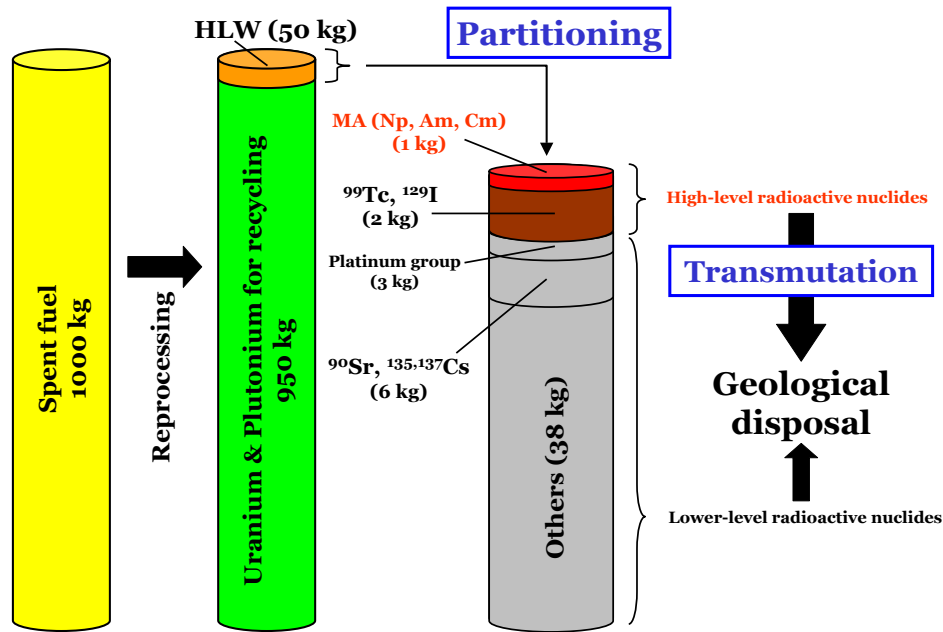
Figure 1-3. Flowchart of the partitioning and transmutation strategy for the reduction of high-level radioactive wastes [15].

Technetium (Tc) and Iodide (I) are relatively easy to separate from HLW by using ordinary separation techniques, such as solvent extraction or ion exchange. Although Tc is usually recovered with Mn, Mo, and Ru due to their chemical similarity, we can isolate Tc from these elements by the solvent extraction [24, 25], the anion exchange method [26, 27], and the chromatography using an activated carbon adsorber [28] with specific conditions. The chemical property of I is different from those of other metallic nuclides in HLW, allowing us to separate it from other nuclides by several chemical separation methods [29, 30]. On the other hand, the partitioning of TRU nuclides from HLW has been well-investigated for many years and several separation techniques, such as PUREX [31], TRUEX [32–34], DIAMEX [35–37], or TRPO process [38, 39], have successfully separated TRU nuclides from FPs in HLW. However, the partitioning of TRU nuclides from HLW always suffers from one obstacle, that is, the presence of lanthanoids (Ln).

The An and Ln belong to the 3rd group in the periodic table and they are known as the *f*-electron filling group (*i.e. f*-elements). As the atomic number increases, they

fill electrons into their f-orbits, which are not the outer-most orbit. Consequently, the electron configurations of their outer orbits (*i.e.* ($6d7s$) for An and ($5d6s$) for Ln) show almost the same arrangement in the same series, bringing a chemical similarity which gives rise to a difficulty in the separation of these elements.

Fig. 1-4 shows the oxidation states and ionic radii of An and Ln [40]. Although the lighter An of Th, Pa, U, Np, and Pu show various oxidation states and smaller ionic radii compared with other An and Ln, most of the An (Ac, Am∼Lr) and Ln form trivalent cations (M(III)) as their most stable oxidation states with quite similar ionic radii in solution. This means that the inter- and intragroup separation of trivalent An (An(III)) and Ln (Ln(III)) (*i.e.* An(III)/Ln(III) separation and individual separation in each group) are very difficult, while the separation of the lighter An is relatively easy by exploiting the difference in oxidation states and ionic radii. Unfortunately, Am and Cm, which are the important target nuclides for the transmutation strategy, exist as trivalent cations in HLW and, to make matters worse, the HLW contain a considerable amount of Ln as FPs. A typical element constituent of spent fuels from PWR is shown in **Fig. 1-5**. The volume of Ln accounts for 30% of the total volume of FPs in spent fuels and it is comparable to the total volume of An, generating 40% of decay heat of spent fuels. In the present reprocessing process using PUREX, An(III) and Ln(III) show the same behavior and, consequently, the An(III)-contaminated HLW generated after the reprocessing process always contain a considerable amount of Ln(III). As above-mentioned, the target nuclides to be transmuted should be isolated from other nuclides before the transmutation process and, furthermore, in the case of the transmutation by nuclear reactors, the Ln exert a bad influence on the nuclear reactions in reactors due to their large neutron capture cross-sections. Therefore, the separation of An(III) from Ln(III) is one of the most important problems to solve for developing the partitioning and transmutation strategy.

Actinide	2	3	4	5	6	7	Lanthanide	2	3	4
Ac		**3**					La		**3**	
Th			**4**				Ce		**3**	4
Pa			4	**5**			Pr		**3**	
U		3	4	5	**6**		Nd		**3**	
Np		3	4	**5**	6	**7**	Pm		**3**	
Pu		3	**4**	5	6	**7**	Sm	2	**3**	
Am		**3**	4	5	6		Eu	2	**3**	
Cm		**3**	4				Gd		**3**	
Bk		**3**	4				Tb		**3**	
Cf		**3**					Dy		**3**	
Es		**3**					Ho		**3**	
Fm	2	**3**					Er		**3**	
Md	2	**3**					Tm		**3**	
No	2	**3**					Yb	2	**3**	
Lr		**3**					Tm		**3**	

※ **Bold-face type**: most stable oxidation state
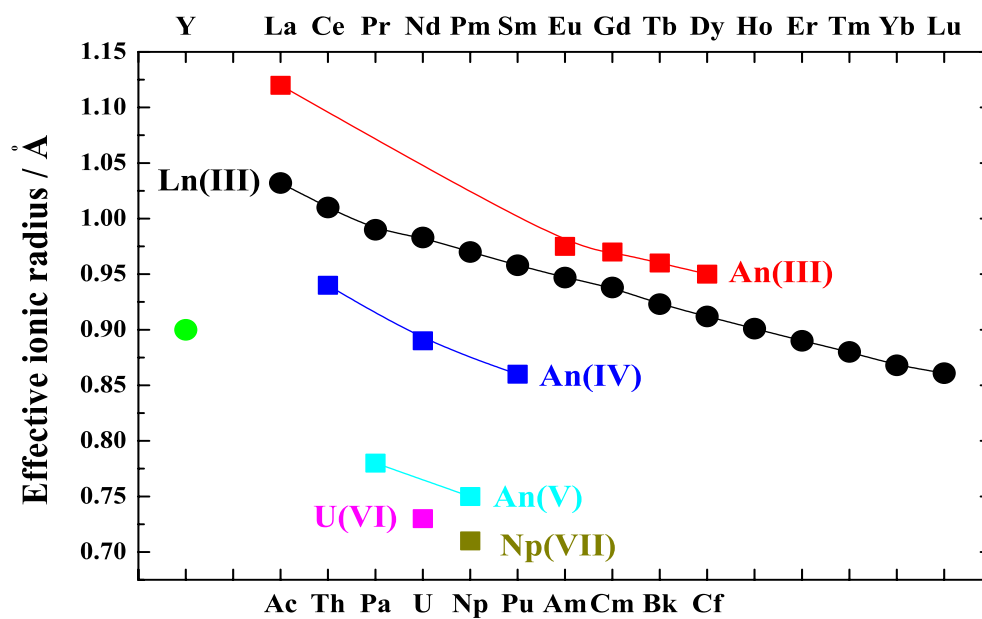
Figure 1-4. Oxidation states and ionic radii (hexagonal) of actinoids and lanthanoids [40].
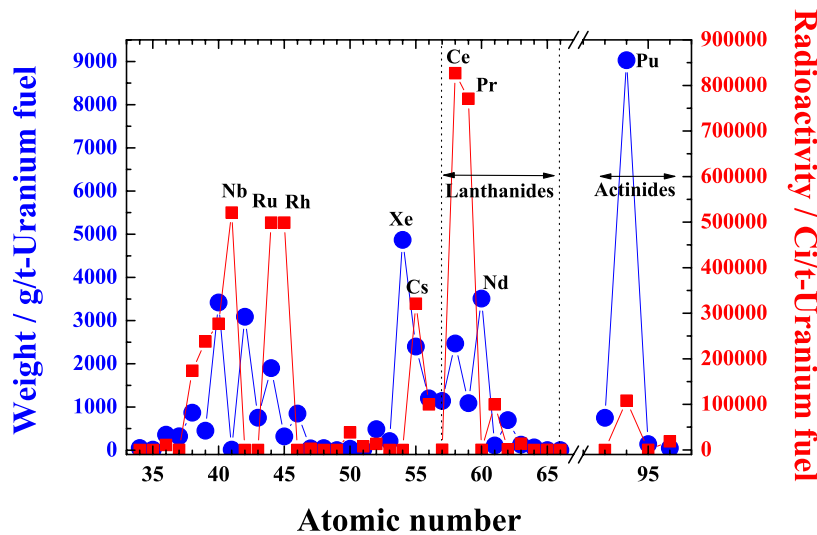
Figure 1-5. A typical element constituent of spent uranium fuels discharged from PWR [41]. (Average exposure: 33 MWd/kg, Average specific power: 30 MW/Mg, 150 days after discharged)

1.4   Precedent Research on the Separation of Trivalent *f*-Elements

As mentioned in the previous section, the separation of An(III) from Ln(III) and the individual separation of An(III) are one of the key processes for the partitioning and transmutation strategy for the reduction of HLW. Besides, an efficient separation technique for each An(III) is also necessary for the basic An science. That is, An samples for research studies are produced by specific reactors with by-products of FPs including Ln(III), and the purification of each An from other nuclides is required to get pure An samples. Moreover, the separation of An(III) is also required for the analytical science of these elements. For example, the alpha spectroscopic determination of Am(III) and Cm(III) requires the individual separation of these elements because their alpha spectra are very close, giving rise to a difficulty in the deconvolution of their mixed spectra. Due to these kinds of necessity, several research studies have been carried out with regard to the separation of An(III) and Ln(III) (*i.e.* trivalent *f*-elements).

In general, there are three techniques for element separation: precipitation, liquid-liquid separation, and liquid-solid separation. There are few reports on the separation of trivalent *f*-elements using the precipitation method because the element selectivity of this method is so low that it is almost impossible to separate these chemically-similar elements, although it is suitable for rough and massive separation. Accordingly, the separation of trivalent *f*-elements has practically been performed by liquid-liquid and liquid-solid separations. The separation process in both methods consists of a transfer of a charged metal cations (or its complex) from one phase to another immiscible phase with the change of solvation structures and concomitant charge neutralization. The effectiveness of any separation process depends on the ability to accomplish phase transfer and the relative affinity of each phase for the chemical species to be separated. In the case of An(III) and Ln(III), efficient separation methods must exploit the slight difference in their ionic radii and (or) covalency/polarizability.

1.4.1   Liquid-Liquid Separation

Liquid-liquid separation, such as solvent extraction, is a method for separating specific components in a mixture by exploiting the differences of the solubility of the components in two different immiscible liquid phases (usually an aqueous phase and a non-aqueous phase are employed). This method can attain high selectivity for one component by using a specific extractant which can selectively extract the target component, and it can easily apply to a larger-scale massive treatment. This method has mainly been developed for the intragroup separation of An(III) and Ln(III) (*i.e.* the separation of An(III) from Ln(III)).

The most extensively studied extractant for An(III)/Ln(III) separation should be neutral organophosphorus extractants since one of this type of ligands, called TBP (tri(*n*-butyl) phosphate), has been successful in the U/Pu separation for reprocessing. Weaver and Kappelmann [42] have reported that a phosphorus-type ligand of di(2-ethylhexyl)phosphoric acid (HDEHP) gives a preferential extraction for Ln(III) over An(III) in lactic acid solutions containing a sodium salt of diethylenetriamine-pentaacetic acid (DTPA), bringing large separation factors (α) between An(III) and Ln(III) (α^{Ln}_{Am}(max) = 770). Horwitz, Muscatello, and his co-workers have demonstrated in a series of their reports [43–45] that carbamoylmethylphosphonate (CMP) extractants can extract An(III) more effectively than Ln(III) in ammonium thiocyanate

solutions and, above all, dihexyl-*N,N*-diisobutylcarbamoylmethylphosphonate (DHDI-BCMP) shows the largest α between Am and Eu (α^{Am}_{Eu} = 10.8). Moreover, the extraction process using di(2-ethylhexyl)phosphoric acid (HDEHP) with aqueous carboxylic acid solutions and diethylenetriaminepentaacetic acid (DTPA), called the TALSPEAK process, can extract Ln(III) from An(III) in pH = 3.0 with larger selectivity (α^{Ce}_{Cm}(max) = 210) [46].

Gerontopulos and his co-workers [47] have employed the extraction system using ammonium thiocyanate solutions and some organic solvents containing a quarternary ammonium salt for the separation of Am and Ln(III) and obtained relatively larger α (α^{Am}_{Ce} = 73). In the TRAMEX process developed in Oak Ridge National Laboratory [48], An(III) are extracted into tertiary amine hydrochloride solution from concentrated lithium chloride solution and they can be separated from several Ln(III). The extraction studies by Kolarik and Müllich [49] have suggested that benzimidazole extractants are also effective for the intragroup separation of An(III) and Ln(III) with aqueous thiocyanate solutions and some organic solvents (α^{Am}_{Eu}(max) = 89).

In addition to the above-mentioned extractants, the new type extractant called soft donor extractants, which coordinate to metal ions by soft donor atoms of nitrogen (N) or sulfur (S) atom [50, 51] and have larger affinity for An(III) over Ln(III) [52], have recently attracted great attention due to the potential for their application to the separation of trivalent *f*-elements. The liquid-liquid extraction using soft donor extractants exploits the slightly greater degree of covalency that appears to exist in An(III) bonds. Although An(III) still prefer hard Lewis bases, they form stronger bonds with soft Lewis bases (*i.e.* soft donor ligands) than Ln(III). The most famous and successful soft donor extractant at present must be bis(2,4,4-trimethylpentyl)dithiophosphinic acid (commercially called CYANEX 301 and supplied by Cytec Industries Inc.). This extractant coordinates to metal cations by S atoms with bidentate, bringing tremendous selectivity between An(III) and Ln(III) in aqueous nitrate solution with kerosene (α^{Am}_{Eu}(max) = 7500) [53, 54]. However, many recent studies have focused on the development of N donor extractants rather than S donor ones in consideration of the CHON principle, which is a trend to design environmentally friendly chemical compounds containing only carbon (C), hydrogen (H), oxygen (O), and nitrogen (N). The CHON compounds produce only innocuous species like H_2O, CO_2, or N_2 on their incineration when they have reached the end of its useful lives, although S compounds produce harmful species such as hydrogen sulfide (H_2S).

Almost all the N donor extractants developed for the separation of trivalent *f*-elements are the derivatives of pyridine (C_5H_5N). The Ensor's group [55] have studied the synergistic extraction of An(III) and Ln(III) by using 4-benzoyl-2,4-dihydro-5-methyl-2-phenyl-3H-pyrazol-3-thione (HBMPPT) and 4,7-diphenyl-1,10-phenanthroline (DPPHEN) and obtained a large α (α^{Am}_{Eu}(max) = 196). Since the bonding between N donor ligands and metal cations is not so strong compared to hard donor ligands such as O donor ligands, N donor extractants must coordinate to metal cations by polydentate mode to stabilize the complexes in extraction process. Cordier and his co-workers [56] have employed several tridentate pyridine type extractants (derivatives of 2,2':6',6"-terpyridine (Tpy) and 2,4,6-tri-2-pyridyl-1,3,5-triazine (TPTZ)) with carboxylic acids and fine selectivity has been observed between Am and Eu (α^{Am}_{Eu} = $\sim$10). Ditriazolyl- and ditriazinylpyridine extractants developed in Karlsruhe [57, 58] have given a efficient separation between Am and Eu with α^{Am}_{Eu} = $\sim$110 in a lower HNO_3 concentration range. Moreover, Watanabe and his co-workers [59] have just recently demonstrated that a hexadentate N donor ligand of *N,N,N',N'*-tetrakis(2-pyridylmethyl)ethylenediamine (TPEN) can selectively extract An(III) from Ln(III), giving a large α^{Am}_{Eu} of 100 in moderate aqueous solution.

Although many successful results have been obtained by liquid-liquid extraction technique on the intergroup separation of An(III) and Ln(III), there is few reports on the intragroup separation of An(III) and Ln(III). The only example of the intragroup separation of An(III) by liquid-liquid extraction seems to be the SESAME process. This process exploits the fact that Am has various oxidation states (III$\sim$VI). That is, the chemical behavior of oxidized Am (An(IV)$\sim$(VI)) is quite different from other An(III), enabling the separation of Am from other An(III). This process is based on several basic research [60–62] and developed by CEA [63–66].

1.4.2 Liquid-Solid Separation

Liquid-solid separation is a separation method which exploits the different affinity of chemical species for two different phases (*i.e.* the mobile (solution) phase and the stationary (solid) phase). This method is classified under two types according to its extraction mechanism, that is, ordinary extraction and ion exchange. In the extraction process of ordinary extraction, chemical species are extracted (adsorbed) to the solid phase as "neutralized" species. On the other hand, chemical species are extracted to the solid phase as "charged (*i.e.* cationic or anionic)" species in the ion

exchange process.

The most common material for the stationary phase of liquid-solid extraction chromatography is organic polymers (resins). The organic polymers are composed of an organic framework and functional sites (such as ion exchange sites or coordinative sites). It is hard to attach so complex functional sites on the polymers due to the difficulty in synthesis, causing lower selectivity compared with liquid-liquid separation. However, liquid-solid separation has the advantage of the application to chromatography which enables multistage separation process with a simple device.

The liquid-solid separation is generally applied to the chromatographic separation using columns. The methodology of liquid-solid separation chromatography is mainly divided into two types according to the procedure of development of samples in column, that is, elution and displacement [67, 68]. The elution development is the most common chromatographic technique. In this technique, the sample is placed at one end of the stationary phase (*i.e.* the column bed) and washed (eluted) with fresh solvent. Normally, solvent (the mobile phase) is passed over the stationary phase until all of the species in the sample have been eluted. On the other hand, in the displacement development, the sample is placed at one end of the stationary phase as in solution and the stationary phase can adsorb the sample strongly. Then, the solvent containing a substance that can be adsorbed by the stationary phase more strongly than any of the species in the sample is passed through the column, eluting the sample from the stationary phase. Although the first successful technique for the individual separation of Ln(III) in industry is the displacement chromatography using a cation exchange resin with ammonium citrate solution [69], most of the applications of liquid-solid separation to the separation of An(III) and Ln(III) have employed elution chromatography technique.

Due to its treatment capacity, the application of liquid-solid separation to the separation of An(III) and Ln(III) has been mainly for their separation in analytical scale. Ion exchange chromatography has probably been the most utilized application of liquid-solid separation since a long time ago. The ion exchange chromatography is classified as cation exchange and anion exchange. In the cation exchange process, the chemical species to be separated are adsorbed (extracted) in cation exchange resin (*e.g.* sulfonic acid (R-SO$_3^-$) type) as positively charged (*i.e.* cationic) species, while the chemical species are adsorbed in anion exchange resin (*e.g.* quarternary ammonium (R-NH$_3^+$) type) as negatively charged (*i.e.* anionic) species in the anion exchange process. There are not so many reports concerning the cation exchange

chromatography of An(III) and Ln(III). The first application of cation exchange process (and also the first application of ion exchange process) to the separation of f-elements appeared in a series of the study [69–74] on the Manhattan Project [75] in 1940's. After that, this technique was succeeded by Street, Jr., Seaborg and Diamond [76, 77]. They employed a cation exchange resin with citric acid or hydrochloric acid solution for the separation of various f-elements (Ac, Th$\sim$Cf, Ln). Deelstra and Verbeek [78] performed a cation exchange chromatography using ammonium α-hydroxyisobutyrate and lactate solutions for the individual separation of Ln(III). Hale and Lowe [79] reported gram-scale separation of Cm from Am and Ln by the cation exchange chromatography using diethylenetriaminepentaacetic acid (DTPA) and nitrilotriacetic acid (NTA) as eluent. Usuda and his co-workers [80, 81] employed a cation exchange resin with mineral acid (hydrochloric acid or nitric acid) / methanol mixtures for the separation of An(III) from Ln(III) and FPs. However, not so many sufficient results of An(III)-Ln(III) separation have been obtained yet by using cation exchange process because there is almost no difference in the affinity between trivalent f-element cations and cation exchange sites.

On the other hand, there are a large number of reports on the separation of An(III) and Ln(III) by anion exchange process. In the anion exchange process, the separation is accomplished by exploiting the different stability of metal complexes with various anions or anionic molecules. Coleman and his co-workers [82] employed a strong base anion exchange resin in ammonium thiocyanate solutions to recover gram amounts of Am from large quantities of lighter Ln. After that, the anion exchange behavior of An(III) and Ln(III) have been investigated in various solvents (lithium chloride (LiCl) solution [83, 84], hydrochloric acid (HCl) [85], nitric acid (HNO$_3$) [85, 86], ammonium thiocyanate solution [87]) and several successful results have been obtained for the intergroup separation of An(III) and Ln(III) [83, 85] and intragroup separation of An(III) [83, 86] in analytical scale. Usuda and his co-workers have developed a macro-scale rapid separation system using anion exchange resin with mineral acid (HCl and HNO$_3$) / alcohol mixtures for the separation of An(III) from FPs containing Ln(III) in a series of their work [81, 88–92]. Hubicka and Drobek proposed the use of N-hydroxyethylenediaminetriacetic acid (HEDTA) with anion exchange resins for the individual separation of Ln(III) [93].

Although the number of reports is not so large compared with ion exchange chromatography, the extraction chromatography has also been applied to the separation of An(III) and Ln(III). Kooi, Boden, and Wijkstra [94] employed the extraction chro-

matography using HDEHP impregnated on silica keiselguhr with HCl eluent for the separation of An(III) (Am, Cm, Bk, and Cf). Horwitz and his co-workers developed a preconcentration technique for the An in radioactive wastes by extraction chromatography in a series of their work [95–100]. Furthermore, a Japanese group at IRI (Institute of Research and Inovation) has recently proposed an extraction chromatography process using 4-(1-methylbenzimidazole-2-yl)phenyl (called AR-01) [101, 102], 2,6-bis-(5,6-dibutyl-1,2,4-triazine-3-yl)pyridine (*n*Bu-BTP) [103], and *N,N,N',N'*-tetra-octyl-3-oxapentane-1,5-diamide (TODGA) [104] impregnated resins for the separation of An and Ln from FPs [101, 102] and their inter- and intragroup separation [103, 104].

1.5   Concept of Overall Separation System for Partitioning and Transmutation Strategy

The present partitioning and transmutation strategy requires (1) the separation of An(III) from other non-trivalent An (*i.e.* U, Np, and Pu) and FPs containing Ln(III) in HLW, and (2) the individual separation of the An(III) to be transmuted (*i.e.* Am and Cm). The precedent studies described in the previous section suggest that the liquid-liquid separation is suitable mainly for the separation of An(III) from other nuclides and, on the other hand, the chromatographic separation technique exploiting liquid-solid separation is effective for their individual separation. However, it is impracticable to combine a liquid-liquid separation process with a liquid-solid separation process because their solvent properties are quite different from each other, complicating the change of solvent. Therefore, despite a considerable number of the precedent works, an overall partitioning system which attains the above two requirements at the same time is still expected.

Table 1-**5** summarizes the advantages and disadvantages of liquid-liquid separation and liquid-solid separation processes. Basically, it is relatively easy to improve the selectivity of An(III) over other elements in liquid-liquid separation process by optimizing extractants. Besides, this process is suitable for larger scale treatment, while it is unsuitable for rigorous individual separation of An(III) due to the properties of its separation system and equipment. On the other hand, the liquid-solid separation is of great advantage to the individual separation by employing chromatography technique, while it is difficult for this process to treat in large quantities. Although it

is probably possible to apply liquid-liquid separation process to the individual separation of An(III) by employing mixer-settlers, the equipment will become very large and it is unrealistic. Therefore, it seems more practicable to develop the liquid-solid separation process using chromatographic technique to an overall separation system for the partitioning and transmutation strategy rather than liquid-liquid separation process.

Table 1-5. Advantages and disadvantages of liquid-liquid separation and liquid-solid separation.

	Liquid-liquid separation	Liquid-solid separation
Separation of An(III) from FPs	◯	△
Individual separation of An(III)	△	◯
Large scale treatment	◯	△
Multistage operation	Massive	Simple
Equipment for multistage operation	Mixer settler	Column
Separation reagent	Special, complicated	Basically simple
Recyclability of reagent	△	◯

The present study aims to develop the overall separation system, in which An(III) are separated from other non-trivalent An and FPs in HLW and also separated individually, using liquid-solid separation chromatography for the partitioning and transmutation strategy. As above-mentioned, the weak points of liquid-solid separation process are lower selectivity for one element (in the present case, the selectivity for An(III) over Ln(III)) and lower treatment capacity. Most of the existing solid extractants for liquid-solid separation chromatography are ion exchange resins and organic polymers in which some extractants are impregnated. Ion exchange resins have large adsorption capacity and their functional groups are relatively stable for chemicals because they are directly bonded to the resin matrices, while they have less selectivity for An(III) over Ln(III). On the other hand, the extractant-impregnated resins show relatively high selectivity for An(III) over Ln(III). However, in most of the cases, their functional groups (*i.e.* impregnated extractants) are not chemically bonded to the resin matrices but they just stick to the matrices. Therefore, it is difficult to impregnate extractants in large quantities and, furthermore, they are easily

unstuck, resulting that their adsorption capacity are not so large compared with ion exchange resins and they are not chemically durable. In order to combine the large adsorption capacity, chemical endurance, and high An(III) selectivity, a novel solid extractant is proposed in the present study. That is, an efficient An(III) extractant of **pyridine** (N-coordinated soft donor ligand [52, 56–59, 103]) is **resinified** and the resinified materials are employed as a stationary phase of chromatography. Pyridine type resins have already been employed as a solid extractant [105, 106]. However, almost all the existing pyridine resins are a quaternary pyridine type resin and they are used as a strongly basic anion exchange resin. On the other hand, the pyridine resin employed in the present study is a tertiary pyridine type, working both as a N-donor type solid extractant and as a weakly basic anion exchange resin, as shown in **Fig. 1-6**. The resinification of pyridine is expected to bring sufficient adsorption capacity, high chemical endurance of functional group, and high selectivity for An(III) over Ln(III). Furthermore, chromatography technique simplifies multistage operation, which is required for the individual separation of An(III). As shown in **Fig. 1-5**, the volume of An(III) in HLW is far smaller than that of FPs (An(III)/FPs $\cong$ 1/167, An(III)/Ln(III) $\cong$ 1/50). This means that, if only An(III) are selectively adsorbed in the solid extractant and other FPs are hardly adsorbed in the extractant (*i.e.* just pass through the column), not so large adsorption capacity is necessary and, therefore, the chromatographic technique is sufficiently applicable to large scale treatment.

Quaternary pyridinium resin
(Strongly basic anion exchange resin)

Coordinative N-donor

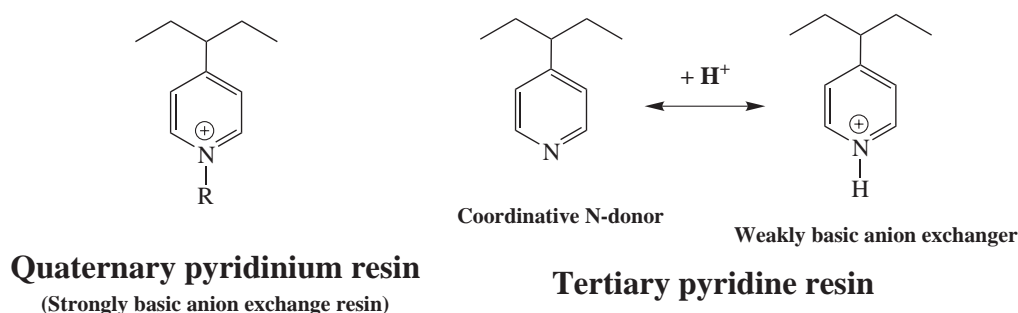Weakly basic anion exchanger

Tertiary pyridine resin

Figure 1-6. Chemical structures of pyridine type resins.

1.6   Contents of Thesis

The final goal of the present study is to develop an overall partitioning system by extraction chromatography using pyridine resin for the transmutation of An(III) in HLW. As the first groundwork for the development of the system, the present study

especially focuses on the separation of An(III) from Ln(III) and the individual separation of An(III), which are considered the most difficult processes on the partitioning of An(III). The study is composed by the following five parts:

   I. Synthesis and properties of pyridine resin (Chapter 2)

  II. Adsorption and separation behavior of trivalent f-elements by pyridine resin in nitrate system (Chapter 3)

 III. Adsorption and separation behavior of trivalent f-elements by pyridine resin in chloride system (Chapter 4)

 IV. Adsorption and separation mechanisms of trivalent f-elements by pyridine resin (Chapter 5)

  V. Practical partitioning experiments using irradiated mixed oxide fuels (Chapter 6)

In part I (Chapter 2), the pyridine resins employed in the present study are synthesized, and their properties (matrix structures, adsorption capacity, resistance to acid and irradiation, and the protonation of pyridine) are examined.

In parts II and III (Chapters 3 and 4), the adsorption and separation behavior of trivalent f-elements by pyridine resin is investigated in various compositions of chloride and nitrate solutions, which are most common solvents for practical separation process. The effects of temperature and flow rates are also examined. Then, on the basis of the results obtained, the operating conditions of chromatography are optimized for the efficient separation of An(III) from Ln(III) and the individual separation of An(III).

In part IV (Chapter 5), the adsorption and separation mechanisms of trivalent f-elements by pyridine resin are discussed in order to elucidate the origin of the observed adsorption and separation phenomena and to develop the present partitioning system using pyridine resin to other separation processes.

In part V (Chapter 6), practical partitioning experiments using real irradiated mixed oxide (MOX) fuels are carried out with the optimized conditions, and the practicability of the partitioning system using pyridine resin is verified. The adsorption and separation behavior of non-trivalent An (U and Pu) and several FPs are also confirmed.

References

[1] EDMC／   ·   ，   ，
    ，Feb. 2004, pp. 22 and 36-37.

[2] ibid., pp. 22 and 30-31.

[3] ibid., pp. 178-179.

[4]   ，   （ 70 ）   3, Dec. 1999.

[5]   15   ，   ，Mar. 2003, pp. 14.

[6] "Nuclear-Waste Transmutation and Incineration", GSI-Nachrichten, Feb. 1999, pp. 14.

[7] J. C. Warf, *J. Am. Chem. Soc.*, **71**, 2187 (1949).

[8] IAEA Technical Report Series, No. 176, 1997, pp. 8-13.

[9] "Reference Design Description for a Geological Repository", *Civilian Radioactive Waste Management System*, 1997.

[10] "Summary of the Environmental Impact Statement on the Concept for Disposal of Canada's Nuclear Fuel Waste", AECL-10721, COG-93-11, 1994.

[11] Jean-Michel Hoorelbeke, "Initial Design Options for Disposal of HLW/TRU Waste in France", *Proceedings of the 18th International Conference on High-Level Radioactive Waste Management*, 1998.

[12] Final Waste Repository and Disposal Projects-Worldwide, DBE, 1995.

[13] Projekt Gewaehr 1985, NAGRA, 1985.

[14] "PLAN 96·Costs for Management of the Radioactive Waste from Nuclear Power Production", SKB TR 96-15, 1996.

[15] H. Takano, K. Nishihara, K. Tsujimoto, T. Sasa, H. Oigawa, T. Takizuka, *Prog. Nucl. Energy*, **37**, 371 (2000).

[16] K. Aizawa, ibid., **40**, 349 (2002).

[17] J.-P. Grouiller, S. Pillon, C. de Saint Jean, F. Varaine, L. Leyval, G. Vambenepe, B. Carlier, *J. Nucl. Mater.*, **320**, 163 (2003).

[18] T. Kase, H. Harada, T. Takahashi, *Prog. Nucl. Energy*, **29**, 335 (1995).

[19] M. Salvatores, I. Slessarev, G. Ritter, P. Fougeras, A. Tchistiakov, G. Youinou, A. Zaetta, *Nucl. Inst. Meth. Phys. Res. A*, **414**, 5 (1998).

[20] T. Mukaiyama, H. Takano, T. Ogawa, T. Takizuka, M. Mizumoto, *Prog. Nucl. Energy*, **40**, 403 (2002).

[21] http://atmimg.tokyo.jst.go.jp/atomica/group2.html

[22] H. Oigawa, T. Yokoo, K. Nishihara, Y. Morita, T. Ikeda, N. Takaki, *Proceedings of GLOBAL 2005*, Paper No. 266 (2005).

[23] S. Chwaszczewski, B. Slowiński, *Appl. Energy*, **75**, 87 (2003).

[24] T. Kiba, K. Terada, N. Okawa, S. Osaki, *Talanta*, **13**, 1385 (1966).

[25] R. D. Neirinckx, A. S. M. de Jesus, *Anal. Chim. Acta*, **59**, 324 (1972).

[26] E. H. Huffman, R. L. Oswalt, L. A. W. Williams, *J. Inorg. Nucl. Chem.*, **3**, 49 (1956).

[27] M. Pirs, R. J. Magee, *Talanta*, **8**, 395 (1961).

[28] B. Gu, K. E. Dowlen, L. Liang, J. L. Clausen, *Sep. Technol.*, **6**, 123 (1996).

[29] P. W. West, A. S. Lorica, *Anal. Chim. Acta*, **25**, 28 (1961).

[30] N. Ikeda, K. Tanaka, *J. Chromatog. A*, **114**, 389 (1975).

[31] N. N. Egorov, *et al.*, "New Approaches to Solving the Management Problem of Long-Lived Radionuclides", *Proceedings of The Third International Conference on Nuclear Fuel Reprocessing and Waste Management. RECOD '91*, Apr. 1991, vol. I, pp. 14.

[32] G. F. Vandergrift, *et al.*, "Development and Demonstration of the TRUEX Solvent Extraction Process", *Technology and Programs for Radioactive Waste Management and Environmental Restoration, Waste Management '93 (R. G. Post Ed.)*, 1993, Vol. 2.

[33] Y. Koma, K. Nomura, M. Ozawa, T. Kawata, "Application of Modified TRUEX Flow-sheet to Minor Actinide Separation from High Level Liquid Waste", ibid.

[34] J. N. Mathur, M. S. Murali, P. R. Natarajan, *Talanta*, **39**, 493 (1992).

[35] L. Nigond, *et al.*, "Recent Advances in the Treatment of Nuclear Wastes by the Use of Diamide and Picolinamide Extractants", *Conference on Separation Science and Technology for Energy Applications*, Gatlinburg TN, USA, Oct. 1993.

[36] L. Nigond, C. Musikas, C. Cuillerdier, "Extraction Chemistry of Actinide Cations by N,N,N',N'-Tetraalkyl Propane-1,3 Diamides", CEACONF 11423, 1993.

[37] C. Madic, *et al.*, "Actinide Partitioning from High-Level Liquid Waste Using the DIAMEX Process", *Proceedings of The Fourth International Conference on Nuclear Fuel Reprocessing and Waste Management. RECOD '94*, Apr. 1994, vol. III, pp. 24.

[38] R. Jiao, S. Wang, S. Fan, B. Liu, Y. Zhu, H. Zheng, S. Zhou, S. Chen, *J. Nucl. Radiochem.*, **7**, 65 (1985).

[39] C. Song, J. Xu, Y. Zhu, ibid., **14**, 193 (1992).

[40] R. D. Shannon, *Acta Cryst.*, **A32**, 751 (1976).

[41] M. Benedict, T. H. Pigford, H. W. Levi, "Nuclear Chemical Engineering, 2nd Ed.", McGraw-Hill, New York, pp. 388 (1981).

[42] B. Weaver, F. A. Kappelmann, *J. Inorg. Nucl. Chem.*, **30**, 263 (1968).

[43] E. P. Horwitz, D. G. Kalina, A. C. Muscatello, *Sep. Sci. Technol.*, **16**, 403 (1981).

[44] E. P. Horwitz, A. C. Muscatello, D. G. Kalina, L. Kaplan, ibid., **16**, 417 (1981).

[45] A. C. Muscatello, E. P. Horwitz, D. G. Kalina, L. Kaplan, ibid., **17**, 859 (1982).

[46] V. N. Kosyakov, E. A. Yerin, *J. Radioanal. Chem.*, **56**, 93 (1980).

[47] P. T. Gerontopulos, L. Rigali, P. G. Barbano, *Radiochim. Acta*, **4**, 75 (1965).

[48] R. E. Leuze, R. D. Baybarz, B. Weaver, *Nucl. Sci. Eng.*, **17**, 252 (1963).

[49] Z. Kolarik, U. Müllich, *Solv. Extr. Ion Exch.*, **15**, 361 (1997).

[50] R. G. Pearson, *J. Am. Chem. Soc.*, **85**, 3533 (1963).

[51] R. G. Pearson, "Chemical Hardness", Wiley-VCH, Weinheim (1997).

[52] C. Musikas, G. le Marois, R. Fitoussi, C. Guillerdier, "Actinide Separations", ACS Symposium Series, Vol. 117 (J.D. Navratil, W.W. Shulz Ed.), American Chemical Society, Washington, D. C., pp. 131 (1980).

[53] J. Chen, Y. Zhu, R. Jiao, *Sep. Sci. Technol.*, **31**, 2723 (1996).

[54] Y. Zhu, J. Chen, R. Jiao, *Solv. Extr. Ion Exch.*, **14**, 61 (1996).

[55] D. D. Ensor, G. D. Jarvinen, B. F. Smith, ibid., **6**, 439 (1988).

[56] P. Y. Cordier, C. Hill, P. Baron, C. Madic, M. J. Hudson, J. O. Liljenzin, *J. Alloys Compd.*, **271**-**273**, 738 (1998).

[57] Z. Kolarik, U. Müllich, F. Gassner, *Solv. Extr. Ion Exch.*, **17**, 23 (1999).

[58] Z. Kolarik, U. Müllich, F. Gassner, ibid., **17**, 1155 (1999).

[59] M. Watanabe, R. Mirvaliev, S. Tachimori, K. Takeshita, Y. Nakano, K. Morikawa, R. Mori, *Chem. Lett.*, **31**, 1230 (2002).

[60] G. W. Manson, A. F. Bollmeier, D. F. Peppard, *J. Inorg. Nucl. Chem.*, **32**, 1011 (1970).

[61] J. J. Fardy, J. M. Buchanan, ibid., **38**, 149 (1976).

[62] B. F. Myasoedov, M. S. Milyukova, E. V. Kuzovkina, D. A. Malikov, N. S. Varezhkina, *J. Less-Comm. Met.*, **122**, 195 (1986)

[63] J. M. Adnet, C. Madic, "New Strategy for Minor Actinides Partitioning: Preliminary Results on the Electrovolatilization of Ruthenium and on the Stabilization of Am(IV) in Nitric with Phosphotungstate Ligand", *Workshop on Partitioning and Transmutation of Minor Actinides*, Karlsruhe, Germany, Oct. 1989.

[64] J. M. Adnet, C. Madic, J. Bourges, "Redox and Extraction Chemistry of Actinides U, Np, Pu, Am Complexed with the Phosphotungstate Ligand: $P_2W_{17}O_{61}{}^{10-}$", *22eme Jounées des Actinides*, Méribel, France, Apr. 1992.

[65] J. M. Adnet, L. Donnet, P. Brossard, J. Bourges, "Oxidation of Americium in Simulated High Level Liquid Wastes", *International Conference on Evaluation of Emerging Nuclear Fuel Cycle Systems, Global 95*, Versailles, France, Sep. 1995.

[66] J. M. Adnet, L. Donnet, P. Brossard, J. Bourges, "The Selective Extraction of Oxidized Americium", *4th International Conference on Nuclear and Radiochemistry (NRC4)*, St. Malo, France, Sep. 1996.

[67] J. M. Miller, "Separation Methods in Chemical Analysis", Wiley & Sons, Inc., New York (1975).

[68] A. Braithwaite, F. J. Smith, "Chromatographic Methods 4th Edition", Chapman and Hall Ltd., London (1985).

[69] F. H. Spedding, E. I. Fulmer, T. A. Butler, E. M. Gladrow, M. Gobush, P. E. Porter, J. E. Powell, J.. M. Wright, *J. Am. Chem. Soc.*, **69**, 2812 (1947).

[70] E. R. Tompkins, J. X. Khym, W. E. Cohn, ibid., **69**, 2769 (1947).

[71] F. H. Spedding, A. F. Voigt, E. M. Gladrow, N. R. Sleight, ibid., **69**, 2777 (1947).

[72] J. A. Marinsky, L. E. Glendenin, C. D. Coryell, ibid., **69**, 2781 (1947).

[73] F. H. Spedding, A. F. Voigt, E. M. Gladrow, N. R. Sleight, J. E. Powell, J. M. Wright, T. A. Butler, P. Figard, ibid., **69**, 2786 (1947).

[74] D. H. Harris, E. R. Tompkins, ibid., **69**, 2792 (1947).

[75] M. A. Bracchini, "The History and Ethics Behind The Manhattan Project", Mechanical Engineering Department, The University of Texas at Austin (1997).

[76] K. Street, Jr., G. T. Seaborg, *J. Am. Chem. Soc.*, **72**, 2790 (1950).

[77] R. M. Diamond, K. Street, Jr., G. T. Seaborg, ibid., **76**, 1461 (1954).

[78] H. Deelstra, F. Verbeek, *J. Chromatog.*, **17**, 558 (1965).

[79] W. H. Hale, J. T. Lowe, *Inorg. Nucl. Chem. Lett.*, **5**, 363 (1969).

[80] S. Usuda, N. Shinohara, H. Yoshikawa, *J. Radioanal. Nucl. Chem., Art.*, **109**, 353 (1987).

[81] S. Usuda, ibid., **123**, 619 (1988).

[82] J. S. Coleman, R. A. Penneman, T. K. Keenan, L. E. LaMar, D. E. Armstrong, L. B. Asprey, *J. Inorg. Nucl. Chem.*, **3**, 327 (1957).

[83] E. K. Hulet, R. G. Gutmacher, M. S. Coops, ibid., **17**, 350 (1961).

[84] Y. Marcus, ibid., **28**, 209 (1966).

[85] R. J. Morrow, *Talanta*, **13**, 1265 (1966).

[86] W. Kraak, W. A. van den Heijden, *J. Inorg. Nucl. Chem.*, **28**, 221 (1966).

[87] J. S. Coleman, L. B. Asprey, R. C. Chisholm, ibid., **31**, 1167 (1969).

[88] S. Usuda, *J. Radioanal. Nucl. Chem., Art.*, **111**, 399 (1987).

[89] S. Usuda, ibid., **111**, 477 (1987).

[90] S. Usuda, N. Shinohara, H. Yoshikawa, S. Ichikawa, T. Suzuki, ibid., **116**, 125 (1987).

[91] S. Usuda, H. Yoshikawa, M. Magara, Y. Hatsukawa, *J. Radioanal. Nucl. Chem., Lett.*, **117**, 329 (1987).

[92] S. Usuda, N. Kohno, *Sep. Sci. Technol.*, **23**, 1119 (1988).

[93] H. Hubicka, D. Drobek, *Hydrometallurgy*, **47**, 127 (1997).

[94] J. Kooi, R. Boden, J. Wijkstra, *J. Inorg. Nucl. Chem.*, **26**, 2300 (1964).

[95] E. P. Horwitz, R. Chiarizia, H. Diamond, R. C. Gatrone, S. D. Alexandratos, A. Q. Trochimczuk, D. W. Crick, *Solv. Extr. Ion Exch.*, **11**, 943 (1993).

[96] R. Chiarizia, E. P. Horwitz, R. C. Gatrone, S. D. Alexandratos, A. Q. Trochimczuk, D. W. Crick, ibid., **11**, 967 (1993).

[97] E. P. Horwitz, M. L. Dietz, D. M. Nelson, J. J. LaRosa, W. D. Fariman, *Anal. Chim. Acta*, **238**, 263 (1990).

[98] E. P. Horwitz, R. Chiarizia, M. L. Dietz, H. Diamond, D. M. Nelson, ibid., **281**, 361 (1993).

[99] E. P. Horwitz, M. L. Dietz, R. Chiarizia, H. Diamond, S. L. Maxwell, III, M. R. Nelson, ibid., **310**, 63 (1995).

[100] E. P. Horwitz, R. Chiarizia, M. L. Dietz, *React. Func. Polym.*, **33**, 25 (1997).

[101] Y.-Z. Wei, M. Kumagai, Y. Takashima, M. Asou, T. Namba, K. Suzuki, A. Maekawa, S. Ohe, *J. Nucl. Sci. Technol.*, **35**, 357 (1998).

[102] Y.-Z. Wei, M. Yamaguchi, M. Kumagai, Y. Takashima, T. Hoshikawa, F. Kawamura, *J. Alloys Compd.*, **271**-**273**, 693 (1998).

[103] Y.-Z. Wei, H. Hoshi, M. Kumagai, T. Asakura, Y. Morita, ibid., **374**, 447 (2004).

[104] H. Hoshi, Y.-Z. Wei, M. Kumagai, T. Asakura, Y. Morita, ibid., **374**, 451 (2004).

[105] M. Chanda, G. L. Rempel, *React. Polym.*, **16**, 149 (1992).

[106] H. B. Sonmez, N. Bicak, *React. Funct. Polym.*, **51**, 55 (2002).

2 Synthesis and Properties of Tertiary Pyridine Resin

2.1 Synthetic Conception

In the present study, an organic polymer (*i.e.* resin) is employed as the stationary (solid) phase for liquid-solid extraction chromatography. The most common resin used for the stationary phase of liquid-solid extraction chromatography is ion exchange resin. The ion exchange resins have been utilized for various processes for a long time and, therefore, its synthesis has been well-developed as well as its applications.

From a synthetic point of view, there are two methods of synthesizing ion exchange resins. The first method consists of building the ion exchange groups into resin structure during the polymerization of resin matrix (*i.e.* backbone polymers). In other words, the ion exchange groups are a constituent of a monomer oil to be polymerize. The second method consists of forming a resin matrix followed by introducing the ion exchange groups into the resin structure. The advantage of the first method over the second one is that the resulting resin is a true homogeneous mass with high mechanical strength. This synthetic principle is applied to other solid extractants, such as chelate resins or extraction resins, by changing ion exchange groups to chelating groups or coordinating groups. Those chemical groups which interact with target chemical species are called "functional groups".

Since the solid-state organic extractants are polymers containing functional groups, their syntheses are achieved by the well-know principle of polymerization. The most common methods for preparing polymers are polymerization-condensation and vinyl polymerization [1, 2]. The first method involves ionic organic reactions in which a backbone polymer is formed from small polyfunctional monomers by splitting them into some products, such as water, alcohol, or ammonia, and new C-C, C-N, C-O, or other bonds. For example, the reaction of phenol and formaldehyde is represented as;
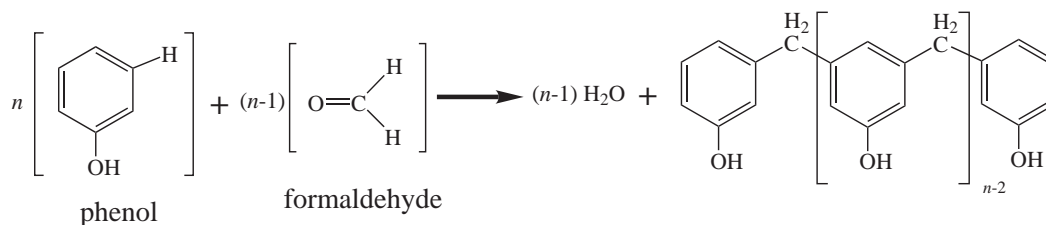
On the other hand, the vinyl polymerization involves polymerization of monomer molecules without the formation of any by-products. For example, butadiene is react with itself and polymerize, forming
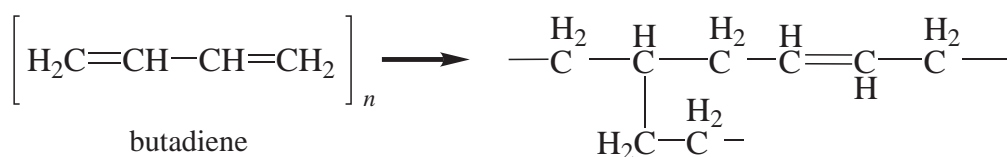
Another example of vinyl polymerization is expressed by the polymerization of styrene, forming polystyrene as follows;
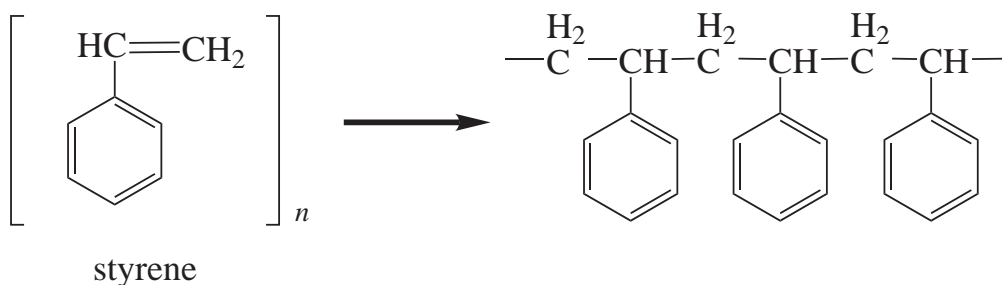
If the polystyrene chains are cross-linked with divinyl benzene (DVB), an insoluble copolymer of polystyrene is formed;
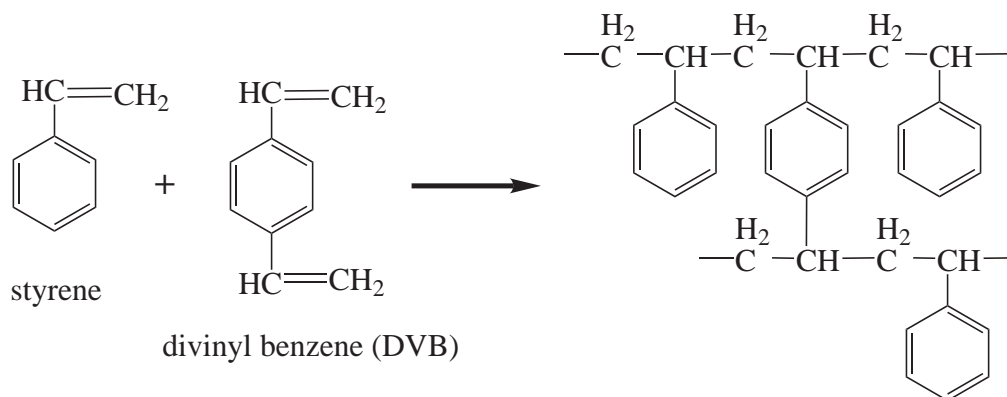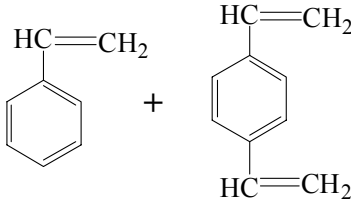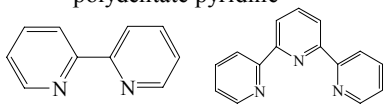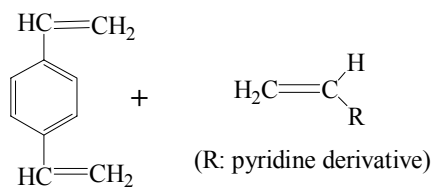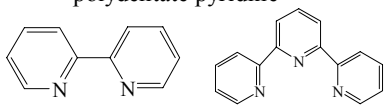
Those types of polymers are employed for the backbone structure of resins in case we can not find an appropriate reaction system in which desired functional groups are introduced into the backbone structure during the polymerization. The polymerization of aliphatic vinyl compounds also produces polymer resins. However, the backbone structure of these polymers is too dense to add further functional groups and to let chemical species penetrate inside the resins in practical separation process. Consequently, almost all the organic polymers for the stationary phase of liquid-solid extraction chromatography have styrene-, DVB-, or phenol-based matrix structure, which has relatively large space in its matrix structure.

Considering these basic principles for the synthesis of polymers, we can conceive several conceptions to synthesize the resins having tertiary pyridine groups. The possible conceptions are outlined in **Table 2-1**. In Conceptions 1 and 2, the functional groups of pyridine groups are introduced after the polymerization of a backbone polymer. These conceptions require more than two steps to complete the synthesis, taking a great deal of time and work. Furthermore, it is not so easy to modify functional groups on the backbone polymer. Thus, it is difficult to accomplish large adsorption capacity (adsorptivity) and homogeneous resin structure for the final products by Conceptions 1 and 2. On the other hand, homogeneous resins with large adsorptivity can be obtained in only one synthetic process by Conceptions 3 and 4. Furthermore, the functional groups of the resins synthesized in these strategies are firmly bonded to the resin matrix, giving high chemical resistance. Therefore, we can conclude that Conceptions 3 and 4 are more favorable for simple and reliable synthesis than Conceptions 1 and 2. As shown in **Table 2-1**, there are two types of pyridine groups for the functional group of the resins, that is, ordinary monodentate pyridine and polydentate pyridine derivatives such as bipyridine (bpy) or terpyridine (tpy). Although the polydentate ligands of bpy and tpy can coordinate to (*i.e.* extract) metal cations more strongly than the monodentate pyridine, their chemical and radiation resistance is lower than the monodentate pyridine due to the presence of single bonds in their structure. In Conception 4, the vinyl compounds of the functional groups (*i.e.* vinyl-bpy or vinyl-tpy) are required for the resinification. However, these vinyl compounds can not be obtained commercially and we have to synthesize ourselves, while vinylpyridine is commercially available. In consequence, it appears that Conception 3 is the most practicable for synthesizing the pyridine type resin. In the present study, a tertiary pyridine type resin is synthesized in accordance with Conception 3.

Table 2-1. Possible conceptions of the synthesis of tertiary pyridine resin.

	Backbone structure	Functional group
1		monodentate pyridine
2		polydentate pyridine *e.g.*
3		monodentate pyridine
4	(R: pyridine derivative)	polydentate pyridine *e.g.*

A concrete scheme for the synthesis of tertiary pyridine resin is as follows;

DVB   **4-Vinylpyridine**   **DVB-Vinylpyridine polymer**
(Tertiary pyridine resin) .
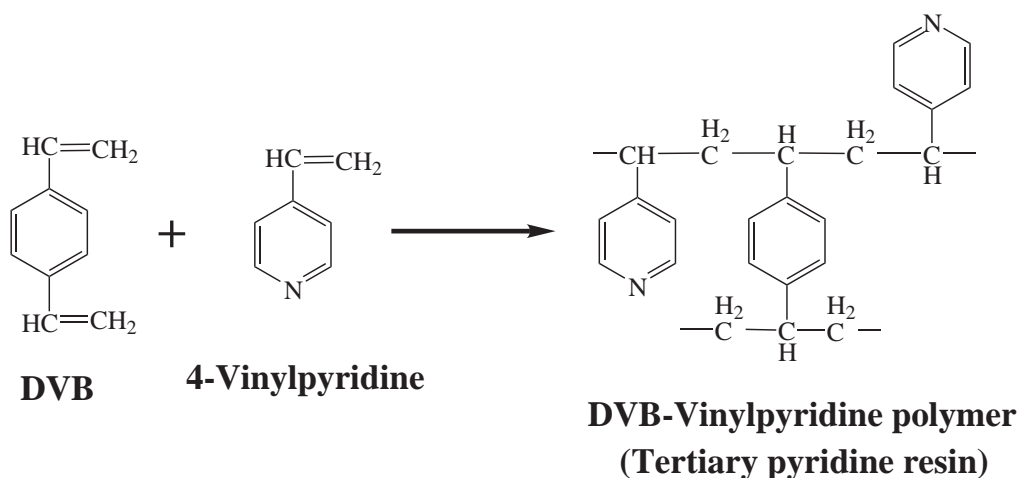
The polymerization of vinylpyridine also gives a tertiary pyridine type polymer. However, the structure of this polymer is so dense that they have small space to retain chemical species and, furthermore, they are brittle. Therefore, in the present

study, vinylpyridine is copolymerized with DVB. In consideration of the flexibility of pyridine groups in the resin structure, 4-vinylpyridine is employed for the copolymerizing vinylpyridine.

2.2   Type of Tertiary Pyridine Resin

Two types of tertiary pyridine resin are synthesized in the present study, that is, a standard polymer type tertiary pyridine resin (called "polymer pyridine resin", hereafter) and a porous silica-based tertiary pyridine resin (called "Si-based pyridine resin"). The former is a pure polymer of 4-vinylpyridine and DVB, while the latter is prepared by embedding polymer pyridine resin in highly porous silica beads. The polymer pyridine resin has plenty of pyridine groups in its structure and the porosity of the resin is relatively easy to control in its synthesis. This polymer pyridine resin is employed for batch experiments and XAFS experiments in Chapter 5. On the other hand, the Si-based pyridine resin is very advantageous to chromatography. The Si-based pyridine resin has uniform particle size, a large internal macro-porous structure, and high mechanical strength owing to the backbone matrix of silica beads. The uniform particle size restrains the deformation of resin in the column, realizing a uniform flow of mobile phase in chromatography. The large macro-porous structure enables chemical species to easily diffuse into the resin and, as a result, we can obtain a sharp chromatogram with well-defined peaks. The high mechanical strength prevents the resin swelling and shrinking which give rise to the deformation of resin column and the fracture of resin.

Table 2-2. Properties of two types of pyridine resins.

	Polymer pyridine resin	Si-based pyridine resin
Backbone matrix	Polymer	Silica beads
Adsorption capacity	Large	Small
Particle size	Need to sieve	Uniform
Mechanical strength	Low	High
Main use	Batch experiments	Chromatography

2.3   Synthesis of Tertiary Pyridine Resin

2.3.1   Polymer Type Tertiary Pyridine Resin

The synthesis of polymer pyridine resin was performed by suspension polymerization. In suspension polymerization technique, the polymerization initiator is soluble in the monomer oil, which is dispersed by comminuting it into the dispersion medium (usually aqueous solution) to form spherical droplets. The solubility of the dispersed monomer oil (and also the resultant polymer) in the dispersion medium are usually low. Polymerization proceeds in the droplet phase and, in most cases, it occurs by a free radical mechanism. Suspension polymerization usually requires the addition of small amounts of a stabilizer for the dispersion medium to control coalescence and breakup of droplets during polymerization. The size distribution of the initial emulsion droplets and, hence, also that of the resultant polymer beads depend on the balance between droplet coalescence and breakup. This balance is changed by the type and speed of agitator, the volume fraction of the monomer oil, and the type and concentration of stabilizer. Therefore, we can control the size distribution of the resultant polymer by modifying these synthetic conditions. When a porous polymer is required, an inert diluent, which is miscible with monomer oil but does not participate the polymerization, is added to the monomer oil. After the polymerization, the inert diluent is removed from the resultant polymer to leave porous structure inside the polymer. This inert diluent is generally called "pore-producing reagent".

Table 2-3 is a list of chemical reagents used for the suspension polymerization of polymer pyridine resin. As mentioned in the previous section, the pyridine resin polymer is produced by the copolymerization of 4-vinylpyridine and DVB. As a initiator of this copolymerization, α,α-Azobisisobutyronitrile (AIBN) and 1,1'-Azobiscyclohexane-1-Carbonitrile (ACCN) were added in the monomer oil. A precedent work by Nogami [3] has suggested that acetophenone and diethyl phthalate are appropriate pore-producing reagents for the 4-vinylpyridine / DVB copolymerization system, and acetophenone produces smaller pores and diethyl phthalate produces larger pores inside the polymer. Suspension reagents were selected by referring to the synthetic procedure of ion exchange resins by Asahi Kasei Corporation [4].

Table 2-4 shows a required quantity of each reagent for 100 g-monomer oil, along with the purity of each reagent employed in the present study. The letters *C*, *M*, and

Table 2-3. Chemical reagents for suspension polymerization of polymer pyridine resin.

Monomer oil	4-vinyl pyridine	Functional groups
	m/p-DVB	Crosslinking reagent
	Acetophenone	Pore-producing reagent (for small pore)
	Diethyl phthalate	Pore-producing reagent (for large pore)
	α,α-Azobisisobutyronitrile (AIBN)	Initiator
	1,1'-Azobiscyclohexane-1-Carbonitrile (ACCN)	Initiator
Suspension	Aqueous NaCl solution	Suspension matrix
	Hydroxyapatite (Super Tight[1])	Suspension reagent
	Methyl cellulose	Suspension reagent
	1,4-Bis(2-ethylhexyl) sodium sulfosuccinate (Rapizol[2])	Surfactant

[1] manufactured by Nippon Chemical Industrial Co., Ltd.

[2] manufactured by Nippon Oil and Fats Co., Ltd.

Table 2-4. Required quantity of each reagent for the polymerization of 100 g-monomer oil.

Reagent	Quantity	Purity / %
4-vinylpyridine	$(100 - C)$ g	95.0
m/p-DVB	C g	98.0
Acetophenone	$3/5 \cdot MP/(1-P)$ cm^3	99.5
Diethyl phthalate	$2/5 \cdot MP/(1-P)$ cm^3	99.0
AIBN	1.5 g	97.0
ACCN	1.0 g	-
Deionized water	$M/(1-P) \times 5$ cm^3	-
NaCl	$(M/(1-P) \times 5) \times 0.05$ g	-
Super Tight	$(M/(1-P) \times 5) \times 0.03$ g	-
Methyl cellulose	$(M/(1-P) \times 5) \times 0.00075$ g	-
Rapizol	$(M/(1-P) \times 5) \times 0.00075$ g	-

P in **Table 2-4** represent the crosslinkage (wt%) of polymer (*i.e.* the weight percent of DVB in monomer oil), the volume of monomer oil (= (C/0.9145)+((100-C)/0.987)), and the porosity of polymer (vol%), respectively. The crosslinkage (*C*) of typical ion exchange resins is around 10 wt%. In the present study, the crosslinkage of polymer pyridine resin was varied from 3 to 20 wt%. The porosity of polymer was also varied from 5 to 50 vol%.

The synthetic procedure is summarized in **Fig. 2-1** and the experimental apparatuses are illustrated in **Fig. 2-2**. The monomer oil and suspension were mixed in a separable flask placed on a heating mantle and stirred by an agitator at 100~200 rpm to form ~100 μm-diameter monomer oil particles. Then the separable flask was gradually heated to 363 K and hold at 363 K for more than 12 h to complete the radical copolymerization of 4-vinylpyridine and m/p-DVB. After the polymerization, a moderate concentration of HCl solution was added to the flask in order to dissolve the suspension reagents which clog filters. The resultant polymer was filtrated by a glass filter and washed by methanol and deionized water several times to remove the pore-producing reagents in the polymer. The well-washed polymer was then dried in a vacuum desiccator at 323 K for 2 days and sieved out into different particle sizes (*i.e.* ~100, 100~200, and 200~ μm). Finally, we got a light orange-colored polymer.

The synthesis succeeded for every crosslinkage and porosity. However, the polymers with below 5 wt%-crosslinkage and those with over 50 vol%-porosity were found to be very brittle and, thus, be of no practical use for batch or chromatography experiments. Accordingly, more than 5 wt%-crosslinkage and below 50 vol%-porosity are necessary composition for the practical polymer resin employed for batch and chromatography experiments. The yield of polymerization calculated from the weight of monomer oil and resultant polymer (*i.e.* weight of well-washed resultant polymer / weight of 4-vinylpyridine and m/p-DVB in monomer oil) was over 95%.

In order to confirm the composition of the resultant polymers, Fourier transform infrared (FT-IR) measurement was carried out. The spectrum is given in **Fig. 2-3**. Several absorption bands corresponding to pyridine group (3080~3010 cm^{-1}: stretching vibration of aromatic C-H, 1600~1430 cm^{-1}: stretching vibration of aromatic C-C and C-N, and ~800 cm^{-1}: deformation vibration of aromatic C-H) and those corresponding to alkane (1300~900 cm^{-1}: deformation vibration of alkane C-H) [5] indicated that 4-vinylpyridine was well polymerized with m/p-DVB and, as a result, pyridine groups were hold in the alkane-benzene backbone structure.

Put deionized water in a separable flask.
Dissolve NaCl in the deionized water.

Put Super Tight and stir the solution under 303 K.

Mix 4-vinylpyridine, DVB, acetophenone, and diethyl phthalate.
Dissolve AIBN and ACCN in the above mixture and stir.
(Monomer oil)

Put the monomer oil into the separable flask
and mixed with the aqueous solution.

Put methyl cellulose and Rapizol into the separable flask
and mixed with the monomer oil-aqueous solution mixture.

Heat the separable flask as follows;
Room temperature ~ 333 K for 30 min.
Hold at 333 K for 1 h.
333 K ~ 343 K for 15 min.
Hold at 343 K for 2 h.
343 K ~ 353 K for 15 min.
Hold at 353 K for 2 h.
353 K ~ 363 K for 15 min.
Hold at 363 K for 12 h.

Cool the separable flask to room temperature.
Add HCl solution to dissolve the suspension reagents.

Filtrate the polymerized material.

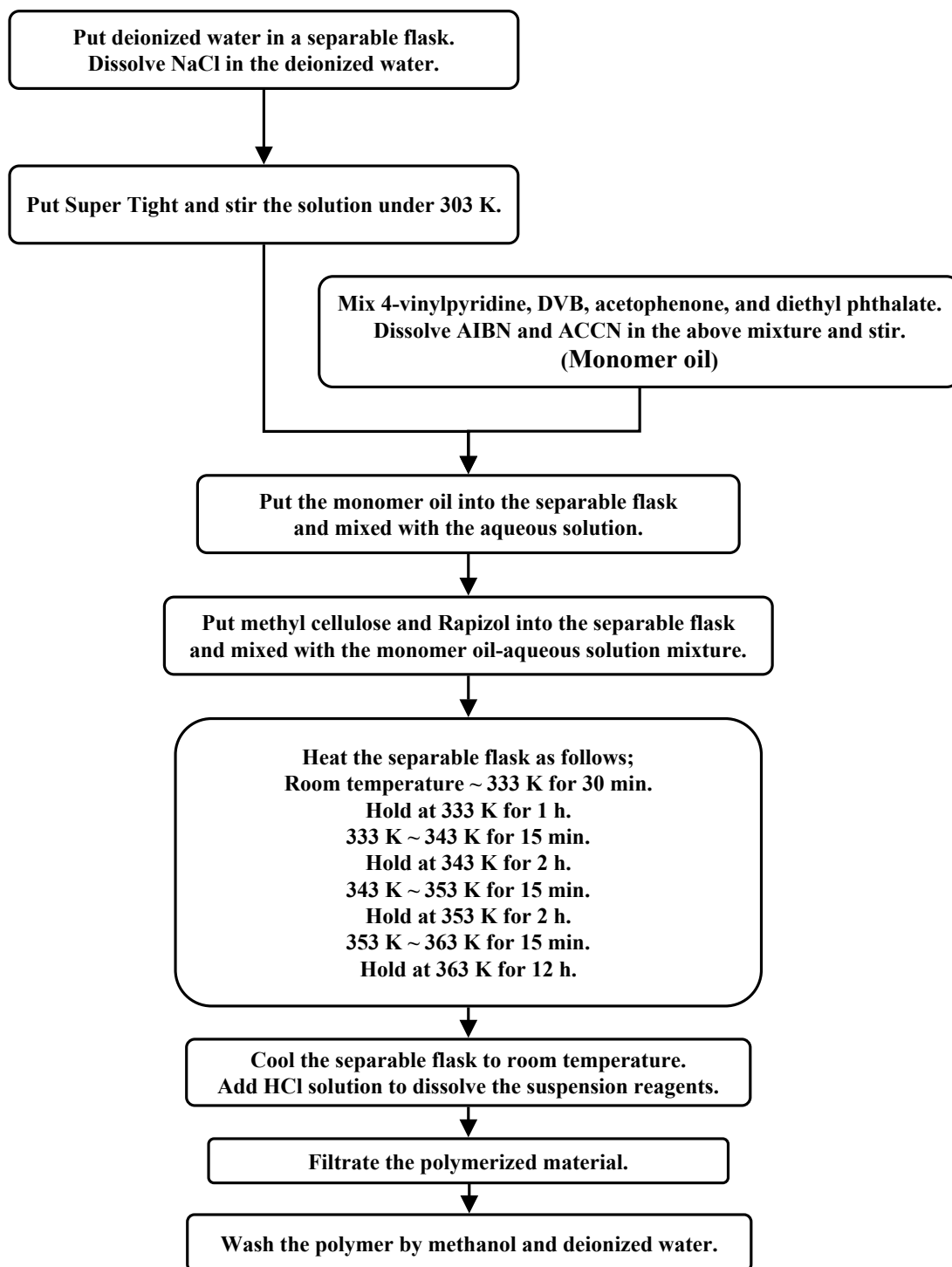Wash the polymer by methanol and deionized water.

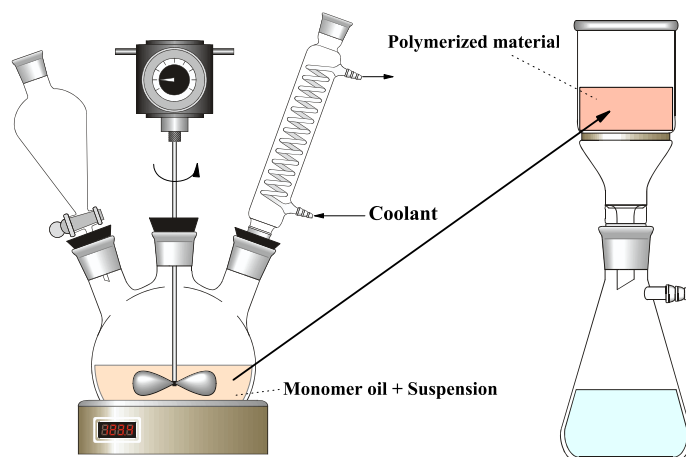Figure 2-1. Synthetic procedure of polymer pyridine resin.

Figure 2-2. Experimental apparatuses for the synthesis of polymer pyridine resin.

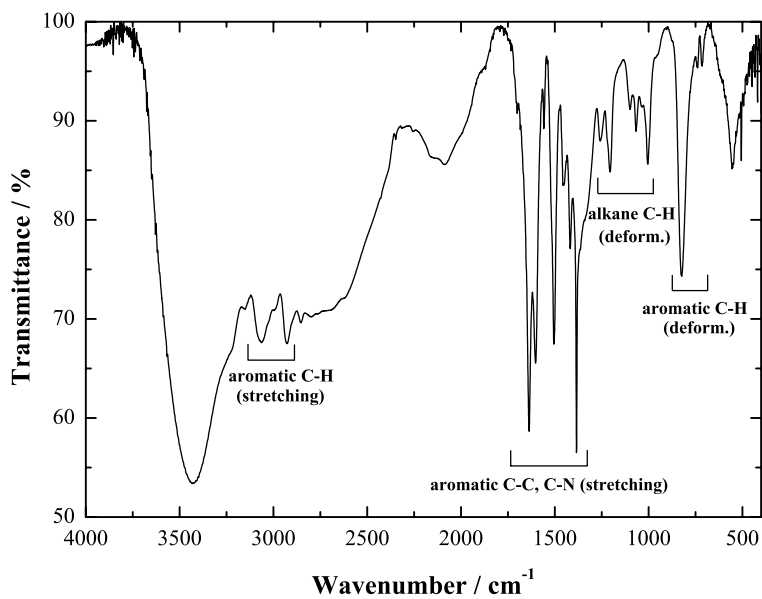

Figure 2-3. FT-IR spectrum of synthesized polymer pyridine resin.

2.3.2 Si-based Type Tertiary Pyridine Resin

In general, there are two ways to synthesize inorganic-organic (generally silica-organic materials) Si-based resins. One way is to "adsorb" organic materials into an inorganic support material. This method is very easy and a variety of organic materials can be introduced as functional groups. However, the durability of these Si-based resins is low because the functional groups are not chemically bonded to the support material but just physically adsorbed and, thus, they easily come off the support material. The other way to synthesize Si-based resins is to polymerize resins in a support material. In this method, monomer oils are impregnated in a support material and polymerized inside the support material. Although this method requires considerably high porous and mechanically strong support materials, the resultant resins have high-durability which is necessary for practical uses. In the present study, the latter method was employed for the synthesis of Si-based type tertiary pyridine resin.

The support material employed in the present study is the silica beads (called KIB) synthesized by Asahi Kasei Corporation. The physical properties of KIB are summarized in **Table 2-5** and typical SEM photos of KIB are shown in **Fig. 2-4**. KIB is composed of SiO_2 having considerably large volume of pores in its structure. Furthermore, it has an uniform particle size. These properties are very favorable for the synthesis of Si-based type resins.

Table 2-5. Physical properties of KIB silica beads.

Framework	SiO_2
Density	2.23 g/cm^3
Particle size	60 μm
Porosity	70 vol%

Fig. 2-5 summarizes the synthetic procedure of Si-based pyridine resin and its experimental apparatuses are illustrated in **Fig. 2-6**. The procedure is almost the same as that employed for the synthesis of polymer pyridine resin. KIB was washed by acetone and water several times and dried in a vacuum desiccator for more than 3 days before use. The dried KIB was put in an eggplant-shaped flask, and the air in the flask was substituted with nitrogen gas. Then the monomer oil that has the same composition as that used for the synthesis of polymer pyridine resin was
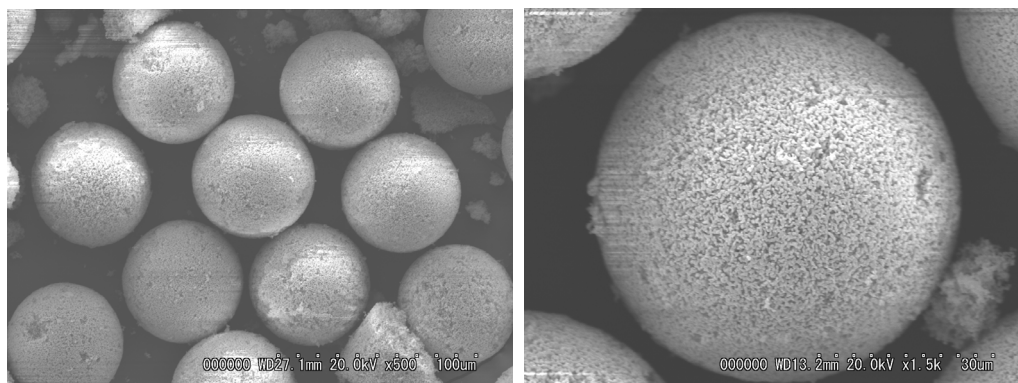
Figure 2-4. SEM photos of KIB.

mixed with KIB in a nitrogen atmosphere to impregnate the monomer oil in the pore structure of KIB homogeneously. The mixture of monomer oil and KIB was then gradually heated in a oil bath to 363 K and hold at 363 K for more than 12 h to polymerize the monomer oil in KIB. The resultant Si-based polymer was washed by acetone, methanol, and water several times and dried in a vacuum desiccator for 2 days. The crosslinkage and porosity of pyridine polymer were fixed at 10 wt% and 60 vol%, respectively. The ratio of monomer oil to KIB was varied from 130 ∕ 100 to 80 ∕ 100 (monomer oil (cm^3) ∕ KIB (g)). Well-polymerized Si-based pyridine resin was obtained for all the ratio of monomer oil to KIB. However, when the ratio of monomer oil to KIB was over 1 (*i.e.* more than 100 cm^3-monomer oil per 100 g-KIB), the resultant Si-based resins stuck to each other and their resin beds packed in a glass column were often clogged up. These mean that the pores of 100 g-KIB are saturated by 100 cm^3 of monomer oil and, hence, an excessive monomer oil chokes the pore structure of KIB and makes the resins stuck to each other. The choked resins are not suitable for practical uses as mentioned above and, therefore, the Si-based pyridine resins that were synthesized from 80 cm^3-monomer oil per 100 g-KIB were employed for chromatography experiments. **Fig. 2-7** is a SEM photo of the Si-based pyridine resin employed for chromatography experiments, showing that the Si-based pyridine resin still holds sufficient pore structures even after the polymerization of monomer oil. The calculated yield of the polymerization of monomer oil was over 95% for all the synthesis. The resultant Si-based resin tinged with pink.

Put dried KIB in an eggplant-shaped flask.
Evacuate the flask.

Substitute the air in the flask for nitrogen gas.
Evacuate the flask.

Mix 4-vinylpyridine, DVB, acetophenone, and diethyl phthalate.
Dissolve AIBN and ACCN in the above mixture and stir.
(Monomer oil)

Put the monomer oil into the eggplant-shaped flask.
Rotate the flask to mix the oil and KIB.

Impregnate the oil in KIB homogeneously
in nitrogen atmosphere.

Heat the eggplant-shaped flask
in an oil bath with rotating as follows;
Room temperature ~ 333 K for 30 min.
Hold at 333 K for 1 h.
333 K ~ 343 K for 15 min.
Hold at 343 K for 2 h.
343 K ~ 353 K for 15 min.
Hold at 353 K for 2 h.
353 K ~ 363 K for 15 min.
Hold at 363 K for 12 h.

Cool the flask to room temperature.

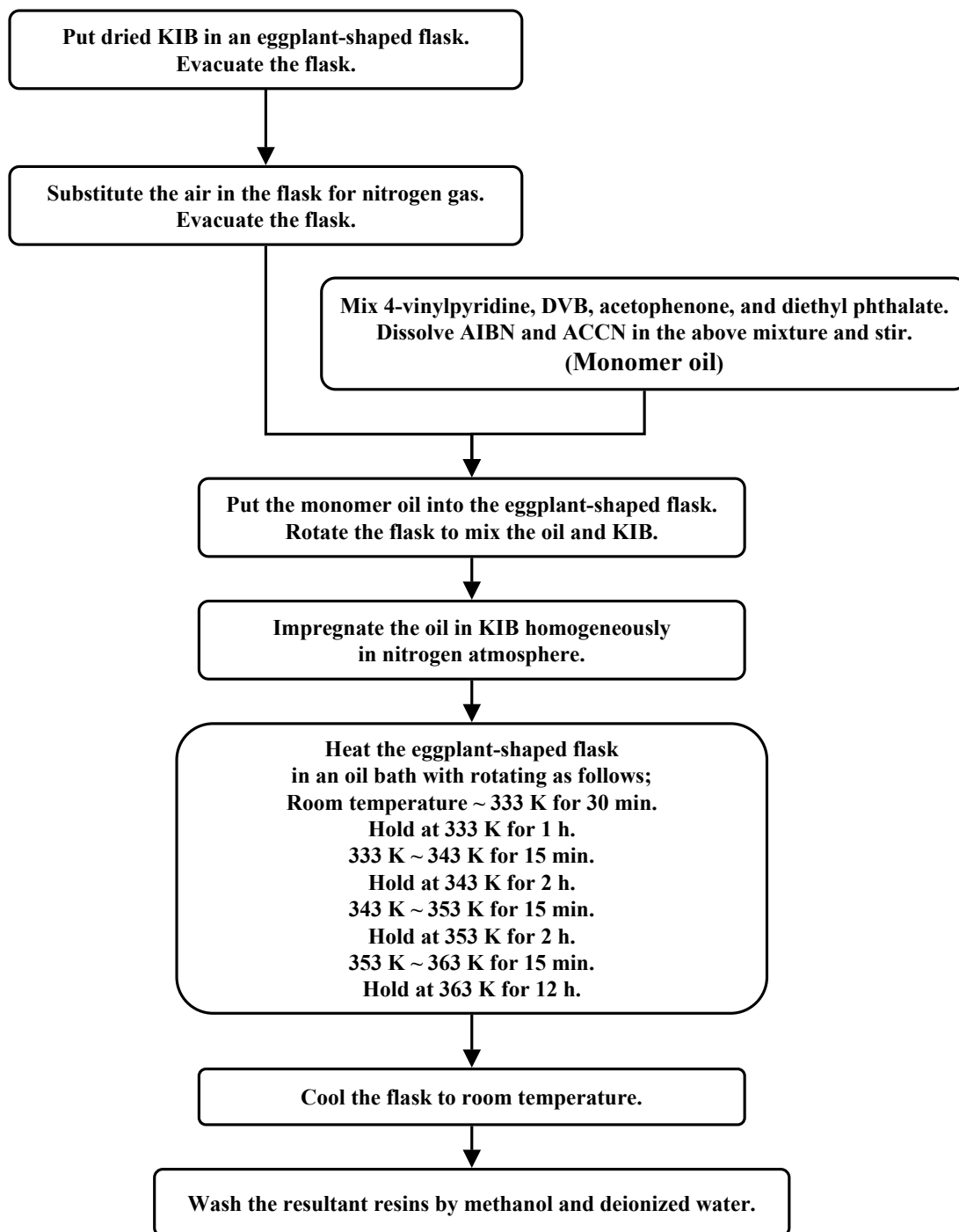Wash the resultant resins by methanol and deionized water.

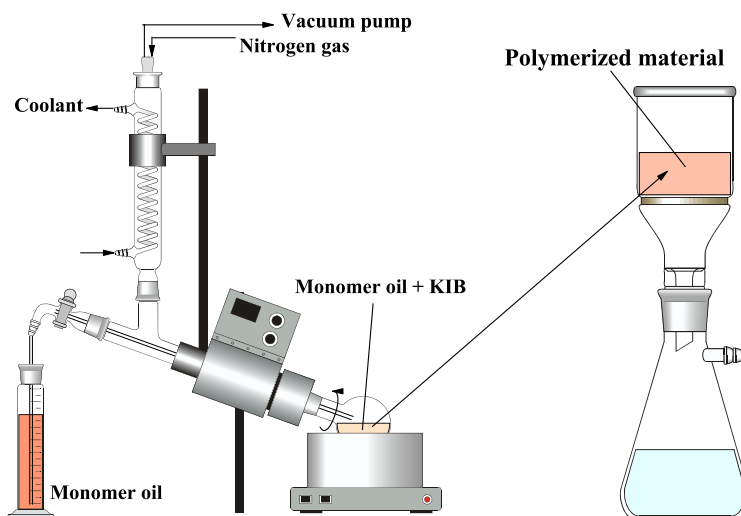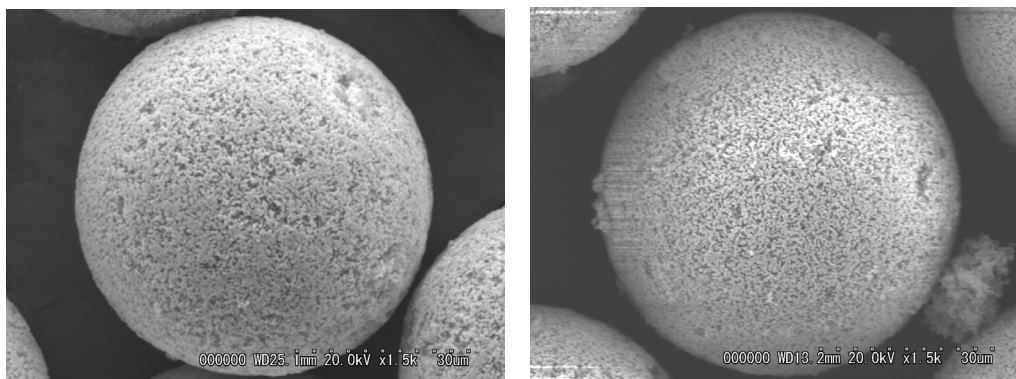Figure 2-5. Synthetic procedure of Si-based pyridine resin.

Figure 2-6. Experimental apparatuses for the synthesis of Si-based pyridine resin.

Hybrid pyridine resin
(80 cm^3-monomer oil / 100 g-KIB)

Raw KIB

Figure 2-7. SEM photos of Si-based pyridine resin and raw KIB.

Spectral comparison between polymer pyridine resin, Si-based pyridine resin, and raw KIB by FT-IR is shown in **Fig. 2-8**. Although a strong absorption peak corresponding to the stretching vibration of Si-O covers the fingerprint region (1400~600 cm^{-1}), we can still identify several absorption bands corresponding to the stretching vibration of aromatic C-H, C-C, and C-N, indicating that the monomer oil is well polymerized and the resultant polymer is "embedded" in KIB.
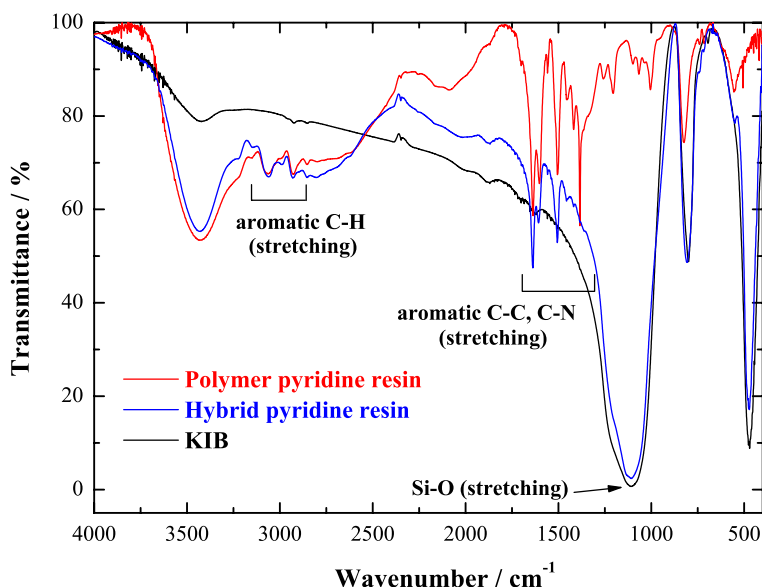

Figure 2-8. FT-IR spectral comparison of polymer pyridine resin, Si-based pyridine resin, and raw KIB.

In the case of ion exchange resins, the adsorption ability (often called "absorptivity") of resins is discussed by using the ion exchange capacity which generally represents the mole equivalent of functional groups per 1 L of resin (*i.e.* mol eq./L-resin or mmol eq./mL-resin). A tertiary pyridine resin can work as a weakly basic anion exchanger and, in principle, the ion exchange capacity of the synthesized resins should be calculated to compare their adsorptivity with other ordinary resins. However, it is very difficult to measure the precise ion exchange capacity of weakly acidic or basic ion exchangers because their capacity depends on pH. Accordingly, instead of the ion exchange capacity, the number of pyridine groups per unit volume was calculated from the compositions of monomer oil and the yield of polymerization

as shown in **Tables 2-6** and **2-7**. Although the number of pyridine groups per unit volume of Si-based resin is almost the half of that of polymer resin, the Si-based resin still has sufficient pyridine groups for practical uses.

Table 2-6. Number of pyridine groups per unit volume of polymer pyridine resin (N_{py}(polym)).

	N_{py}(polym) / mmol/cm^3		
Crosslinkage (wt%)	3	5	10
Porosity / vol% 5	8.63	8.44	7.96
10	8.18	7.99	7.54
20	7.27	7.11	6.71
40	5.45	5.33	5.03

Table 2-7. Number of pyridine groups per unit volume of Si-based pyridine resin (N_{py}(Si-bsd)).

Crosslinkage	10 wt%
Porosity of pyridine resin	60 vol%
Yield of polymerization	95%
Ratio of monomer oil to KIB / cm^3/g-KIB	N_{py}(Si-bsd) / mmol/cm^3
1	2.28
0.9	2.20
0.8	2.11

2.4 Durability of Tertiary Pyridine Resin

2.4.1 Acid Resistance

In the present study, most of the adsorption and separation experiments using the synthesized tertiary pyridine resin are performed in hydrochloric acid or nitric acid solution. These acids are corrosive and nitric acid is a strong oxidizing agent. Furthermore, the mixing of an organic polymer of tertiary pyridine resin with nitric acid

may produce nitro compounds which are well-known as an explosive. Therefore, the decomposition and nitration effects of these acidic solutions on tertiary pyridine resin should be investigated before the following adsorption and separation experiments in order to examine the recyclability of the resin and to ward off the danger of the explosion caused by the nitration of resin.

The effect of hydrochloric acid and nitric acid solutions on the chemical structure of polymer pyridine resin was examined by soaking the resin in concentrated hydrochloric acid (*i.e.* 11.7 mol-HCl/dm^3, written as "conc. HCl" hereafter) or concentrated nitric acid (*i.e.* 13.5 mol-HNO$_3$/dm^3, written as "conc. HNO$_3$" hereafter) and measuring FT-IR spectra before and after soaking. The tested resin was carefully washed by acetone, methanol, and water several times and dried. The resin was soaked in the acid solutions for a certain period of time (1, 2, 4, and 7 days). After soaking, the resin was filtrated and washed by methanol and water several times and then dried in a vacuum desiccator for 2 days before FT-IR measurements.

Fig. 2-9 shows FT-IR spectra of original polymer pyridine resin and the resins after 1 day and 1 week of soaking in conc. HCl (also see Appendix II, **Fig. II-4**). No spectral change was observed before and after soaking even in the fingerprint region (the right graph). Even after 1 week of soaking, the spectra showed no change, suggesting that HCl has no effect on the decomposition of tertiary pyridine resin. Therefore, it is expected that we can recycle the pyridine resin many times after using in a HCl solution system. On the other hand, some spectral changes were observed for the resins soaked in conc. HNO$_3$, as shown in **Fig. 2-10** (and Appendix II, **Fig. II-5**). That is, three new absorption peaks appeared at 1560, 1384, and 1034 cm^{-1} after only 1 day of soaking. The first two peaks at 1560 and 1384 cm^{-1} correspond to the asymmetric and symmetric N-O stretching vibration of nitro group (-NO$_2$) respectively [6, 7], suggesting that some methylene or aromatic hydrogens of the resin are nitrated. The asterisked peak at 1034 cm^{-1} (∗) is probably attributed to the stretching vibration of aromatic C-N bond [6]. The absorption band appeared in 1600∼1430 cm^{-1}, which corresponds to the C-C and C-N stretching vibration of pyridine groups, showed no change even after 1 week of soaking. From these spectral results, it can be concluded that the nitration of methylene and aromatic hydrogens of tertiary pyridine resin occurs for only 1 day of soaking in conc. HNO$_3$, although the functional sites of tertiary pyridine groups are not affected by this nitration. Close attention is required for using the pyridine resin with nitric acid media in order to avoid the explosion caused by the nitrated compounds.
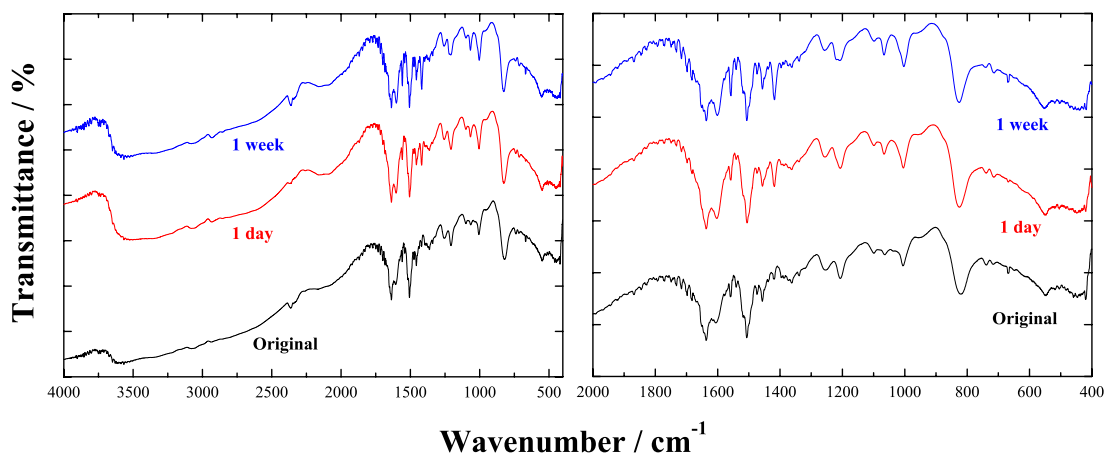
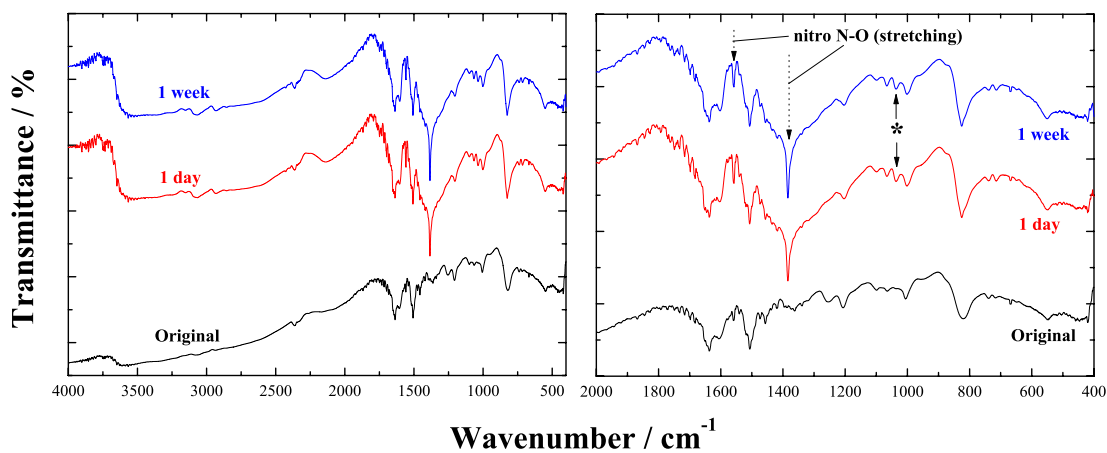**Figure 2-9.** FT-IR spectral comparison of polymer pyridine resins before and after soaking in conc. HCl.

Figure 2-10. FT-IR spectral comparison of polymer pyridine resins before and after soaking in conc. HNO_3.

45

2.4.2   Radiation Resistance

Irradiation can change most of the physical and chemical properties, such as optical [8–11], electrical [12], or mechanical property [13], of organic polymers depending on the irradiation dose and energy and type of beam. The tertiary pyridine resin synthesized in the present study aims at applying to a practical treatment of HLW with high dose of radiation. Therefore, it is important to investigate the durability of the resin against the expected irradiation in order to evaluate its practicability and recyclability.

The durability of pyridine resin (both of polymer type and Si-based type) for γ-ray irradiation (up to 10 MGy) has precedently been investigated both in HCl and HNO_3 solutions by Nogami and his co-workers [14]. They revealed that only less than 10% of the functional pyridine groups of the resin was decomposed after 10 MGy irradiation in 6 M-HCl solution, while approximately 40% of the pyridine groups was damaged by the same irradiation in 6M-HNO_3 solution. It was also found in their research that the Si-based type resin showed higher radiation resistance than the polymer type resin.

In addition to the irradiation of γ-ray, the pyridine resin is exposed to α-ray emitted by An elements in practical processes. In the present study, the effect of α-irradiation on Si-based pyridine resin was investigated in a HCl-methanol mixed solution, which is going to be found to be one of the efficient solvents for An(III)-Ln(III) separation in chapter 4.

A 0.5 g of Si-based pyridine resin was soaked in 2 cm^3 of 70 vol%-conc. HCl/30 vol%-methanol mixed solution (written as conc. HCl/MeOH = 7/3, hereafter) containing Am and Cm ($\sim$6 kBq) for 70 days. (It was, unfortunately, impossible to examine in nitric acid solution due to the danger of the explosion caused by nitration). The resin samples before and after the irradiation were filtrated, washed by deionized water and methanol several times and dried in a vacuum desiccator for 2 days. Then the FT-IR spectra of the samples were measured.

Fig. 2-11 shows the spectral comparison of the Si-based pyridine resin before and after α- (and γ-) irradiation. Several spectral changes were observed in the fingerprint region, that is, the absorbance of two absorption bands corresponding to the alkane C-H deformation vibration (1450$\sim$1300 and 1100$\sim$1000 cm^{-1}) increased or decreased before and after the irradiation. This probably means that the methylene groups of the backbone structure of the resin are decomposed by α-ray (or the

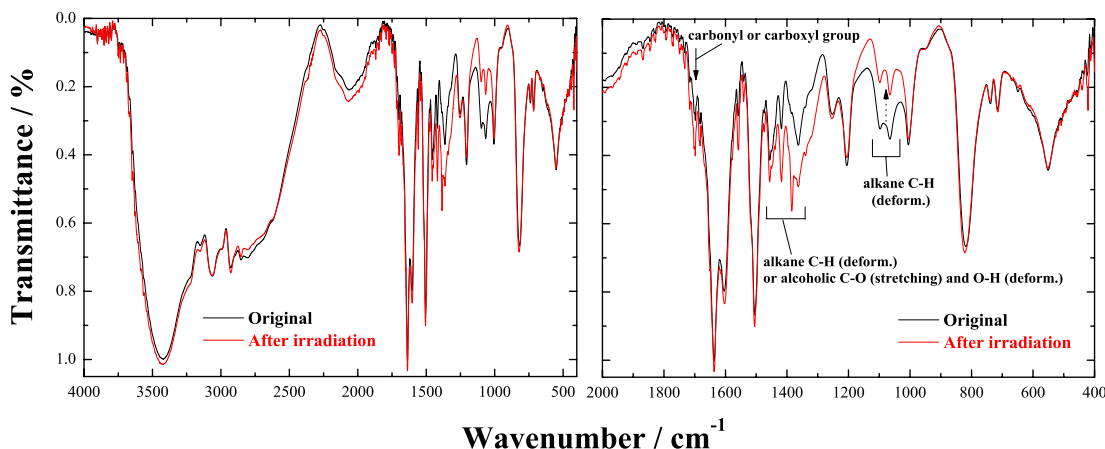synergic effect of α-ray and HCl) and, consequently, other types of alkane are produced.

Figure 2-11. FT-IR spectral comparison of Si-based pyridine resins before and after α-irradiation.

The new peak which appeared at 1700 cm^{-1} after the irradiation indicates the presence of carbonyl or carboxylic group [6] due to the oxygenation of the resin [14], as shown in **Fig. 2-12**. The increasing absorption band at 1450~1300 cm^{-1}, which can be assigned to the stretching vibration of alcoholic C-O and the deformation vibration of alcoholic O-H, may support this decomposition mechanism. However, despite of the decomposition of the backbone structure, the absorption bands corresponding to the pyridine groups (3080~3010 and 1600~1430 cm^{-1}) showed no change, suggesting that the α- (and γ-) irradiation in conc.HCl/MeOH mixed solvent has no influence on the pyridine groups. This is consistent with the previous results of γ-ray irradiation [14]. Furthermore, the adsorptivity of the resin was unchanged before and after the irradiation. Therefore, we can conclude that the tertiary pyridine resin has sufficient radiation resistance in HCl solution system, although the decomposition by irradiation is not negligible in HNO$_3$ solution system.
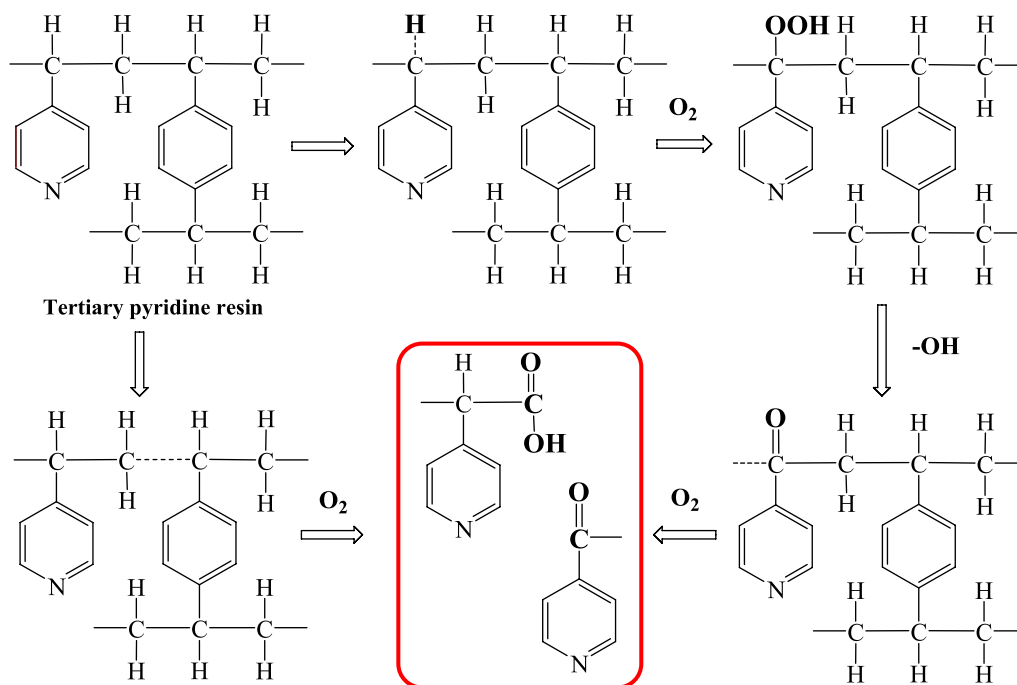
Figure 2-12. Decomposition mechanism of tertiary pyridine resin by irradiation [14].

2.5   Protonation of Pyridine

The protonation of pyridine groups is one of the important factors which affect the adsorptivity of tertiary pyridine resins because the protonated pyridine groups do not work as coordinative functional sites but work as anion exchangers. In the case of metal cation adsorption, coordinative pyridine groups directly interact with the cations by coordinate bonds, while protonated pyridine groups adsorb the cations as a result of the ionic interaction between positively charged pyridine groups and negatively charged anionic complexes of the cations. This difference in adsorption mechanism should lead to the different adsorption and separation properties of tertiary pyridine resin and, consequently, these properties depend on the degree of protonation of pyridine groups.

In order to evaluate the degree of protonation of pyridine groups, the protonation constants of several pyridine derivatives (pyridine (Bpy), bipyridine (Bpy), and terpyridine (Tpy)) were determined by spectrophotometric titrations. UV-visible measurements were made by a V-560 series UV-visible spectrophotometer (JASCO, Ap-

pendix I, **Fig. I-2**) with 200~350 nm scanning range to follow the change in absorption attributed to the $\pi \rightarrow \pi^*$ transitions of the pyridine type ligands. Spectrophotometric titrations were performed by first introducing a given portion of the ligand solution, which contains a pyridine ligand in an alcohol solution, directly into a quartz cuvette (path length = 1 cm). Then tiny aliquots (2 mm^3) of HCl in alcohol were introduced directly into the cuvette. The increase in solution volume after each H$^+$ addition was corrected in a calculation step. The temperature was not controlled but monitored: the monitored temperatures were 293~298 K. The data-processing ranges were selected around the major absorption maxima of the pyridine type ligands as follows: Py 205~280; Bpy 205~330; Tpy 200~350. Singular value decomposition analysis (SVD) was employed to determine the number of spectrophotometrically distinguishable species in the scanning absorption range by using the calculation programs SPECFIT/32 [15–18] and Hyperquad 2003 [19]. The analysis assumes only the validity of the Lambert-Beer's law of optical absorbance for multicomponent mixtures.

Fig. 2-13 shows the results of the spectrophotometric titrations, and the protonation constants calculated from the results are listed in **Table 2-8**. The calculated protonation constant for pyridine was similar to those previously reported ($p\beta_1$ = 5.1~5.5) [20–25], while the calculated constant for bipyridine was a little larger than the reported value in water ($p\beta_1$ = 4.33) [26] probably due to the difference in solvent and determination method. It was difficult to determine $p\beta_1$ for Tpy due to the poor spectral change. Interestingly, the degree of protonation seems to increase with an increase of the number of pyridine groups in the molecule.

The speciation diagrams for H-Py and H-Bpy systems calculated from the obtained protonation constants are shown in **Fig. 2-14**. The protonation of pyridine is considerably strong and almost all the pyridine groups are protonated even in 0.0002 mol-HCl/dm^3 solution. Furthermore, it has been reported [25, 27] that there is a substitution effect on the protonation of pyridine, that is, the substitution by alkyl groups increases the acidity of endocyclic nitrogen of pyridine groups. The pyridine groups in the resin have similar structure to 4-isopropylpyridine that has larger protonation constant than pyridine. Therefore, the pyridine groups in the resin are expected to protonated almost completely even in very low acidic solvent ([H$^+$] $\cong$ 0.1 mmol/dm^3).
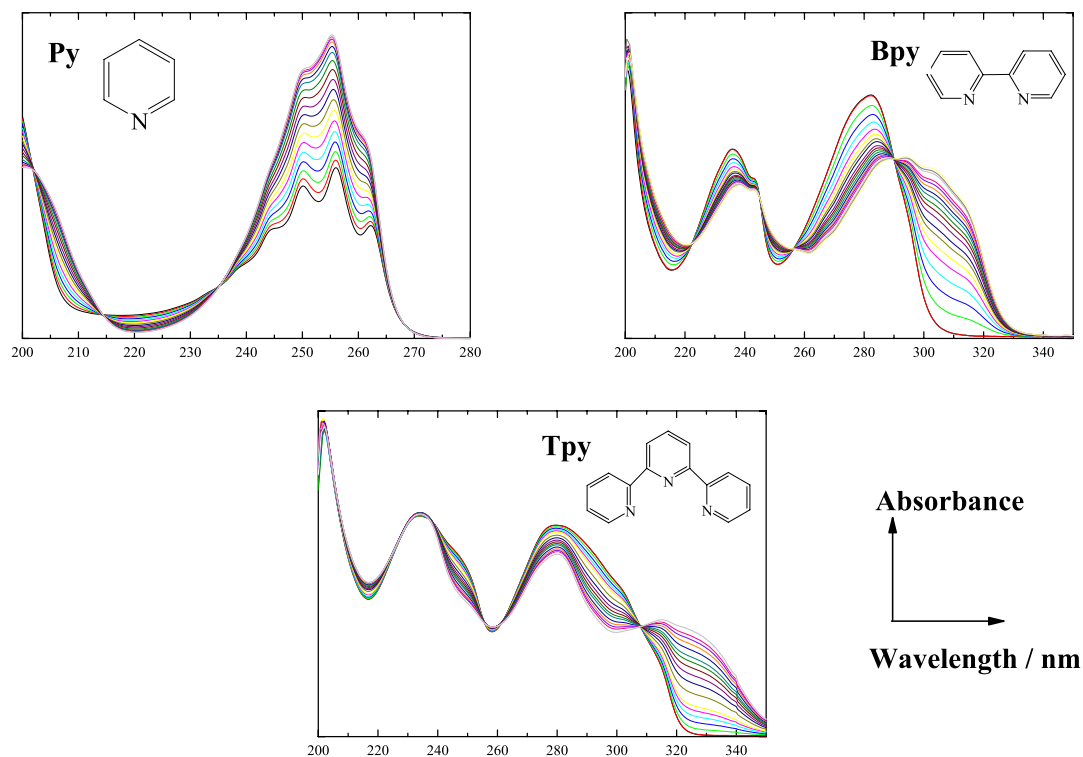
Figure 2-13. Spectral titration data for the protonation of pyridine derivatives with HCl in ethanol.

Table 2-8. Overall protonation constants (β_1 and β_2) of pyridine derivatives in ethanol.

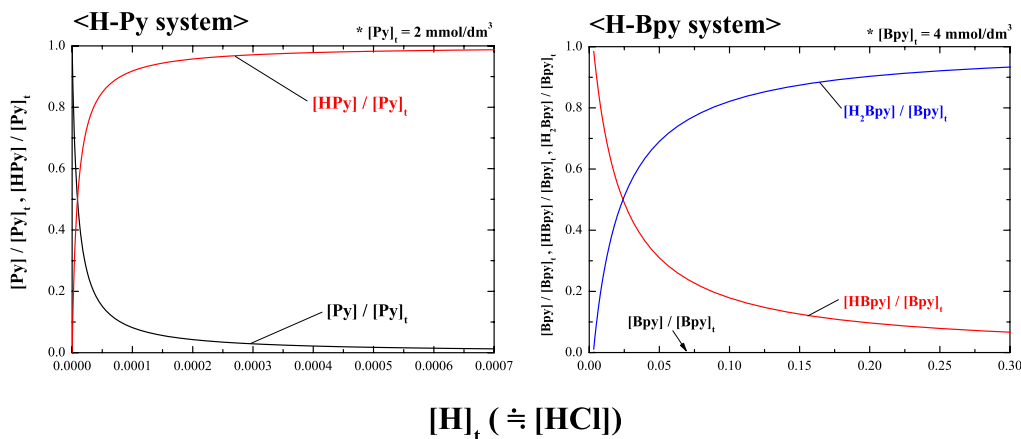|	$log\beta_1$	$log\beta_2$
Pyridine (Py)	5.05$\pm$0.04	-
Bipyridine (Bpy)	5.98$\pm$0.01	10.02$\pm$0.01
Terpyridine (Tpy)	-	10.24$\pm$0.02

Figure 2-14. Speciation diagrams for H-Py and H-Bpy systems in ethanol.

The degree of protonation also depends on the type of solvent because the acidity (and basicity) of solvent molecules has an influence on the activity of H^+, affecting the protonation of pyridine groups. In the present study, different types of alcohols (both normal and branched chain types) are employed for batch and chromatography experiments. The protonation constants of Bpy determined in different alcohols are shown in **Table 2-9** and **Fig. 2-15**. ($*$ Bpy was employed for this experiments instead of Py because the titration data for Bpy showed larger spectral change than those for Py (as shown in **Fig. 2-13**), giving less errors in calculation process.) Although almost all the physical and chemical properties of alcohols increase or decrease monotonously with increasing the number of carbon (Appendix II, **Table II-1**), the protonation constants of Bpy showed an irregular variation with the increase of the number of carbon. This suggests that the protonation of pyridine groups is not dominated by only one factor, but it involves several factors.

Table 2-9. Overall protonation constants (β_1 and β_2) of Bpy in water and several alcohols.

Solvent	$log\beta_1$	$log\beta_2$
Water	5.52±0.01	9.59±0.01
Methanol	5.13±0.02	9.91±0.01
Ethanol	5.98±0.01	10.02±0.01
1-Propanol	4.72±0.02	9.32±0.01
2-Propanol	5.64±0.01	9.15±0.01
1-Butanol	5.06±0.01	9.29±0.01
2-Butanol	5.01±0.01	8.77±0.01
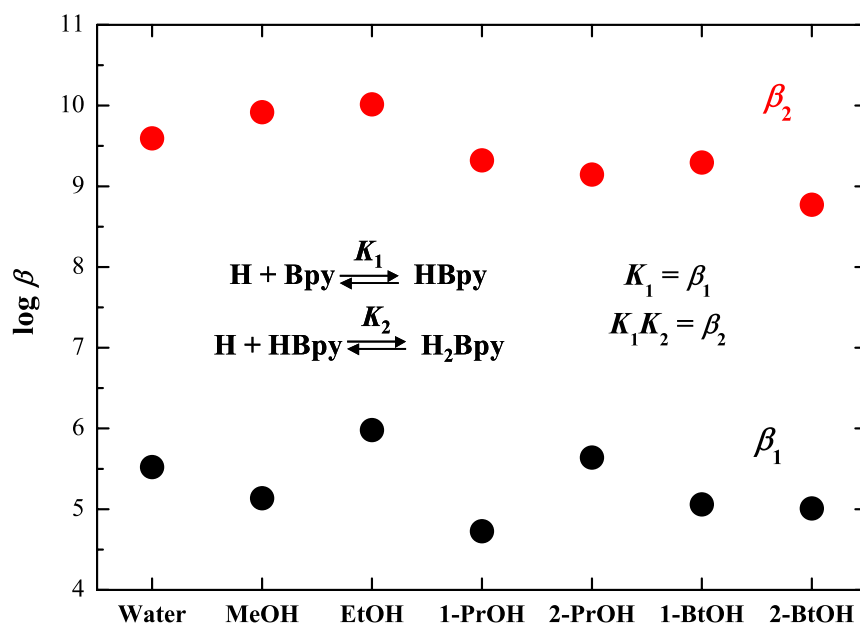
Figure 2-15. Overall protonation constants (β_1 and β_2) of Bpy in water and several alcohols.

In the present study, we investigate the adsorption and separation behavior of trivalent f-elements by the pyridine resin in the mixed solvents of mineral acid (hydrochloric acid and nitric acid) solutions and alcohol because several reports [28–36] have suggested that adding alcohol in aqueous solution often promotes the adsorptivity and separability of solid extractants such as ion exchange resins. Therefore, the protonation reaction of pyridine groups in the water-alcohol mixed system should also be considered in order to understand the adsorption and separation properties of the pyridine resin in this system.

Kılıç and his co-workers have performed a systematic investigation on the protonation constants of pyridine derivatives in a water-ethanol mixed solvent system [37], revealing that the protonation constants of pyridine derivatives decrease almost linearly as the volume fraction of ethanol increases, as shown in **Fig. 2-16**. Furthermore, the protonation constants for other ligands (anilines [38], alkylamines [39], and esters [40]) show similar decreasing tendency with the increase of alcohol in solvent. Therefore, although the solvent properties of water-alcohol binary solvent systems greatly depend on the type of alcohol added [41–44], it still can be expected that adding alcohol in solvent restrains the protonation of pyridine groups of the resin in the water-alcohol mixed system.
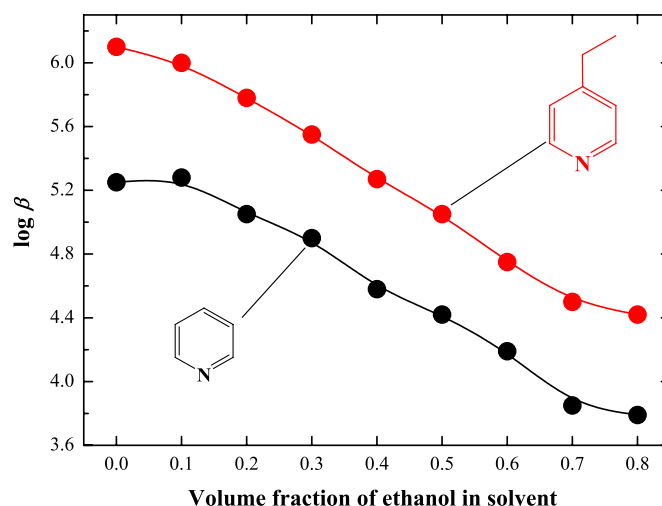

Figure 2-16. Variation of the protonation constants of pyridine and 4-ethylpyridine in water-ethanol mixed system [37].

2.6   Summary

Two types of tertiary pyridine resin (*i.e.* polymer type and Si-based type) were synthesized by the copolymerization of 4-vinylpyridine and m/p-divinylbenzene. The synthesized pyridine resins showed no chemical change by soaking in a HCl solution, while a HNO_3 solution caused the nitration of backbone polymers. The resins also showed remarkable resistance to α- and γ-irradiation. These properties are very favorable for the practical use with high radiation dose and acidic solvent conditions.

The pyridine groups of a tertiary pyridine resin are easily protonated even in weak acid solutions ($[H^+] \cong 0.1$ mmol/dm^3). The protonation of pyridine groups depends on the type of solvent. In water-alcohol binary solvent systems, an increase of alcohol content weakens the protonation of pyridine groups.

References

[1] R. Kunin, R. J. Myers, "Ion Exchange Resins", John Wiley & Sons, Inc., New York, 1950.

[2] J. A. Marinsky, "Ion Exchange -A Series of Advances-", Marcel Dekker, Inc., New York, 1969.

[3] M. Nogami, Doctor Thesis, Department of Nuclear Engineering, Tokyo Institute of Technology, Tokyo (1996).

[4] Asahi Kasei, Private communication, Asahi Kasei (1992).

[5] R. M. Silverstein, F. X. Webster, "Spectrometric Identification of Organic Compounds 6th Ed.", John Wiley & Sons, Inc., New York, 1998.

[6] J. R. Dyer, "Application of Absorption Spectroscopy of Organic Compounds", Prentice-Hall, Inc., New Jersey, 1965.

[7] J. P. Agrawal, R. N. Surve, Mehilal, S. H. Sonawane, *J. Hazard. Mater.*, **A77**, 11 (2000).

[8] B. S. Elman, M. K. Thakur, D. J. Sandman, M. A. Newkirk, *J. Appl. Phys.*, **57**, 4996 (1985).

[9] J. Davenas, X. L. Xu, G. Boiteux, D. Sage, *Nucl. Inst. Meth. Phys. Res. B*, **39**, 754 (1989).

[10] D. M. Rück, J. Schulz, N. Deusch, ibid., **131**, 149 (1997).

[11] E. Yap, D. G. McCulloch, D. R. Mckenzie, M. V. Swain, L. S. Wielunski, R. A. Clissold, *J. Appl. Phys.*, **83**, 3404 (1998).

[12] G. Marletta, S. Pignataro, C. Oliveri, *Nucl. Inst. Meth. Phys. Res. B*, **39**, 773 (1989).

[13] E. H. Lee, M. B. Lewis, P. J. Blau, L. K. Mansur, *J. Mater. Res.*, **6**, 610 (1991).

[14] M. Nogami, Y. Fujii, T. Sugo, *J. Radioanal. Nucl. Chem., Art.*, **203**, 109 (1996).

[15] H. Gampp, M. Maeder, C. J. Meyer, A. D. Zuberbühler, *Talanta*, **32**, 95 (1985).

[16] H. Gampp, M. Maeder, C. J. Meyer, A. D. Zuberbühler, ibid., **32**, 257 (1985).

[17] H. Gampp, M. Maeder, C. J. Meyer, A. D. Zuberbühler, ibid., **32**, 1133 (1985).

[18] H. Gampp, M. Maeder, C. J. Meyer, A. D. Zuberbühler, ibid., **33**, 943 (1986).

[19] P. Gans, A. Sabatini, A. Vacca, ibid., **43**, 1739 (1996).

[20] A. Albert, R. Goldacre, J. Phillips, *J. Chem. Soc.*, 2240 (1948).

[21] E. B. Hughes, H. H. G. Jellinek, B. A. Ambrose, *J. Phys. Colloid Chem.*, **53**, 410 (1949).

[22] C. Golumbic, M. Orchin, *J. Am. Chem. Soc.*, **72**, 4125 (1950).

[23] A. Gero, J. J. Markham, *J. Org. Chem.*, **16**, 1835 (1951).

[24] H. H. Jaffé, G. O. Doak, *J. Am. Chem. Soc.*, **77**, 4441 (1955).

[25] L. E. Kapinos, H. Sigel, *Inorg. Chim. Acta*, **337**, 131 (2002).

[26] T. R. Harkins, H. Freiser, *J. Am. Chem. Soc.*, **77**, 1374 (1955).

[27] R. G. Pearson, F. V. Williams, ibid., **75**, 3073 (1953).

[28] J. Korkisch, P. Antal, F. Hecht, *J. Inorg. Nucl. Chem.*, **14**, 247 (1960).

[29] P. Antal, J. Korkisch, F. Hecht, ibid., **14**, 251 (1960).

[30] J. Korkisch, F. Tera, ibid., **15**, 177 (1960).

[31] F. Tera, J. Korkisch, F. Hecht, ibid., **16**, 345 (1961).

[32] F. Tera, J. Korkisch, ibid., **20**, 335 (1961).

[33] J. P. Faris, J. W. Warton, *Anal. Chem.*, **34**, 1077 (1962).

[34] J. Korkisch, G. E. Janauer, *Talanta*, **9**, 957 (1962).

[35] J. Korkisch, I. Hazan, ibid., **11**, 1157 (1964).

[36] R. J. Morrow, ibid., **13**, 1265 (1966).

[37] E. Kılıç, F. Köseoğlu, Ö. Başgut, *Anal. Chim. Acta*, **294**, 215 (1994).

[38] M. A. Akay, E. Canel, E. Kılıç, F. Köseoğlu, *Turk. J. Chem.*, **26**, 37 (2002).

[39] E. Kılıç, G. Gökçe, E. Canel, ibid., **26**, 843 (2002).

[40] A. Doğan, E. Kılıç, ibid., **29**, 41 (2005).

[41] S. Mashimo, S. Kuwabara, S. Yagihara, K. Higashi, *J. Chem. Phys.*, **90**, 3292 (1989).

[42] N. Asaka, N. Shinyashiki, T. Umehara, S. Mashimo, ibid., **93**, 8273 (1990).

[43] S. Mashimo, T. Umehara, H. Redlin, ibid., **95**, 6257 (1991).

[44] H. Hayashi, K. Nishikawa, T. Iijima, *J. Phys. Chem.*, **94**, 8334 (1990).

3 Adsorption and Separation Behavior of Trivalent *f*-Elements in Nitrate Solution System

3.1 Introduction

A nitrate solution is one of the most frequently-used solvents for various separation processes. Especially, in the present nuclear industry, the fuel reprocessing or the treatment of radioactive wastes is performed in nitric acid solutions for the most part in order to combine the processes with the well-developed PUREX process. In fact, we can find a number of reports concerning the R&D of the treatment of radioactive nuclides using nitrate solution media.

The nitrate solution system has also been applied to the separation of trivalent *f*-elements. Adar and his co-workers investigated the anion exchange behavior of An(III) in LiNO$_3$ solutions and obtained a good chromatographic separation result [1]. Kraak and Van Der Heijden demonstrated a complete chromatographic separation between Am and Cm using an anion exchange resin with an aqueous Al(NO$_3$)$_3$ solution [2]. Hamaguchi and his co-workers investigated the anion exchange behavior of U, Th, and rare earth elements (Sc, Y, and Ln(III)) in Mg(NO$_3$)$_2$ solutions for the separation of U and Th from the FPs containing Ln(III) [3]. Numerous batch studies performed by Faris and his co-workers brought systematic information about the anion exchange behavior of An(III) and Ln(III) in HNO$_3$ solutions [4] and HNO$_3$ / MeOH mixed solutions [5]. In addition, the anion exchange behavior of Ln(III) in different alcoholic HNO$_3$ solutions was reported by Edge [6]. On the other hand, a gram-scale separation of Cm from Am and Ln(III) was achieved by cation exchange chromatography using a HNO$_3$ solution in combination with diethylenetriaminepentaacetic acid (DTPA) and nitrilotriacetic acid (NTA) eluents [7]. Usuda and his co-workers developed a chromatographic separation method using cation and anion exchange resins in HCl and HNO$_3$ solutions for the separation of TRU elements in a series of their

study [8–13]. Sato investigated a cation exchange behavior of FPs containing Ln(III) in a dilute HNO_3 solution [14].

Although the ion exchange study of An(III) and Ln(III) in the nitrate solution system has been carried out lively, much more energy has been thrown into the extraction study. The intergroup separation of An(III) and Ln(III) by solvent extraction using Cyanex, that is one of the most powerful extractants for An(III) / Ln(III) separation at the moment, has been developed on the assumption that its aqueous phase is a nitric acid solution [15, 16]. A large number of other effective extractants (*e.g.* dihexyl-*N,N*-diethylcarbamoylmethylphosphonate (DHDECMP) [17, 18], di-(2-ethylhexyl)phosphoric acid (HDEHP) and diethylenetriaminepentaacetic acid (DTPA) in TALSPEAK [19], TRPO [20, 21], terdentate pyridine derivatives [22], aromatic dithiophosphinic acids (R_2PSSH) [23], and 2,6-di-(5,6-dipropyl-1,2,4-triazin-3-yl)-pyridine [24]) exhibit their sufficient separability for An(III) / Ln(III) separation in combination with the aqueous phase of nitric acid solutions. Besides, most of the recently-developed processes for large-scale separation of An and FPs containing Ln(III) are operated in the nitric acid solution system (*e.g.* IMPUREX [25], TRUEX [26], or DIAMEX [27]) and the chromatographic separation technique using solid extractants has also employed nitrate solution media in most cases [28–33].

Considering these precedent studies and the fact that the present high-level liquid wastes are produced as nitric acid solutions, the adsorption and separation properties of the tertiary pyridine resin should be investigated in the nitrate solution system at first. In this chapter, the chromatographic behavior of trivalent *f*-elements by the tertiary pyridine resin is investigated in various nitrate solution media.

3.2   Experimental

3.2.1   Chromatography Experiments Using Stable Ln(III)

Chemicals   Ln(III) and Y samples for chromatography experiments were prepared from their hydrated nitrate ($Ln(NO_3)_3$) or oxide (Ln_2O_3) compounds supplied by Wako Pure Chemical Ind., Ltd. and Kanto Kagaku. Other chemicals and solvents were reagent grade and supplied by Wako Pure Chemical Ind., Ltd. and Kanto Kagaku. The pyridine resin used for chromatography was Si-based pyridine resin (Crosslinkage: 10 wt%, ratio of monomer oil to KIB: 0.9). In addition, strongly-basic an-

ion exchange resins of Dowex 1X8 (100~200 mesh, The Dow Chemical Company) and quaternary pyridinium resin (Si-based type, synthesized by Dr. Arai [34]) were also employed for chromatography experiments in order to compare their chromatographic behavior with those of the tertiary pyridine resin.

Apparatus and Procedure   The experimental apparatus for chromatography experiments is illustrated in **Fig. 3-1**. A resin column was prepared by packing 1 cm-ϕ × 50 cm of Si-based pyridine resin in 1 cm-ϕ × 55 cm of Pyrex glass column. The column was wrapped with a water jacket to keep the column temperature constant. In case of explosive emergency which may caused by the nitration of the resin, the column was enclosed by acryl boards. Prior to experiments, the resin column was conditioned by 300 cm^3 of deionized water and 200 cm^3 of a desired nitrate solution. A quaternary pyridinium resin was preliminarily treated by HNO$_3$ solution to give and NO$_3^-$ form and then conditioned by the desired nitrate solution. Sample solutions for chromatography experiments were prepared by dissolving the hydrated nitrate compounds into a desired solution. The volume of sample solutions was 10.0 cm^3 and the concentration of each metal in sample solutions was 1 mmol/dm^3. The sample solution was pumped into the column at a constant flow rate of 0.8 cm^3/min, and then eluted with the same solvent which was used to prepare the sample solution. The effluent from the column was collected in fractions and the metal concentrations in the fractions were determined by ICP-atomic emission spectrometer (OPTIMA-3000, PerkinElmer Inc. (Appendix I, **Fig. I-3**)) using selected emission lines [35, 36] to avoid their spectroscopic interference.

The distribution coefficients were calculated from the obtained chromatograms (**Fig. 3-2**). The distribution coefficient is defined as:

$$K_d = \frac{V_M - V_S}{V_R} \tag{1}$$

where V_M is the volume of effluent at elution peak, V_S is the dead volume of resin column and V_R is the volume of resin. In a preliminary experiment, it has been observed that the silica beads themselves do not adsorb any metal cations in a HCl or HNO$_3$ solution (see Appendix IV, **Fig. IV-1**). This means that the adsorption observed in this study is caused by the pyridine resin of stationary-phase, not by silica beads. Hence, V_R should be defined as the volume of the resin part of stationary-phase and, thus, was calculated from the mixing ratio of resin polymer and silica beads when
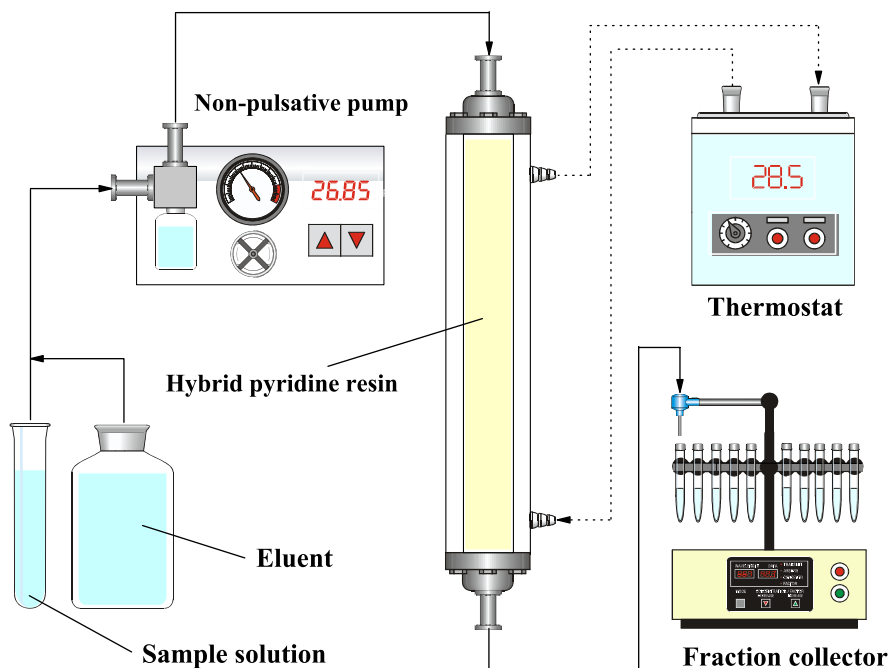
Figure 3-1. Experimental apparatus for chromatography experiments.

synthesized. The V_S was calculated from the water content in the resin column. It has also been confirmed in preliminary experiments that the elution curves in the present chromatography system fit Gaussian curves very well. Therefore, the elution curves obtained in this study were fitted with Gaussian curves. Then the V_M was calculated from the Gaussian curve fitted. The separation factors (α) were subsequently calculated from the distribution coefficients. The separation factor between *A* and *B* is defined as follows:

$$\alpha^A{}_B = \frac{K_d(A)}{K_d(B)} \tag{2}$$

V_R : **Volume of Resin in Column**

$$K_d = (V_M - V_S) / V_R$$

Gaussian curve
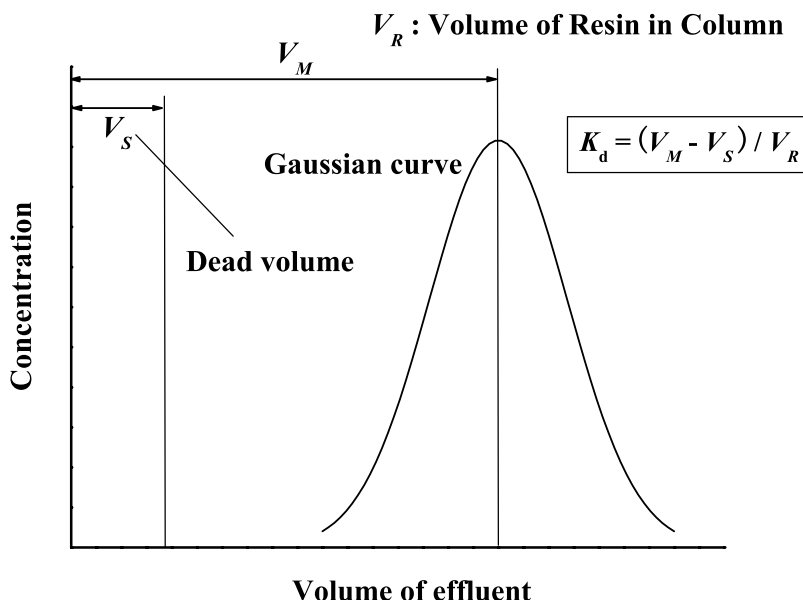
Dead volume

Concentration

Volume of effluent

Figure 3-2. Calculation of distribution coefficient (K_d) from chromatograms.

3.2.2 Chromatography Experiments Using An(III) and Radioactive Ln(III)

Chemicals In the present study, Ac, Am, Cm, and Cf were employed for trivalent An samples. A mixed trivalent An sample of ^{241}Am and ^{242}Cm was produced by the irradiation of ^{241}AmO$_2$ shielded sample in the Japan Materials Testing Reactor (JMTR, Japan Atomic Energy Research Institute (JAERI)-Oharai) followed by chemical separation for removing the majority of FPs. A mixed sample of ^{243}Cm and ^{244}Cm was produced by the irradiation of mixed oxide (MOX) fuels in the experimental FBR JOYO (Japan Nuclear Cycle Development Institute (JNC)-Oharai) followed by an appropriate separation process to isolate ^{243}Cm. A ^{249}Cf sample was prepared from a spent ^{252}Cf neutron source followed by the separation of FPs and daughter Cm isotopes. An ^{225}Ac sample was prepared by separating from its milking source of ^{229}Th. A radioactive ^{144}Ce was contained in the irradiated ^{241}AmO$_2$ sample as its FPs. Other radioactive Ln samples of ^{139,141}Ce, ^{147}Nd, ^{160}Tb, ^{168}Tm, and ^{169}Yb were produced by the irradiation of their stable isotopes using an electron linac at the Laboratory of Nuclear Science, Tohoku University. These radioactive samples were

dissolved into HCl solution and the dried samples were then dissolved in a desired nitrate or chloride solution. Other chemicals, solvents, and resin were the same as those used in the experiments using stable Ln. All the hot experiments were carried out at International Research Center for Nuclear Materials Science, Institute for Materials Research (IMR), Tohoku University (Oharai, Ibaraki).

Procedure   Feed samples for chromatography experiments were prepared by dissolving a dried mixture of trivalent An and radioactive Ln in a desired solution. A 0.5 cm^3 of feed sample was introduced into the plastic column, in which 1 cm-ϕ × 10 cm or 1 cm-ϕ × 50 cm of Si-based pyridine resin was packed. The sample was subsequently eluted using the same solution used to prepare the sample. The experiments were performed at a constant flow rate of 100 cm^3/h at ambient temperature (about 293 K). The effluent from the column was collected in fractions. The trivalent An of Am, Cm, and Cf in the collected fractions were detected using an α-ray spectrometer (IPC500-100-21EM, Eurisys Mesures or PG900-27AM, Canberra Industries, Appendix I, **Fig. I-4**). The Ln(III) in the fractions were detected using a coaxial n-type germanium detector (Eurisys Mesures, EGC 20-195-R, Appendix I, **Fig. I-5**). The amount of ^{225}Ac was determined by tracing its daughter nuclides of ^{221}Fr (E$_\gamma$ = 218.0 keV) and ^{217}At (E$_\alpha$ = 7.07 MeV). Samples for α-ray spectroscopy were prepared by drying a given portion of each fraction on a Nb plate and coating it with polycarbonate, while γ-ray spectra were measured by loading the sample tube of the fractions directly in the germanium detector. The radioactivity of each nuclide was defined as the net counts around the peak for α-ray measurements and as the gross counts for γ-ray measurements. The detection energy of each nuclide is listed in **Table 3-1** [37]. Distribution coefficients and separation factors were calculated by the same way as mentioned above using equations (2) and (3).

Table 3-1. Trivalent An and radioactive Ln employed in this study and their detection energy.

Element	Nuclide	Half life [37]	Detection
Ac	^{225}Ac	10.0 days	E_γ = 218.0 keV (^{221}Fr)
			E_α = 7.07 MeV (^{217}At)
Am	^{241}Am	432 y	E_α = 5.48 MeV
			E_γ = 59.54 keV
Cm	^{242}Cm	162.8 days	E_α = 6.11 MeV
			E_γ = 44.08 keV
	^{243}Cm	28.5 y	E_γ = 228.20 keV
			E_γ = 277.60 keV
	^{244}Cm	18.1 y	E_α = 5.80 MeV
Cf	^{249}Cf	351 y	E_α = 5.81 MeV
			E_γ = 387.95 keV
	^{252}Cf	2.638 y	E_α = 6.11 MeV
			E_γ = 43.40 keV
Ce	^{141}Ce	32.5 days	E_γ = 145.44 keV
	^{144}Ce	284.3 days	E_γ = 133.54 keV
Nd	^{147}Nd	32.5 days	E_γ = 91.11 keV
Tb	^{160}Tb	72.1 days	E_γ = 197.04 keV
Tm	^{168}Tm	93.1 days	E_γ = 720.32 keV
			E_γ = 815.95 keV
Yb	^{169}Yb	30.0 days	E_γ = 177.21 keV
			E_γ = 197.95 keV

3.3 Results

3.3.1 Chromatographic Behavior of Ln(III) by Tertiary Pyridine Resin in Nitrate Solution System

The experiments using radioactive nuclides (*i.e.* An(III) and radioactive Ln), generally called "hot" experiments, require thorough preliminary experiments in order to optimize experimental conditions before the real experiments because these radioactive sources are very rare and, thus, we can not use them in large quantities. Therefore, chromatography experiments using stable Ln were carried out in a variety of experimental conditions so that we can optimize the separating conditions (solvent composition, temperature, and flow rate) before the after-mentioned hot experiments and predict the adsorption and separation behavior of An(III) and Ln(III) mixture.

Solvent effect I. HNO_3-Alcohol   Nitric acid is the most common nitrate solution for chemical separation. In fact, the present reprocessing process (PUREX) employs nitric acid solution with tributyl phosphate (TBP). Therefore, the chromatographic behavior of Ln(III) was investigated in a nitric acid solution system in the first place.

The upper left graph in **Fig. 3-3** shows a chromatogram of Y and Ln(III) by the tertiary pyridine resin in a concentrated nitric acid solution (*i.e.* 13.5 mol-HNO_3/dm^3, written as "conc. HNO_3", hereafter). The elution curves were roughly divided into two groups of heavier Ln (Sm-Lu) and lighter one (La-Nd). However, the obtained distribution coefficients (K_d) and separation factors (α) were so low that it seems difficult to achieve sufficient separation in this solution. It is well-known that the addition of alcohols in mineral acids promotes the adsorptivity of solid extractants such as ion exchange resins [38–45]. Therefore, the adsorptivity of tertiary pyridine resin may also be promoted by adding alcohols in solvent. In order to confirm the effect of alcohol on K_d and α, methanol was added into a nitric acid solution, in the same way as the chloride solution system in the previous chapter. The obtained chromatograms in different conc. HNO_3 / MeOH solutions are shown in **Fig. 3-3** and Appendix III, **Fig. III-1**.
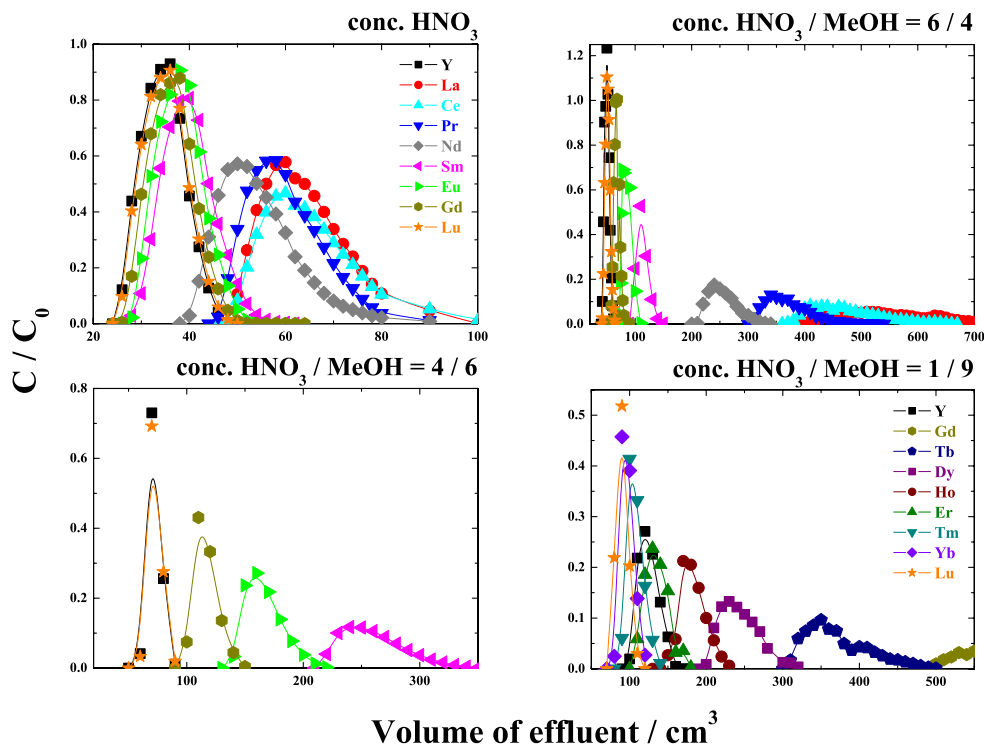
Figure 3-3.   Elution chromatograms of Y and Ln(III) by tertiary pyridine resin in different conc. HNO_3 / MeOH mixed solutions at 298 K. (Flow rate: 100 cm^3/h, Resin column: 1 cm-$\phi \times$ 50 cm, C: concentration in effluent, C_0: concentration in feed solution)

As the volume fraction of MeOH (X_{MeOH}) increased, the retention volume of each element increased. Interestingly, the increasing tendency of retention volume for lighter Ln(III) (La-Nd) is far larger than that for heavier Ln(III) (Sm-Lu), enabling a complete separation between the lighter Ln(III) and the heavier ones when X_{MeOH} is 20% and over. Besides, an individual separation of the heavier Ln(III) was also obtained when X_{MeOH} is over 60%, although the separation of the lighter Ln(III) seems to be difficult because they are adsorbed in the resin too strongly in this solution system to get sharp elution curves. **Fig. 3-4** illustrates the variations of K_d and α as a function of X_{MeOH}. The K_d exhibit exponential increases with the increase of X_{MeOH} and this increasing tendency becomes smaller as the atomic number decreases. The α also increase with increasing X_{MeOH}.
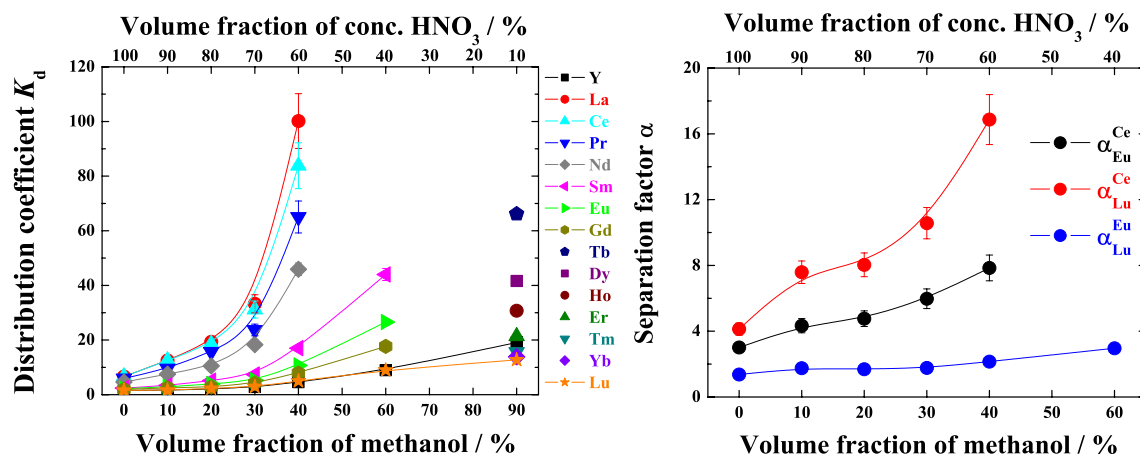
Figure 3-4. Variation of distribution coefficients of Y and Ln(III) and their separation factors by tertiary pyridine resin in conc. HNO_3 / MeOH mixed solutions at 298 K. (Flow rate: 100 cm^3/h, Resin column: 1 cm-$\phi \times$ 50 cm)

Practical separation processes require as a mild solvent condition as possible, that is, lower acid concentration is desired. Thus, the [HNO_3] dependence of the chromatographic behavior was investigated. In order to obtain enough large K_d and α values for a comparative study, methanol was added in the solution with 30 vol%. The chromatograms in different [HNO_3] solutions are given in **Fig. 3-5** and Appendix III, **Fig. III-2**. Contrary to the expectation, the retention volume showed no monotonous decrease and the maximum retention volume obtained at 6~7 mol-HNO_3/dm^3-mixed solvent in the present methanolic solution, although the elution curves began to overlap when [HNO_3] was below 2 mol-HNO_3/dm^3-mixed solvent.
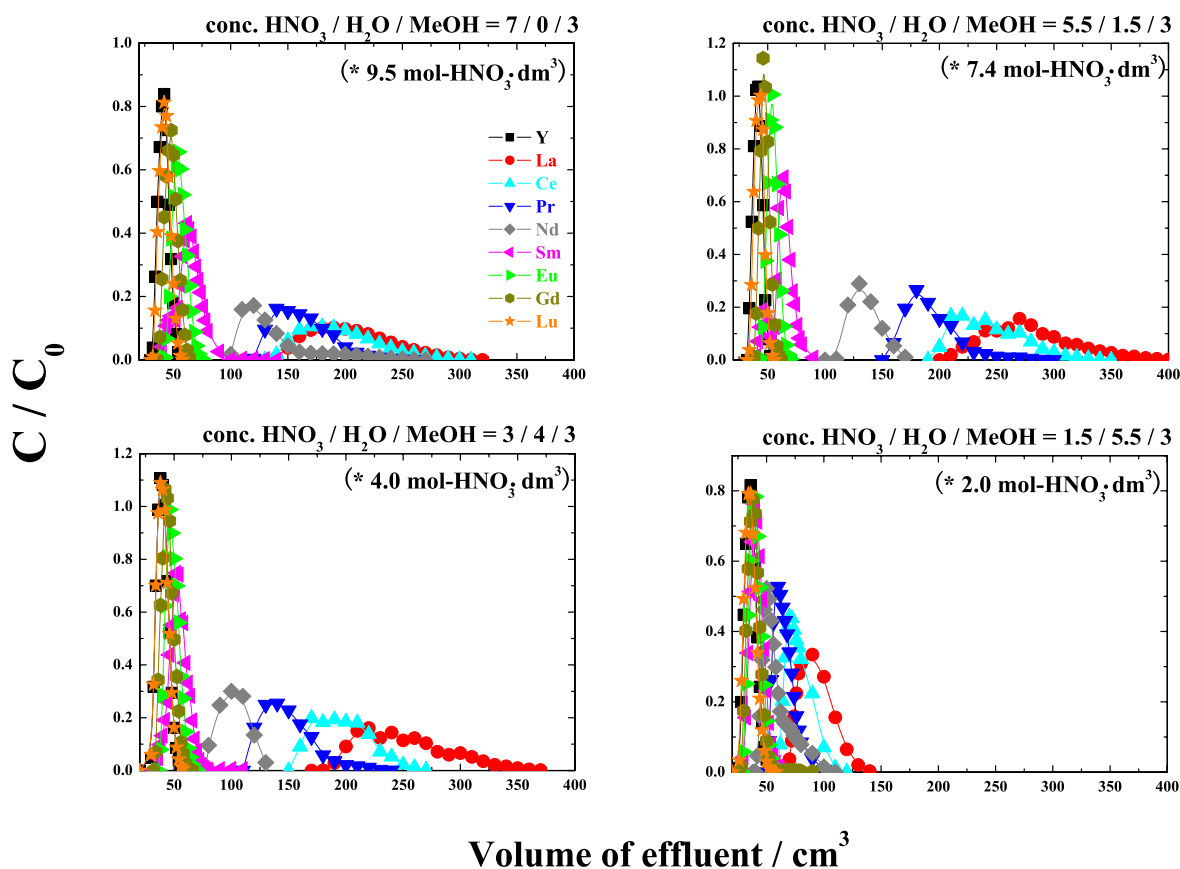
Figure 3-5. Elution chromatograms of Y and Ln(III) by tertiary pyridine resin in different methanolic HNO_3 solutions at 298 K. (Flow rate: 100 cm^3/h, Resin column: 1 cm-ϕ $\times$ 50 cm, Solvent: 30 vol%-MeOH)

The calculated K_d and α from the chromatograms are plotted in **Fig. 3-6**. As corresponding to the retention volume, the K_d exhibit a convex variation with the decrease of [HNO_3] and they become maximum at around 6~8 mol-HNO_3/dm^3, being analogous to the anion exchange behavior of Y and Ln(III) by a strongly basic anion exchange resin in HNO_3 medium [4]. The α shows the similar convex variation, while the maximum values are obtained at around 4 mol-HNO_3/dm^3. The K_d and α decrease drastically when [HNO_3] is under 4 mol-HNO_3/dm^3. These results indicate that conc. HNO_3 is not necessary and 4~6 mol-HNO_3/dm^3 is enough for achieving the best separability in the HNO_3 solution system.
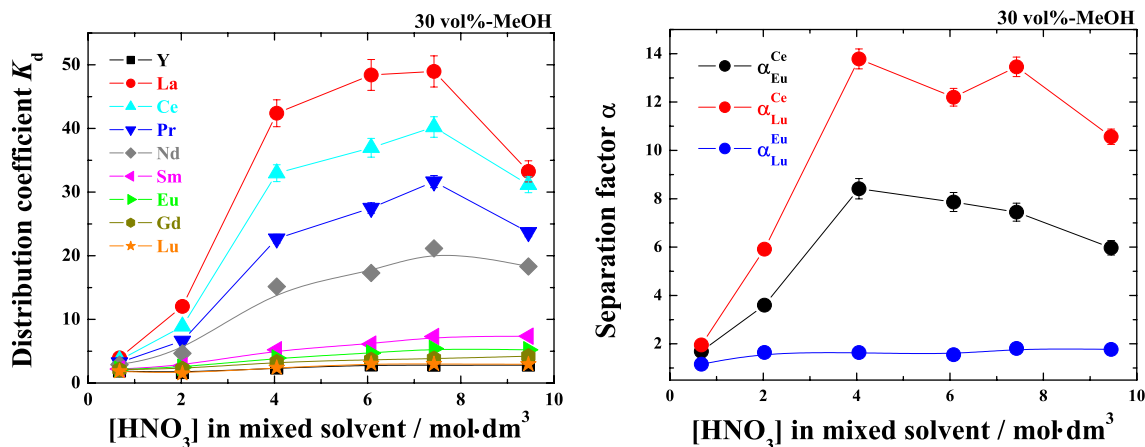
Figure 3-6. [HNO$_3$] dependence of distribution coefficients of Y and Ln(III) and their separation factors by tertiary pyridine resin in methanolic HNO$_3$ solutions at 298 K. (Flow rate: 100 cm^3/h, Resin column: 1 cm-$\phi \times$ 50 cm, Solvent: 30 vol%-MeOH)

In the conc. HNO$_3$ / alcohol mixed solution system as given in **Figs. 3-3** and **3-4**, both [HNO$_3$] and X_{MeOH} are changed at the same time with a variation of their mixing ratio and it is not appropriate for investigating the X_{MeOH} dependence of the chromatographic behavior. Hence, other chromatography experiments were carried out in various mixing ratios of water / MeOH mixed solutions with a constant [HNO$_3$] (4.05 mol/dm^3). **Fig. 3-7** and Appendix III, **Fig. III-3** show the obtained chromatograms. It is clear that the adsorption of each element becomes stronger with an increase of X_{MeOH} and the elution curves are clearly divided into two groups (lighter Ln (La-Nd) and heavier ones (Gd-Lu)) in higher X_{MeOH} solutions. The variation of K_d and α are given in **Fig. 3-8**. Both the K_d and α show exponentially increasing tendency with the increase of X_{MeOH}. This increasing tendency is also similar to the anion exchange behavior by a strongly basic anion exchange resin [5].
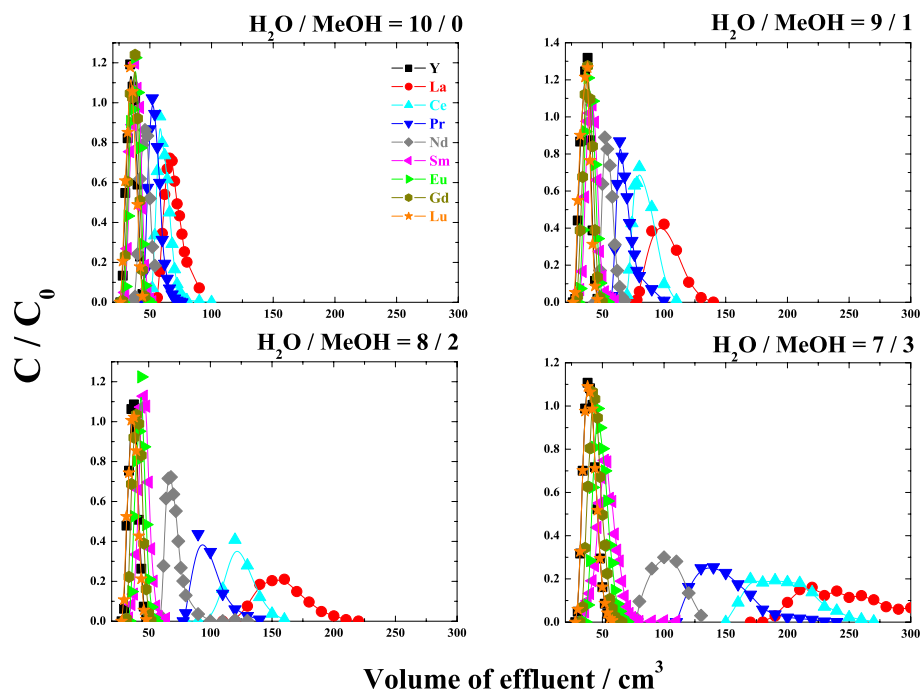
Figure 3-7. Elution chromatograms of Y and Ln(III) by tertiary pyridine resin in different methanolic HNO_3 solutions at 298 K. (Flow rate: 100 cm^3/h, Resin column: 1 cm-ϕ × 50 cm, Solvent: [HNO_3] = 4.05 mol/dm^3)

It has been found in the previous experiments using HCl solutions that the adsorbability and separability of the tertiary pyridine resin are influenced by the type of alcohol added in solvent. In order to confirm the effect of alcohol type in the present HNO_3 solution system, the chromatographic behavior in different alcoholic HNO_3 solutions were investigated by using three monohydric normal-chain alcohols (methanol, ethanol, and 1-propanol). The observed chromatograms are given in **Fig. III-4** in Appendix III and the comparison of K_d and α are illustrated in **Fig. 3-9**. Among the tested three alcohols, ethanol displayed the largest enhancing effect on K_d, corresponding to the results in the HCl solution system and the anion exchange system using alcoholic nitric acid solutions [6]. On the other hand, no considerable change was observed in the α. It seems that the type of alcohol has a less influence on the separability in the HNO_3 solutions system, although ethanol brings a slight improvement on the separation between lighter Ln (La-Nd) compared with methanol
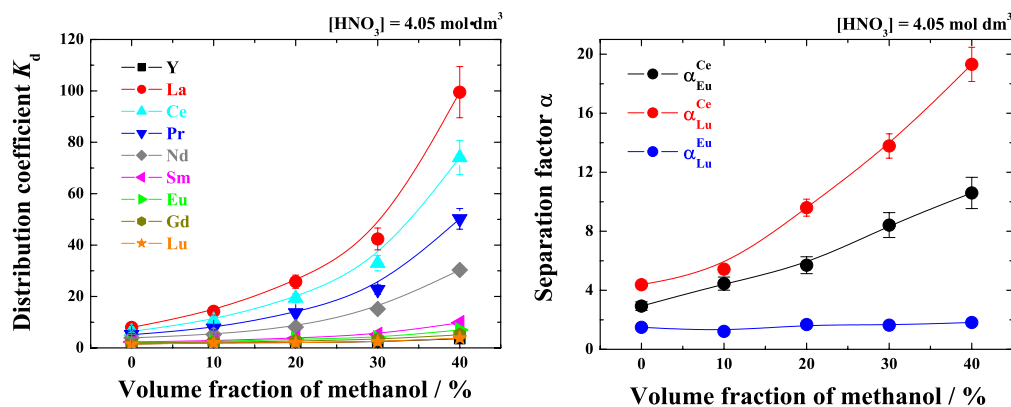
Figure 3-8. X_{MeOH} **dependence of distribution coefficients of Y and Ln(III) and their separation factors by tertiary pyridine resin in methanolic HNO$_3$ solutions at 298 K. (Flow rate: 100 cm^3/h, Resin column: 1 cm-$\phi \times$ 50 cm, Solvent: [HNO$_3$] = 4.05 mol/dm^3)**
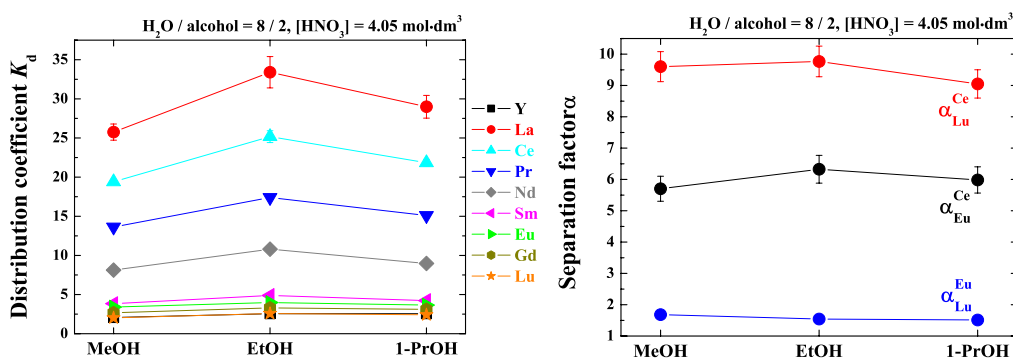

Figure 3-9. Variation of distribution coefficients of Y and Ln(III) and their separation factors by tertiary pyridine resin in different alcoholic HNO$_3$ solutions at 298 K. (Flow rate: 100 cm^3/h, Resin column: 1 cm-$\phi \times$ 50 cm, Solvent: conc. HNO$_3$ / alcohol = 8 / 2 (vol/vol))

(Appendix III, **Fig. III-4**).

From the results mentioned above, it can be concluded that the HNO_3 solution system has higher potential for the individual (*i.e.* intragroup) separation of Ln(III) than the HCl solution system.

Solvent effect II. LiNO$_3$-Alcohol In order to investigate the chromatographic behavior in a non-acidic nitrate solution system, aqueous $LiNO_3$ solutions were employed in this study. **Fig. 3-10** shows a chromatogram of Y and Ln(III) in an aqueous $LiNO_3$ solution ($[LiNO_3]$ = 4.0 mol/dm^3). The obtained chromatogram was similar to that obtained in the HNO_3 solution system and the elements were eluted in the reverse order of atomic number. However, the retention volume (=K_d) of each element was far larger than that in the corresponding HNO_3 solution (*i.e.* $[HNO_3]$ = 4.05 mol/dm^3). In fact, the K_d of Nd in the $LiNO_3$ solution was three times larger than that in the HNO_3 solution (K_d(Nd) in the $LiNO_3$ solution: 11.57, that in the HNO_3 solution: 3.90, Appendix III, **Tables III-3** and **5**).
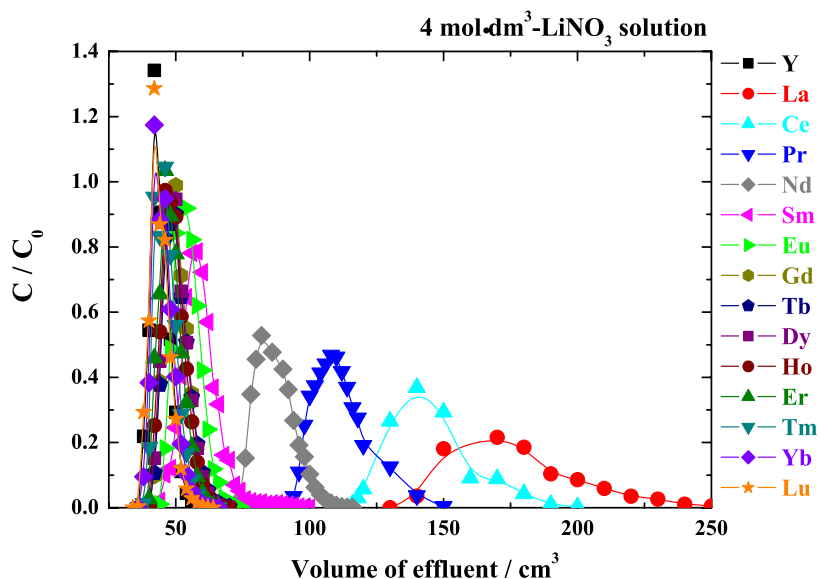

Figure 3-10. Elution chromatogram of Y and Ln(III) by tertiary pyridine resin in an aqueous $LiNO_3$ solution at 298 K. (Flow rate: 100 cm^3/h, Resin column: 1 cm-$\phi \times$ 50 cm, Solvent: $[LiNO_3]$ = 4.0 mol/dm^3)

The experiment was also carried out in a methanolic LiNO$_3$ solution (see Appendix III, **Fig. III-5**). **Fig. 3-11** shows the comparison of K_d between aqueous and methanolic LiNO$_3$ solutions. The K_d increased with an increase of X_{MeOH} in solvent. Furthermore, this increasing tendency became larger as a decrease in atomic number, bringing a clear individual separation for lighter Ln (La-Nd), as shown in the lower graph of **Fig. III-5**, Appendix III. These results suggest that non-acidic nitrate solution is also useful for the individual separation of Ln(III).
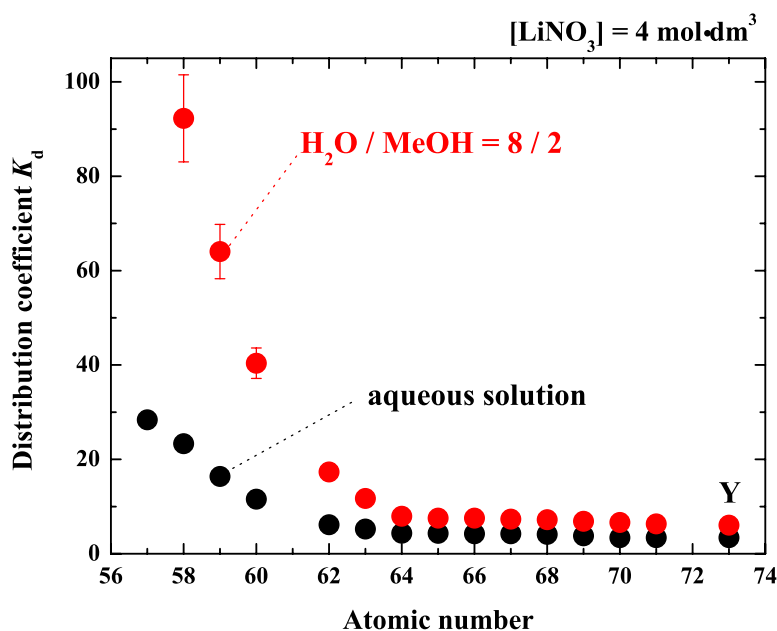
Figure 3-11. Variation of distribution coefficients of Y and Ln(III) by tertiary pyridine resin in methanolic LiNO$_3$ solutions at 298 K. (Flow rate: 100 cm^3/h, Resin column: 1 cm-$\phi \times$ 50 cm, Solvent: [LiNO$_3$] = 4.0 mol/dm^3)

Anion Exchange Behavior The tertiary pyridine resin is expected to work both as a coordinative extractant and as an anion exchanger. In order to compare the adsorption and separation properties of the pyridine resin with those of anion exchange resins, another experiment was performed using a strongly basic anion exchange resin (Dowex 1X8). **Fig. 3-12** shows a chromatogram of Y and Ln(III) by

73

Dowex 1X8 in a methanolic HNO$_3$ solution ([HNO$_3$] = 4.05 mol/dm^3, X_{MeOH} = 20%).

Figure 3-12. Elution chromatogram of Y and Ln(III) by strongly basic anion exchange resin Dowex 1X8 in a conc. HNO$_3$ / MeOH mixed solution at 298 K. (Flow rate: 100 cm^3/h, Resin column: 1 cm-ϕ × 50 cm, Solvent: conc. HNO$_3$ / MeOH = 8 / 2 (vol/vol))
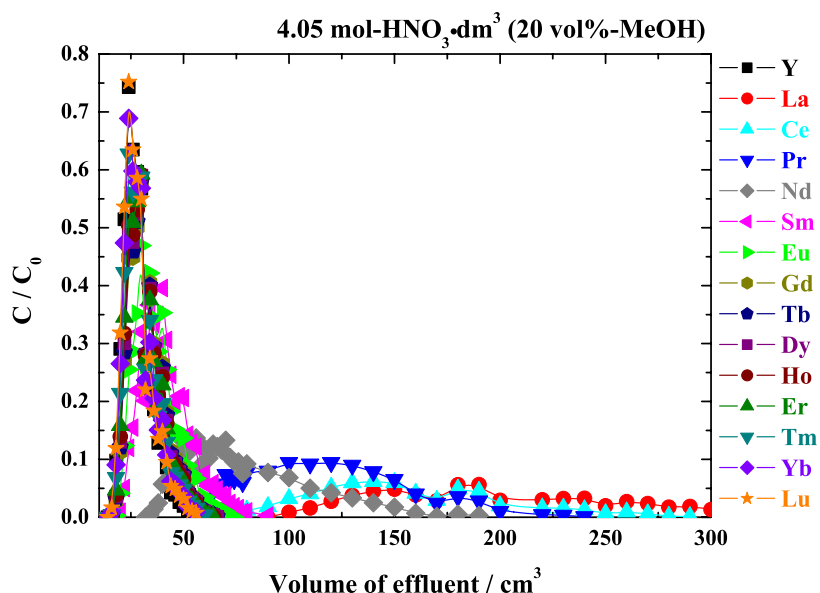
The tested anion exchange resin exhibited stronger adsorption for lighter Ln (La-Nd) than the pyridine resin although its smaller ion exchange capacity (Dowex 1X8: 1.2 meq/cm^3, Si-based pyridine resin: N$_{Py}$ = ~2.2 mmol/dm^3). As a result, their elution curves became so broad that it is difficult to calculate K_d from the chromatogram. From this result, Y and Ln(III) (especially the lighter Ln) are expected to form some anionic complexes with nitrate ions (NO$_3^-$) to adsorb in the anion exchange resin. This is consistent with the reported results [4, 5]. Considering the fact that the chromatographic behavior of Y and Ln(III) by the pyridine resin is analogous to that by the anion exchanger, the pyridine resin appears to behave as an anion exchanger in the nitric acid solution system. However, the pyridine resin also exhibited stronger adsorption in non-acidic solution of LiNO$_3$ solution, in which almost no pyridine groups are protonated. Consequently, there is still two possibility left on the adsorption mechanism by tertiary pyridine resin. Further discussion will be held

in chapter 5.

Temperature dependence   The effect of temperature on the chromatographic behavior was investigated in a methanolic HNO_3 solution ($[HNO_3]$ = 4.05 mol/dm^3, X_{MeOH} = 20%). **Fig. 3-13** gives the variations of K_d and α as a function of temperature. (The obtained chromatograms are shown in Appendix III, **Fig. III- 6**.) Both K_d and α decreased exponentially with a decrease in temperature. It should be noted that the K_d of lighter Ln (La-Nd) became $1/2\sim1/3$ as the temperature increased from 278 to 323 K (Appendix III, **Table III-6**). This drastic change of K_d in temperature can be used for controlling the elution behavior of these elements.

Figure 3-13. Temperature dependence of distribution coefficients of Y and Ln(III) and their separation factors by tertiary pyridine resin in a methanolic HNO_3 solution. (Flow rate: 100 cm^3/h, Resin column: 1 cm-ϕ $\times$ 50 cm, Solvent: $[HNO_3]$ = 4.05 mol/dm^3, X_{MeOH} = 20%)

Flow rate dependence   The flow rate is one of the important operating conditions to consider because the treatment capacity of practical separation process is determined by the flow rate. In order to confirm the flow rate dependence of the

present separation system, other chromatography experiments were carried out in a methanolic HNO_3 solution ($[HNO_3]$ = 4.05 mol/dm^3, X_{MeOH} = 20%) at 293 K with different flow rates. The obtained chromatograms are given in Appendix III, **Fig. III-7** and the K_d and α calculated from the chromatograms are plotted in **Fig. 3-15**. The K_d showed no considerable change as increasing temperature, while α changed slightly. The flow rate seems to have almost no influence on the adsorbability and separability of the tertiary pyridine resin in the present HNO_3 solution system (at least up to 380 cm/h-linear flow rate).
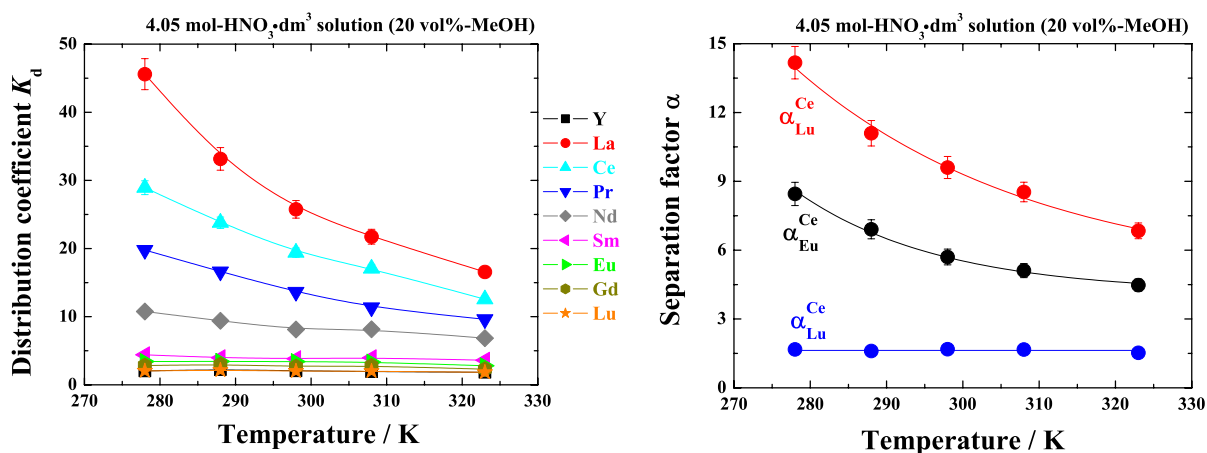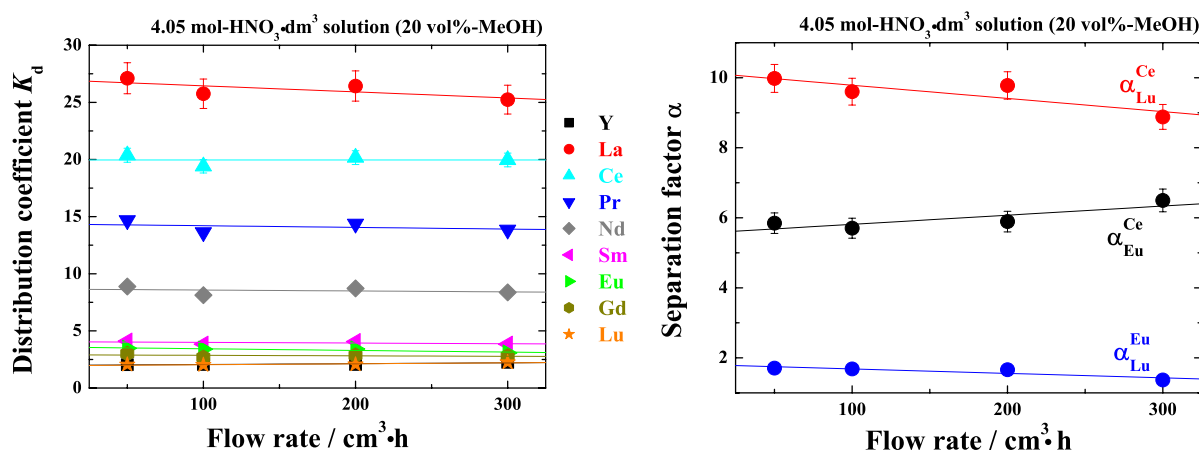

Figure 3-14. Flow rate dependence of distribution coefficients of Y and Ln(III) and their separation factors by tertiary pyridine resin in a methanolic HNO_3 / solution at 298 K. (Resin column: 1 cm-ϕ × 50 cm, Solvent: $[HNO_3]$ = 4.05 mol/dm^3, X_{MeOH} = 20%)

Individual (intragroup) separation of Ln(III) The above-mentioned investigations have revealed that the present nitrate solution system with the tertiary pyridine resin has a great potential for the individual separation of Ln(III). That is, these elements can be separated chromatographically by changing the composition of solvent (*i.e.* the mixing ratio of HNO_3, H_2O, and alcohol). Hence, the chromato-

graphic separation of Y and Ln(III) was performed by optimizing the solvent compositions during the operation. The result is given in **Fig. 3-15**.
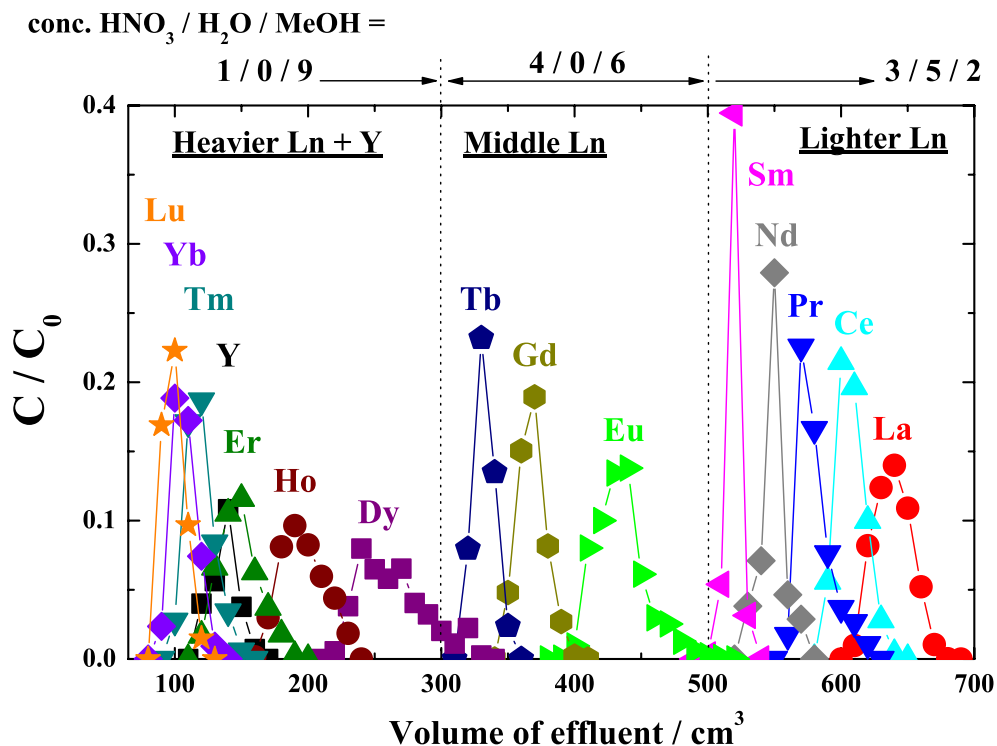
Figure 3-15. Chromatographic separation of Y and Ln(III) by tertiary pyridine resin in methanolic HNO_3 solutions at 298 K. (Flow rate: 100 cm^3/h, Resin column: 1 cm-$\phi \times$ 50 cm)

First, the heavier Ln (Dy-Lu) and Y were eluted by a methanolic HNO_3 solution with high X_{MeOH} (conc. HNO_3 / MeOH = 1 / 9) and, subsequently, the middle Ln (Eu-Tb) were eluted in sequence by a methanolic HNO_3 solution with relatively high [HNO_3] (conc. HNO_3 / MeOH = 4 / 6). Lastly, the lighter Ln (La-Sm) were eluted by a moderate methanolic HNO_3 solution (conc. HNO_3 / H_2O / MeOH = 3 / 5 / 2). As a result, a rough individual separation of Ln(III) was accomplished by this simple and easy separation system. This result also means that the present separation system using alcoholic HNO_3 solutions has sufficient potential for the individual separation of An(III)

3.3.2   Chromatographic Behavior of An(III) and Ln(III) by Tertiary Pyridine Resin in Nitrate Solution System

The preliminary experiments using stable Ln have revealed that the nitrate solution system is very effective for the individual separation of Ln(III). In order to investigate the applicability of this solution system to the separation of An(III) and Ln(III) mixture, further chromatography experiments were carried out using An(III) and Ln(III). The experiments were performed at room temperature ($\cong 293$ K) with a constant flow rate of 100 cm^3/h.

Solvent effect I. conc. HNO$_3$ / MeOH system   At first, chromatographic behavior of An(III) and Ln(III) in the nitrate solution system was investigated in conc. HNO$_3$ solution (*i.e.* 13.5 mol-HNO$_3$/dm^3). The obtained chromatogram is shown in the upper left graph of **Fig. 3-16**. All the nuclides in the introduced sample were eluted within 50 cm^3 of effluent volume, meaning that the adsorbability (K_d) of the tertiary pyridine resin for An(III) and Ln(III) was very small in conc. HNO$_3$ solution. Besides, it should be noted that the elution of An(III) (Am and Cm) occurred before the elution of Ln(III) (Ce and Nd).

Then, methanol was added in the solvent to examine its effect on the adsorbability and separability. As shown in **Fig. 3-16**, the retention volume of each nuclide increased and the elution curves were clearly separated with a increase of X_{MeOH}, corresponding to the results of the previous experiments using stable Ln (**Fig. 3-3**). It was also found that the An(III) of Am, Cm, and Cf were eluted between Nd and Tb. This means that the HNO$_3$ solution system is not appropriate for the intergroup separation of An(III) and Ln(III).

There was a trouble with the determination of Cm and Cf species in the experiment using "conc. HNO$_3$ / MeOH = 4 / 6" solvent: at first, we intended to observe the elution behavior of Cf by using the α-peak of ^{249}Cf (E_α = 5.81 MeV) and ^{252}Cf was regarded as a sort of impurity. However, unfortunately, the amount of ^{249}Cf in the sample was too small to identify its α-peak. Accordingly, we tried to follow the elution behavior of Cf by ^{252}Cf. Although the amount of ^{252}Cf seemed to be enough large to identify, the α-peaks of ^{252}Cf (E_α = 6.12 MeV) were detected so closely to those of ^{242}Cm (E_α = 6.11 MeV) that it was difficult to distinguish them individually.
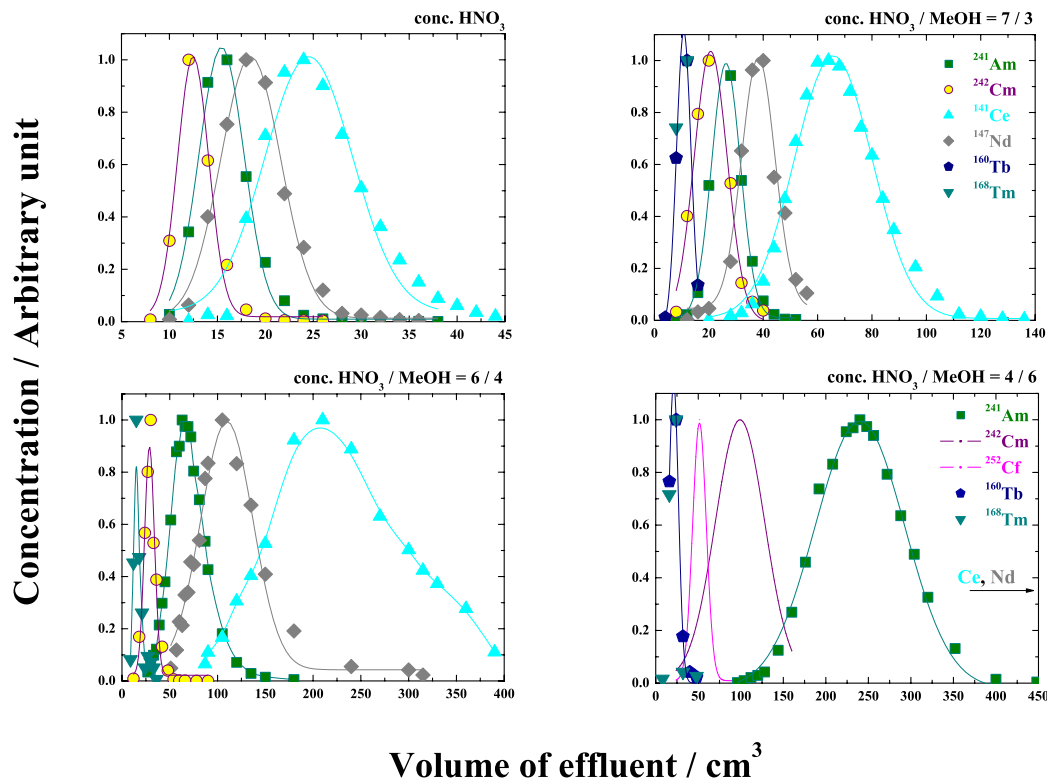
Figure 3-16. Elution chromatograms of An(III) and Ln(III) by tertiary pyridine resin in conc. HNO_3 / MeOH mixed solutions at 293 K. (Flow rate: 100 cm^3/h, Resin column: 1 cm-ϕ × 10 cm)

Hence, the elution curves of Cm and Cf were first drawn together by using the gross of their α-peaks, as shown in the upper graph of **Fig. IV-8**, Appendix IV. This lump elution curve of Cm and Cf had two peaks at 50 cm^3 and 100 cm^3 of effluent volume. These two peaks probably attribute to the individual elution of Cm and Cf. In order to identify these two peaks, γ-ray spectra were measured for the fraction samples around these peaks. As a result, a sharp peak was observed in the fractions of the first elution peak at 40-45 keV, attributing to the γ emission of ^{252}Cf (E_γ = 43.4 keV), while no considerable peak was observed in the spectra of the fractions around the second elution peak. Furthermore, a slight peak of ^{249}Cf was also observed at 385-390 keV (E_γ = 387.95 keV) in the fractions of the first elution peak (Appendix III, **Fig. III-9**). Hence, we concluded that the first peak of the lump elution curve attributed

to Cf and the second one ascribed to Cm. As a matter of fact, the shape of the first elution peak is in good agreement with the elution curve drawn from the γ-peaks of ^{252}Cf, as shown in **Fig. III-8**, Appendix III. The lower graph in the **Fig. III-8** and shows the result of peak-separation for the overlapped elution curves of Cm and Cf by two-peaks Gaussian fitting.

Figure 3-17 shows the calculated K_d of Am and Cm, along with their α. The K_d drastically increased when X_{MeOH} was over 30%. Besides, this drastic increase in K_d involved an increase of the α. In fact, the α became double when X_{MeOH} was over 30%. This suggests that the HNO_3 solution system still has the potential for the individual separation of An(III) in addition to that of Ln(III), although the inter-group separation of An(III) and Ln(III) is difficult in this solution system. Thus, the experiments mentioned hereafter focus on the individual separation of An(III).

Figure 3-17. Variation of distribution coefficients of Am and Cm and their separation factors by tertiary pyridine resin in conc. HNO_3 / MeOH mixed solutions at 293 K. The error bars are smaller than the plotted points. (Flow rate: 100 cm^3/h, Resin column: 1 cm-$\phi \times$ 10 cm)

Solvent effect II. [HNO$_3$] dependence   In the preliminary experiments using stable Ln, it has been found that the adsorbability and separability of the tertiary pyridine resin for Ln(III) exhibits the irregular variation for the variation of [HNO$_3$] in solvent. In order to determine the appropriate [HNO$_3$] for an efficient separation of An(III), the [HNO$_3$] dependence of the chromatographic behavior of An(III) was investigated. The X_{MeOH} was fixed at 60% to obtain enough large K_d and α values for comparison. The chromatograms are given in Appendix III, **Fig. III**-**10** and the calculated K_d and α are plotted in **Fig. 3**-**18**. The K_d of Am and Cm showed a convex change with a variation of [HNO$_3$] and they became maximum at around 4.0 mol-HNO^3/dm^3 in the present X_{MeOH}. On the other hand, their α showed an irregular variation and the maximum value was obtained at around 3.5 mol-HNO^3/dm^3. It seems that the separability of the tertiary pyridine resin is very sensitive to the concentration of HNO$_3$ and, consequently, a detailed investigation is required to optimize [HNO$_3$] for the most efficient separation. In any case, conc. HNO$_3$ solution is not necessary for the efficient individual separations of An(III) and Ln(III).

Figure 3-18. [HNO$_3$] dependence of distribution coefficients of Am and Cm and their separation factors by tertiary pyridine resin in methanolic HNO$_3$ solutions at 293 K. (Flow rate: 100 cm^3/h, Resin column: 1 cm-ϕ × 10 cm, Solvent: X_{MeOH} = 60%)

Individual (intergroup) separation of An(III)   Further chromatography experiments were carried out using a various compositions of methanolic HNO_3 solutions to optimize the solvent composition for the efficient separation of An(III) (Am and Cm). From the results mentioned above, the α between Am and Cm is expected to become maximum when we employ 6~10 mol/dm^3 of HNO_3 solution with alcohol. Hence, the experiments were performed by mixing an 8 $mol \cdot dm^3$-HNO_3 solution with methanol. **Fig. III-11** in Appendix III shows the chromatograms of Am and Cm in different 8 $mol \cdot dm^3$-HNO_3 / MeOH mixtures and the calculated K_d and α are given in **Fig. 3-19**. The K_d increased exponentially as increasing X_{MeOH}. In addition, the α also increased with the increase in X_{MeOH}. In consequence, Am were completely separated from Cm in "8 $mol \cdot dm^3$-HNO_3 / MeOH = 4 / 6" solvent, as shown in **Fig. 3-20**. It was also found in another experiment that a clear separation of Am and Cm was possible by using the methanolic HNO_3 solution with high X_{MeOH} (~90%), as shown in **Fig. 3-21**. From these results, it can be concluded that the alcoholic HNO_3 solution is a powerful solvent for the individual separation of An(III) and Ln(III), although it is not appropriate for the intergroup separation of An(III) and Ln(III).
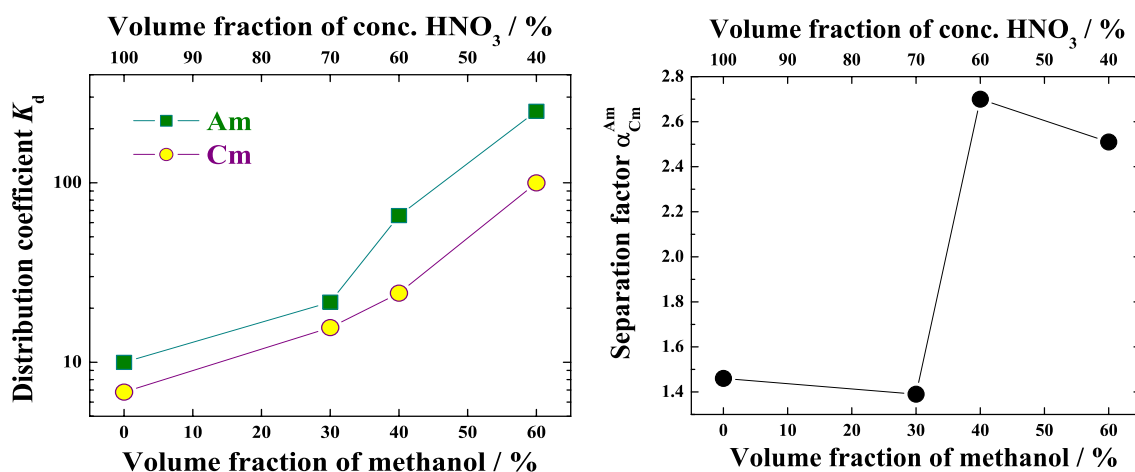

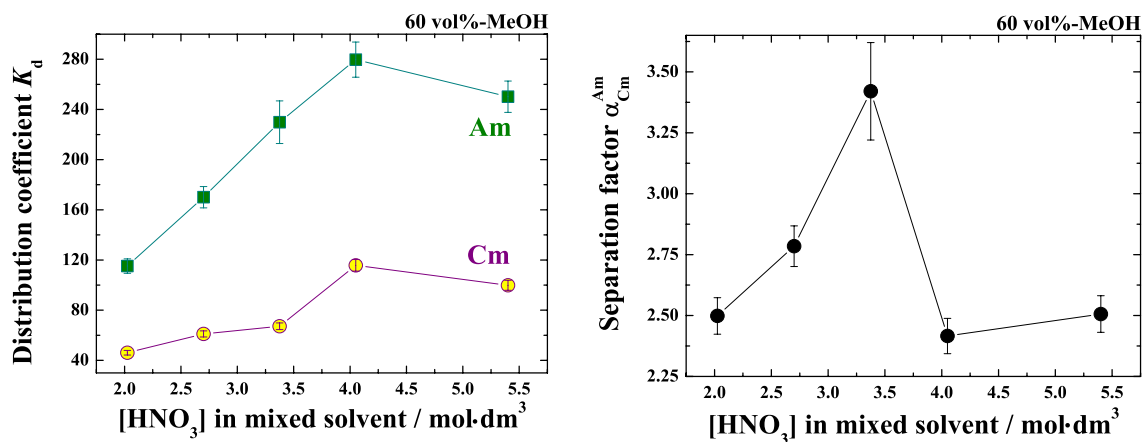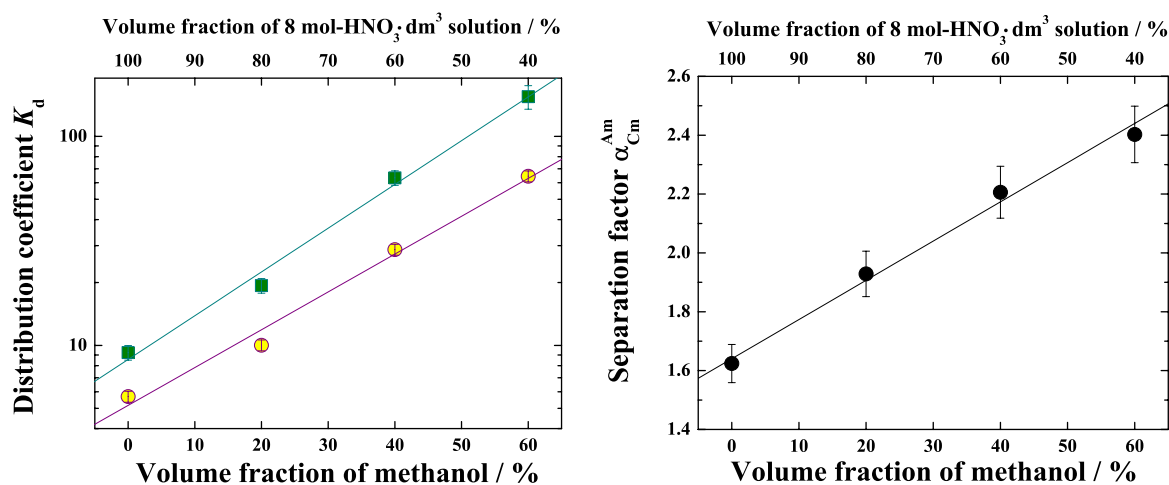
Figure 3-19. Variation of distribution coefficients of Am and Cm and their separation factors by tertiary pyridine resin in 8.0 $mol \cdot dm^3$-HNO_3 / MeOH mixed solutions at 293 K. (Flow rate: 100 cm^3/h, Resin column: 1 cm-ϕ × 10 cm)
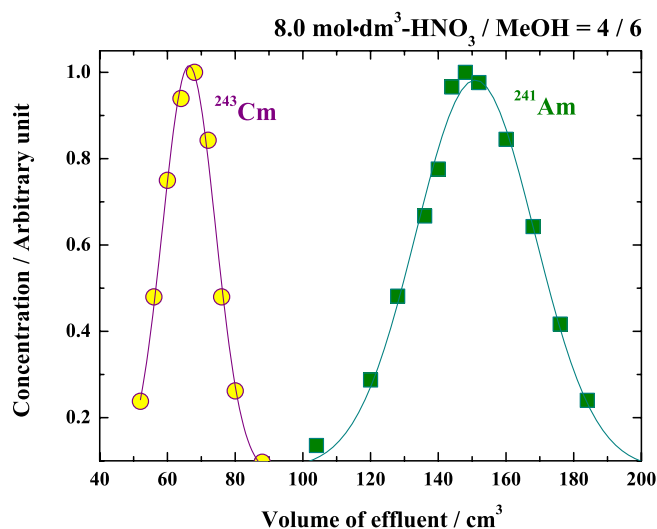
Figure 3-20. Elution chromatogram of Am and Cm by tertiary pyridine resin in a methanolic HNO_3 solution at 293 K. (Flow rate: 100 cm^3/h, Resin column: 1 cm-ϕ $\times$ 10 cm, Solvent: 8.0 mol·dm^3-HNO_3 / MeOH = 4 / 6 (vol/vol), [HNO_3] = 3.2 mol/dm^3)
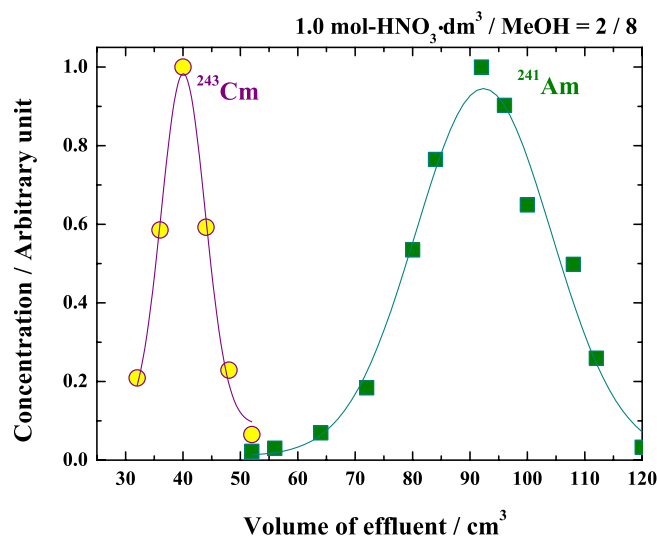
Figure 3-21. Elution chromatogram of Am and Cm by tertiary pyridine resin in a methanolic HNO_3 solution at 293 K. (Flow rate: 100 cm^3/h, Resin column: 1 cm-ϕ $\times$ 10 cm, Solvent: 1.0 mol·dm^3-HNO_3 / MeOH = 2 / 8 (vol/vol), [HNO_3] = 0.2 mol/dm^3)

Chromatographic behavior of An(III) by quaternary pyridinium resin

It has been found in the preliminary experiments using stable Ln that the chromato-graphic behavior of Ln(III) by the tertiary pyridine resin is similar to that by a typical anion exchange resin in HNO_3 solutions. In order to confirm the anion exchange behavior of An(III) in the HNO_3 solution, further experiments were carried out by employing a strongly anion exchange resin of quaternary pyridinium resin. **Fig. 3-22** gives the chromatograms of An(III) and Ln(III) mixture by the quaternary pyridinium resin in conc. HNO_3 / MeOH mixed solutions.
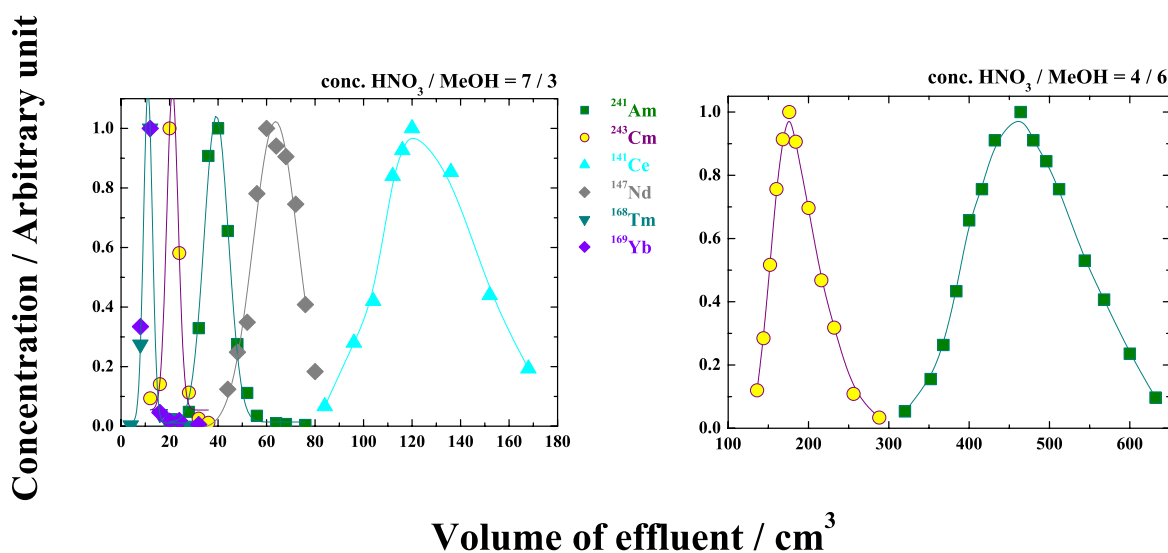
Figure 3-22. Elution chromatograms of An(III) and Ln(III) by quaternary pyridinium resin in conc. HNO_3 / MeOH mixed solutions at 293 K. (Flow rate: 100 cm^3/h, Resin column: 1 cm-$\phi \times$ 10 cm)

The obtained chromatograms were quite similar to those by the tertiary pyridine resin: Am and Cm were eluted before the elution Nd and, furthermore, a clear separation between Am and Cm was observed in "conc. HNO_3 / MeOH = 4 / 6" solvent. On the other hand, the calculated K_d and α (Appendix III, **Table III-12**) indicate that the adsorbability and separability of the quaternary pyridinium resin is larger than those of the tertiary one. The quaternary pyridinium resin is a strongly basic anion exchange resin, while the tertiary pyridine resin can work both as a weakly basic anion exchanger and as a coordinative extractant. If the tertiary pyridine resin

works as a coordinative extractant in the present HNO_3 solution, its adsorptivity and separability should be different from those of anion exchange resins. Therefore, the tertiary pyridine resin appears to behave as an anion exchanger in the HNO_3 solution. However, the tertiary pyridine resin has also exhibited strong adsorbability in a non-acidic solution of $LiNO_3$ solution. It seems difficult to elucidate the adsorption mechanism of tertiary pyridine resin only from its adsorption and separation properties. Further detailed discussion is postponed to chapter 5.

Adsorptivity of tertiary pyridine resin for An(III) and Ln(III)   **Figure 3-23** gives a summary of the adsorptivity of the tertiary pyridine resin for An(III) and Ln(III) in the HNO_3 solution medium. The K_d of An(III) and Ln(III) simply depend on their ionic radii and they decrease as a decrease of their ionic radii. The difference of K_d between neighboring elements is so large especially for lighter Ln and Am/Cm that clear individual separations are possible between Am and Cm, and between Nd and Sm in the present HNO_3 solution system.
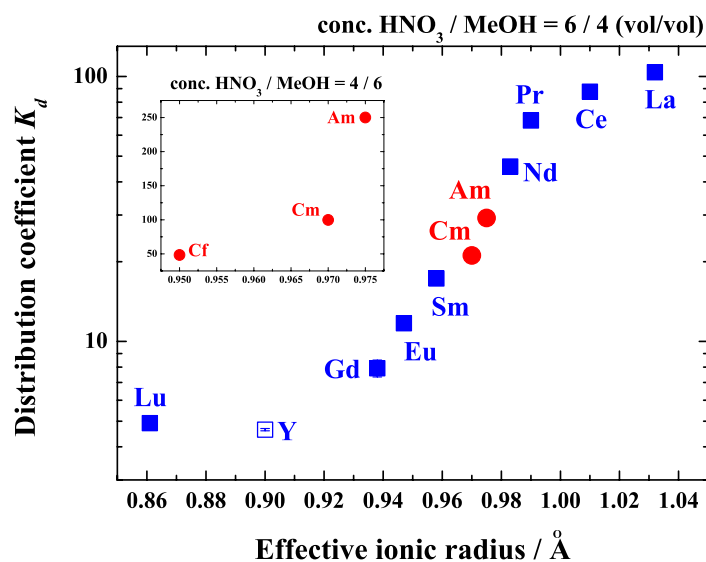
Figure 3-23. Variation of distribution coefficients of An(III), Ln(III), and Y in conc. HNO_3 / MeOH mixed solutions as a function of their ionic radii. The error bars are smaller than the plotted points. (Ionic radii: refer to [46])

3.4 Summary

The chromatographic behavior of An(III), Ln(III), and Y by a tertiary pyridine resin was examined in various nitrate solutions. The adsorbability (= K_d) of these elements depends on [HNO$_3$], X_{alcohol}, and the type of alcohol added in solvent. The K_d showed an irregular change with the variation of [HNO$_3$] and they became maximum when $6{\sim}10$ mol/dm^3-HNO$_3$ solutions were mixed with alcohol. On the other hand, they increased exponentially as increasing X_{alcohol} and ethanol was the most effective alcohol to enhance the adsorbability of the pyridine resin. A non-acidic nitrate solution of LiNO$_3$ solution also gave strong adsorption of Y and Ln(III) and the obtained K_d were larger than those in the corresponding HNO$_3$ solution. The adsorbability of the pyridine resin in the HNO$_3$ solution was governed by temperature, while the flow rate had no effect on the adsorbability.

In HNO$_3$ solutions, An(III) and Ln(III) were eluted from the tertiary pyridine resin column in the reverse order of their ionic radii and no intergroup separation between An(III) and Ln(III) was observed. However, the individual separations of An(III) and several Ln(III) were achieved by using the optimized alcoholic HNO$_3$ solutions. The separation behavior of Y and Ln(III) in LiNO$_3$ solution was similar to that in the HNO$_3$ solution.

A comparative study using anion exchange resins (Dowex 1X8 and quaternary pyridinium resin) has indicated that the chromatographic behavior of An(III), Ln(III), and Y by the tertiary pyridine resin is quite similar to that by the anion exchange resin in the HNO$_3$ solution system. A sufficient individual separation between Am and Cm was also achieved by the quaternary pyridinium resin.

References

[1] S. Adar, R. K. Sjoblom, R. F. Barnes, P. R. Fields, E. K. Hulet, H. D. Wilson, *J. Inorg. Nucl. Chem.*, **25**, 447 (1963).

[2] W. Kraak, W. A. Van Der Heijden, ibid., **28**, 221 (1966).

[3] H. Hamaguchi, I. Hikawa, R. Kuroda, *J. Chromatog.*, **18**, 556 (1965).

[4] J. P. Faris, R. F. Buchanan, *Anal. Chem.*, **36**, 1157 (1964).

[5] J. P. Faris, J. W. Warton, ibid., **34**, 1077 (1962).

[6] R. A. Edge, *J. Chromatog.*, **8**, 419 (1962).

[7] W. H. Hale, J. T. Lowe, *Inorg. Nucl. Chem. Lett.*, **5**, 363 (1969).

[8] S. Usuda, N. Shinohara, H. Yoshikawa, *J. Radioanal. Nucl. Chem., Art.*, **109**, 353 (1987).

[9] S. Usuda, ibid., **111**, 399 (1987).

[10] S. Usuda, N. Shinohara, H. Yoshikawa, S. Ichikawa, T. Suzuki, ibid., **116**, 125 (1987).

[11] S. Usuda, H. Yoshikawa, M. Magara, Y. Hatsukawa, *J. Radioanal. Nucl. Chem., Lett.*, **117**, 329 (1987).

[12] S. Usuda, *J. Radioanal. Nucl. Chem., Art.*, **123**, 619 (1988).

[13] S. Usuda, N. Kohno, *Sep. Sci. Technol.*, **23**, 1119 (1988).

[14] T. Sato, *J. Radioanal. Nucl. Chem., Art.*, **139**, 79 (1990).

[15] J. Chen, Y. Zhu, R. Jiao, *Sep. Sci. Technol.*, **31**, 2723 (1996).

[16] Y. Zhu, J. Chen, R. Jiao, *Solv. Extr. Ion Exch.*, **14**, 61 (1996).

[17] E. P. Horwitz, A. C. Muscatello, D. G. Kalina, L. Kaplan, *Sep. Sci. Technol.*, **16**, 417 (1981).

[18] A. C. Muscatello, E. P. Horwitz, D. G. Kalina, L. Kaplan, ibid., **17**, 859 (1982).

[19] G. Persson, I. Svantesson , S. Wingefors, J. O. Liljenzin, ibid., **2**, 89 (1984).

[20] R. Jiao, S. Wang, S. Fan, B. Liu, Y. Zhu, H. Zheng, S. Zhou, S. Chen, *J. Nucl. Radiochem.*, **7**, 65 (1985).

[21] C. Song, J. Xu, Y. Zhu, ibid., **14**, 193 (1992).

[22] P. Y. Cordier, C. Hill, P. Baron, C. Madic, M. J. Hudson, J. O. Liljenzin, *J. Alloys Compd.*, **271**-**273**, 738 (1998)

[23] G. Modolo, R. Odoj, *Solv. Extr. Ion Exch.*, **17**, 33 (1999).

[24] Z. Kolarik, U. Müllich, F. Gassner, ibid., **17**, 1155 (1999).

[25] H. Schmieder, G. Petrich, *Radiochim. Acta*, **48**, 181 (1989).

[26] M. Ozawa, Y. Koma, K. Nomura, Y. Tanaka, *J. Alloys Compd.*, **271**-**273**, 538 (1998).

[27] G. R. Mahajan, D. R. Prabhu, V. K. Manchanda, L. P. Badheka, *Waste Managem.*, **18**, 125 (1998).

[28] E. P. Horwitz, R. Chiarizia, M. L. Dietz, H. Diamond, D. M. Nelson, *Anal. Chim. Acta*, **281**, 361 (1993).

[29] E. P. Horwitz, M. L. Dietz, R. Chiarizia, H. Diamond, S. L. Maxwell, III, M. R. Nelson, ibid., **310**, 63 (1995).

[30] Y. Wei, M. Kumagai, Y. Takashima, M. Asou, T. Namba, K. Suzuki, A. Maekawa, S. Ohe, *J. Nucl. Sci. Technol.*, **35**, 357 (1998).

[31] Y.-Z. Wei, M. Yamaguchi, M. Kumagai, Y. Takashima, T. Hoshikawa, F. Kawamura, *J. Alloys Compd.*, **271**-**273**, 693 (1998).

[32] Y.-Z. Wei, H. Hoshi, M. Kumagai, T. Asakura, Y. Morita, ibid.,**374**, 447 (2004).

[33] H. Hoshi, Y.-Z. Wei, M. Kumagai, T. Asakura, Y. Morita, ibid.,**374**, 451 (2004).

[34] T. Arai, Doctor Thesis, School of Materials Science and Engineering, Shibaura Institute of Technology, Tokyo (2002).

[35] J. A. C. Broekaert, F. Leis, K. Laqua, *Spectrochim. Acta*, **34B**, 73 (1979).

[36] K. Toyoda, H. Haraguchi, *Chem. Lett.,* 981 (1985).

[37]   ,   ,   , “   ”,   , 1982.

[38] J. Korkisch, I. Hazan, *Talanta*, **11**, 1157 (1964).

[39] R. J. Morrow, ibid., **13**, 1265 (1966).

[40] J. Korkisch, P. Antal, F. Hecht, *J. Inorg. Nucl. Chem.*, **14**, 247 (1960).

[41] P. Antal, J. Korkisch, F. Hecht, ibid., **14**, 251 (1960).

[42] J. Korkisch, F. Tera, ibid., **15**, 177 (1960).

[43] F. Tera, J. Korkisch, F. Hecht, ibid., **16**, 345 (1961).

[44] F. Tera, J. Korkisch, ibid., **20**, 335 (1961).

[45] J. Korkisch, G. E. Janauer, *Talanta*, **9**, 957 (1962).

[46] R. D. Shannon, *Acta Cryst.*, **A32**, 751 (1976).

[47] R. M. Nur, M. Nogami, Y. Fujii, T. Mitsugashira, *J. Nucl. Sci. Technol.*, **36**, 707 (1999).

4 Adsorption and Separation Behavior of Trivalent *f*-Elements in Chloride Solution System

4.1 Introduction

In addition to the nitrate solution system as mentioned in the previous chapter, chloride solutions, such as hydrochloric acid (HCl) or aqueous alkali chloride solution, are also frequently-used solvents for various chemical separation processes. Especially, this solution system has often been applied to ion exchange separations. The ion exchange processes using chloride solutions have been investigated for a long period [1] and several researchers have reported its applications to the separation of trivalent *f*-elements. Diamond and his co-workers employed hydrochloric acid with a cation exchange resin for the separation of trivalent *f*-elements and suggested the possibility their intra-group separations in this system [2,3]. Korkisch and Hazan investigated the anion exchange behavior of many elements including U, Th, and Ln(III) in various HCl-organic solvent mixed media [4]. Morrow demonstrated good inter- and intragroup separations of trivalent *f*-elements using an anion exchange resin with HCl-MeOH mixture [5]. Usuda and his co-workers investigated the cation and anion exchange behavior of An and FPs including trivalent *f*-elements in various HCl solutions in a series of their papers [6–10]. As compared with hydrochloric acid, there are few studies using aqueous alkali chloride solutions. The report by Hulet and his co-workers [11] seems to be the only example of the application of aqueous alkali chloride solutions to the separation of trivalent *f*-elements, showing a good intragroup separation between several An(III) in aqueous LiCl solution.

On the other hand, there are few reports on the extraction studies of trivalent *f*-elements in the chloride solution system because most of the studies have taken account of the compatibility with the present reprocessing process of PUREX process using nitric acid solutions. There is almost no available reports about the separation of trivalent *f*-elements by liquid-liquid extraction in chloride media, although several liquid-solid extraction studies using chloride solutions have given successful results

on the separation of An [12–15].

Although hydrochloric acid is very corrosive, it has several advantages for chemical separations; it is a nonoxidizing acid and, therefore, it does not cause so much chemical complexity such as disproportionation of chemical species. Furthermore, no nitration of organic compounds occurs in this solution system, restraining organic materials from the deterioration and eliminating the potential danger of the explosion caused by the nitration. On the other hand, aqueous alkali chloride solutions are not corrosive. Alkali chloride compounds have so high solubility for water that we can prepare high concentration of aqueous alkali chloride solutions (*e.g.* saturated molarities for aqueous LiCl, NaCl, and KCl solutions are 20.0, 6.1, and 4.8 mol/dm^3, respectively.). Therefore, we believe that the chloride solution system is still one of the suitable solvent system for chemical separations.

In this chapter, the adsorption and separation behavior of trivalent f-elements on the tertiary pyridine resin is investigated in various chloride solutions in order to confirm its applicability for the partitioning of An(III) and Ln(III) and determine appropriate solvent conditions for the practical separation process. The obtained results are compared with those of the nitrate solution system.

4.2   Experimental

4.2.1   Chromatography Experiments

Chemicals   Ln(III) and Y samples for chromatography experiments were prepared from their hydrated chloride compounds or their oxides (Ln$_2$O$_3$) supplied by Wako Pure Chemical Ind., Ltd. and Kanto Kagaku. Other chemicals and solvents were the same as those used in the batch experiments. The resin used for chromatography experiments was Si-based pyridine resin (Crosslinkage: 10 wt%, ratio of monomer oil to KIB: 0.9). In addition to the pyridine resin, several ion exchange resins were also employed in order to compare their adsorption and separation behavior for Ln(III) with those of pyridine resin. These ion exchange resins were supplied by The Dow Chemical Company, Mitsubishi Chemical Corporation and Asahi Kasei Corporation.

Apparatus and Procedure   The experimental apparatus and procedure for chromatography were the same as employed in the previous experiments using nitrate solutions. Prior to experiments, the resin column was conditioned by 300

cm^3 of deionized water and 200 cm^3 of a desired chloride solution. The distribution coefficients (K_d) and separation factors (α) were calculated from the obtained chromatograms by the same calculation used in the previous chapter.

4.2.2 Batch Experiments

Chemicals Ln(III) and Y samples for batch experiments were prepared from their hydrated chloride compounds (LnCl·nH$_2$O, n = 6~7) supplied by Rare Metallic, Inc. with more than 99.9% purity. All chemicals and solvents used in this study were reagent grade and supplied by Wako Pure Chemical Ind., Ltd. and Kanto Kagaku. The purities of the alcohols were 99.8, 99.5, 99.5, 99.5, 99.0, and 99.0% for methanol, ethanol, 1-propanol, 2-propanol, 1-butanol, and 2-butanol, respectively. Distilled and deionized water was used for preparing aqueous samples. Aqueous lithium chloride solutions were prepared by dissolving LiCl (purity: > 99%) in the distilled and deionized water. The pyridine resin used for batch experiments was polymer pyridine resin with 10 wt% crosslinkage. The resin was washed by acetone, ethanol, and water several times and dried in a vacuum desiccator at 323 K for more than 2 days before use.

Procedure Stock solutions for batch experiments were prepared by dissolving the chloride compounds in methanol. A portion of each stock solution was mixed together and dried to evaporate the solvent. The dried sample was then dissolved in 5.0 cm^3 of desired solvent to give a concentration of 2 mmol/dm^3 for each metal. This solution was used as a sample solution. A 1.0 g of dried pyridine resin was put into the sample solution, and the mixture was shaken for 24 hours at 288 K. The concentrations of metals in solution phase before and after adsorption equilibrium were determined by ICP-mass spectrometer (SPQ9200, Seiko Instruments Inc. (Appendix I, **Fig. I-2**)). The distribution coefficients (K_d) were calculated as follows:

$$K_d = \frac{C_I - C_F}{V_R} \Big/ \frac{C_F}{V_S} = \frac{(C_I - C_F)V_S}{C_F V_R} \tag{1}$$

where C_I and C_F represent the concentrations of metals in solution before (initial) and after (final) the equilibrium, respectively. V_R and V_S represent the volume of pyridine resin and sample solution, respectively.

4.3   Results of Chromatography Experiments

4.3.1   Chromatographic Behavior of Ln(III) by Tertiary Pyridine Resin in Chloride Solution System

As described in the previous chapter, preliminary experiments using non-radioactive materials are required before hot experiments in order to optimize the experimental conditions. Accordingly, several experiments using stable Ln were carried out prior to the hot experiments using An and radioactive Ln.

Solvent effect I. HCl-Alcohol   As mentioned in the section 4.1, hydrochloric acid is the most commonly used solvent as a chloride solution. Accordingly, the first chromatography experiment was carried out by employing a conc. HCl solution (**Fig. IV-2** in Appendix IV). However, Ln(III) showed no adsorption in this solvent. In order to obtain distinguishable K_d and α, methanol was added into a nitric acid solution, in the same way as the chloride solution system in the previous chapter. **Fig. 4-1** shows typical chromatograms of Y and Ln(III) in methanolic HCl solutions (also see Appendix IV, **Fig. IV-2**). The retention volume of each element increased as increasing X_{MeOH} and, moreover, each element began to separate individually with the increase of X_{MeOH}, although these enhanced adsorbability and separability turned to decrease when X_{MeOH} was over 80%, being different from the results obtained in the methanolic HNO$_3$ solutions.

Figure 4-2 shows a variation of K_d with the increase of X_{MeOH} and the separation factors (α between Ce and Eu, Ce and Lu, and Eu and Lu. (Ce, Eu, and Lu represent light, middle, and heavy Ln, respectively) The K_d of each element varied to form a convex curve with the increase of X_{MeOH}, giving the maximum value when X_{MeOH} was 60%. However, the α showed an irregular variation with the increase of X_{MeOH} and the maximum values were at $X_{\mathrm{MeOH}} = 20\%$. This means that higher X_{MeOH} is not necessarily required for the intragroup separation of Ln(III) (and An(III)). As mentioned in the first section of this chapter, hydrochloric acid is a very corrosive solvent. Higher concentration of this solution erodes equipment and, therefore, we should keep the concentration of HCl in separating solvent as low as possible for a long-term operation. **Fig. 4-3** represents the effect of HCl concentration in methanolic HCl solution on the adsorbability (K_d) and separability (α) of the pyridine resin (also see Appendix IV, **Fig. IV-3**). The K_d rapidly decreased with a decrease

in HCl concentration, although higher X_{MeOH} solvent gave larger K_d in the same HCl concentration. On the other hand, the α showed the similar tendency, that is, the α decreased with the decrease of HCl concentration and higher X_{MeOH} gave larger α in the same HCl concentration. However, it should also be noted that higher HCl concentration brings the larger absolute value of α. These results suggests that we can lower the concentration of HCl in separating solvent by adding alcohol in the solvent, although higher HCl concentration brings larger α.
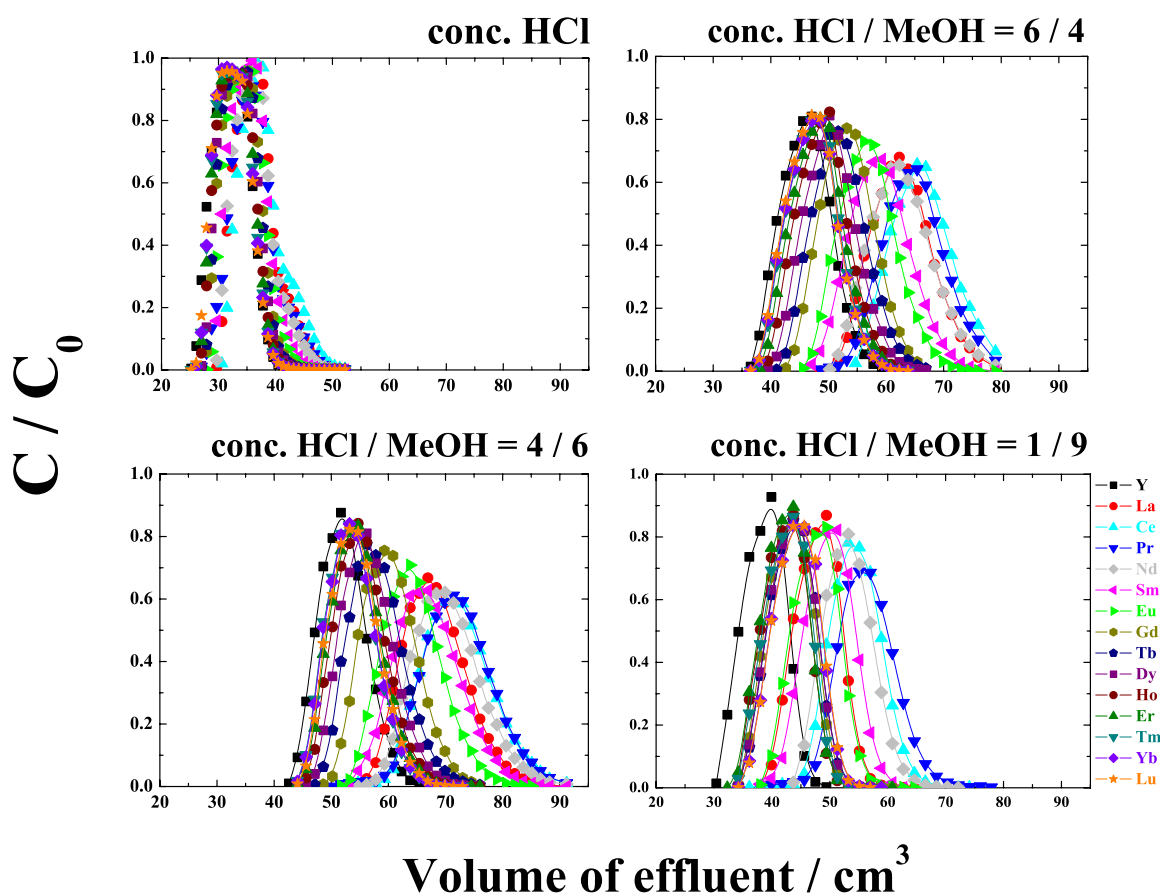
Figure 4-1.   Elution chromatograms of Y and Ln(III) by tertiary pyridine resin in different conc. HCl / MeOH mixed solutions at 293 K. (Flow rate: 50 cm^3/h, Resin column: 1 cm-ϕ × 51 cm, C: concentration in effluent, C$_0$: concentration in feed solution)
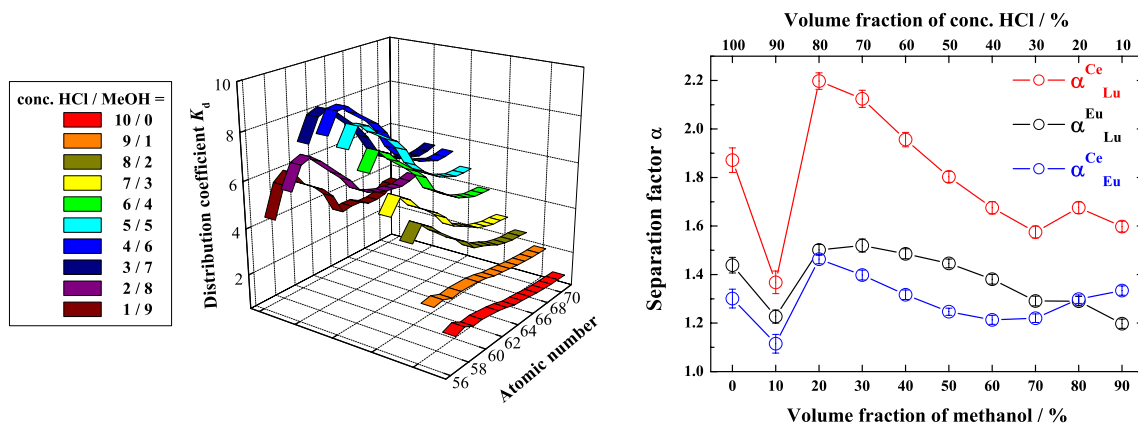
Figure 4-2. Variation of distribution coefficients of Y and Ln(III) and their separation factors by tertiary pyridine resin in conc. HCl / MeOH mixed solutions at 293 K. (Flow rate: 50 cm^3/h, Resin column: 1 cm-ϕ × 51 cm)
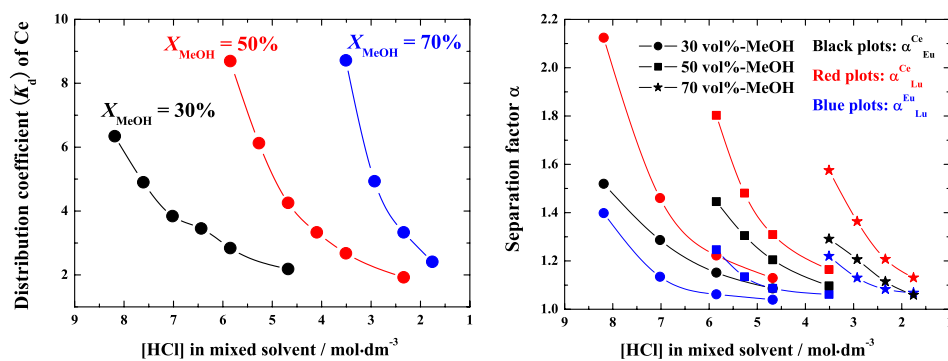
Figure 4-3. [HCl] dependence of distribution coefficient of Ce and separation factors between several lanthanoids in different HCl / MeOH mixed solutions at 293 K. The error bars are smaller than the plotted points. (Flow rate: 50 cm^3/h, Resin column: 1 cm-ϕ × 51 cm)

It has also been reported in some previous papers [16–19] that the adsorbability (*i.e.* the degree of adsorption) of metal cations in alcoholic acid solutions depends on the type of alcohol added. Accordingly, in order to confirm the effect of alcohol type on the chromatographic behavior, several chromatography experiments were carried out in different alcoholic HCl solutions (Appendix IV, **Fig. IV-4**). The K_d of Ce and the α between Ce and Lu calculated from the obtained chromatograms are plotted in **Fig. 4-4**. For normal chain monohydric alcohols, ethanol and propanol showed the largest K_d and α. However, branched alcohols of 2-propanol and 2-butanol showed larger K_d and α than their corresponding normal alcohols of 1-propanol and 1-butanol, respectively. Consequently, 2-propanol was the best alcohol among the tested six monohydric alcohols for enhancing the adsorbability and separability of the pyridine resin. Interestingly, a dihydric alcohol of ethylene glycol exhibited no considerable effect on the adsorbability or separability. That is, no adsorption or separation was observed in a conc. HCl / ethylene glycol mixed solution (see Appendix IV, **Fig. IV-5**).
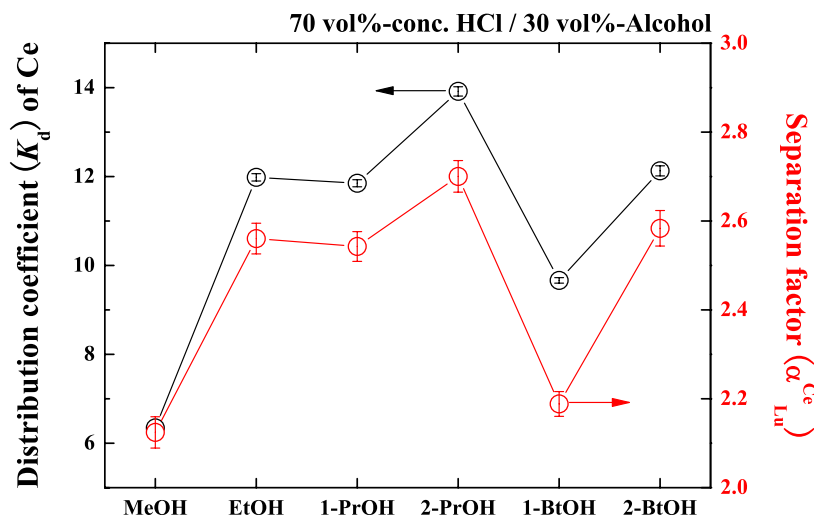
Figure 4-4. Variation of distribution coefficients of Ce and separation factors between Ce and Lu by tertiary pyridine resin in different alcoholic HCl solutions at 293 K. (Flow rate: 50 cm^3/h, Resin column: 1 cm-$\phi \times$ 51 cm, Solvent: 70 vol%-conc. HCl / 30 vol%-alcohol)

Solvent effect II. LiCl-Alcohol   The adsorption manner of tertiary pyridine resin (*i.e.* coordinative or anion exchange) is expected to depend on the acidity of solvent. In order to discuss this issue, the information about the adsorptivity of the pyridine resin in non-acidic solutions is indispensable. Furthermore, supposing that we can accomplish the separation without using any acidic solution, the operating conditions of the separation system will become mild. Therefore, we should confirm the chromatographic behavior by the pyridine resin in a non-acidic solution system.

Figure 4-5 shows the chromatogram of Y and Ln(III) in a methanolic LiCl solution and the calculated K_d. The elution order was quite different from that in alcoholic HCl solutions. Moreover, as compared with the HCl solution system, the adsorbability of the resin became larger in the LiCl solution. However, the middle and heavier Ln were adsorbed in the resin so strongly that the separability became low and, furthermore, the tailing of their chromatograms occurred. It seems that non-acidic solution systems such as LiCl solution are not so suitable for the separation of trivalent f-elements by tertiary pyridine resin, although its adsorption and separation behavior is interesting. This information is also important for understanding the adsorption and separation mechanism of tertiary pyridine resin.
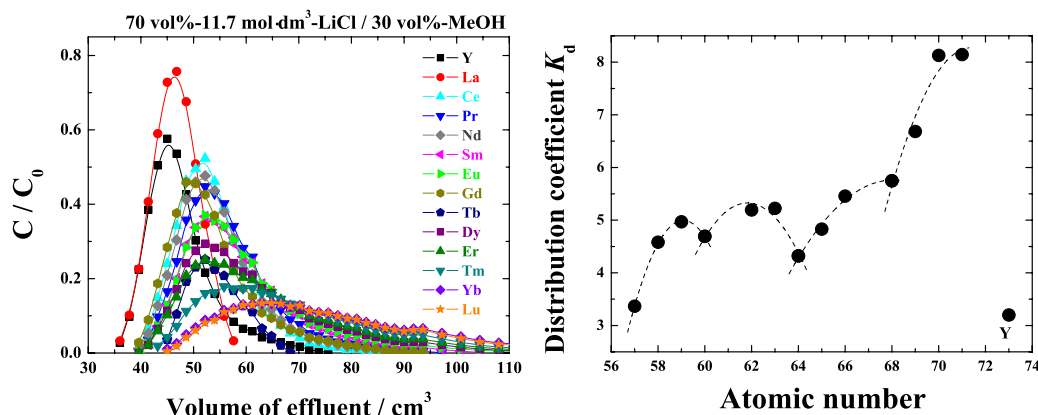
Figure 4-5.   Elution chromatogram of Y and Ln(III) by tertiary pyridine resin in methanolic LiCl solution at 293 K and their calculated distribution coefficients. The error bars are smaller than the plotted points. (Flow rate: 50 cm^3/h, Resin column: 1 cm-$\phi \times$ 50 cm, Solvent: 70 vol%-11.7 mol·dm^3-LiCl / 30 vol%-alcohol)

Temperature dependence The effect of temperature on chromatographic be-
havior was studied using a 70 vol%-conc. HCl / 30 vol%-MeOH Mixed solution by
changing the column temperature from 278 to 323 K (*i.e.* 278, 293, 308, and 323
K). To make the description simple, the mixing ratio of conc. HCl and methanol (al-
cohol) is described as "conc. HCl / MeOH (alcohol) = X / Y" (vol/vol), hereafter. The
K_d and α calculated from the obtained chromatograms (Appendix IV, **Fig. IV-6**) are
shown in **Fig. 4-6**. The observed K_d showed slight concave curves with an increase
of temperature and seem to have their minimum values at around 293 K, while the
α exhibited the opposite tendency and they seem to have the maximum values at
around 293 K. Lowering the temperature increases the adsorptivity of the resin but
it also occurs the broadening of chromatograms (see Appendix IV, **Fig. IV-6**), caus-
ing the decrease of α. On the other hand, the present separation system using HCl
and alcohols is not applicable to higher-temperature operation because these sol-
vents have low boiling points as listed in **Table 4-1**, and, thus, they may vaporize
in a resin column at higher temperature. The vaporization of solvent in the column
disturbs the homogeneous flow of solvent in the column and, consequently, the ob-
tained chromatogram becomes broad and poor-defined. Therefore, we can conclude
that room temperature ($\cong$ 293 K) is the best temperature to perform the separation
and we do not need to control the temperature during the operation, simplifying the
separation system.

Table 4-1. Boiling points of conc. HCl and alcohols.

Solvent	Boiling point / K [20]
conc. HCl	61.0
MeOH	64.5
EtOH	78.3
1-PrOH	97.2
2-PrOH	82.4
1-BtOH	117.7
2-BtOH	99.5
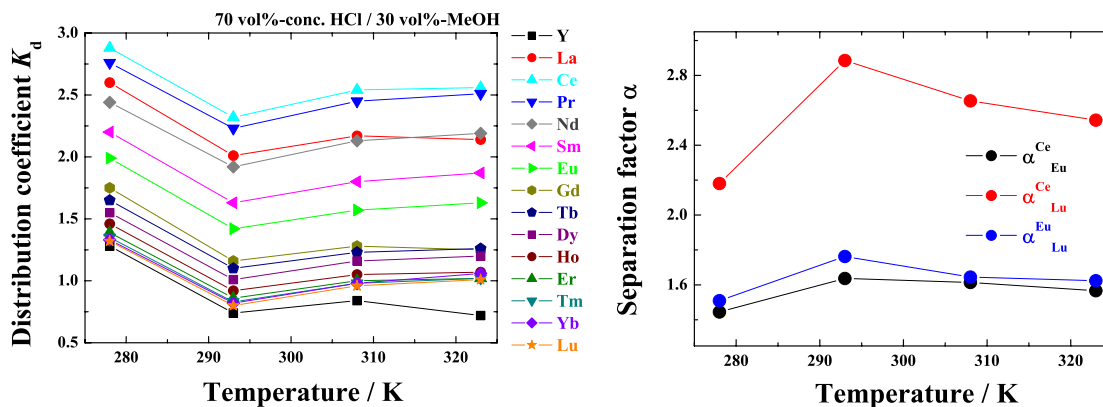
Figure 4-6. Temperature dependence of distribution coefficients of Y and Ln(III) and their separation factors by tertiary pyridine resin in conc. HCl / MeOH mixed solution at 293 K. The error bars are smaller than the plotted points. (Flow rate: 50 cm^3/h, Resin column: 1 cm-ϕ × 50 cm, Solvent: 70 vol%-conc. HCl / 30 vol%-alcohol)

Flow rate dependence The flow rate dependence of K_d and α in the HCl solution system was also confirmed using "conc. HCl / MeOH = 7 / 3" solvent at 293 K. The flow rate was varied from 13 to 92 cm^3/h. (The maximum flow rate of the pump used in this study is ∼100 cm^3/h.) The resultant chromatograms and their corresponding K_d and α are shown in Appendix IV, **Fig. IV-7** and **Table IV-6**. There were no significant change both in the K_d and in α within the tested flow rate range. The flow rate of 92 cm^3/h with 1 cm-ϕ column equals to a linear flow rate of 117 cm/h. Therefore, we can operate the practical separation process with at least ∼120 cm/h-linear flow rate.

Chromatography using longer resin column It has been found in the above-mentioned sections that the elution curves of Y and Ln(III) by the pyridine resin are split individually in alcoholic HCl solutions. The height of resin column in chromatography corresponds to the number of theoretical plate [21] and, hence, using longer resin column will accomplish further clear separation. The chromatograms

of Y and Ln(III) using a longer resin column (0.8 cm-ϕ × 100 cm) are shown in **Fig. 4-7**. In "conc. HCl / MeOH = 5 / 5", the elution curves of lighter Ln (La-Nd) were separated from those of heavier Ln (Gd-Lu), although the elution curves of Sm and Eu overlapped with those of the lighter and heavier ones (Upper left in **Fig. 4-7**). On the other hand, the chromatogram in "conc. HCl / 2-PrOH = 5 / 5" showed a clear peak separation even between heavier Ln and the elution curves of heavier Ln were separated from those of middle Ln (Sm and Eu) (Upper right in **Fig. 4-7**). It should be noted that good individual separations between lighter Ln and between heavier Ln were observed in pure MeOH solvent as shown in the lower graphs of **Fig. 4-7**; the lighter Ln of La, Ce, Pr (Nd), and Sm were separated individually in MeOH (lower left), while the elution curves of the heavier Ln (Tb-Lu) and Y were also split out (lower right). These results suggest that there is a possibility to use the alcoholic chloride solution system for the individual separation of specific trivalent f-elements.

Figure 4-7. Elution chromatograms of Y and Ln(III) in several alcoholic chloride solutions at 323 K. (Flow rate: 100 cm^3/h, Resin column: 0.8 cm-ϕ × 100 cm)
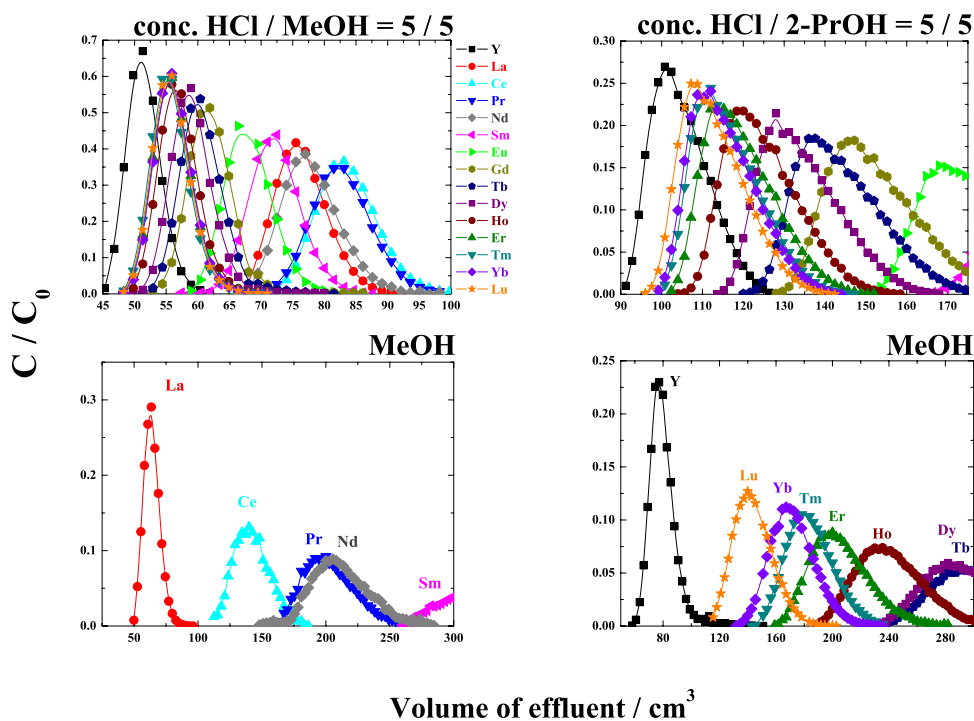
Other solid extractants   As before mentioned, a tertiary pyridine resin can work both as a coordinative extractant and as an anion exchange resin. Supposing that the pyridine resin mainly works as the anion exchanger in the present alcoholic chloride solution, other anion exchange resins should show similar adsorption and separation behavior in the same solvent system. Or, to the contrary, if the adsorption by the pyridine resin is attributed to the direct interaction of pyridine groups, other coordinative extractants should give similar adsorption and separation. In order to reveal the adsorption property of tertiary pyridine resin, further chromatography experiments were carried out by employing several ion exchange resins and solid type extractants.

The ion exchange resins and solid extractants employed in this study are listed in **Table 4-2** and their chemical structures are illustrated in **Fig. 4-8**. Strongly acidic or basic ion exchange resins (SQS, Dowex 1X8, and PA416) can work in any acidic or basic solvent conditions, while weakly basic anion exchange resins of WA30 and WA21 function as an anion exchanger only in acidic solvent conditions. AR-01 is a mixture of coordinative extractant and anion exchanger: one nitrogen atom of imidazol groups behaves as a coordinative site and its methylated nitrogen atom works as an anion exchange site. DMAA resin has O(oxygen)-donor sites in its structure and works as a coordinative extractant.

Figure 4-9 shows the elution chromatograms using SQS, WA21, and DMAA resins, respectively. A cation exchanger of SQS showed strong adsorption for Y and Ln(III) in conc. HCl / MeOH mixed solution and the Ln(III) were eluted in the reverse order of their atomic numbers, corresponding to the reported results in aqueous HCl solutions [2, 3, 6]. In the present study, lighter Ln of La$\sim$Nd were adsorbed in SQS far more strongly than heavier Ln, that is, their elution curves became very broad and they were difficult to define their elution peaks. On the other hand, most of the tested anion exchange resins showed no adsorption and separation for Y and Ln(III) (Appendix IV, **Fig. IV-8**). WA21 was the only resin which gave separated elution curves in the conc. HCl / MeOH solution. Unfortunately, most of the elution curves for WA21 became broad due to the large particle size ($\sim$ 200 μm-ϕ) of the resin, giving rise to a difficulty on the calculation of K_d. However, it is clear that the elution order of Ln(III) (including the deviation of La) is identical with that observed in the chromatogram by the pyridine resin.

Table 4-2. Properties of anion exchange resins and solid extractants used in this study.

Product name	Manufacturer	Type
SQS	Asahi Kasei	Strongly acidic cation exchange resin
Dowex 1X8	Dow Chemical	Strongly basic anion exchange resin (Type-I)
PA 416	Mitsubishi Chemical	Strongly basic anion exchange resin (Type-II)
WA 30	Mitsubishi Chemical	Weakly basic anion exchange resin
WA 21	Mitsubishi Chemical	Weakly basic anion exchange resin
AR-01	Asahi Kasei	Coordinative & anion exchange resin
DMAA	Ishihara [22]	Coordinative polymer resin

Product name	Functional group	Particle size (μm)	Chemical structure
SQS	Sulfonic acid	⊃100	Fig. 3-16 I
Dowex 1X8	Quaternary ammonium	⊃100	II
PA 416	Quaternary ammonium	⊃200	III
WA 30	Tertiary ammonium	⊃200	IV
WA 21	Secondary ammonium	⊃200	V
AR-01	Benzimidazolium	40⊃60	VI
DMAA	N,N-Dimethylacrylamide	⊃50	VII
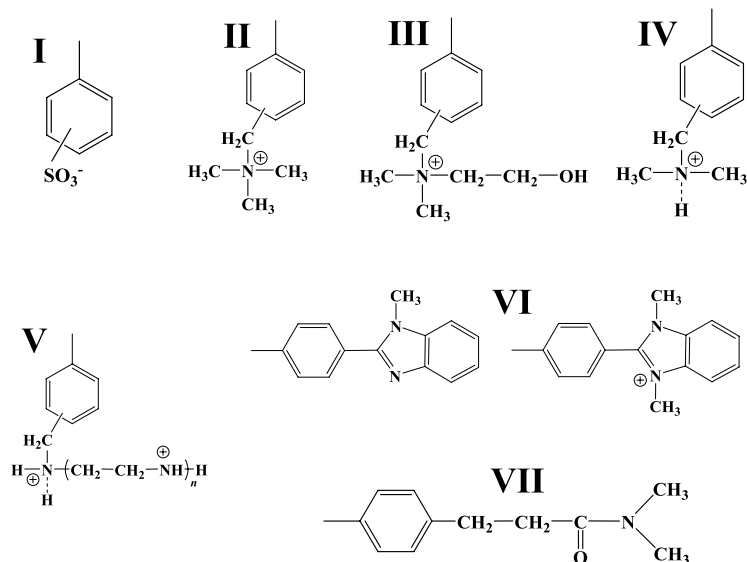
Figure 4-8. Chemical structures of ion exchange resins and solid type extractants used in this study.
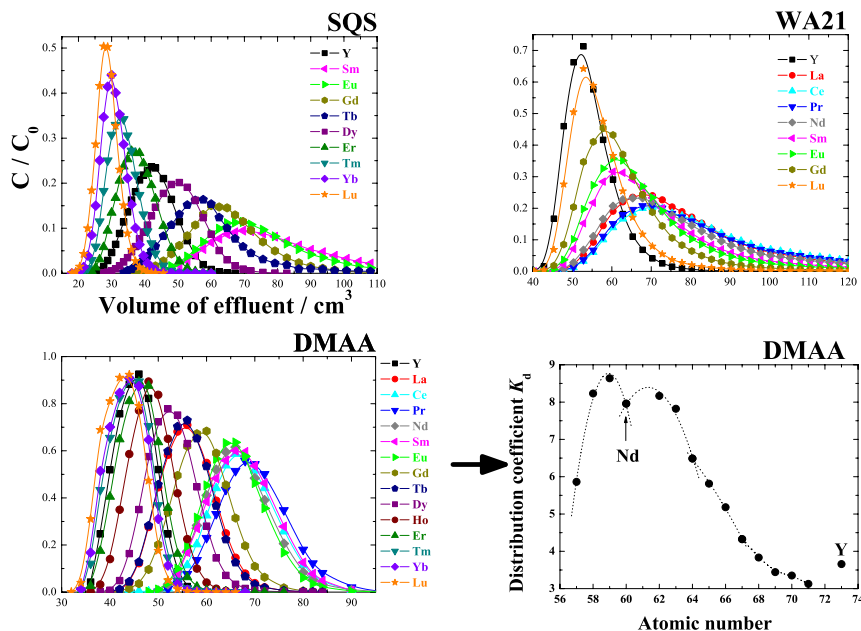
Figure 4-9. Elution chromatograms of Y and Ln(III) using SQS, WA21, and DMAA resins in conc. HCl / MeOH mixed solution at 298 K. The error bars are smaller than the plotted points. (Flow rate: 50 cm^3/h, Resin column: 1 cm-ϕ × 10 cm for SQS, 1 cm-ϕ × 50 cm for WA21 and DMAA, Solvent: 70 vol%-conc. HCl / 30 vol%-alcohol)

AR-01 is a relatively newly-developed anion exchanger and coordinative extractant, which has been found to be effective for the separation of U from several fission products in nitric acid solutions [23, 24]. However, it brought no adsorption and separation for Y and Ln(III) in the conc. HCl / MeOH mixed solution (Appendix IV, **Fig. IV-8**). On the other hand, an O-donor extractant of DMAA resin showed a fine chromatogram, in which elution curves were separated individually, as shown in the lower left of **Fig. 4-9**. O-donors are classified as a hard donor in HSAB theory and their affinity for hard metals like Ln(III) is larger than that of soft donors such as pyridine ligands [25, 26]. The larger K_d of DMAA resin over the pyridine resin (*e.g* K_d(Ce) = 8.23 for DMAA and 6.35 for tertiary pyridine resin) probably reflects this fact. The elution order (*i.e.* lanthanoid pattern of K_d) of Y and Ln(III) by DMAA resin was somewhat different from that by the pyridine resin; lighter Ln(III) of La∼Gd showed clear "tetrad effect", as appeared in other O-donor ligand [27], instead of the

103

linear relationship observed for the pyridine resin. The eluting position of Y was also different from that by the pyridine resin.

The adsorptivity of the tested resins are summarized in **Table 4-3**. It seems that Y and Ln cations basically form no anionic species, which can be adsorbed in anion exchange resins, with Cl^- in alcoholic HCl solutions even in the resin phase. This is consistent with the several reports indicating the weak interaction between Ln cations and Cl^- [28–30]. On the other hand, these cations can be adsorbed in cation exchangers and some coordinative extractants even though their hydration structures are very tight [31, 32]. It is supposed from these facts that Y and Ln cations are adsorbed in the pyridine resin mainly by the direct coordination of nitrogen atoms of pyridine groups in alcoholic HCl solutions, although we still can not deny the possibility of the ionic interaction between the protonated pyridine groups and the anionic Cl^- complexes of the cations completely.

Table 4-3. Table 4-3. Adsorptivity of ion exchange resins and solid type extractants in conc. HCl / MeOH mixed solution. (Solvent: 70 vol%-conc. HCl / 30 vol%-alcohol)

Product name	Type	Adsorptivity
SQS	Strongly acidic cation exchange resin	◯
Dowex 1X8	Strongly basic anion exchange resin (Type-I)	×
PA 416	Strongly basic anion exchange resin (Type-II)	×
WA 30	Weakly basic anion exchange resin	×
WA 21	Weakly basic anion exchange resin	△
AR-01	Coordinative & anion exchange resin	×
DMAA	Coordinative polymer resin	◯

4.3.2   Chromatographic Behavior of An(III) and Ln(III) by Tertiary Pyridine Resin in Chloride Solution System

On the basis of the results obtained in the preliminary experiments using stable Ln, chromatography experiments using radioactive trivalent An (An(III)) and Ln(III) were carried out in order to investigate their chromatographic behavior for a tertiary pyridine resin in the alcoholic chloride solution system. All the experiments were carried out at room temperature ($\cong$ 293 K) and the flow rate was adjusted at 100 cm^3/h.

Solvent effect I. HCl-Alcohol   **Figure 4-10** shows elution chromatograms of An(III) and Ln(III) in different compositions of conc. HCl / MeOH mixed solution (also see Appendix IV, **Fig. IV-9**). In a conc. HCl solution, the Ln(III) were instantly eluted from the column, while the An(III) slightly adsorbed in the resin, causing relatively slower elution compared with the Ln(III). However, as X_{MeOH} in the solvent increased, the retention volume of each element increased and, furthermore, An(III) were clearly separated from Ln(III). This means that adding methanol in the solvent promotes both the adsorption of An(III) in the resin and the separability of the pyridine resin for An(III) over Ln(III). Furthermore, the elution order of Ac and Cf were unexpected (middle graph in **Fig. 4-10** and Appendix IV, **Fig. IV-10**); Ac is the first element of the An series and its ionic radius is far larger than other An(III) and Ln(III) [36], as shown in **Fig. 1-4**. Cf is a heavier element than Am and Cm and its ionic radius is smaller than those of Am and Cm. If the elution order of An(III) is analogous to that of Ln(III) (*i.e.* basically depends on the ionic radii), Ac should be eluted far after the other three An(III) and Cf should be eluted before Cm. However, the result was quite different from that as expected, indeed the opposite. That is, the largest An of Ac was eluted with Ln(III), while the smaller An of Cf was strongly adsorbed in the resin and hardly eluted from the column. This irregular elution of An(III) is different from the order in the cation exchange system using HCl solutions [3, 6] and the anion exchange system using nitric acid solutions [10, 33], but similar to that in the anion exchange system using HCl solutions [7–10] and LiCl solutions [11]. On the other hand, the nitrate solution system gave no intergroup separation between An(III) and Ln(III) as observed in the present HCl solutions.

Figure 4-10. Elution chromatograms of An(III) and Ln(III) by tertiary pyridine resin in different conc. HCl / MeOH mixed solutions at 293 K. (Flow rate: 100 cm^3/h, Resin column: 1 cm-$\phi \times$ 10 cm)

The elution curves in **Fig. 4-10** and **Fig. IV-9**, especially those of Am and Cm, show tailing profiles. This is probably due to the presence of a liquid layer on the resin bed. That is, in these hot experiments, a 0.5 mm-height of liquid layer was retained at the top of the resin bed in the column in order to avoid the inhalation of air into the resin bed. This liquid layer encourages the diffusion of sample solutions out of the stationary-phase, broadening the tails of elution curves. Therefore, the plotted points within the full width at half maximum (FWHM) of the elution curves were used for the Gaussian-curve fitting to calculate K_d (Appendix IV, **Fig. IV-11**).

The K_d of Am(III) and Ce(III) calculated from the elution chromatograms are plotted in **Fig. 4-11**, along with their separation factors (α^{Am}_{Ce}). Although both the K_d of Am(III) and Ce(III) increased as increasing X_{MeOH}, its increasing tendency of Am(III) was more drastic than that of Ce(III). As a result, the α^{Am}_{Ce} increased as the increase of X_{MeOH}. On the other hand, when the HCl concentration in solvent was lowered (*i.e.* the concentration of water increased), the retention volume of each element drastically decreased and no clear group separation between An(III) and Ln(III) was observed any more (**Fig. 4-12**). Consequently, the K_d and α decreased drastically, as shown in **Fig. 4-13**. Therefore, it seems that we have to use as higher [HCl] solution as possible for the efficient separation of An(III) and Ln(III) in this separation system.

Figure 4-11. Variation of distribution coefficients of Am, Cm, and Ce and their separation factors by tertiary pyridine resin in conc. HCl / MeOH mixed solutions at 293 K. (Flow rate: 100 cm^3/h, Resin column: 1 cm-ϕ × 10 cm)
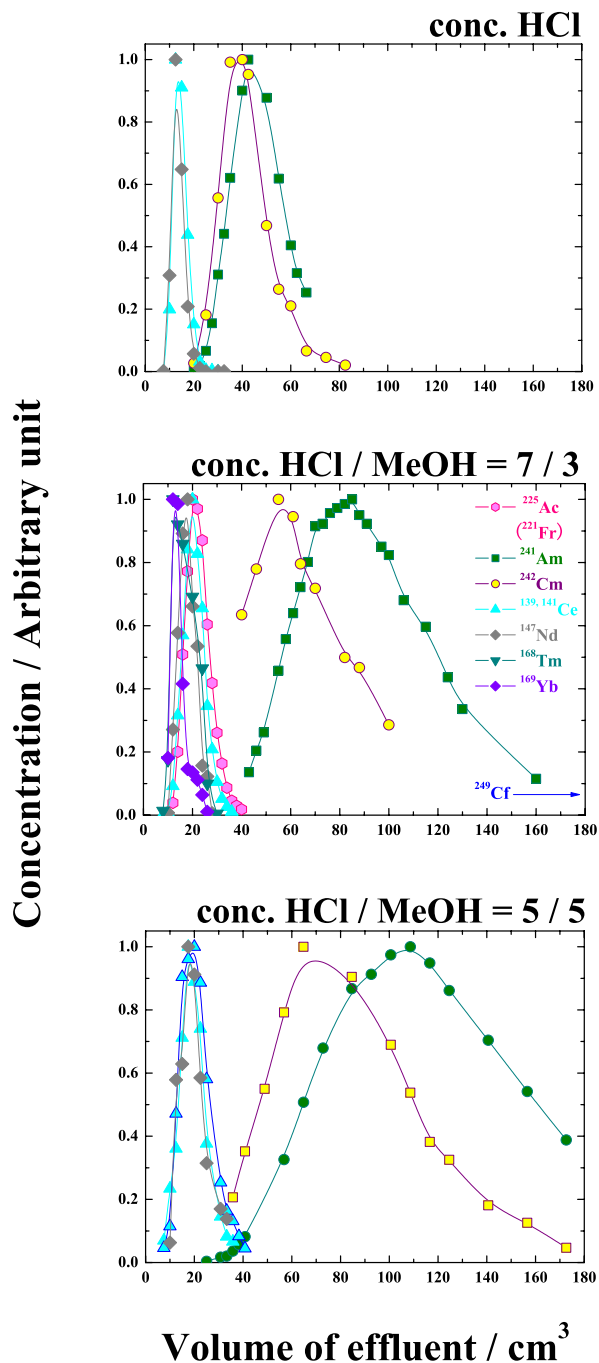
Figure 4-12. Elution chromatograms of An(III) and Ln(III) by tertiary pyridine resin in different HCl / MeOH mixed solutions at 293 K. (Flow rate: 100 cm^3/h, Resin column: 1 cm-ϕ $\times$ 10 cm)
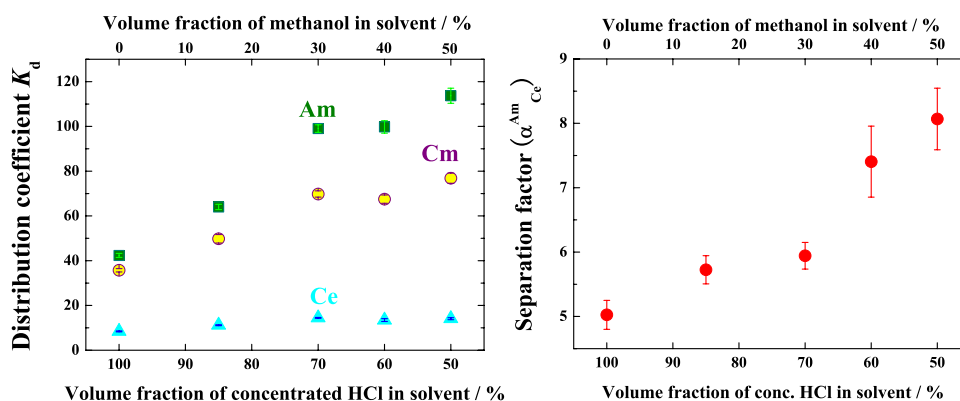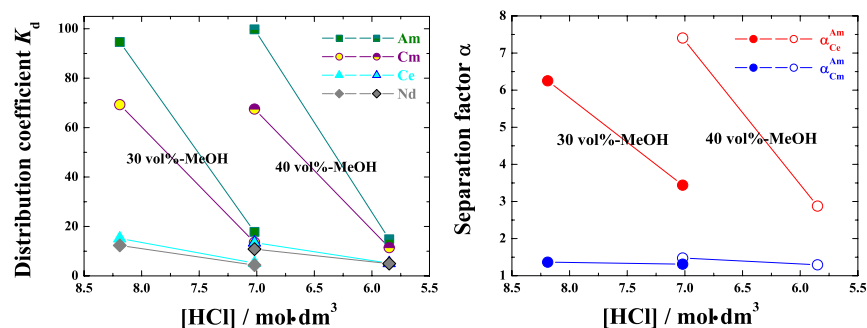
Figure 4-13. Variation of distribution coefficients of Am and Ce and their separation factors by tertiary pyridine resin in HCl / MeOH mixed solutions at 293 K. (Flow rate: 100 cm^3/h, Resin column: 1 cm-ϕ $\times$ 10 cm)

As observed in the previous section, the type of alcohol has a great influence on the adsorption and separation properties of the tertiary pyridine resin. In order to investigate the effect of alcohol types on the adsorption and separation behavior of An(III) and Ln(III), further chromatography experiments were performed using four different normal chain monohydric alcohols (*i.e.* methanol, ethanol, 1-propanol, and 1-butanol). **Fig. 4-14** (and Appendix IV, **Fig. IV-12**) shows a variation of K_d of Am and α^{Am}_{Ce} for the four different alcoholic HCl solutions.
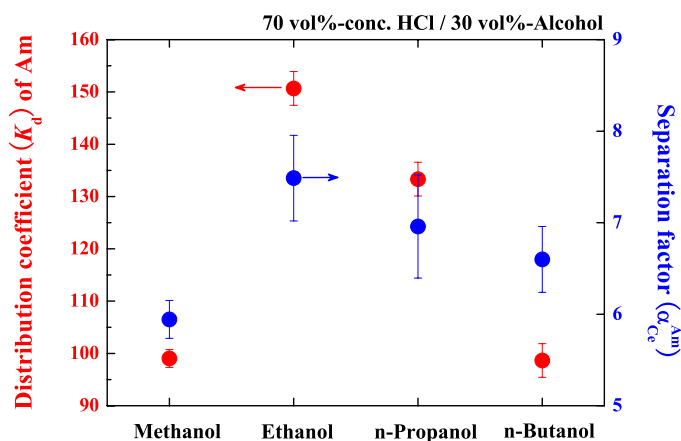
Figure 4-14. Variation of distribution coefficients of Am the separation factors between Am and Ce by tertiary pyridine resin in different alcoholic conc. HCl solutions at 293 K. (Flow rate: 100 cm^3/h, Resin column: 1 cm-$\phi \times$ 10 cm)

The mixing ratio of conc. HCl and alcohol was fixed at 70 vol% and 30 vol%, respectively. Convex-upward changes, that are similar to the previous results using stable Ln, were observed with an increase in carbon number of the alkyl group both in K_d and α: both of the K_d and α were at a maximum in the ethanolic mixed solvent and decreased as the carbon number increased above ethanol. Among the four alcoholic solvents, MeOH gave the minimum K_d and α. However, the chromatogram by the methanolic solution showed a sufficiently clear peak separation between An(III) and Ln(III) in this system, while the elution curves for the ethanolic solution were rather broad and a greater amount of eluent was required to elute the whole components of the sample completely from the column. Therefore, the ethanol mixed solvent was not necessarily considered the best solvent for the separation of An(III) from Ln(III). In order to determine the most practical solvent for the separation, the

overall separation system should be taken into consideration; such as the size of resin column or the post-treatment for the produced wastes.

Chromatography using longer resin column As described in the previous paragraph, it was found that the pyridine resin exhibited sufficient potential for the separation of An(III) from Ln(III) in the alcoholic HCl solution system with a very short resin column (1 cm-ϕ × 10 cm). Hence, a longer resin column was employed to achieve a complete separation between An(III) and Ln(III). **Fig. 4-15** shows elution chromatograms in conc. HCl / MeOH mixed solutions using a 1 cm-ϕ × 49 cm resin column. In "conc. HCl / MeOH = 7 / 3" solvent, the elution curves of Am and Cm were clearly separated from those of other Ln, giving a complete separation between An(III) and Ln(III) (In fact, no radioactivity was detected in the effluent from 110 to 160 cm^3.). On the other hand, An(III) and Ln(III) were hardly separated when the HCl concentration in the solvent decreased (the H_2O concentration increased) even though a longer resin column was utilized (right graph in **Fig. 4-15**). These results indicate that the chromatography system using the pyridine resin in combination with conc. HCl / alcohol mixed solutions is sufficiently applicable to a practical group separation between An(III) and Ln(III).
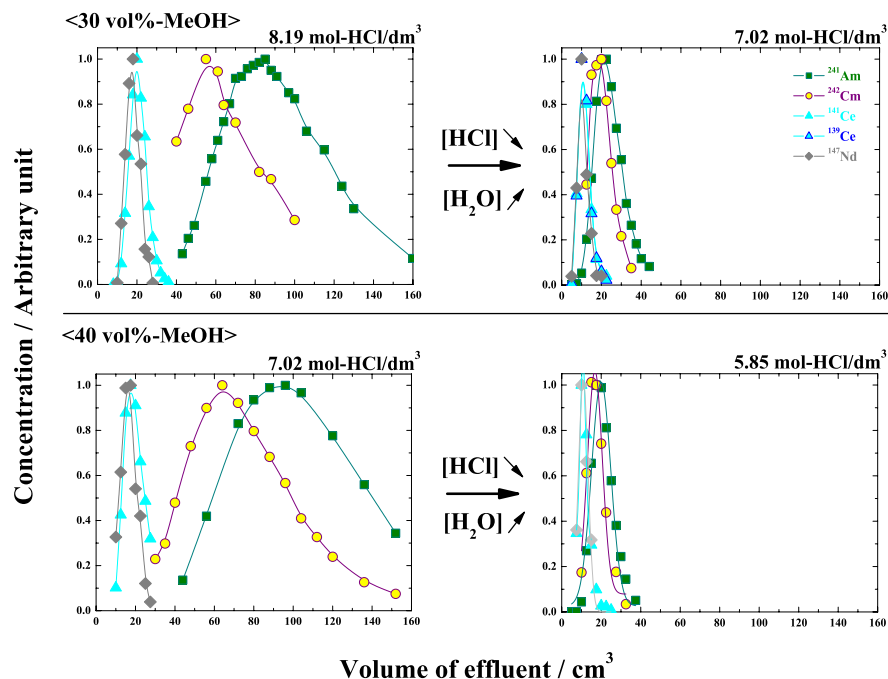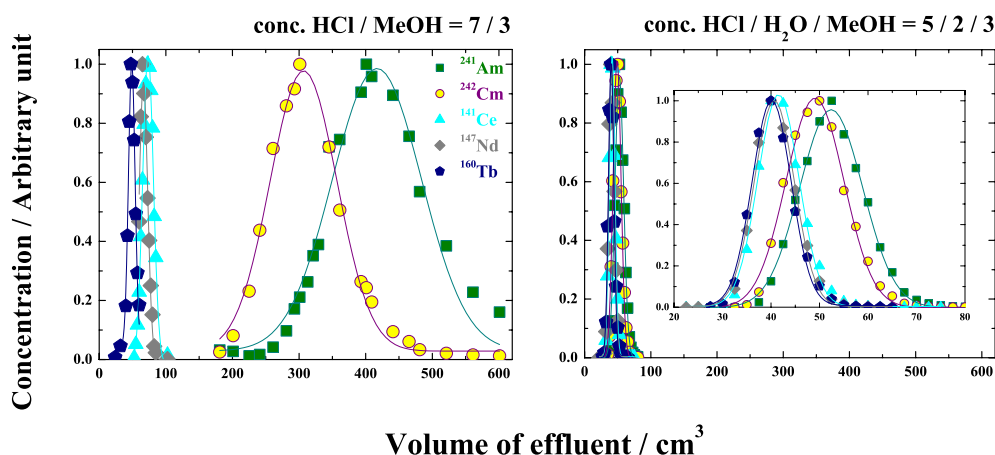

Figure 4-15. Elution chromatograms of An(III) and Ln(III) by tertiary pyridine resin in methanolic HCl solutions at 293 K. (Flow rate: 100 cm^3/h, Resin column: 1 cm-ϕ × 49 cm)

Solvent effect II. LiCl-Alcohol   Interesting adsorption and separation behavior has been observed in in the preliminary experiments using non-acidic LiCl solutions.   Therefore, it is necessary to examine the chromatographic behavior of An(III) and Ln(III) mixture in the LiCl solution system in order to confirm the possibility of this solution system for the separation of An(III) and Ln(III), and to understand the adsorption and separation mechanism of tertiary pyridine resin.   The elution chromatogram of An(III) and Ln(III) in "LiCl solution (11.7 mol-LiCl/dm^3) / MeOH = 7 / 3" is given in **Fig. 4-16**.
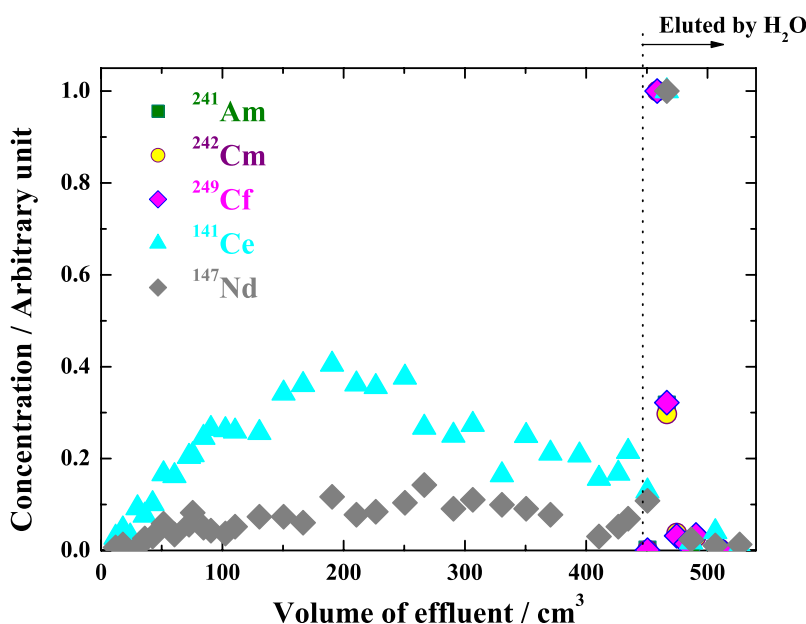
Figure 4-16. Elution chromatogram of An(III) and Ln(III) by tertiary pyridine resin in a methanolic LiCl solution at 293 K. (Flow rate: 100 cm^3/h, Resin column: 1 cm-ϕ × 10 cm, Solvent: 70 vol%-LiCl solution (11.7 mol-LiCl/dm^3) / 30 vol%-MeOH)

   The elution of Ln(III) was considerably slow, meaning that Ln(III) were strongly adsorbed in the pyridine resin.   On the other hand, there was no elution of An(III) observed even by over 400 cm^3 of eluent. Then, when deionized water was introduced to wash the resin column, An(III) and the rest of Ln(III) in the column were rapidly eluted. This result indicates that An(III) are adsorbed in the pyridine resin far more strongly than Ln(III) in LiCl solutions.   This tendency is similar to that observed in the anion exchange system using LiCl solutions [11]. Furthermore, the adsorbability

in this solution system becomes far larger than that in the HCl system. It should be noted that the adsorbed species in the pyridine resin are easily and rapidly eluted by water. This makes the regeneration of the resin easy and also makes the separation process simple. These advantages are very favorable for practical uses.

Chromatographic behavior by anion exchange resins   So far, the tertiary pyridine resin has exhibited unique selectivity for An(III) over Ln(III) in alcoholic chloride solutions. In order to clarify this singularity of the pyridine resin for the separation of An(III) and Ln(III), the chromatographic behavior by other typical anion exchange resins in the alcoholic chloride solution should be confirmed. Therefore, two types of anion exchange resins (quaternary ammonium type and quaternary pyridinium anion exchange resins) were employed. As a solvent, "conc. HCl / MeOH = 7 / 3" solvent was used for chromatography experiments.

A chromatographic result by quaternary ammonium type anion exchange resin (Dowex 1X8, strongly basic anion exchange resin) is given in **Fig. IV-13** in Appendix IV. The elution of An(III) and Ln(III) was observed right after introducing the sample solution and their elution curves were overlapped for the most part, although the elution peaks of An(III) were slightly separated from those of Ln(III). This result is consistent with the previously reported results in conc. HCl / MeOH mixtures [4], while the water / MeOH mixed solutions saturated by HCl gas (*i.e.* the HCl concentration in the mixtures is more than 11.7 mol/dm^3) gave several successful results on both the inter- and intragroup separation of An(III) and Ln(III) [5]. A non-acidic solution of LiCl solution also brought strong adsorption of An(III) (and weaker adsorption of Ln(III)) in the same resin [11]. These results indicate that An(III) and Ln(III) cations hardly form anionic complexes with Cl$^-$ to adsorb in anion exchange resins in the present HCl / alcohol mixtures, although the anionic complexes will form in the water / alcohol mixtures saturated by HCl gas or in higher LiCl concentration.

Figure 4-17 shows a chromatogram of An(III) and Ln(III) by quaternary pyridinium resin. The quaternary pyridinium resin was synthesized by the methylation of tertiary pyridine resin. The introduced sample was instantly eluted from the column and, consequently, the adsorbability (K_d) was found to be very low. However, the elution curves were split into four groups: heavier Ln (Tm and Yb), lighter Ln (Ce and Nd), Cm, and Am. Supposing that this peak separation was caused by the ionic interaction of the methylated pyridine groups, the An(III) and Ln(III) should form

some anionic complexes with Cl⁻ in the present HCl / MeOH solution, being contra-
dictory to the previous result by Dowex 1X8. The methylation rate for the present
quaternary pyridinium resin is reported to be less than 80% [34, 35]. This means
that at least 20% of pyridine groups in the resin is still a tertiary pyridine group.
Hence, it seems pertinent to consider that the observed peak separation is not at-
tributed to the ionic interaction by the quaternary pyridinium groups, but to the
covalent or coordinative (still not declared, further discussion will appear in chapter
5) interaction by the rest tertiary pyridine groups.
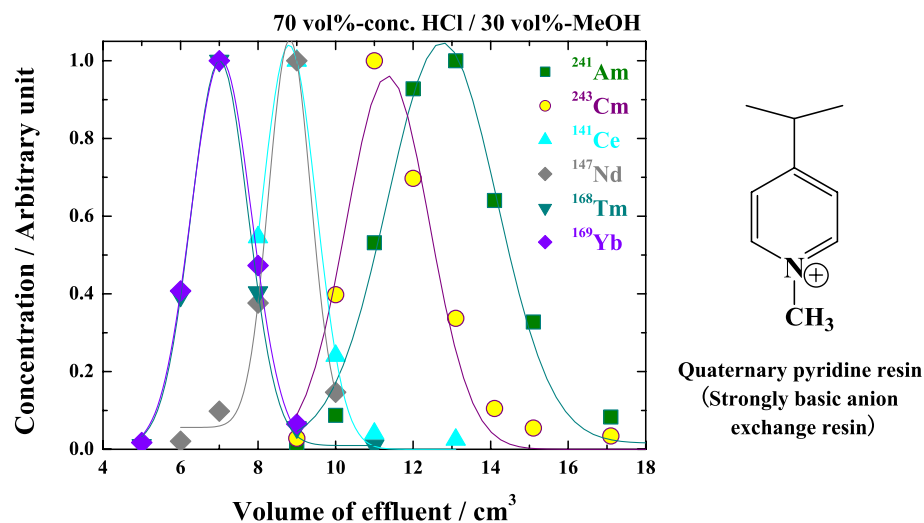
Figure 4-17. Elution chromatogram of An(III) and Ln(III) by quaternary pyridinium
resin in a conc. HCl / MeOH solution at 293 K. (Flow rate: 100 cm^3/h, Resin column:
1 cm-ϕ × 10 cm, Solvent: 70 vol%-conc. HCl / 30 vol%-MeOH)

Considering the above-mentioned results by anion exchange resins, we can con-
clude that the tertiary pyridine resin has singular separability for An(III) and Ln(III)
in alcoholic chloride solutions.

Adsorptivity of tertiary pyridine resin for An(III) and Ln(III)   From
the obtained results mentioned above, it can be concluded that the alcoholic HCl
solution system is the most suitable solvent system for the separation of An(III) and

Ln(III) by using tertiary pyridine resin. Then, the adsorptivity of the tertiary pyridine resin for An(III) and Ln(III) in the mixed solution system is summarized here before the consideration of its application to practical uses. **Fig. 4-18** illustrates the K_d of tertiary pyridine resin for An(III), Ln(III), and Y in "conc. HCl / MeOH = 7 / 3" solvent as a function of their ionic radii [36]. The An(III) except Ac have far larger K_d values than Ln(III) (and Y), enabling a clear chromatographic separation between An(III) and Ln(III). The order of K_d of An(III) is irregular (Cf $\gg$ Am $>$ Cm $\gg$ Ac) and shows no dependence on their ionic radii. The chromatographic behavior of Ac is more like Ln(III) rather than An(III). On the other hand, the K_d of Ln(III) show a regular decreasing tendency with decreasing their ionic radii (atomic number), although La deviates this regularity. From a different point of view, the K_d of Ln(III) represent a relatively clear tetrad effect [37]. Y has a lowest K_d among the tested elements. Further discussion about this adsorptivity of the pyridine resin will be made in the next section.
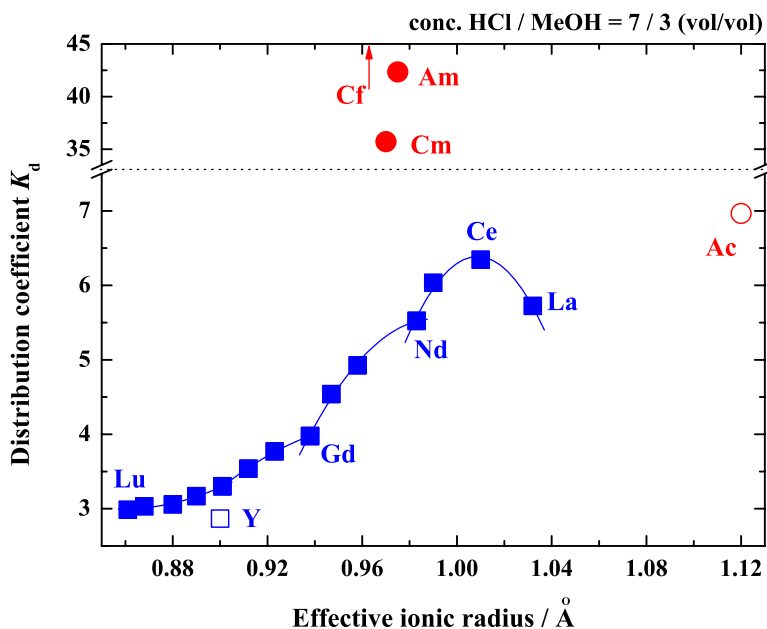
Figure 4-18. Variation of distribution coefficients of An(III), Ln(III), and Y in a conc. HCl / MeOH mixed solution as a function of their ionic radii. The error bars are smaller than the plotted points. (Solvent: 70 vol%-conc. HCl / 30 vol%-MeOH, Temperature: 293 K, Ionic radii: refer to [36])

4.4 Adsorption Equilibria in Chloride Solution System

In the previous sections, the adsorption and separation properties of the tertiary pyridine resin for An(III) and Ln(III) have been investigated by chromatography experiments. However, the chromatography process contains a variety of physical and chemical phenomena, such as diffusion or physical and chemical interactions, and, consequently, its adsorption and separation behavior are not necessarily consistent with the adsorption equilibrium that relates directly with the adsorptivity of the resin. Therefore, in order to investigate the net adsorption and separation properties of the pyridine resin more closely, batch experiments should be performed. Additionally, the tetrad effect observed in **Fig. 4-18** might be the evidence of the direct interaction of pyridine groups since it is generally considered that the tetrad effects observed in the complexation of Ln(III) (An(III)) ions originate in the different electron configurations of these cations [37–40], while the anion exchange reaction of Ln(III) (and An(III)) is mainly dominated by the size of their cations, obtaining a linear relationship between K_d and ionic radii as shown in **Fig. 3-23**. Further detailed discussion on this issue also requires the fundamental information obtained by batch experiments.

At first, adsorption (*i.e.* batch) experiments were performed in various HCl-LiCl mixed solutions in order to investigate the H$^+$ dependence of K_d. 11.7 mol/dm^3-LiCl solution was mixed with conc. HCl to give a constant Cl$^-$ concentration for all the mixtures. **Fig. 4-19** shows a variation of K_d of Ce, that gives the maximum K_d for all the Ln(III), as a function of [H$^+$]. The K_d gradually increased with a decrease of H$^+$ in solvent and this increasing tendency became drastic when [H$^+$] was lower than 2 mol/dm^3. The K_d in 11.7 mol/dm^3-LiCl solution was 20 times larger than that in conc. HCl. These results indicate that the pyridine resin can adsorb Ln(III) (and An(III)) ions more strongly in lower [H$^+$] conditions. On the other hand, **Fig. 4-20** shows a variation of K_d of Ce in different concentration of LiCl solutions. The pH of the solutions were lower than 5.5 and, accordingly, no hydrolysis of Ln cations should occur in these solutions [41]. (In fact, no precipitation was observed during the experiments.) The K_d decreased exponentially with a decrease of LiCl concentration and they became below 1 when [LiCl] ($\cong$ [Cl$^-$]) was lower than 6 mol/dm^3.
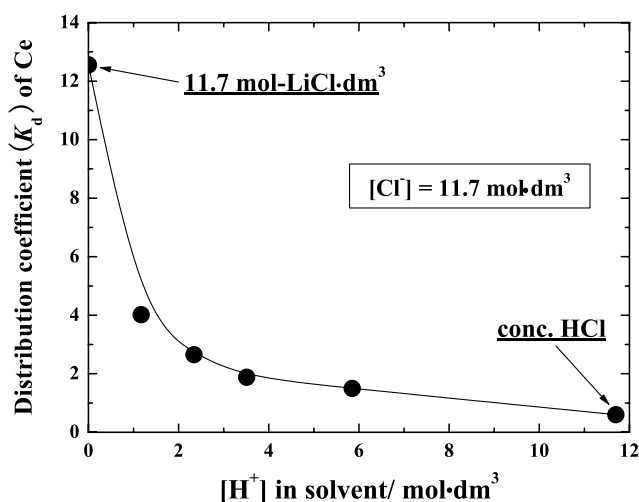
Figure 4-19. H$^+$ dependence of distribution coefficients of Ce in HCl/LiCl mixed solutions at 288 K. Concentration of Cl was fixed at 11.7 mol/dm^3. The error bars are smaller than the plotted points.

Figure 4-20. Variation of distribution coefficients of Ce in LiCl solutions at 288 K. The error bars are smaller than the plotted points.

Figure 4-21 represents the K_d variation of Ln(III) in conc. HCl / methanol (MeOH) mixed solutions (see also **Fig. IV-15** in Appendix IV). The adsorption of Ln(III) was enhanced by the addition of MeOH in solvent; distribution coefficients became maximum when the volume fraction of MeOH (X_{MeOH}) was 40-60%, although the distribution coefficients turned to decrease in higher X_{MeOH} range (*i.e.* $X_{MeOH} \geq 70\%$). This is in good agreement with the results of chromatography experiments (**4-2**). Similar convex variation was observed in the anion exchange systems using alcoholic mineral acid solutions [16–18], although the maximum K_d of these systems were found to be at over 90 vol% of alcohol. It should be noted that the ordinality of K_d of Ln(III) (*i.e.* lanthanoid pattern) showed clearer tetrad effect with an increase of atomic number than that observed in chromatography experiments and, furthermore, it changed drastically in larger X_{MeOH} solutions.
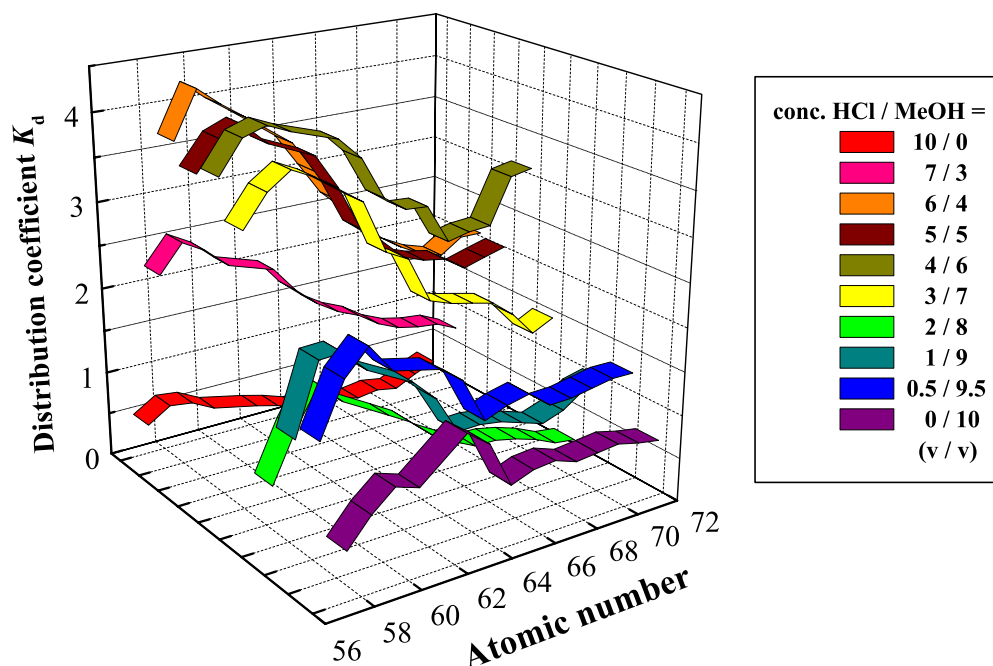
Figure 4-21. Variation of distribution coefficients of Ln(III) in different conc. HCl / methanol mixed solutions at 288K.

Figure 4-22 shows the lanthanoid patterns for "conc. HCl ∕ MeOH = 1 ∕ 9", "0.5 ∕ 9.5", and "0 ∕ 10", along with that for "conc. HCl ∕ MeOH = 7 ∕ 3". Until X_{MeOH} was 80% or below, the K_d of the Ln(III) except La showed a monotonous decreasing pattern, as shown in the upper graph of **Fig. 4-22**, with an increase in atomic number. However, this monotonous pattern began to break when X_{MeOH} was over 90%, presenting unique tetrad effects. Particularly, the tetrad effect for "conc. HCl ∕ MeOH = 0 ∕ 10", corresponding to pure methanol, was unprecedented and it showed no dependence on atomic number any longer. These results strongly support the presence of direct interaction between the cations and the pyridine groups of the resin. Moreover, the difference in the shape of tetrad effect may suggest that the interaction manner between the cations and the pyridine groups varies according to the solvent compositions.

It has already been found in the chromatography experiments that the adsorbability and separability of the pyridine resin are influenced by the type of alcohol employed. Accordingly, other batch experiments were performed in mixtures of conc. HCl and different six alcohols (four normal-chain and two branched-chain alcohols) in order to confirm the effect of alcohol types on the adsorption equilibria. The mixing ratio of conc. HCl and alcohol was fixed at "conc. HCl ∕ alcohol = 5 ∕ 5". The K_d of Ce in these different alcoholic HCl solutions are plotted in **Fig. 4-23**. A convex variation was observed for normal-chain alcohols, although most of their physical and chemical properties exhibit monotonous increasing or decreasing tendency with an increase of carbon number [20, 42]. Furthermore, branched-chain alcohols showed larger K_d than those of their corresponding normal-chain alcohols. The observed convex variation for normal-chain alcohols and the larger K_d of branched-chain alcohols over normal-chain ones are similar to the reported results of uranium adsorption on an anion exchange resin in alcoholic HCl solutions [18]. The results are also consistent with the results of chromatography experiments (**Fig. 4-4**).
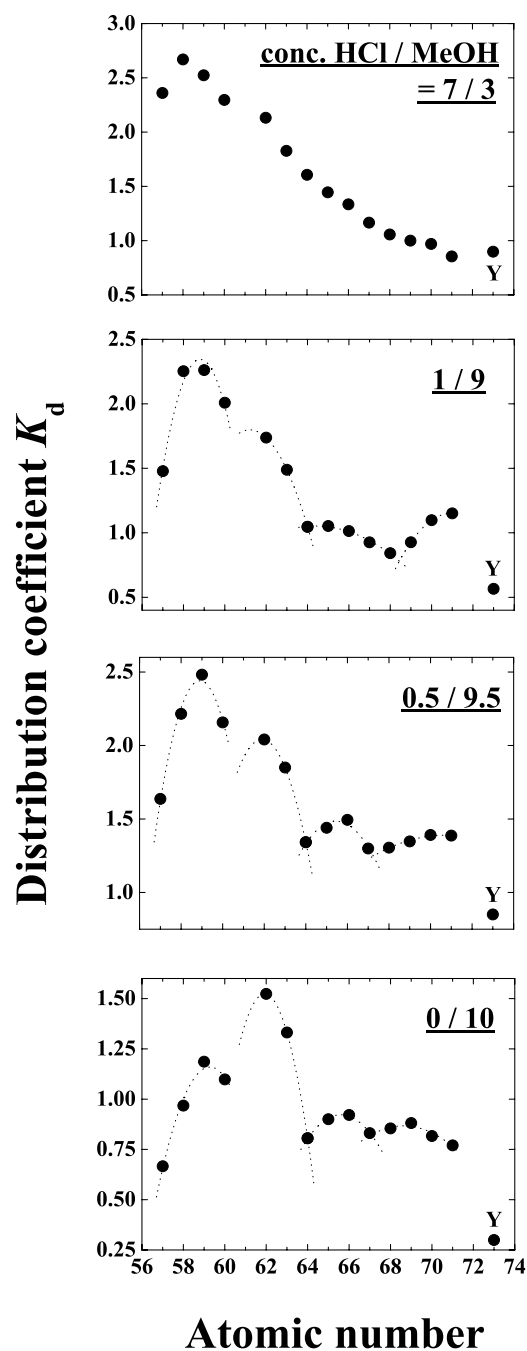
Figure 4-22. Distribution coefficients of Y and Ln(III) in different conc. HCl / methanol solutions at 288 K. The error bars are smaller than the plotted points.
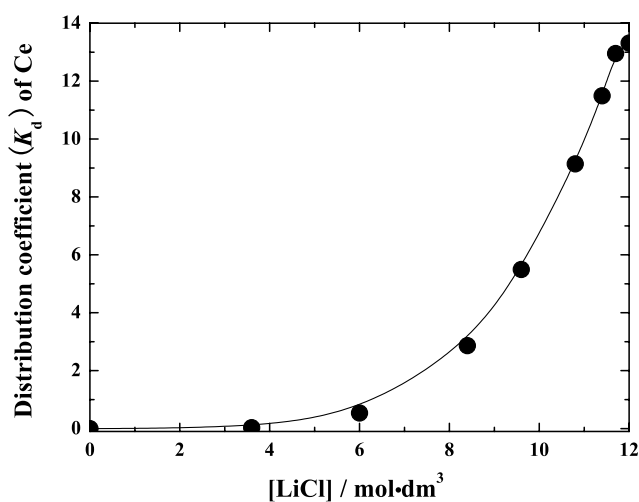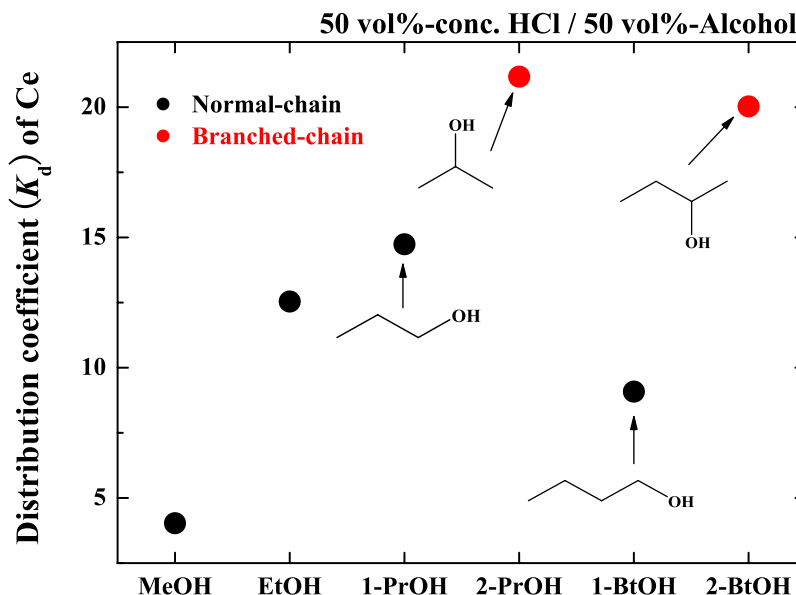
Figure 4-23. Variation of distribution coefficients of Ce in different alcoholic HCl solutions at 288 K. The error bars are smaller than the plotted points.

Although the H$^+$ dependence of K_d has already been investigated in aqueous HCl / LiCl solutions (**Fig. 4-19**), we should also confirm the dependence in the mixture of aqueous solution and alcohol because the solvent properties of water / alcohol mixed solutions are different from those of their pure solvents [43]. Then, the K_d of Ln(III) were determined in various methanolic HCl/LiCl mixed solutions and the results of Ce are shown in **Fig. 4-24**, along with the lanthanoid patterns for "conc. HCl / MeOH = 5 / 5" and "LiCl solution / MeOH = 5 / 5". X_{MeOH} was fixed at 50%, and the mixed solutions have a constant Cl$^-$ concentration of 5.85 mol/dm^3. The K_d lowered with a decrease of HCl concentration ($\cong$ [H$^+$]) in a higher HCl concentration range ($\sim$2 mol-HCl/dm^3). However, this decreasing tendency turned to a sudden increase when HCl concentration became lower than 1 mol/dm^3, giving different lanthanoid patterns. The observed variations in K_d and lanthanoid patterns for different solvent systems probably reflect the change of adsorption mechanism of tertiary pyridine resin. Further discussion will be made in chapter 5.
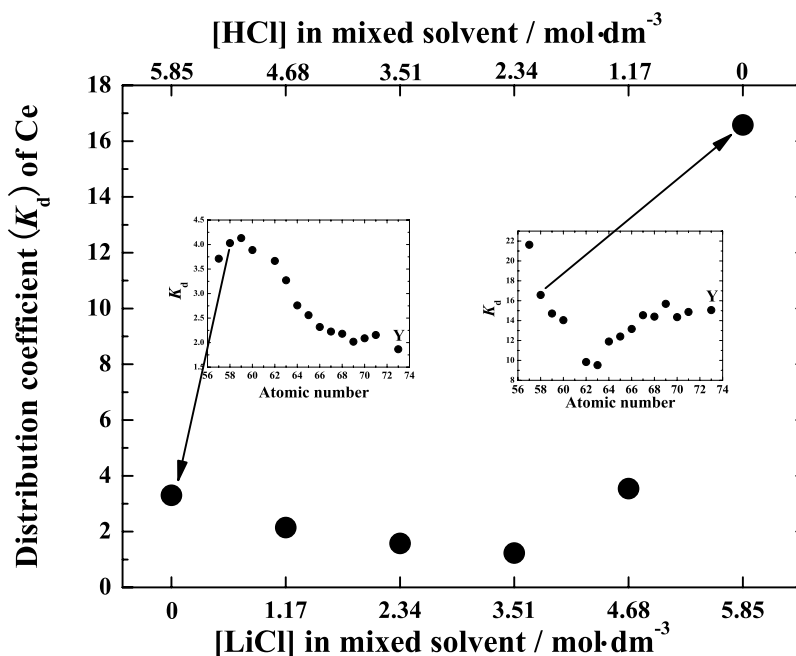
Figure 4-24. Variation of Distribution coefficients of Y and Ln(III) in methanolic HCl / LiCl solutions at 288 K. The volume fraction of methanol was fixed at 50%. The error bars are smaller than the plotted points.

4.5 Summary

The adsorption and separation behavior of An(III), Ln(III), and Y by a tertiary pyridine resin was investigated in various chloride solution systems both by chromatography and by batch experiments. The adsorbability of the pyridine resin for these elements depends on [H$^+$], [Cl$^-$], [H$_2$O], X_{alcohol}, and the type of alcohol. The adsorbability (= K_d) increases with a decrease of [H$^+$] or [H$_2$O], but decreases with a decrease of [Cl$^-$] and X_{alcohol}. A non-acidic solution system of LiCl solution shows far larger K_d than HCl system. The LiCl solution system has so large K_d that it is difficult to apply this solution system to a practical separation process. On the other hand, the HCl solution system exhibits moderate adsorbability and fine separability for the intergroup separation of An(III) and Ln(III) by adding alcohol in the solvent. Among the four normal chain monohydric alcohols (MeOH, EtOH, 1-PrOH, and 1-BtOH) and two branched monohydric alcohols (2-PrOH and 2-BtOH), 2-PrOH is the

most effective alcohol on the promotion of K_d and α, although even the most ineffective alcohol of MeOH brings sufficient intergroup separation. Dihydric alcohols such as ethylene glycol have no influence on the promotion of K_d or α. A mixed solution of conc. HCl and monohydric alcohol is the best solution for the separation of An(III) and Ln(III) by the pyridine resin.

The adsorptivity of the pyridine resin is also influenced by the properties of solvent, such as acidity. That is, the adsorptivity in the HCl system is quite different from that in the LiCl system or the alcoholic chloride solution system with higher X_{alcohol} (> ~90 vol%), bringing different lanthanoid (or actinoid) patterns and separability. That is, the LiCl and the alcoholic chloride solution systems show clear and unique tetrad effects on the K_d of Ln(III), while the tetrad effect does not appear so clearly in the HCl system.

In addition to the effect of solvent, the effects of temperature and flow rate were also investigated and optimized. The chromatographic behavior of An(III) and Ln(III) depends on the temperature and the adsorbability of the pyridine resin becomes larger in lower temperature, while the largest separability would be obtained at around 293 K. The effect of flow rate on the chromatographic behavior is so small that we can perform the chromatographic operation with sufficiently high flow rate (at least ~120 cm/h).

The chromatographic behavior of An(III) and Ln(III) in alcoholic chloride solutions was also confirmed by using various ion exchange resins and solid extractants and the results were compared with those of the pyridine resin. This comparative study suggests that the tertiary pyridine resin has outstanding selectivity for An(III) over Ln(III). This selectivity of the pyridine resin is probably attributed to the coordinative interaction of pyridine groups, not to the ionic interaction such as anion exchange reaction.

References

[1] *e.g.* H. F. Walton, "Ion-Exchange Chromatography", Dowden, Hutchinson & Ross, Inc., Pennsylvania (1976).

[2] K. Street, Jr., G. T. Seaborg, *J. Am. Chem. Soc.*, **72**, 2790 (1950).

[3] R. M. Diamond, K. Street, Jr., G. T. Seaborg, ibid., **76**, 1461 (1954).

[4] J. Korkisch, I. Hazan, *Talanta*, **11**, 1157 (1964).

[5] R. J. Morrow, ibid., **13**, 1265 (1966).

[6] S. Usuda, N. Shinohara, H. Yoshikawa, *J. Radioanal. Nucl. Chem., Art.*, **109**, 353 (1987).

[7] S. Usuda, ibid., **111**, 477 (1987).

[8] S. Usuda, N. Shinohara, H. Yoshikawa, S. Ichikawa, T. Suzuki, ibid., **116**, 125 (1987).

[9] S. Usuda, H. Yoshikawa, M. Magara, Y. Hatsukawa, *J. Radioanal. Nucl. Chem., Let.*, **117**, 329 (1987).

[10] S. Usuda, *J. Radioanal. Nucl. Chem., Art.*, **123**, 619 (1988).

[11] E. K. Hulet, R. G. Gutmacher, M. S. Coops, *J. Inorg. Nucl. Chem.*, **17**, 350 (1961).

[12] A. Dellesite, C. Testa, *Anal. Chim. Acta*, **72**, 155 (1974).

[13] E. P. Horwitz, R. Chiarizia, M. L. Dietz, H. Diamond, D. M. Nelson, ibid., **281**, 361 (1993).

[14] E. P. Horwitz, M. L. Dietz, R. Chiarizia, H. Diamond, S. L. Maxwell, III, M. R. Nelson, ibid., **310**, 63 (1995).

[15] E. P. Horwitz, R. Chiarizia, M. L. Dietz, *React. Func. Polym.*, **33**, 25 (1997).

[16] J. Korkisch, F. Tera, *J. Inorg. Nucl. Chem.*, **15**, 177 (1960).

[17] F. Tera, J. Korkisch, F. Hecht, ibid., **16**, 345 (1961).

[18] F. Tera, J. Korkisch, ibid., **20**, 335 (1961).

[19] J. Korkisch, G. E. Janauer, *Talanta*, **9**, 957 (1962).

[20]   ,   ,   ,   ,   , "   ",   , 1991.

[21] *e.g.* O. Mikeš, "Laboratory Handbook of Chromatographic Methods", D. Van Nostrand Company, Ltd., London (1966). or E. Heftmann, "Chromatography, 2nd Ed.", Reinhold Publishing Corporation, New York (1967).

[22] T. Ishihara, Master Thesis, Department of Nuclear Engineering, Tokyo Institute of Technology, Tokyo (2003).

[23] Y.-Z. Wei, M. Kumagai, Y. Takashima, M. Asou, T. Namba, K. Suzuki, A. Maekawa, S. Ohe, *J. Nucl. Sci. Technol.*, **35**, 357 (1998).

[24] Y.-Z. Wei, M. Yamaguchi, M. Kumagai, Y. Takashima, T. Hoshikawa, F. Kawamura, *J. Alloys Compd.*, **271**-**273**, 693 (1998).

[25] R. G. Pearson, *J. Am. Chem. Soc.*, **85**, 3533 (1963).

[26] R. G. Pearson, "Chemical Hardness", Wiley-VCH, Weinheim (1997).

[27] T. Yaita, S. Tachimori, *Radiochim. Acta*, **73**, 27 (1996).

[28] D. F. Peppard, G. W. Mason, I. Hucher, *J. Inorg. Nucl. Chem.*, **24**, 881 (1962).

[29] G. R. Choppin, P. J. Unrein, ibid., **25**, 387 (1963).

[30] T. Sekine, ibid., **26**, 1463 (1964).

[31] F. David, *J. Less-Comm. Met.*, **121**, 27 (1986).

[32] E. N. Rizkalla, G. R. Choppin, *J. Alloys Compd.*, **180**, 325 (1992).

[33] S. Usuda, *J. Radioanal. Nucl. Chem., Art.*, **111**, 399 (1987).

[34] M. Nogami, Doctor Thesis, Department of Nuclear Engineering, Tokyo Institute of Technology, Tokyo (1996).

[35] T. Arai, Doctor Thesis, School of Materials Science and Engineering, Shibaura Institute of Technology, Tokyo (2002).

[36] R. D. Shannon, *Acta Cryst.*, **A32**, 751 (1976).

[37] D. F. Peppard, G. W. Mason, S. Lewey, *J, Inorg. Nucl. Chem.*, **31**, 2271 (1969).

[38] S. Siekierski, ibid., **32**, 519 (1970).

[39] C. K. Jørgensen, ibid., **32**, 3127 (1970).

[40] L. J. Nugent, ibid., **32**, 3485 (1970).

[41] Y. Suzuki, T. Nagayama, M. Sekine, A. Mizuno, K. Yamaguchi, *J. Less-Comm. Met.*, **126**, 351 (1986).

[42] " ( )", , , 2000.

[43] K. Burger, "Solvation, Ionic and Complex Formation Reactions in Non-Aqueous Solvents", Akadémiai Kiadó, Budapest, 1983.

5   Adsorption and Separation Mechanisms of Trivalent *f*-Elements by Tertiary Pyridine Resin

5.1   Introduction

In the previous two chapters (chapters 3 and 4), the tertiary pyridine resin has displayed singular separability for trivalent *f*-elements, and several successful results, which give a bright prospect of the application of the separation system using the tertiary pyridine resin to the practical partitioning process for the treatment of HLW, have been achieved for the inter- and intragroup separations of An(III) and Ln(III) in alcoholic chloride and nitrate solution systems. However, these previous investigations have also brought up several questions about the adsorption and separation properties of the resin as follows:

- How does the pyridine resin adsorb An(III) and Ln(III)? (Is the interaction electrostatic (ion exchange) or coordinative?)

- What is the origin of the observed successful inter- and intergroup separations?

- Why is the adsorptivity, adsorbability, and separability in the chloride solution system different from those in the nitrate solution system?

- Why does the addition of alcohol in solvent promote the adsorption and separation?

As a matter of fact, these fundamental knowledge concerning the adsorption and separation mechanisms by organic polymers is essential for selecting appropriate solvent, optimizing solvent compositions, and designing the functional sites. Nevertheless, these kinds of phenomena occurred in organic polymer resins is still an open discussion for the most part even in the most well-developed system of ion exchange due to the poor available technique for analyzing this peculiar chemical system (*i.e.* the solid-liquid interface in solid). Therefore, it is significant to reveal the origin of the adsorption and separation phenomena by organic polymer resins not only for the engineering aspects, but also for their basic science.

In this chapter, the adsorptivity, adsorbability, and separability of the tertiary pyridine resin are discussed from several points of view. The adsorption and separation phenomena by the pyridine resin involve many factors.
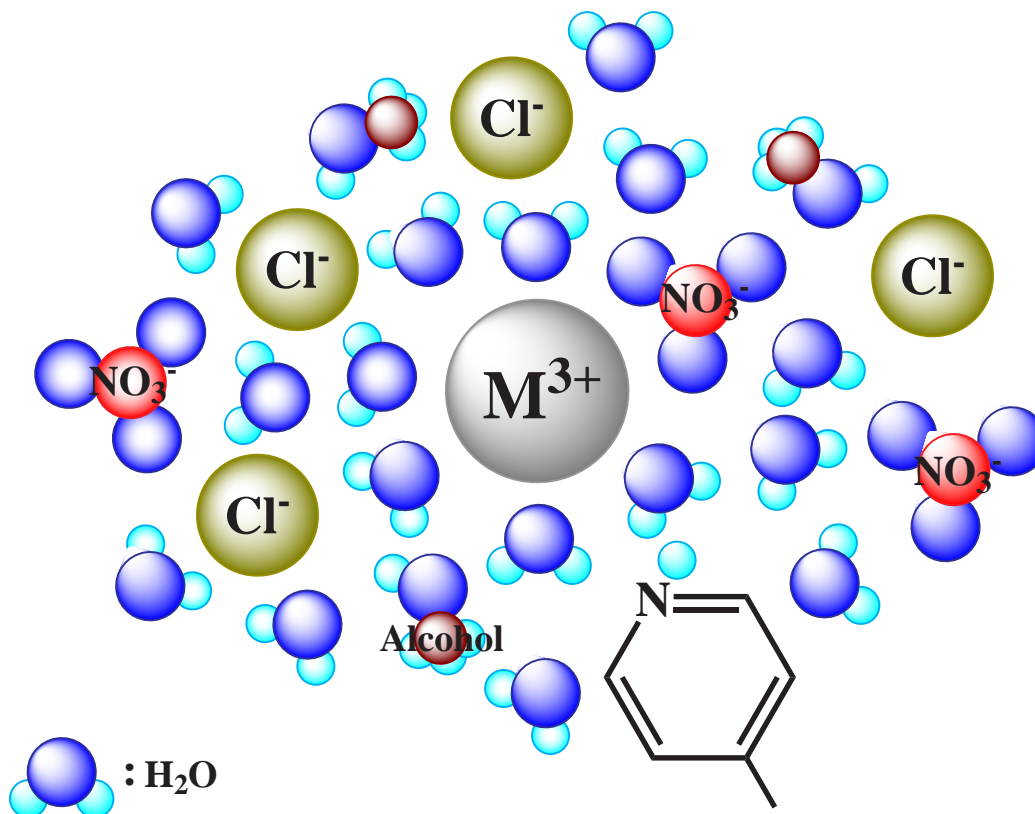
Figure 5-1. Chemical environment around metal cations in the present system.

As shown in **Fig. 5-1**, metal cations (in this study, An(III) and Ln(III)) are, first of all, hydrated by water molecules in aqueous solution. Then if there are some counter ion (*e.g.* Cl^- in chloride solution, or NO_3^- in nitrate solution) around the cations, the cations should form some complexes with these anions. When alcohol is added in the solvent, the alcohol molecules must have an influence on these hydration and anion complexation and, furthermore, the alcohol molecules may coordinate (solvate) to the cations directly. The metal cations diffuse in the solution phase with such complicated chemical environment and, when they approach the pyridine groups of the resin, they finally interact with the pyridine groups in some manner. The pyridine groups in the resin are also affected by the protonation. Considering these phenomena, the adsorption and separation mechanisms by the tertiary pyridine resin are discussed on the following four aspects in this chapter:

1 Solvation in the solution phase

2 Complexation property between trivalent f-element cations and pyridine ligands

3 Selectivity of pyridine ligands for An(III) and Ln(III)

4 Chemical species adsorbed in the pyridine resin

5.1.1   Hydration of Trivalent An and Ln

The present separation system using the tertiary pyridine resin is performed in aqueous solutions. Therefore, the hydration of metal cations (An(III) and Ln(III)) is the most primary factor for understanding the adsorption and separation behavior by the pyridine resin.

The hydration of Ln(III) ions have been well investigated from many points of view, while only a few reports can be found for the hydration of An(III) ions. The hydration of An(III) and Ln(III) ions have been structurally determined by XRD [1, 2], ND [3–6], and XAFS [7, 8]. The results are summarized in **Table 5-1** along with the theoretical M-O distances calculated from their effective ionic radii [9, 10]. The effective ionic radii of Ln(III) (and An(III)) gradually decrease with an increase of atomic number due to the lanthanoid (actinoid) contraction. Corresponding to this decrease of ionic radii, the M-O(H_2O) distances in the primary sphere also decrease with the decrease of atomic number. The M-O distances for An(III) are slightly larger than those for Ln(III) due to their larger ionic radii. Hence, the An(III) of Am and Cm are similar to the Ln(III) of Nd-Pm in the size of aquo complexes. The Ln(III) ions are hydrated by 8~9 water molecules in the primary sphere on average, while the An(III) ions hold 9~10 water molecules in the primary sphere. The hydration number (N_O) decreases from 9 to 8 for Ln(III) and from 10 to 9 for An(III) as increasing in atomic number. A transition state of N_O appears at around Eu-Gd for Ln(III) (*i.e.* $N_O = 9 \rightarrow 8$), giving a mixture of octaaqua and nonaaqua complexes [11]. The variation of apparent molar volume of aqueous Ln solutions also suggests this transition state [12, 13]. On the other hand, the transition state for An(III) is expected to be at around Cm-Cf [14].

In addition to these structural information, the thermodynamic data are also very informative for understanding the hydration of ions. The hydration enthalpy (ΔH_{hyd}) reflects the stability of the formed aquo complexes. It has been reported that the ΔH_{hyd} for An(III) and Ln(III) decrease (-ΔH_{hyd} increase) with the increase in

Table 5-1. Structural parameters of the hydration of An(III) and Ln(III) ions determined by different methods.

| | Theoretical | | XRD [1, 2] | | ND [6] | | XAFS [7] | | XAFS [8] | |
| | Octa [1] | Nona [2] | | | | | | | | |
	R (Å) [3]	R	R	N_O [4]	R	N_O	R	N_O	R	N_O
Y	2.379	2.435							2.36	9.7
La	2.520	2.576	2.580	9.13					2.54	9.2
Ce	2.503	2.556							2.52	9.3
Pr	2.486	2.539	2.539	9.22						
Nd	2.469	2.523	2.513	8.90	2.50	8.9	2.51	9.5	2.49	9.5
Pm	2.453	2.504								
Sm	2.439	2.492			2.46	8.5	2.45	9.3		
Eu	2.426	2.480					2.43	8.6	2.43	9.3
Gd	2.413	2.467					2.41	7.6		
Tb	2.400	2.455	2.409	8.18			2.39	7.5		
Dy	2.387	2.443	2.396	7.93	2.38	7.9	2.37	8.1		
Ho	2.375	2.432								
Er	2.364	2.422	2.369	8.19			2.34	7.8		
Tm	2.354	2.412	2.358	8.12			2.33	8.0		
Yb	2.346	2.402			2.32	7.9			2.32	8.7
Lu	2.337	2.392	2.338	7.97			2.31	7.7		
Ac	2.600	2.650								
Pa	2.520	2.570								
U	2.505	2.555								
Np	2.490	2.540								
Pu	2.480	2.530							2.51	9.2
Am	2.455	2.505							2.48	10.3
Cm	2.450	2.500							2.45	10.2
Bk	2.440	2.490								
Cf	2.430	2.480								

([1] Octagonal [M(H$_2$O)$_8$], [2] Nonagonal [M(H$_2$O)$_9$], [3] M-O(H$_2$O) distance, [4] hydration number)
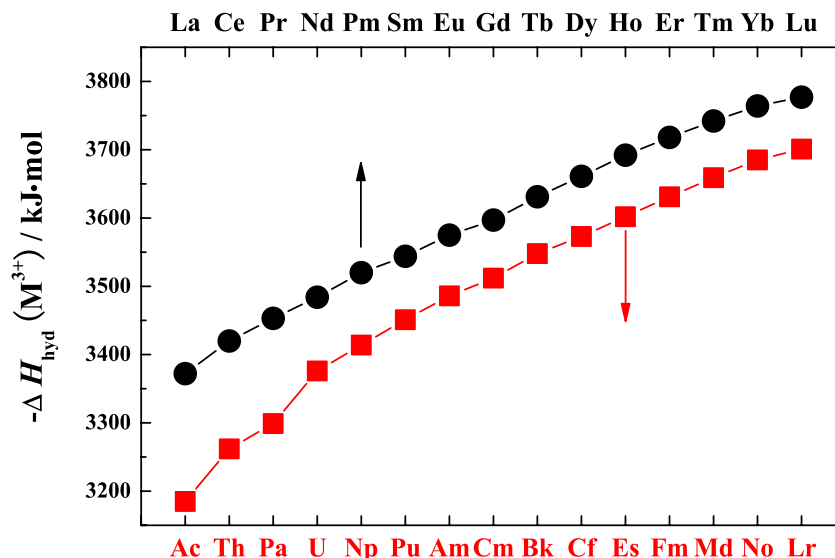
Figure 5-2. Variation of hydration enthalpy (ΔH_{hyd}) of An(III) and Ln(III) [15].

atomic number [15] (**Fig. 5-2**), indicating that the hydration of An(III) and Ln(III) ions becomes tighter as proceeding across the series and that the hydration of Ln(III) ions is tighter than that of An(III) ions.

On the other hand, an ^{17}O NMR study has revealed that the water exchange rate of Ln(III) aquo complexes decreases regularly with an increase of atomic number [16, 17]. Although the interpretation of these results are still open for discussion, this is in good agreement with the thermodynamic results mentioned above. That is, the aquo complexes of the heavier Ln are more stable than those of the lighter Ln, meaning that the heavier Ln are hydrated more tightly than the lighter ones. These phenomena can be interpreted as a result of the larger charge density of the heavier Ln over the lighter ones due to the lanthanoid contraction. Considering the facts that the hydration structures of An(III) ions are similar to those of Ln(III) ions and An(III) exhibit the actinoid contraction, the hydration of An(III) ions is also expected to be tighter as increasing atomic number.

To sum up these results, the following can be concluded:

• An(III) ions are hydrated by 9-10 water molecules in aqueous solutions, while Ln(III) ions are hydrated by 8-9 water molecules.

- The hydration number decreases gradually as an increase of atomic number for both An(III) and Ln(III) series.

- The M-O(H_2O) distance also decreases as the increase of atomic number for both series.

- The hydration becomes tighter with the increase of atomic number.

- The hydration of An(III) ions is expected to be weaker than that of corresponding Ln(III) ions.

5.1.2   Complexation with Chloride and Nitrate Ions

In the present study, An(III) and Ln(III) are separated by the pyridine resin in considerably high concentration of chloride or nitrate solution. Hence, the complexation of chloride ions (Cl^-) or nitrate ions (NO_3^-) must participate in the adsorption and separation phenomena to no small extent.

The stability (formation) constant of complex is the most simple and useful value to grasp their complexation behavior. The stability constants for the Cl^- complexes of An(III) and Ln(III) have been determined by several methods [18–22]. The obtained stability constants of the Cl^- complexes indicate that (1) the complexation between Cl^- ions and the cations is very weak, (2) it becomes weaker with an increase in atomic number, and (3) the complexation of An(III) is slightly stronger than that of Ln(III). Structural investigations also support these results: no Cl^- ion is observed in the primary (inner-) sphere of An(III) ions [8] and Ln(III) ions [1–5, 7, 8] but it is located in the secondary sphere [8, 23–25] in aqueous solution with moderate Cl^- concentration. The Cl^- ions can penetrate the primary sphere to coordinate the metal cations directly in higher Cl^- concentration ($[Cl^-] \geq 10$ mol·dm^3), but the coordination number of the nearest Cl^- (N_{Cl}) decreases as increasing atomic number for Ln(III) [8, 26].

To the contrary, the complex formation with NO_3^- ions is rather firm. The stability constants indicate that NO_3^- ions form firmer complexes with An(III) and Ln(III) ions than Cl^- ions [18, 20], although no significant difference can be observed between An(III) and Ln(III) [18, 20, 27]. In addition, UV/visible absorption [28–31], IR and Raman [32–34], NMR [35–38], and ultrasonic absorption [39] spectroscopic investigations and fluorescence lifetime measurement [40] have suggested that NO_3^-

ions directly coordinate to An(III) and Ln(III) ions and they form inner-sphere complexes even at low NO_3^- concentration ($[NO_3^-] = \sim 0.1$ mol·dm^3), while Cl$^-$ ions hardly form inner-sphere complexes, as described above. Furthermore, their coordination manner has been determined as bidentate and symmetric mode by XRD [41] and XAFS [42, 43]. The bond distances between the cations and NO_3^- decrease with an increase of atomic number [43].

The above-mentioned difference in coordination property brings not only the different complexation modes (*i.e.* inner- or outer-sphere complexation), but also the difference in the hydration dynamics of aquo complexes. Ions in aqueous solution can be classified into two groups according to their effects on the hydrogen-bonding network of water molecules: structure-breaking and structure making ions [44]. Both chloride ions and nitrate ions are basically categorized as structure-breaking ions. However, Yaita and his co-workers [38] have demonstrated by ^{139}La-NMR measurements that these two anions have different influence on the kinetics of the aqua-complexes of Ln(III): The structure-breaking ions break the hydrogen-bonding network of structured water by cutting the hydrogen bonds around them. Assuming that structure-breaking anions exist in the secondary sphere of aqua complexes of metal cations (in the present case, Cl$^-$ ions in the secondary sphere of An(III) and Ln(III) aqua complexes), the anions will break the hydrogen bonds between the water molecules in the primary sphere and those in the secondary sphere. This isolates the water molecules in the primary sphere from the hydrogen-bonding network formed in the outer-sphere of metal cations and, as a result, the hydration of metal cations becomes stronger in the primary sphere (the upper schematic of **Fig. 5-3**). On the other hand, the structure-making ions enhance the hydrogen-bonding network of structured water. Although NO_3^- ions are basically classified under structure-breaking ions, they have three oxygen atoms which can form some hydrogen bonds with water molecules. When NO_3^- ions are located in the primary sphere of An(III) and Ln(III) aqua complexes, hydrogen bonds will be formed between the anions and the structured water in the outer-sphere as the hydration water in the primary sphere forms the hydrogen bonds with the structured water in the outer-sphere (the lower schematic of **Fig. 5-3**). In this case, the water molecules in the primary sphere is pulled toward the outer-sphere by the hydrogen-bonded water molecules in the secondary sphere, as well as it is attracted by the metal cation. In consequence, the hydration structure in aqueous nitrate solution becomes looser compared with that in aqueous chloride solution. Thus, there is a large difference in the chemical

environment around the metal cations between the chloride solution system and the nitrate solution system and the difference affects the diffusion the cations in aqueous solution. This is surely one of the important factors to understand the different adsorption and separation behavior in these solution systems.

< in chloride solution>
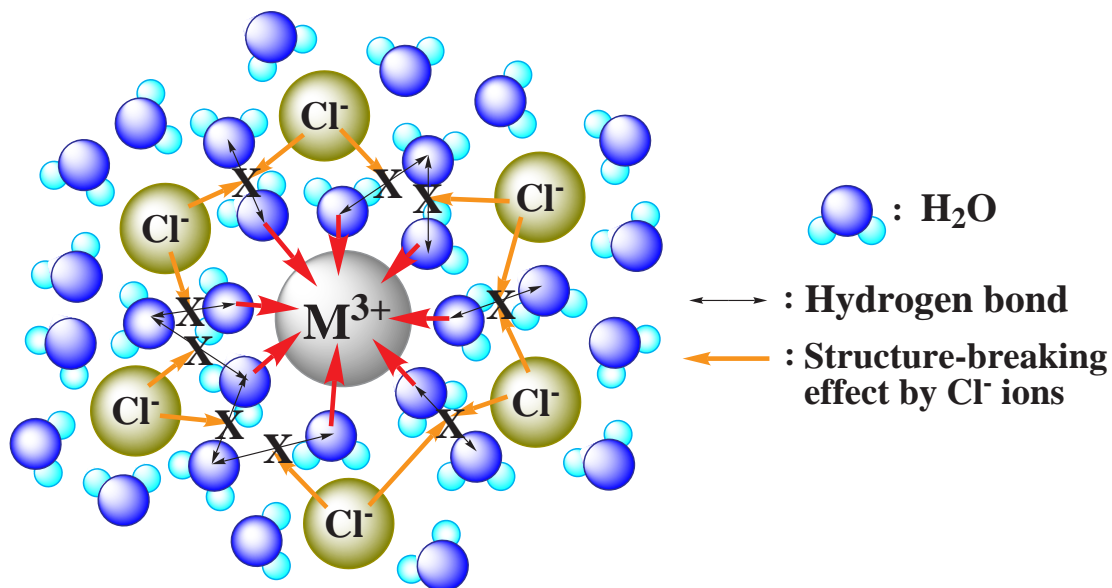
< in nitrate solution>
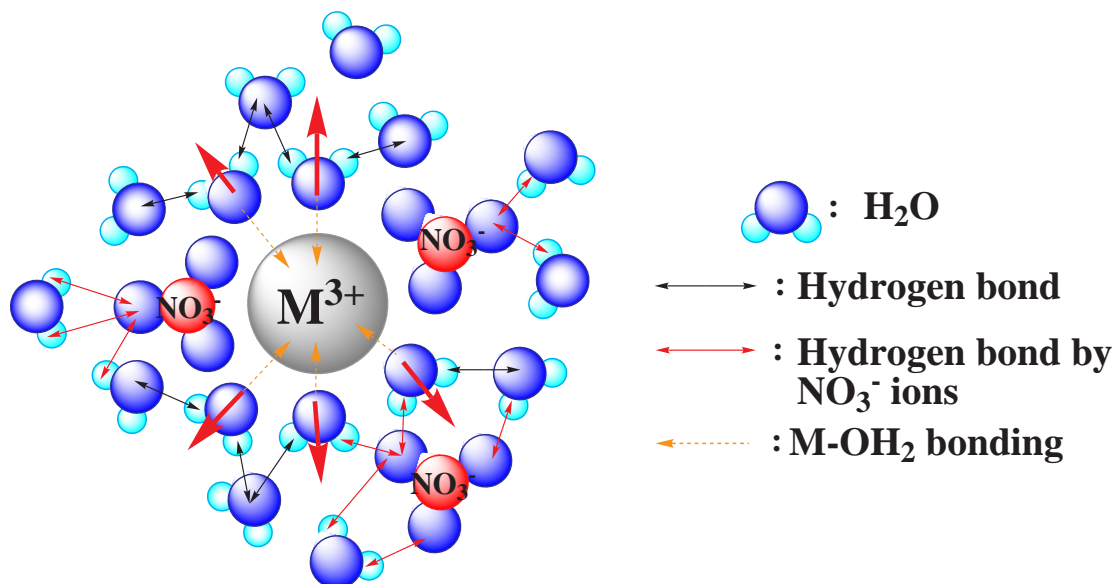
Figure 5-3. Different hydration dynamics of An(III) and Ln(III) aqua complexes in chloride and nitrate solutions. [38]

From the viewpoint of solvent, the addition of electrolytes in aqueous solution involves various phenomena, such as the rearrangement of hydrogen-bonding network or hydration of electrolytes, affecting the water activity (a_w). The a_w is closely related to the hydration and complexation of ions in aqueous solution. **Fig. 5-4** shows the variations of a_w in aqueous HCl, LiCl, and HNO_3 solutions (the data were reported in [45, 46]). The a_w decrease monotonously with increasing the concentration of electrolytes for all the solutions. Interestingly, these three electrolytes show no significant difference in their decreasing tendency for a_w. This means that the a_w simply depends on the concentration of electrolytes and it is independent of the type of electrolytes. **Fig. 5-4** also indicates that the a_w in conc. HCl (11.7 mol-HCl/dm^3) and conc. HNO_3 (13.5 mol-HNO_3/dm^3) are 60~70% smaller than that in water. This promotes the dehydration of ions and the complexation of ions with their couter ions.
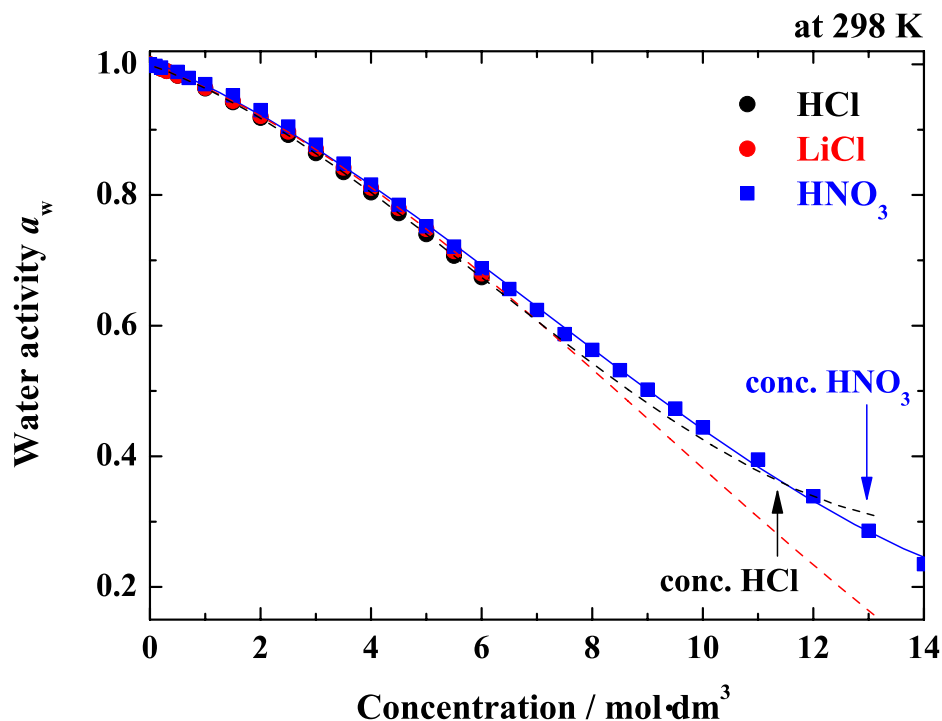
Figure 5-4. Variation of water activity (a_w) as a function of concentration of electrolyte at 293 K (HCl, LiCl: [45], HNO_3: [46]). The dotted lines for HCl and LiCl were drawn by the extrapolation of the plotted data using cubic functions.

5.1.3   Selectivity of Pyridine Type Extractants for Trivalent An and Ln

At this stage, two possibilities should be considered for the origin of the observed adsorption and separation phenomena by the tertiary pyridine resin, that is, the direct coordination of pyridine groups and the anion exchange interaction of protonated pyridine groups.

As described in **1.4** of chapter 1, soft donor type extractants have displayed sufficient selectivity for the intergroup separation of An(III) and Ln(III). Several soft donor extractants and their separation factors for Am over Eu ($\alpha_{Am/Eu}$) are summarized in **Table 5-2**. Obviously, the soft donor extractants prefer to extract An(III) rather than Ln(III). Although the origin of this high selectivity of soft donor ligands for An(III) still remains a subject of continuing scientific investigation, several studies have indicated that An(III) have a thermodynamic advantage on their complexation and extraction with soft donor ligands compared with Ln(III) [47–52]. Considering these facts, the direct coordination of pyridine groups is likely to be the origin of the enhanced adsorption of An(III) by the pyridine resin.

Table 5-2. Reported soft donor type extractants and their separation factors between Am and Eu on liquid-liquid extraction.

	Ligand	Organic phase	Aqueous phase	$\alpha_{Am/Eu}$(max.)	Ref.
N-donor	HBMPPT DPPhen	toluene	NaClO$_4$	196	[53]
	DPTP	TPH	HNO$_3$/NaNO$_3$	143	[54]
	TPEN	nitrobenzene	NH$_4$NO$_3$	100	[55]
	MPBIZ	chlorobenzene	NH$_4$SCN	65	[56]
	T^{t}BPTZ	TPH	HNO$_3$	11.9	[57]
S-donor	Cyanex 301	kerosene	NaNO$_3$	7.5×10^3	[47]

(HBMPPT: 4-Benzoyl-2,4-dihydro-5-methyl-2-phenyl-3H-pyrazol-3-thione, DPPhen: 4,7-Diphenyl-1,10-phenanthroline, DPTP: 2,6-Di(5,6-dipropyl-1,2,4-triazin-3-yl)-pyridine, MPBIZ: 6-Methyl-2-(2-pyridyl)benzimidazole, T^{t}BPTZ: Tritertiarybutyl-tri-pyridyltriazine, Cyanex 301: Bis(2,4,4-trimethylpentyl)dithiophosphinic acid, TPH: Hydrogenated tetrapropene)

On the other hand, the ion exchange technique has also been applied for the separation of An(III) and Ln(III) using various solvent systems (cation exchange in HCl [58–62], HNO$_3$ [63], ammonium citrate solution [58], and anion exchange in HCl [64, 65], HCl/LiCl [66], HNO$_3$ [62, 65, 67], several nitrate solutions [68], ammonium thiocyanate solution [69, 70]). However, no complete intergroup separation between An(III) and Ln(III) (*i.e.* An(III) are completely separated from the whole Ln(III)) has been achieved by these ion exchange separation systems. An anion exchange separation using high concentration of LiCl solution ([LiCl] = 10 mol·dm^3) seems to be the only successful example for the complete intergroup separation between An(III) and Ln(III) by ion exchange [71]. Interestingly, the adsorption and separation behavior of An(III) and Ln(III) in this anion exchange system is quite similar to that observed in the present separation system using the pyridine resin with LiCl solution. That is, An(III) are adsorbed in the resin more strongly than Ln(III), and the K_d of Ln(III) increase as an increase of atomic number (see **Fig. 4-5** in chapter 4). It should also be noted that this enhanced adsorption of An(III) appears only in a non-acidic chloride solution like LiCl solution, while it does not appear in the anion exchange system using an acidic chloride solution of HCl (*e.g.* **Fig. 4-17** in chapter 4 or **Fig. IV-13** in Appendix IV) or other electrolyte solutions such as nitrate solution. These results suggest that the chloride complexation can also be the origin of the higher selectivity of the pyridine resin for An(III) and, in addition, the pyridine resin adsorbs the cations in aqueous LiCl solution in the same way that anion exchange resin does, even if the pyridine groups are not protonated.

Considering these facts, both the direct coordination of pyridine groups and the chloride complexation have a potential for the intergroup separation of An(III) and Ln(III) and, accordingly, the origin of the observed selectivity of the pyridine resin is still unclear. Further discussion requires the information about the adsorption mechanism described in the next section.

5.2   Experimental

5.2.1   UV/Visible Absorption Measurements

The stability constants of Ln complexes with pyridine derivatives were determined by spectrophotometric titration to observe the chemical environment of pyridine in various conditions. All the measurements were made on an UV-visible spectrometer (JASCO V-560, **Fig. I-2** in Appendix I) with a 200 to 350 nm scanning range at room temperature ($\sim$293 K). The sample solutions were held in quartz cuvettes with 1.00 cm path length. In order to evaluate the stability constants, the spectrophotometric titration data were treated by the two calculation programs described in chapter 2. All the spectra were referred to the matrix solvent of sample solution. All the samples used in the measurements were prepared from reagent grade compounds and solvents supplied by Wako Pure Chemical Ind., Ltd. and Rare Metallic Inc.

5.2.2   XAFS Measurements

XAFS spectroscopy   The X-ray Absorption Fine Structure (XAFS) spectroscopy (also called X-ray Absorption Spectroscopy (XAS)) is a relatively recently established technique to obtain the information about the local structure (*i.e.* atomic arrangement) around a target atom. This technique is based on the excitation and scattering phenomena of electrons induced by the x-ray absorption of orbital electrons and it has been theoretically developed in the 1970s by Sayers, Lytle, and Stern [72–74], although its phenomenon has already been discovered in the early 1920s [75–79].

The left picture in **Fig. 5-5** shows a typical XAFS spectrum. When an atom is irradiated by x-ray, the atom absorbs specific energy of x-ray to excite its orbital electrons. This specific energy is called "x-ray absorption edge" or just called "absorption edge". When the excited electrons are the most tightly bound ones in the *1s*-orbit (n = 1), the edge is called the K-edge. For the next most tightly bound electrons in the *2s*- or *2p*-orbits (l = 1), the corresponding edges are called the L-edges. These absorption edges are peculiar to each element, giving XAFS spectroscopy high element selectivity.

In the photon range around the absorption edge (20$\sim$30 eV), the x-ray photons are absorbed to excite the orbital electrons to higher unoccupied levels of the atom
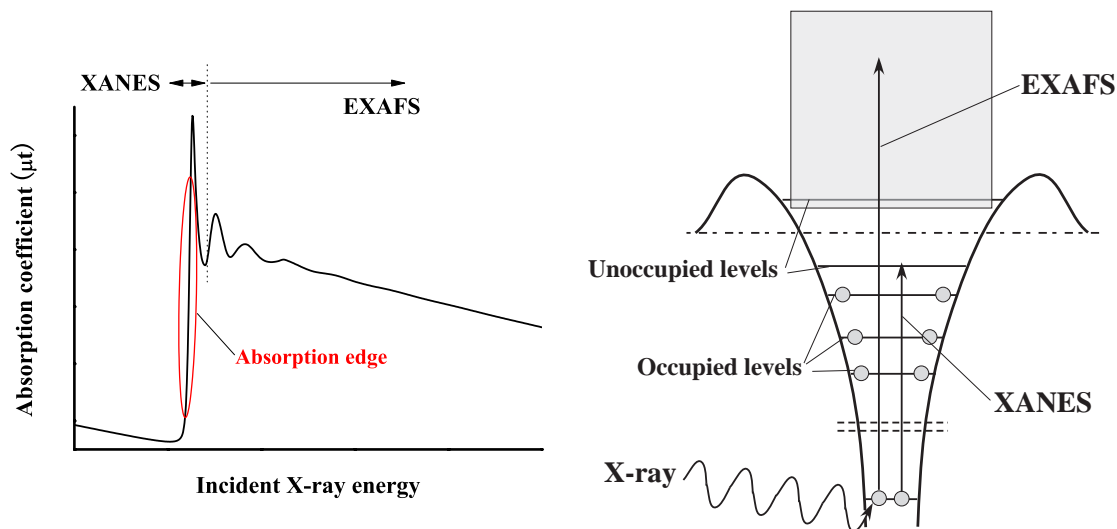
Figure 5-5. Typical XAFS spectrum (left) and schematic of x-ray absorption phenomena (right).

(right graph in **Fig. 5-5**). This absorption process, called XANES (X-ray Absorption Near-Edge Structure), reflects the electronic property of the absorbing atom and, therefore, analyzing this XANES region brings us some electronic information of the atom, such as oxidation states or electronic configurations. On the other hand, when x-ray photons give the atom enough energy to free its bound electrons from the orbits, the atom releases the electrons and the released electrons are scattered around the atom. If the atom is isolated from other atoms (*i.e.* if it is a "single" atom), the scattering electrons are just spread out and, as a result, no XAFS is observed in the absorption spectrum. However, if the atom is surrounded by other atoms, some of the outgoing electrons will be backscattered by the surrounding atoms and come back the original atom. This backscattering phenomena affects the orbital function (ψ) of the initial atom, causing a wiggly structure in the absorption spectrum up to 40 keV as EXAFS (Extended X-ray Absorption Fine Structure). Obviously, this electron-scattering process which causes EXAFS is dominated by the type and arrangement of surrounding atoms. Consequently, interpreting the EXAFS spectrum gives the information about the local structure of the target atom. Theoretical details of XAFS are described in several famous books and articles [80–82]. In the present study, the structural information (*i.e.* solvation and coordination structures) of metal cations (Ln(III)) both in solution phase and in resin phase are determined by analyzing this EXAFS region.

The advantages of XAFS spectroscopy for structural analysis are as follows:

1 Any form (*i.e.* solid, liquid, gaseous) of sample can be measured in the same manner.

2 In principle, any element is measurable.

3 As mentioned above, high element selectivity is obtained.

4 The measurements are simple, easy, and rapid.

In order to understand the adsorption mechanism by the resin, the chemical information of adsorbed ions both in the solution phase and in the resin phase is required. There are several methods, such as UV-visible absorption, NMR, or some electrochemical measurements, to study the chemical species in solution. However, these methods give no structural information (*e.g.* distance or coordination number) directly and, moreover, the measurable elements are often limited. X-ray diffraction (XRD) or neutron diffraction (ND) method can be applied to the structural analysis of solution samples by using specific technique such as isotopic substitution [83] or anomalous scattering [84], although measurable elements are limited and considerably high concentration (< 1 mol·dm^3) of sample is required. On the other hand, few methods are available for acquiring the chemical information in the resin phase. This is the main reason why the phenomena occurred in the resin phase is still unclear. Organic resins do not transmit UV-visible light. The application of NMR to solid samples is still very limited. IR spectroscopy is not applicable for the samples holding water. It is also difficult to measure noncrystalline resin samples by diffraction methods. Considering these facts, we can conclude that XAFS spectroscopy is the only method to obtain the chemical information in the solution and resin phases in the same manner.

Data treatment   In XAFS measurements, the intensities of incident x-ray (I_0) and those of transmitted x-ray (I_T) or fluorescent x-ray (I_F) are monitored at each energy step and the x-ray absorbance ($\mu(E)$) is calculated from these values as follows:

$$\mu(E_T) = \ln\left(\frac{I_0(E)}{I_T(E)}\right) \tag{1}$$

or

$$\mu(E_F) = \frac{I_F(E)}{I_0(E)} \tag{2}$$

In the present study, the obtained XAFS spectra ($\mu(E)$) were treated according to a standard procedure [81]: background subtraction using Victoreen function, and normalization, extraction of XAFS oscillations by cubic spline fitting. Then the extracted XAFS oscillation ($\chi(k)$) was fitted by the following standard XAFS formula:

$$\chi(k) = S_0^2 \sum_j \frac{N_j F_j(k)}{kR_j^2} \cdot \exp\left(-2k^2\sigma_j^2\right) \cdot \exp\left(\frac{-2R_j}{\lambda}\right) \cdot \sin[2kR_j + \delta_j(k)] \tag{3}$$

where S_0^2 is the probability of intrinsic loss (generally called "amplitude reduction factor"), N_j and R_j are the coordination number and distance of the *j*-th atom, $F_j(k)$ and $\delta_j(k)$ are the amplitude of backscattering and the phase shift by the *j*-th atom, σ is related with the thermal vibration of scattering atoms (so called "Debye-Waller factor"), and $\exp(-2R_j/\lambda)$ is the term of extrinsic loss. In the present study, $F_j(k)$, $\delta_j(k)$, and λ (photoelectron mean free path) were calculated by the *ab-initio* self-consistent real space multiple-scattering program FEFF 8.00 [85, 86] using appropriate reference samples or hypothetical compounds based on the reported crystal structures. The fitting was done both in the *k*-space and in the *R*-space. Structural parameters (coordination number (*N*), inter-atomic distance (*R*), and Debye-Waller factor (σ)) were obtained from the curve fitting both in *k*-space (raw and back Fourier transformed spectra) and *R*-space. The shifts in threshold energy, ΔE_0, were allowed to vary from -10 to 10 eV for each fitting, but it was held constant for all coordination shells. These data treatments and fittings were performed on the same program WinXAS (Ver. 3.1) [87].

Necessity of synchrotron XAFS spectra are measured by changing the energy of incident x-ray and by monitoring the intensity of incident and transmitted (or fluorescence) x-rays. Therefore, the ideal right (x-ray) source for XAFS measurements should have flat and continuous radiation spectrum in a wide range of photon energy with high brightness. To the contrary, if the right source generating monochromatic or quasi-monochromatic spectrum is employed for XAFS measurements, the intensity of incident x-ray changes for each photon energy, breaking the linearity of detection efficiency of detectors during the measurements. Furthermore, a bright right source is required for obtaining as low signal-to-noise ratio (S/N ratio) as possible.

An x-ray tube is the most common x-ray source in laboratory scale. The x-ray tube generates x-rays by the bremsstrahlung of electrons. This x-ray source is very

simple and easy to handle. However, it has a very peaky radiation spectrum due to the characteristic x-rays (**Fig. 5-6**) and its x-ray intensity is not sufficiently large to perform XAFS measurements even using rotating anode type source. (In fact, we can perform XAFS measurements with the x-ray tube by avoiding the characteristic x-rays of anode materials. However, it needs many hours to obtain a spectrum with sufficient S/N ratio. For instance, I measured one solution sample by using the x-ray tube (rotating anode type) and it took ∼24 hours to obtain a sufficient spectrum for data treatment.) These properties of x-ray tubes surely deteriorate the quality of XAFS measurements.

On the other hand, the synchrotron radiation, which has been developed in the 1970s, is a desirable light source for XAFS measurements. That is, it can generate a flat, wide, and continuous radiation spectrum with considerably high brightness (10^4∼ larger than that by the x-ray tube), as shown in **Fig. 5-6**. These properties of synchrotron radiation allow much more rapid and reliable XAFS measurements.In fact, the development of synchrotron radiation facilities has greatly expanded the use of XAFS technique. In the present study, XAFS measurements were carried out by using two synchrotron radiation facilities, SPring-8 and Photon Factory (High Energy Accelerator Research Organization (KEK)).
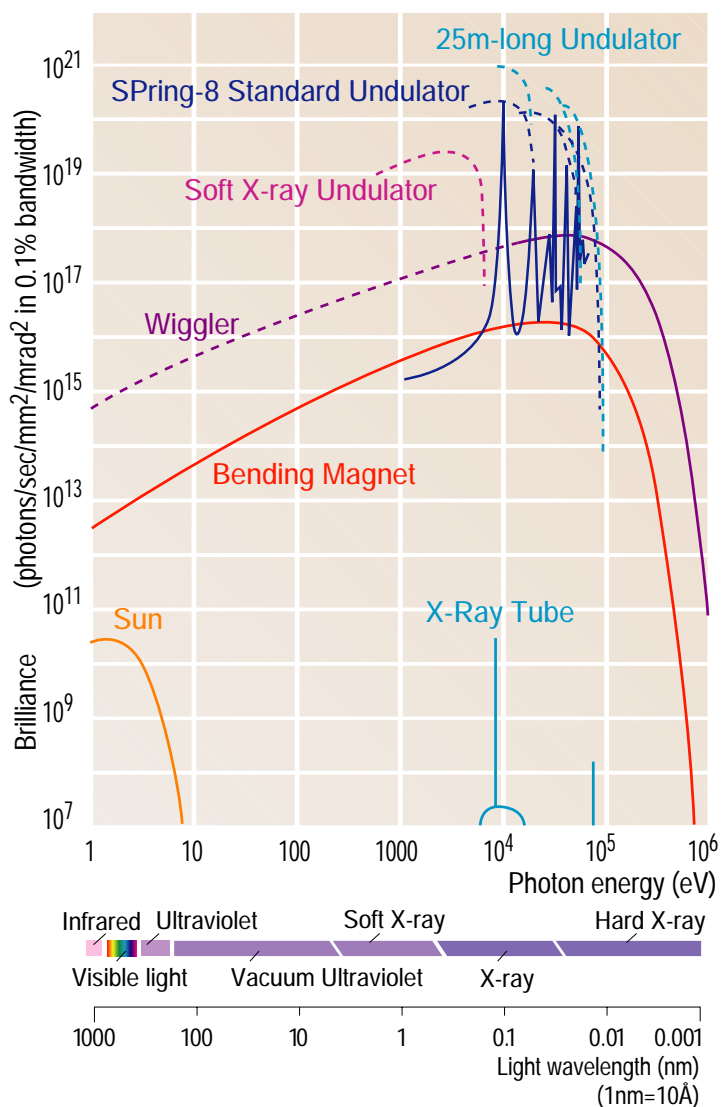
Figure 5-6. Radiation spectra from different light sources [88].

Samples, apparatus, and procedures   Solution samples for XAFS measurements were prepared by dissolving hydrated Ln(III) chlorides (LnCl3 nH2O, 99.9%-purity) or their nitrates (Ln(NO$_3$)$_3 \cdot n$H$_2$O, 99.9%-purity) into a desired solution to give a constant metal concentration of 0.1 mol·dm^3. Then the sample solution was doubly sealed in a polyethylene bag and was held between two Al plates with a Teflon spacer of suitable thickness. The Ln compounds were supplied by Rare Metallic Co., Ltd., Japan. Other chemicals such as solvents were reagent grade and supplied by

Wako Pure Chemical Ind., Ltd., Japan.

Resin samples were prepared by mixing polymer pyridine resin (10 vol%-closslinkage, 20 wt%-porosity) with a solution containing 0.1 mol·dm^3 of Ln(III) in a desired solvent, shaking the mixture for 24 h at 288 K, and filtering the resin from the solution. When the sample was measured by transmission mode (La-Nd K-edges), the filtered sample was packed in polystyrene cuvettes and sealed up by Parafilm. On the other hand, the samples were doubly sealed in a polyethylene bag without any spacer and placed on a polystyrene plate for fluorescence mode measurements (Ln L_{III}-edges).

In the present study, XAFS spectra of Ln samples were basically collected at their L_{III}-edges. However, it is well-known that the L_{III}-edge XAFS spectra of lighter Ln (especially La-Nd) suffer from the multielectron excitations [89], which make another undesirable XAFS oscillation. In addition, their available spectrum ranges are so short ($k = \sim11$ Å^{-1}) that their Fourier transformed spectra (*i.e.* radial structural function (RSF)) become broad and unclear. In order to avoid these problems, the XAFS spectra of the lighter Ln (La-Nd) were also collected at their K-edges. One sample was measured repeatedly at least three times and the obtained spectra were averaged for data treatment.

Ln(III) L_{III}-edges and Y K-edge XAFS spectra were measured at the beamlines BL-7C, BL-12C, and BL-27B of Photon Factory (2.5 GeV, 350-400 mA), KEK using a Si(111) monochromator. All the solution samples were measured in transmission mode using ion chambers which are filled with suitable gases (He, N$_2$, Ar, and their mixtures) for monitoring the intensities of incident and transmitted x-rays. On the other hand, the resin samples were measured in fluorescence mode using a 7-element solid-state detector. All the measurements were performed at room temperature. The incident flux from the synchrotron was reduced to 60-70% of its maximum at around adsorption edges to remove the effect of higher-order harmonics. The detection system for XAFS measurements in transmission and fluorescence modes is illustrated in **Fig. 5-7**. In the fluorescence mode measurements, samples were arranged at an angle of $45°$ (the fluorescent x-rays were detected at a right angle) to the incident x-ray in order to minimize the influence of scattering x-rays.

K-edge XAFS measurements for lighter Ln (La-Nd) were performed at the beamline BL11XU of SPring-8 (8 GeV, 99 mA) using Si(311) monochromator. All the measurements were carried out in transmission mode using ion chambers filled with N$_2$ and 50 vol%-N$_2$ / 50 vol%-Ar mixed gases for monitoring the intensities of incident and transmitted x-rays, respectively. The beamline BL11XU utilizes an in-vacuum
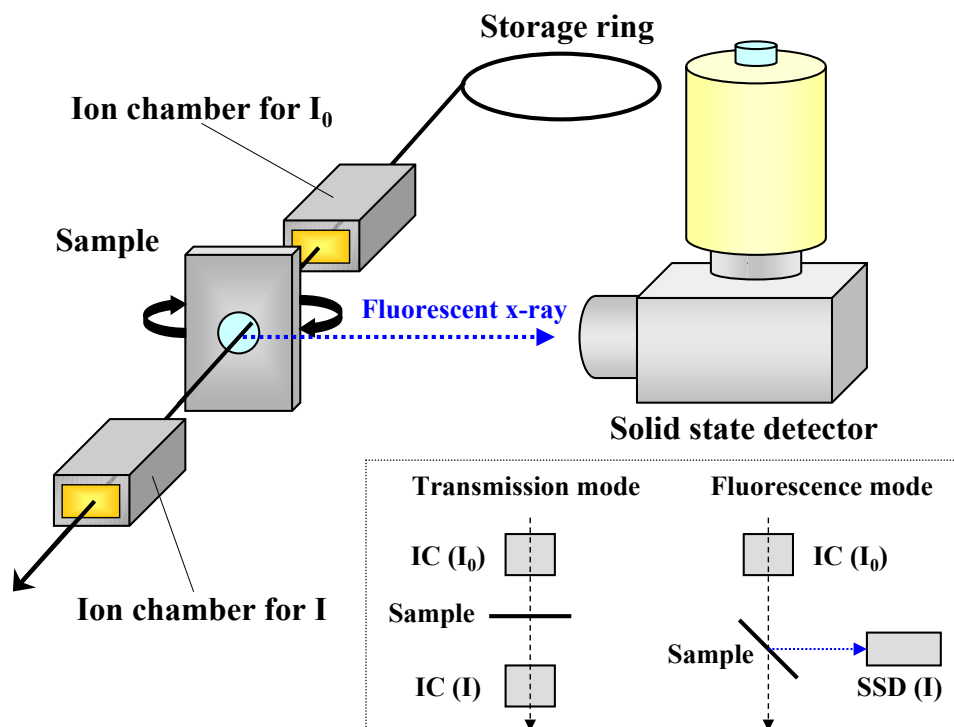
Figure 5-7. Detection system for XAFS measurements in transmission and fluorescence modes.

type linear undulator as an insertion device for generating extremely high-flux x-ray [90]. Although undulator beamlines can produce considerably higher flux of x-ray than the beamlines using bending magnets, their radiation spectra become quasi-monochromatic (**Fig. 5-6**) and, therefore, it is not a desirable light source for XAFS measurements. In order to apply this quasi-monochromatic (but extremely high-flux) light source to XAFS spectroscopy, the gap (the distance between the magnets of undulator) was adjusted to obtain the strongest x-ray intensity for each energy step in the present study, coping both with high flux and smooth radiation spectrum. The Si(311) monochromator employed was cooled by liquid nitrogen to prevent the crystals from melting. However, this cooling system by liquid nitrogen vibrates the monochromator, destabilizing the position and intensity of incident x-ray. Then, in the present study, the monochromator stabilization system (MOSTAB [91]) was employed to stabilize the incident x-ray [92, 93] (**Fig. I-10** in Appendix I).

Further information about the detection systems for XAFS measurements are summarized in **Table I-1** in Appendix I.

5.3   Results and Discussion I
Solvation Structure in Solution Phase

5.3.1   Property of Water-Alcohol Mixed Solvents

It is well-known that the solvent property of water-organic solvent mixed solutions is different both from that of pure water and from that of pure alcohol and, moreover, it often shows an irregular variation with a change of its solvent composition (*i.e.* mixing ratio). The separation system developed in this study employs water-alcohol mixed solutions as separating solvent of chromatography. Therefore, the consideration of the solvent property of water-alcohol mixed solutions must be very important to understand the adsorption and separation mechanisms in the present separation system.

Dielectric constants   The dielectric constants (DC: ε) of solvent is one of the most fundamental and important values which express the solvent property. Fortunately, the ε of various water-alcohol mixtures have already been investigated in detail by Åkerlöf [94]. **Fig. 5-8** shows variations of ε for several alcohols-water mixed solutions as a function of the volume fraction of alcohol in solvent ($X_{alcohol}$) (left graph) and their temperature dependence (right graph). The ε decrease monotonously as an increase of $X_{alcohol}$ for all the mixtures. The degree of the decreasing tendency becomes larger as the following order: EtGly > MeOH > EtOH > 1-PrOH > 2-PrOH, corresponding to the order of the ε of their pure alcohols. These results indicate that the macroscopic polarity of water-alcohol mixed solutions decreases with the increase of $X_{alcohol}$ and its decreasing tendency depends on the type of alcohol added. The polarity of solvent has an influence on the hydration and complexation of metal cations in the solvent. Of course, the macroscopic property is not necessarily connected directly with the microscopic phenomenon. However, the polarity of solvent is still one of the important factors to be considered. The ε also decrease with increasing temperature. This tendency is usually interpreted as the disruption of the cooperative effect of hydrogen-bonding network [44]: the increase in temperature promotes the thermal motion of solvent molecules and some part of the associated solvent molecule group formed by the cooperative effect of hydrogen bonds is broken. This probably changes the dipole moment of the associated solvent molecule

groups and, consequently, the ε decreases. Viscosity measurements of water-alcohol mixtures also support this model [97].
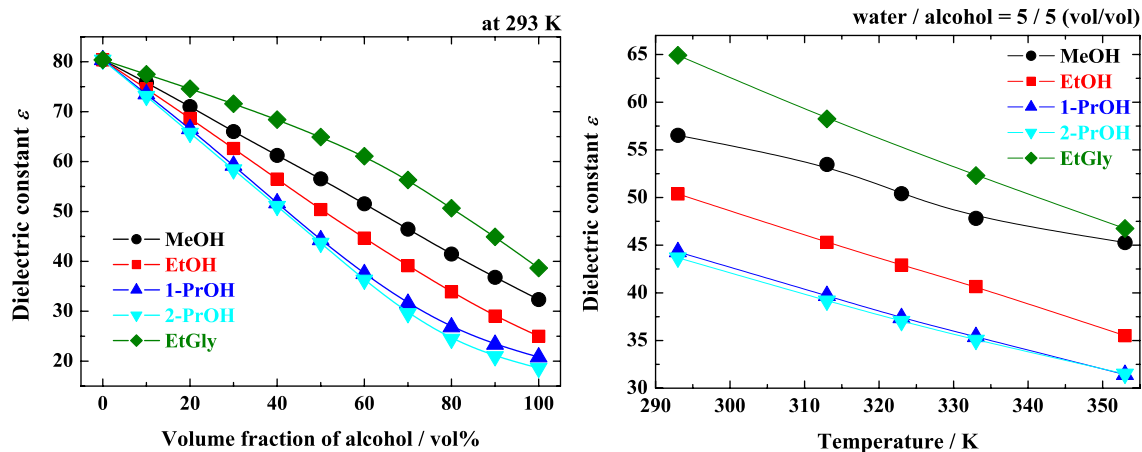
Figure 5-8. $X_{alcohol}$ (left) and temperature (right) dependence of dielectric constants (ε) of water-alcohol mixed solutions. [94]

Association of solvent molecules   The association (cluster) structure of solvent molecules has a great influence not only on the basic properties of the solvent but also on various phenomena occurred in the solvent, such as hydration, solvation, or complexation. The association structure of solvent molecules in water-alcohol binary solution system have been extensively studied by several researchers using general XRD [98–100], small-angle x-ray scattering (SAXS) [101–103], NMR [104], Rayleigh light scattering [105], mass spectrometry [99, 100], and frequency dielectric measurements [106–108]. These studies suggest that alcohol molecules added in water are hydrated by several tens of water molecules in a lower $X_{alcohol}$ region ($X_{alcohol} < \sim$15 vol%), then some clusters are formed with the hydrated alcohols in a moderate $X_{alcohol}$ region ($\sim$15 $< X_{alcohol} <$ 60$\sim$70 vol%), and finally the aggregation of alcohol molecules occurs in a higher $X_{alcohol}$ region ($X_{alcohol} <$ 70$\sim$ vol%). The hydration number (N_{hyd}) of the hydrated alcohols depends on the size of alcohol molecule and it increases with increasing carbon number of alcohol. Branched-chain alcohol

molecules, such as 2-PrOH or 2-BtOH, seem to be hydrated more easily than the corresponding normal-chain alcohols because the branched alcohol molecules have spherical hydrophobic groups and it causes less distortion of the hydrogen-bonding network of water compared with the corresponding normal alcohols which have linear hydrophobic groups [102, 105]. Although it is still unclear how the structural change of associated solvent molecules affects the activity coefficients (γ_w) of water molecules and other electrolytes in the solvent, the hydration and complexation of ions in the solvent are surely influenced by this change. At least, adding alcohols in aqueous solution decreases the water activity ($a_w = \gamma_w\, m_w$, where m_w is the concentration of water) by just lowering m_w.

Thermodynamics of solvation of ions   Thanks to the extensive work by Hefter, Marcus, and Waghorne [109], very informative thermodynamic parameters are available concerning the transfer of ions from water to water-alcohol mixed solvents, which reflects the preferential solvation in the mixed solvents. **Fig. 5-9** gives the variation of the standard enthalpies of transfer ($\Delta_{trans}H^O$) of protons (H^+, left) and chloride ions (Cl^-, right) from water to water-alcohol mixed solvents for several alcohols. The $\Delta_{trans}H^O$ vary irregularly with an increase of $X_{alcohol}$ and each alcohol shows its own variation pattern. To judge from the values of $\Delta_{trans}H^O$, H^+ seem to be solvated in the mixed solvents more preferably than in pure water ($\Delta_{trans}H^O$ become negative) in higher $X_{alcohol}$ region, although $\Delta_{trans}H^O$ become positive when $X_{alcohol}$ is under 60% for MeOH and 20% for EtOH and 1-PrOH, respectively. To the contrary, Cl^- show positive $\Delta_{trans}H^O$ for almost the whole $X_{alcohol}$ region except for MeOH mixture, suggesting that Cl^- prefer to be solvated in pure water rather than in the mixed solvents. **Fig. 5-10** shows the variation of $\Delta_{trans}H^O$ of several cations (left) and anions (right) for the transfer from water to water-MeOH mixed solvent. H^+ and Li^+ exhibit a similar variation and they are preferably solvated in the MeOH mixed solvent when X_{MeOH} is over 60%. La^{3+} also exibits similar variation, but it shows far larger $\Delta_{trans}H^O$ in higher X_{MeOH} region, indicating that the solvation of La^{3+} (and probably An(III) and Ln(III)) becomes stronger in water-alcohol mixed solvents than in pure water. This means that excessive alcohol in solvent hinders the complexation of metal cations due to its strong solvation effect. On the other hand, Cl^- and NO_3^- show similar irregular $\Delta_{trans}H^O$ variations and they prefer to be solvated in pure water in lower and higher X_{MeOH} regions. These kinds of information is very helpful in the interpretation of the effect of alcohol on the adsorption and separation mechanisms.
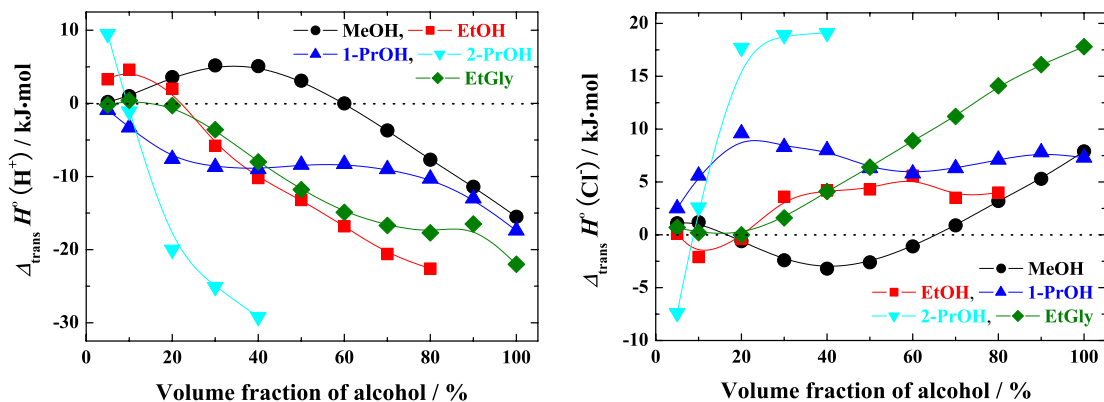
Figure 5-9. Variation of $\Delta_{trans}H^O$ of protons (left) and chloride ions (right) from water to water-alcohol mixed solvents [109].
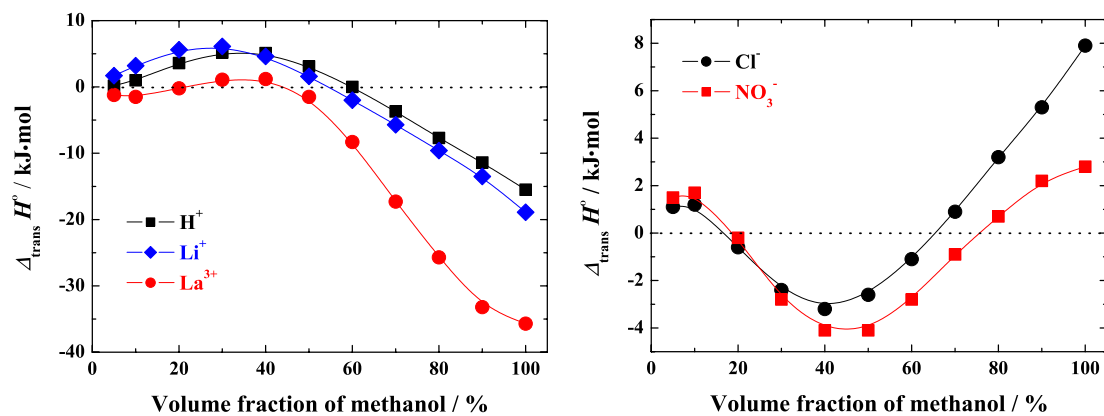

Figure 5-10. Variation of $\Delta_{trans}H^O$ of several cations and anions from water to water-MeOH mixed solvent [109].

Hydration and anion complexation in water-alcohol mixed solvents As described above, the property of water-alcohol mixed solvents is different from that of pure water or that of pure alcohols. Hence, the hydration and anion complexation of metal cations in the mixed solvents must also be different from those in the pure solvents. The hydration and anion complexation of the cations are the essential factors that are related directly with the adsorption and separation phenomena by the pyridine resin.

There are few studies dealing with the hydration and anion complexation of An(III) and Ln(III) ions in the mixed solvents. Reidler and Silber investigated the complexation of Er^{3+} ions with Cl^- and NO_3^- ions in water-MeOH mixtures by ultrasonic relaxation measurements and revealed that (1) Cl^- complexation of Er^{3+} varied from outer-sphere complexation to inner-sphere one when X_{MeOH} became over 90%, and (2) NO_3^- ions formed inner-sphere complexes with Er^{3+} in the whole X_{MeOH} range but its coordination number would change with increasing X_{MeOH} [110, 111]. Arisaka and his co-workers studied the hydration states of Cm^{3+} and Eu^{3+} in alcoholic HCl/LiCl solutions by employing time-resolved laser-induced fluorescence spectroscopy (TRLFS) [112–116]. They demonstrated that the inner-sphere hydration numbers of these cations decreased as increases of X_{MeOH}, [HCl], and [LiCl] in solvent and the decreasing tendency of Cm^{3+} was more drastic than that of Eu^{3+}. These previous works indicate that adding alcohols in aqueous solution brings the dehydration of An(III) and Ln(III) ions and, simultaneously, it also promotes their anion complexations.

When we try to understand a certain separation phenomenon of elements, we need to know their elemental difference relating to the separation phenomenon. Therefore, in order to understand the separation phenomenon of An(III) and Ln(III) by the pyridine resin, it is indispensable to obtain systematic information about the hydration and anion complexations of An(III) and Ln(III) in water-alcohol mixed solvents. However, unfortunately, such kind of systematic study has not been reported as yet. Then, in the present study, the hydration and anion complexation in the mixed solvents were determined for the whole Ln(III) by using XAFS spectroscopy.

Figure 5-11 shows k^3-weighted EXAFS spectra of Ln(III) and Y in water along with their corresponding Fourier transforms (FTs). Each spectrum in the upper graph of **Fig. 5-11** appears to be dominated by a single oscillation pattern, indicating that there is only one type of coordination shell around Ln(III) and Y ions in water. The corresponding FTs in **Fig. 5-11** also exhibited single peak for each element.
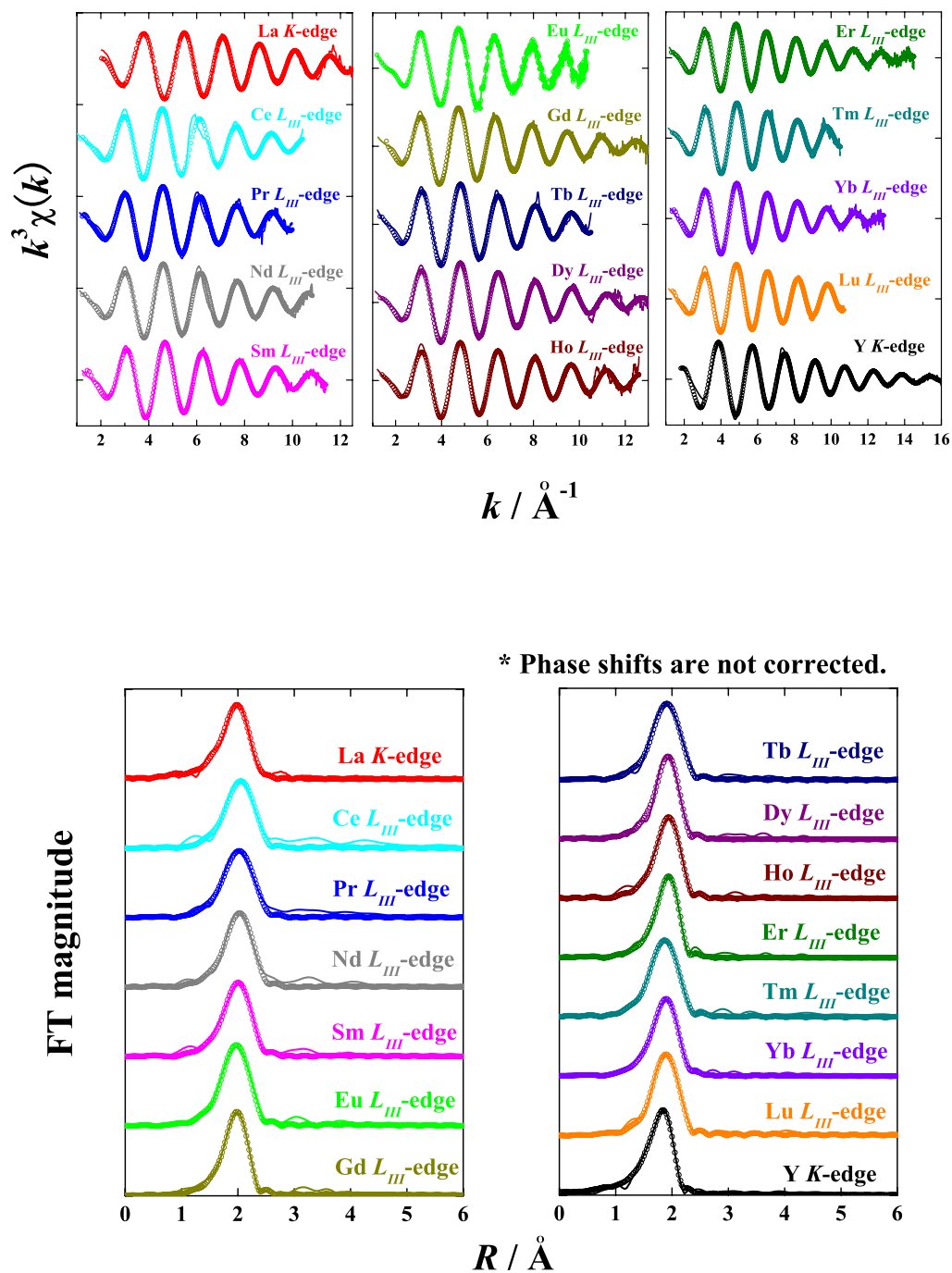
Figure 5-11. k^3-weighted EXAFS spectra of Ln(III) and Y in water (upper) and their corresponding Fourier transforms (lower). (solid lines: experimental data, ○: curve fitting results)

The curve fitting results indicate that the primary sphere of Ln(III) and Y ions are composed of 8-9 water molecules in water and the hydration number gradually decreases with an increase of atomic number. The distance between the cations and hydrated water molecules also decreases as the increase of atomic number, reflecting the lanthanoid contraction. The EXAFS structural parameters obtained from the curve fitting are summarized in **Table 5-3** and **Table V-1** in Appendix V. The obtained inter-atomic distances (R) and coordination numbers (N) are in good agreement with the reported values listed in **Table 5-1**. The curve fitting for the lighter Ln (Ce-Nd) L_{III}-edges generated slightly larger residuals. This is due to the multielectron excitations [89] which give rise to distortion on EXAFS oscillation.

Table 5-3. EXAFS structural parameters of Ln(III) and Y in water and conc. HCl / MeOH mixed solution. (conc. HCl / MeOH = 7 / 3 (vol/vol), Error: $R \pm 0.01$ Å, $N \pm$ 5%)

| | | in water | | in conc. HCl / MeOH = 7 / 3 | | | |
| | | O (H$_2$O) | | O (H$_2$O) | | Cl | |
Element	Edge	R / Å	N	R / Å	N	R / Å	N
La	K	2.55	9.5	2.55	7.9	2.88	1.6
Ce	L_{III}	2.52	9.2	2.53	8.1	2.85	1.2
Pr	L_{III}	2.51	9.4	2.51	8.4	2.86	0.9
Nd	L_{III}	2.48	9.3	2.50	7.8	2.82	0.9
Sm	L_{III}	2.46	9.4	2.46	8.6		
Eu	L_{III}	2.42	9.0	2.42	8.7		
Gd	L_{III}	2.41	8.4	2.40	8.3		
Tb	L_{III}	2.38	8.4	2.39	8.6		
Dy	L_{III}	2.36	8.6	2.36	8.3		
Ho	L_{III}	2.36	8.3	2.35	8.5		
Er	L_{III}	2.35	8.2	2.35	8.0		
Tm	L_{III}	2.34	8.0				
Yb	L_{III}	2.32	8.2	2.33	8.0		
Lu	L_{III}	2.32	8.2	2.31	7.7		
Y	K	2.33	8.3	2.33	8.2		

The EXAFS spectra ($k^3\chi(k)$ and FTs) of Ln(III) and Y in a conc. HCl / MeOH mixed solution are given in **Fig.   5-12** and their EXAFS structural parameters obtained from the curve fitting are summarized in the right columns of **Table 5-3** and **Table V-2** in Appendix V. Although the spectra were noisy probably due to the presence of Cl with high concentration, the k^3-weighted EXAFS spectra exhibited the clear single frequency that is similar to that observed in water. However, their corresponding FTs (the lower graph in **Fig.   5-12**) and curve fitting results suggested that there was a slight contribution of Cl$^-$ ions on the EXAFS spectra for the lighter Ln (La-Nd), Gd, and Er. The spectra of Sm and Eu were too noisy to distinguish the slight contribution of Cl$^-$ ions. To the contrary, a clear spectrum was obtained for Er L_{III}-edge with an sufficient long k-range, providing a distinguishable FT between O (H$_2$O) and Cl shells in spite of a considerably small contribution of Cl $^-$ ions (see Appendix V, **Figs. V-2**).

The obtained structural parameters indicate that the hydration of Ln(III) and Y ions are so tight that Cl$^-$ ions hardly form inner-sphere complexation with the cations even in an extreme solvent of conc. HCl / MeOH mixture. This is consistent with the previous results described in **5.1.2**. However, a small number ($\sim$2) of Cl$^-$ ions can penetrate the primary sphere of the lighter Ln in the conc. HCl / MeOH mixture. The number of Cl$^-$ ions in the primary sphere (N_{Cl}) decreases as increasing the atomic number, reflecting the stronger hydration of lighter Ln over heavier Ln as described in **5.3.1**. The inter-atomic distances (R) between the cations and hydrated water molecules in the conc. HCl / MeOH mixture are almost identical with those in water (**Fig.   5-13**). The R_{Cl} decrease with the increase of atomic number, also reflecting the lanthanoid contraction. These structural parameters are in agreement with the previously reported values by XAFS [7, 8], but slightly shorter R than those by XRD [1, 2] and ND [6].

∗ Theoretical parameters ($F_j(k)$, $\delta_j(k)$, and λ) for the curve fitting of O and Cl shells were calculated from the crystal structures of hydrated Ln chloride compounds [117–120] using FEFF code. (see **Fig. V-18** in Appendix V)
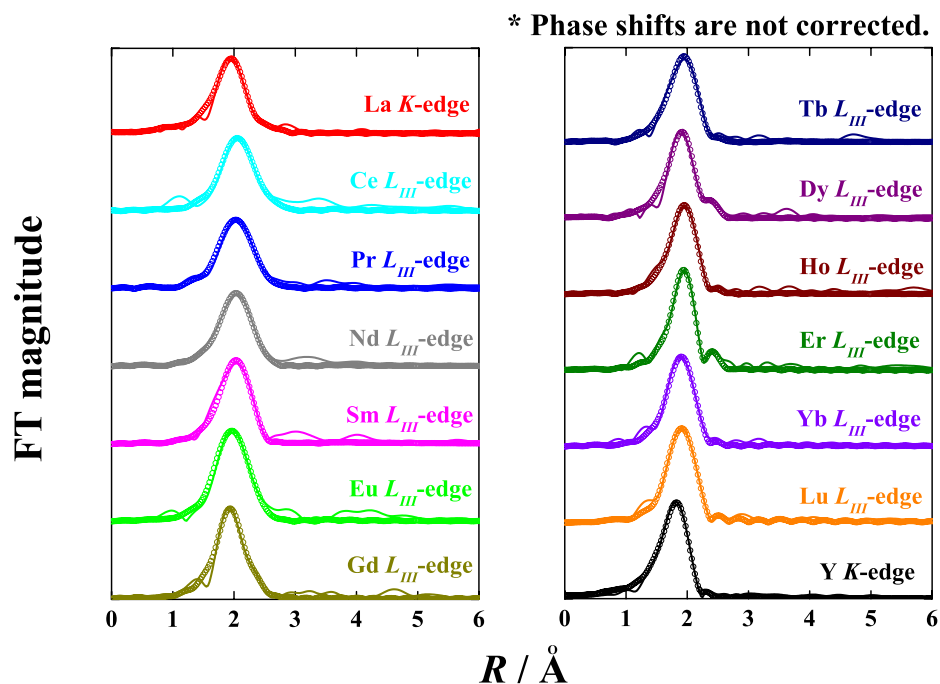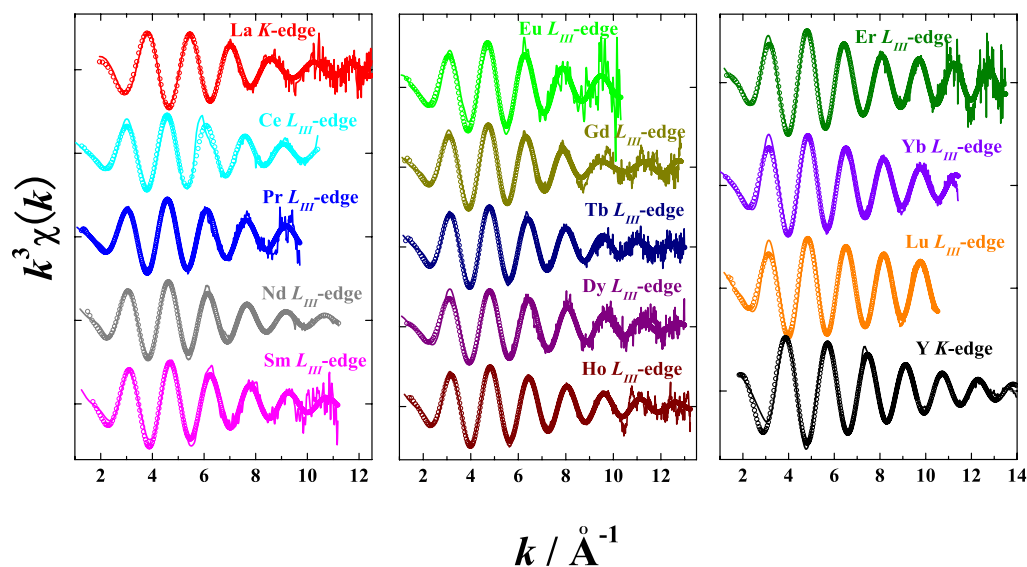
Figure 5-12. k^3-weighted EXAFS spectra of Ln(III) and Y in conc. HCl / MeOH mixed solution (upper) and their corresponding Fourier transforms (lower). (conc. HCl / MeOH = 7 / 3 (vol/vol), solid lines: experimental data, ○: curve fitting results)
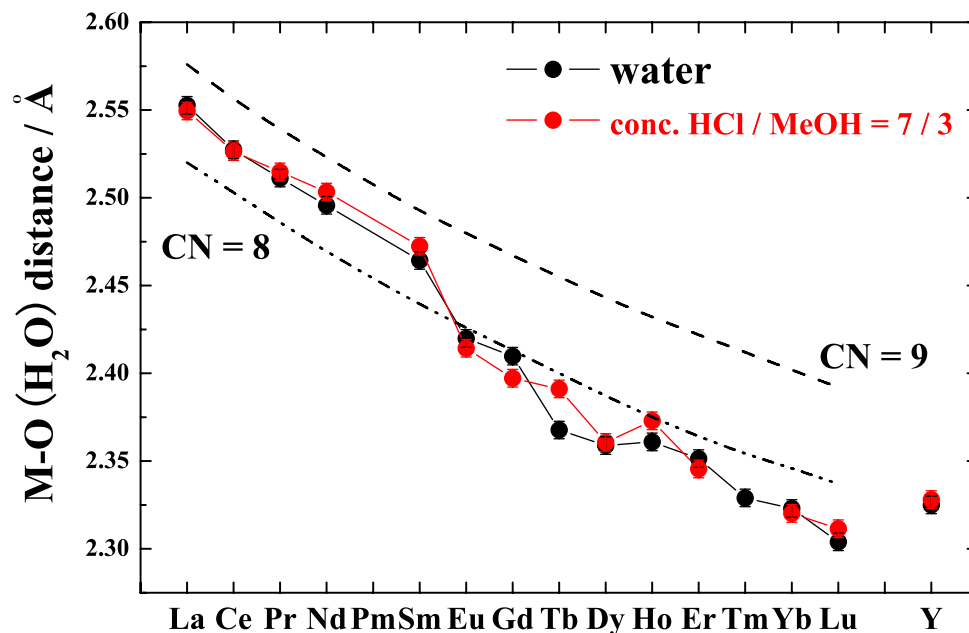
Figure 5-13. Comparison of inter-atomic distances between Ln(III) and Y ions and hydrated water molecules in water and conc. HCl / MeOH mixed solution. (conc. HCl / MeOH = 7 / 3 (vol/vol), theoretical distances (dotted lines) were calculated from the effective ionic radii reported in [9], *CN*: coordination number)

Nd and Er L_{III}-edge EXAFS were also measured for various compositions of conc. HCl / MeOH solution. The obtained EXAFS spectra ($k^3\chi(k)$ and FTs) are given in **Fig. 5-14**. The k^3-weighted EXAFS spectra and their corresponding FTs showed no considerable change as the solvent composition varied. Furthermore, the obtained EXAFS structural parameters summarized in **Table 5-4** and **Tables. V-3** and **V-4** in Appendix V also indicate no significant difference for every composition. Similar results have been obtained by TRLFS measurements in HCl / MeOH system [114] and LiCl / MeOH system [115, 116]. Therefore, we can conclude that the primary co-ordination sphere of Ln(III) and Y ions is dominated by water molecules for the most part even in higher $X_{alcohol}$ ($\approx$ 90 vol%) region in solution phase although the water activity (a_w) surely decreases with the increase of $X_{alcohol}$ in solvent. The coordination

number of Cl$^-$ was almost constant for every $X_{alcohol}$ sample despite the decrease of [Cl$^-$] with an increase of $X_{alcohol}$. This indicates that the stability constants (K_d) of Ln-Cl complexes increase as increasing $X_{alcohol}$, probably due to the decrease of a_w. It should be noted that the spectrum of Er in "conc. HCl / MeOH = 1 / 9" exhibited a little different frequency in the imaginary part of FT (Appendix V, **Fig. V-2**), indicating that methanol molecules slightly coordinate to Er in this solution. This means that the solvation by alcohol molecules is stronger than the Cl$^-$ complexation for heavier Ln.

Table 5-4. EXAFS structural parameters of Nd and Er in water and in different compositions of conc. HCl / MeOH mixed solutions. (Solvent: conc. HCl / MeOH (vol / vol), Error: $R \pm 0.01$ Å, $N \pm 5\%$)

		O (H$_2$O)		Cl		O (MeOH)		C (MeOH)	
	Solvent	R / Å	N	R / Å	N	R / Å	N	R / Å	N
Nd L_{III}-edge	water	2.48	9.3						
	7 / 3	2.50	7.8	2.82	0.9				
	5 / 5	2.48	8.0	2.82	1.0				
	3 / 7	2.49	8.0	2.82	1.0				
	2 / 8	2.49	8.0	2.83	1.0				
	1 / 9	2.49	8.0	2.81	1.0				
Er L_{III}-edge	water	2.35	8.2	2.74	0.3				
	7 / 3	2.35	8.0	2.74	0.6				
	5 / 5	2.36	8.5	2.75	0.4				
	3 / 7	2.36	8.0	2.74	0.5				
	2 / 8	2.35	8.3	2.73	0.5				
	1 / 9	2.35	8.1			2.47	0.6	2.97	0.6

Figure 5-14. k^3-weighted EXAFS spectra of Nd and Er L_{III}-edges in different compositions of conc. HCl / MeOH mixed solutions (upper) and their corresponding Fourier transforms (lower). (conc. HCl / MeOH (vol/vol), solid lines: experimental data, ○: curve fitting results)

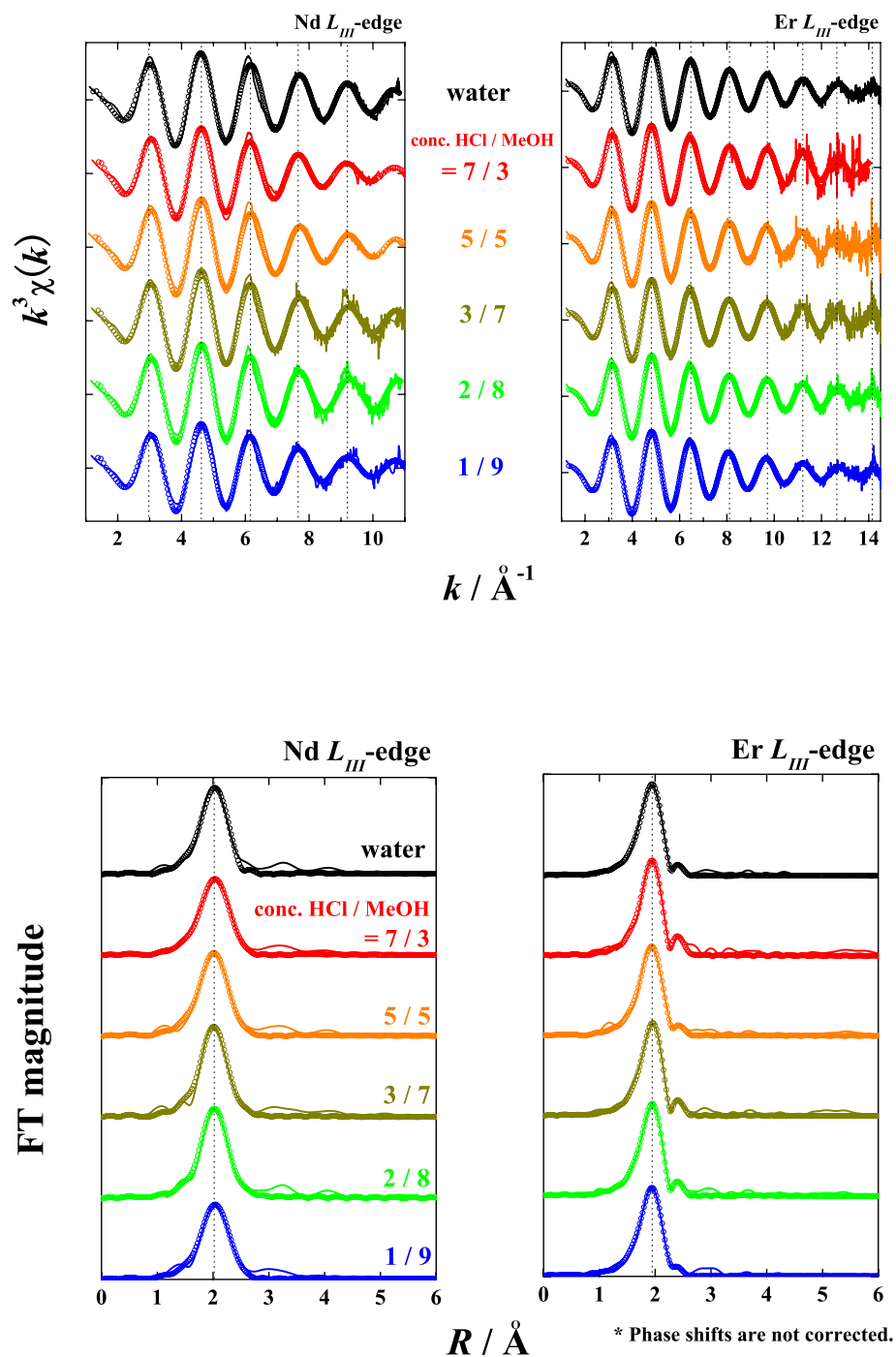The EXAFS spectra of Ln(III) were also collected in a conc. HNO_3 / MeOH mixed solution (conc. HNO_3 / MeOH = 5 / 5 (vol/vol)). The obtained spectra are shown in **Fig. 5-15**. The k^3-weighted EXAFS spectra exhibited much more complicated oscillation pattern compared with that of water and HCl solutions: the main EXAFS oscillations shape broke after their third peaks. The corresponding FTs gave broader first peaks than those in water (*e.g.* **Fig. V-3** in Appendix V) and, furthermore, small but distinguishable second peaks appeared at around 3.5-3.8 Å. As a result of curve fitting, the first broadened peaks were identified as the mixture of two O atoms (H_2O and NO_3) and one N atom (NO_3), and the second peaks were attributed to the multiple scattering (MS) [81] of NO_3 molecules (see **Fig. 5-16**). **Table 5-5** summarizes the obtained EXAFS structural parameters.

Table 5-5. EXAFS structural parameters of Ln(III) in conc. HNO_3 / MeOH mixed solution. (Solvent: conc. HNO_3 / MeOH = 5 / 5 (vol/vol), Error: $R \pm 0.01$ Å, $N \pm 5\%$)

| | | in conc. HNO_3 / MeOH = 5 / 5 (vol/vol) | | | | | |
| | | O (H_2O) | | O (NO_3) | | N (NO_3) | |
Element	Edge	R / Å	N	R / Å	N	R / Å	N
La	K	2.55	5.0	2.66	4.0	3.45	2.0
Ce	L_{III}	2.52	4.6	2.60	4.4	3.10	2.2
Pr	L_{III}	2.51	4.9	2.59	4.1	3.11	2.1
Nd	L_{III}	2.49	5.0	2.57	4.0	3.03	2.0
Sm	L_{III}	2.44	5.0	2.52	4.0	2.99	2.0
Eu	L_{III}	2.41	5.3	2.50	3.9	2.95	2.0
Gd	L_{III}	2.39	5.0	2.48	4.1	2.98	2.0
Tb	L_{III}	2.38	5.0	2.47	4.2	2.96	2.1
Dy	L_{III}	2.36	5.1	2.48	4.1	2.93	2.1
Ho	L_{III}	2.34	4.1	2.42	4.1	2.92	2.1
Er	L_{III}	2.34	4.3	2.43	4.1	2.91	2.1
Tm	L_{III}	2.33	4.1	2.41	3.9	2.91	1.9
Yb	L_{III}	2.31	4.1	2.38	3.9	2.90	2.0
Lu	L_{III}	2.29	3.9	2.38	4.1	2.85	2.1

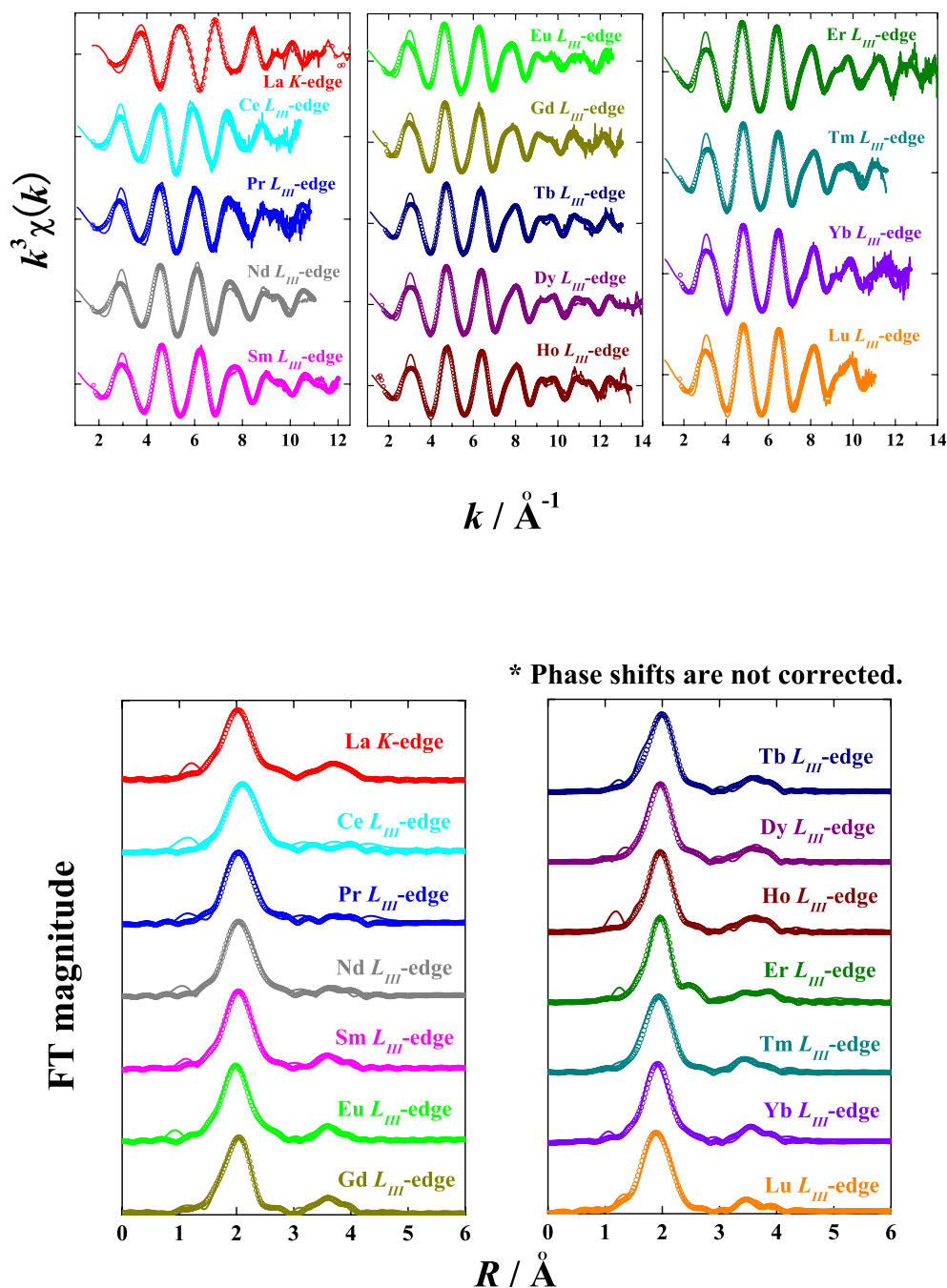**Figure 5-15.** k^3-weighted EXAFS spectra of Ln(III) in conc. HNO_3 / MeOH mixed solution (upper) and their corresponding Fourier transforms (lower). (conc. HNO_3 / MeOH = 5 / 5 (vol/vol), solid lines: experimental data, ○: curve fitting results)

The lighter to middle Ln (La-Dy) cations are surrounded by $\sim$5 water molecules and 2 nitrate ions (NO_3^-) in the present conc. HNO_3 / MeOH mixture, while the heavier Ln (Ho-Lu) are coordinated by 4 water molecules and 2 NO_3^- ions in their primary spheres. The whole Ln has two NO_3^- ions in their primary sphere and the NO_3^- ions coordinate to the Ln(III) ions with bidentate mode. These results are consistent with the previous studies mentioned in **5.1.2**.

The inter-atomic distances (R) of Ln-O (H_2O), Ln-O (NO_3), and Ln-N (NO_3) in the conc. HNO_3 / MeOH mixed solution are plotted in the upper graph of **Fig. 5-16**. These R gradually decreased with an increase of atomic number regardless of the inflection of CN_{H2O} and CN_{NO3}, also reflecting the lanthanoid contraction. The R of hydrated water molecules are unchanged even in conc. HNO_3 / MeOH mixed solutions. The R between the cations and the O atoms of NO_3 are slightly longer (0.08$\sim$0.1 Å) than those between the cations and hydrated water molecules.

Figure 5-17 gives the k^3-weighted EXAFS spectra of Nd and Gd L_{III}-edges in various compositions of conc. HNO_3 / MeOH mixed solutions along with their FTs. The obtained EXAFS spectra showed no considerable change for every composition both in k-space and in R-space. The structural parameters summarized in **Table 5-6** and **Tables V-6** and **V-7** in Appendix V also indicate no considerable difference: both Nd and Gd ions are coordinated by $\sim$5 water molecules and 2 NO_3^- ions in every composition of conc. HNO_3 / MeOH mixed solutions. It seems that alcohols have almost no significant influence on the primary coordination sphere of Ln(III) ions both in chloride solutions and nitrate solutions even if $X_{alcohol}$ is 90%.

$*$ Theoretical parameters ($F_j(k)$, $\delta_j(k)$, and λ) for the curve fitting of O and N shells were calculated from the crystal structures of hydrated Ln nitrate compounds [121–124] using FEFF code. (see **Fig. V-18** in Appendix V)
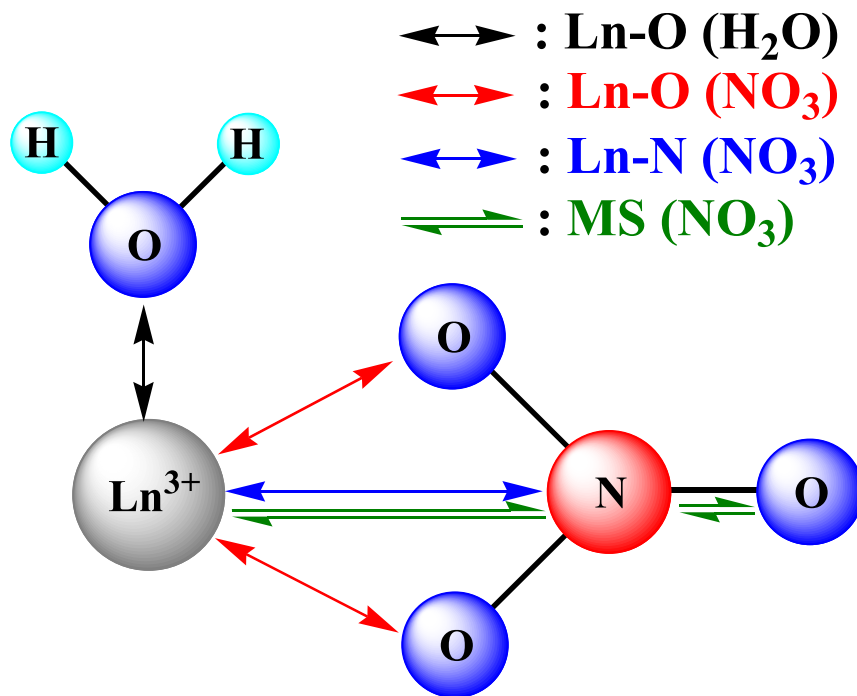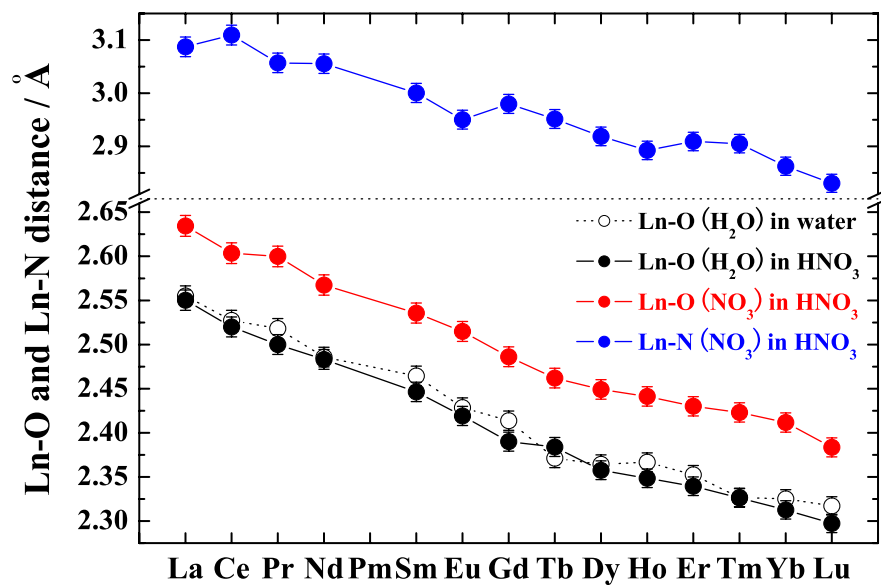
Figure 5-16. Comparison of inter-atomic distances of Ln(III) ions in conc. HNO_3 / MeOH mixed solution. (conc. HNO_3 / MeOH = 5 / 5 (vol/vol), *CN*: coordination number)
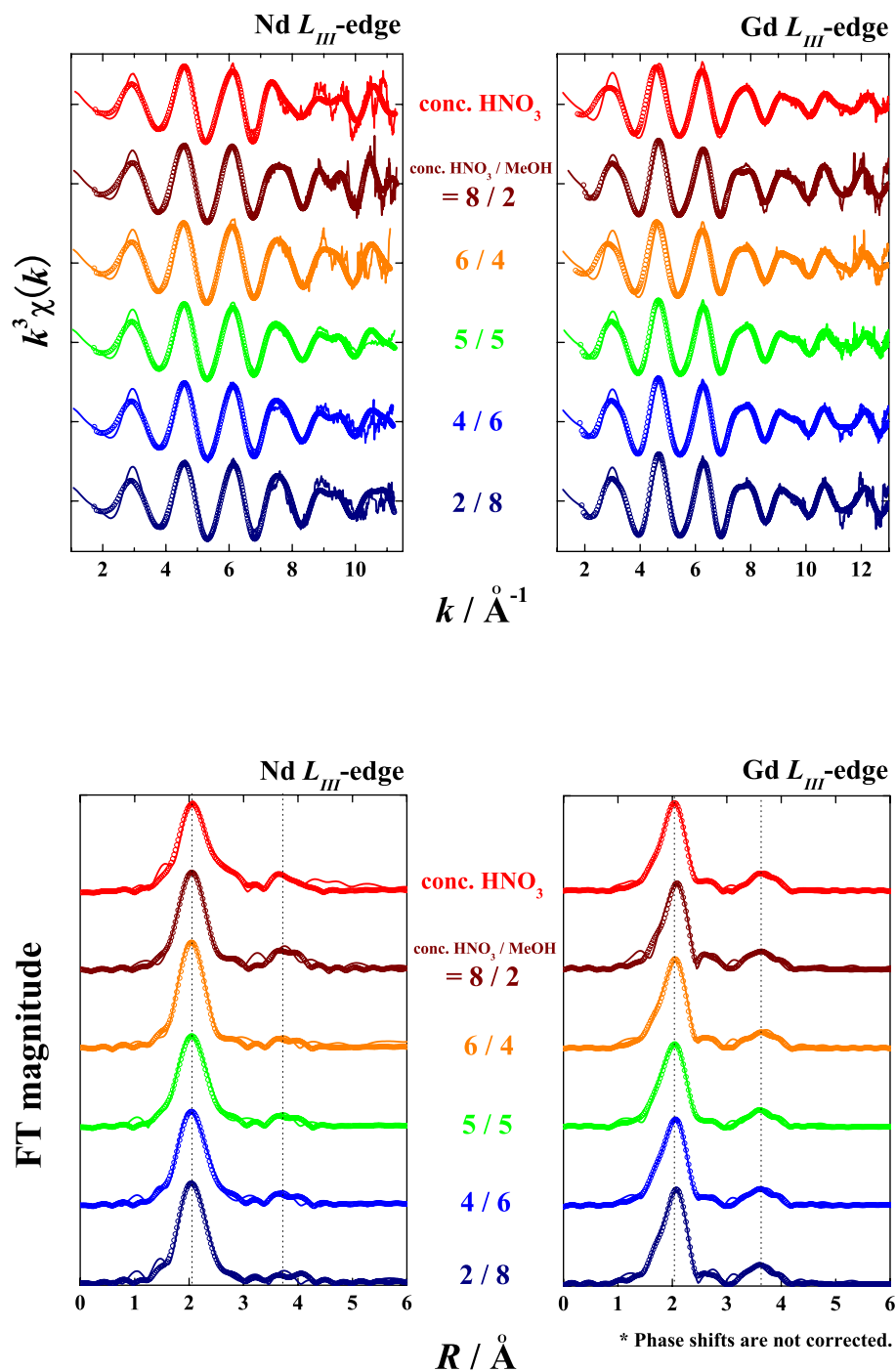
Figure 5-17. k^3-weighted EXAFS spectra of Nd and Gd L_{III}-edges in various compositions of conc. HNO_3 / MeOH mixed solutions (upper) and their corresponding Fourier transforms (lower). (conc. HNO_3 / MeOH (vol/vol), solid lines: experimental data, ○: curve fitting results)

Table 5-6. EXAFS structural parameters of Nd and Gd in various compositions of conc. HNO_3 / MeOH mixed solutions. (Solvent: conc. HNO_3 / MeOH (vol/vol), Error: $R \pm 0.01$ Å, $N \pm 5\%$)

		O (H_2O)		O (NO_3)		N (NO_3)	
	Solvent	R / Å	N	R / Å	N	R / Å	N
	conc. HNO_3	2.49	4.6	2.58	4.4	3.07	2.2
	8 / 2	2.48	4.8	2.58	4.2	3.07	2.1
Nd L_{III}-edge	6 / 4	2.49	5.0	2.57	4.0	3.09	2.0
	5 / 5	2.49	5.0	2.57	4.0	3.03	2.0
	4 / 6	2.49	4.9	2.57	4.1	3.06	2.0
	2 / 8	2.49	4.7	2.57	4.3	3.04	2.2
	conc. HNO_3	2.40	4.8	2.49	4.0	2.99	2.0
	8 / 2	2.40	4.4	2.50	4.0	3.01	2.0
Gd L_{III}-edge	6 / 4	2.40	4.7	2.49	4.0	3.02	2.0
	5 / 5	2.39	5.0	2.48	4.1	2.98	2.0
	4 / 6	2.40	4.6	2.49	4.0	3.01	2.0
	2 / 8	2.40	4.7	2.49	4.0	3.01	2.0

In addition to the above-mentioned aqueous chloride and nitrate solution samples, EXAFS measurements were also performed for 95~% alcohol samples . As mentioned in chapter 3, the adsorption and separation behavior by the pyridine resin in pure alcohols was quite different from that in aqueous solutions. Therefore, the information about the solvation structure in pure alcohols is also important to understand the adsorption and separation mechanisms by the pyridine resin.

The samples for EXAFS measurements were prepared by dissolving hydrated Ln trichloride compounds ($LnCl_3 \cdot nH_2O$) in pure alcohols (more than 99.5%-purity). The results of Er L_{III}-edge EXAFS in various alcohols are given in **Fig. 5-18**, along with the result in water. The EXAFS structural parameters obtained from the best curve fits are listed in **Table 5-7**. The $k^3\chi(k)$ in alcohols showed similar but a little weaker frequencies compared with that in water. The corresponding FTs gave broader first peaks than that in water and the peak tops shifted to longer distance. The shapes of their imaginary parts were also different from that in water (see **Fig. V-2** in Appendix V). The structural parameters obtained from curve fitting indicated that the

primary sphere were occupied by 4 water molecules and 3 alcohol molecules. The dehydration of Ln(III) ions in pure alcohols has also been observed by TRLFS measurements [113]. It should be noted that the degree of dehydration is independent of the type of alcohol and the coordination distances of alcoholic hydroxy groups are almost the same for all the tested alcohols. Nd L_{III}-edge EXAFS spectrum in MeOH also suggested that Nd ions are surrounded by 6 water molecules and 3 methanol molecules in pure MeOH (**Table V-3** in Appendix V). This means that Ln(III) ions are coordinated by 3 alcohol molecules in pure alcohol solvent regardless of their size and coordination number, although their hydration numbers are different. These dehydration and alcohol coordination must have some influence on the adsorption and separation mechanisms by the pyridine resin, bringing the unexpected adsorption and separation behavior demonstrated in chapter 3.

To sum up the EXAFS results, adding alcohol in aqueous solution does not affect the hydration and anion complexation of Ln(III) ions in their primary spheres even $X_{alcohol}$ is 90% from the viewpoint of the structure in the primary sphere of the ions. However, as mentioned in the first half of this section, the solvent properties of water-alcohol mixed solvents are quite different from those of pure water or pure alcohol. Therefore, alcohols may have an influence on the secondary spheres or further, or rather macro-scale phenomena such as diffusion of ions. On the other hand, there is an obvious difference between Ln-Cl$^-$ complexation and Ln-NO$_3^-$ complexation in aqueous solution: Cl$^-$ ions forms outer-sphere complexes with Ln(III) ions even in high Cl$^-$ concentration, while NO$_3^-$ ions form stronger inner-sphere complexes using their two O atoms as bidentate mode. This difference must cause the observed different adsorption and separation behavior between these two solution systems. Further discussion is made in the latter section of this chapter.
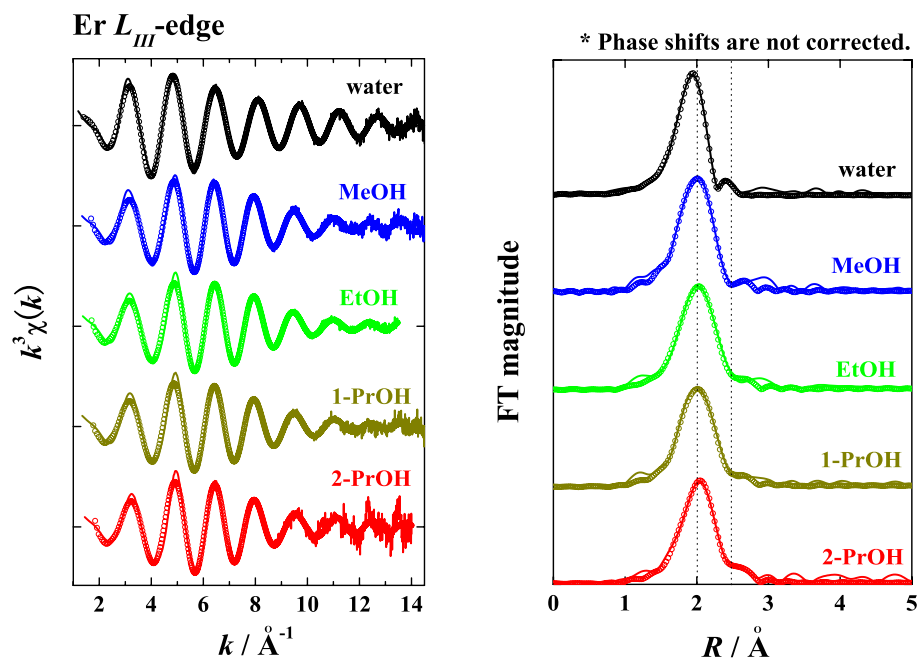
Figure 5-18. k^3-weighted EXAFS spectra of Er L_{III}-edge in different pure alcohols (left) and their corresponding Fourier transforms (right). (solid lines: experimental data, ○: curve fitting results)

Table 5-7. EXAFS structural parameters of Er in different pure alcohols. (Error: $R \pm$ 0.01 Å, $N \pm$ 5%)

Solvent	O (H_2O)		O (alcohol)		C (alcohol)	
	R / Å	N	R / Å	N	R / Å	N
water	2.35	8.2				
MeOH	2.33	4.4	2.45	3.1	2.85	3.1
EtOH	2.33	4.4	2.44	3.1	2.84	3.1
1-PrOH	2.33	4.4	2.45	3.1	2.85	3.1
2-PrOH	2.33	4.2	2.44	3.0	2.87	3.0

5.4 Results and Discussion II
Coordination Properties of Pyridine

As mentioned in chapter 1, a tertiary pyridine resin can work both as a coordinative solid extractant and as a weakly basic anion exchange resin. When the resin functions as an anion exchanger, their adsorptivity and separability for An(III) and Ln(III) simply depend on the anion complexation of the cations. However, as described in **5.3.2**, An(III) and Ln(III) ions hardly form anionic complexes ($[MA_n]^{(n-3)-}$, where A is a counter anion) with Cl^- or NO_3^- ions at least in their primary spheres in solution phase, whereas they are adsorbed in the pyridine resin both in HCl and HNO_3 solutions. Additionally, the pyridine resin also displayed strong adsorption even in non-acidic solvents of aqueous LiCl and $LiNO_3$ solutions in which the pyridine groups are hardly protonated. Hence, there is every possibility that the pyridine groups in the resin directly interact with the cations and work as an "extractant", not as an "anion exchanger". If this is the case, the affinity of pyridine groups to An(III) and Ln(III) ions has a great influence on the adsorptivity and separability of the pyridine resin.

As described in **1.4.1** of chapter 1, pyridine type ligands are classified as a soft donor type ligand whose affinity for An(III) is larger than that for Ln(III) [125]. This larger affinity of soft donor ligands for An(III) over Ln(III) is attributed to the slightly greater covalency appeared in the An bonding. That is, An form stronger covalent bonding with soft donor ligands using their slightly more extended unoccupied $7p$- [126, 127], $6d$- [128], and $5f$ orbitals [126], while $6s$ orbital is dominant in Ln(III) bonding [129]. This is considered one of the most probable interpretation of the large enthalpy difference observed in the extraction of An(III) and Ln(III) by soft donor extractants, such as Cyanex (S-donor) [47].

In this section, the coordination properties of pyridine type ligands for An(III) and Ln(III) are summarized from several viewpoints.

5.4.1 Stability of Trivalent An/Ln-Pyridine Complexes

Stability (formation) constant is the most fundamental information to estimate the complexation behavior. However, unfortunately, there seems to be no precedent report surveying the stability constants of An(III)/Ln(III)-pyridine ligand complexes

systematically. Then, in this study, spectrophotometric titrations were carried out to determine the stability constants of Ln(III)-pyridine ligand complexes using the $\pi \rightarrow \pi*$ transitions of the ligands in UV/visible absorption region. All the titrations were performed by adding a given small portion of metal solution into an alcohol solution of ligand. The metal solutions were prepared by dissolving $LnCl_3 \cdot nH_2O$ in the same alcohol used for preparing the ligand solution.

The first attempt was made for Ln(III)-pyridine (Py) complexes. **Fig. V-7** in Appendix V shows a typical spectral change of the $\pi \rightarrow \pi*$ transition of Py. The spectra indicated almost no change for metal titration and, in consequence, it was impossible to calculate their stability constants. But to put it the other way around, this means that the complexation between Ln(III) ions and Py is very weak.

Then, the next attempt was done for Ln(III)-1,10-phenanthroline (Phen, see **Fig. 5-20**) complexes. It is well-known that Phen forms stronger complexes with transition metals than Py and, therefore, their complexes with Ln(III) ions are expected to be stronger than the Py complexes. The spectral titration data are given in **Fig. V-8** in Appendix V. The stability constants (β_n) calculated from the spectra are listed in **Table V-8** in Appendix V and they are plotted in **Fig. 5-19**. The β_1 and β_2 varied irregularly as increasing atomic number, seeming to form the tetrad effect [130] especially for lighter Ln. However, Phen is a bidentate ligand and its complexation with Ln(III) ions may affected by the size of Ln(III) ions. Hence, we can not discuss the stability constants of Ln(III)-Phen complexes directly with the affinity of pyridine ligands for Ln(III) ions, although comparing the β of neighboring elements is still informative.
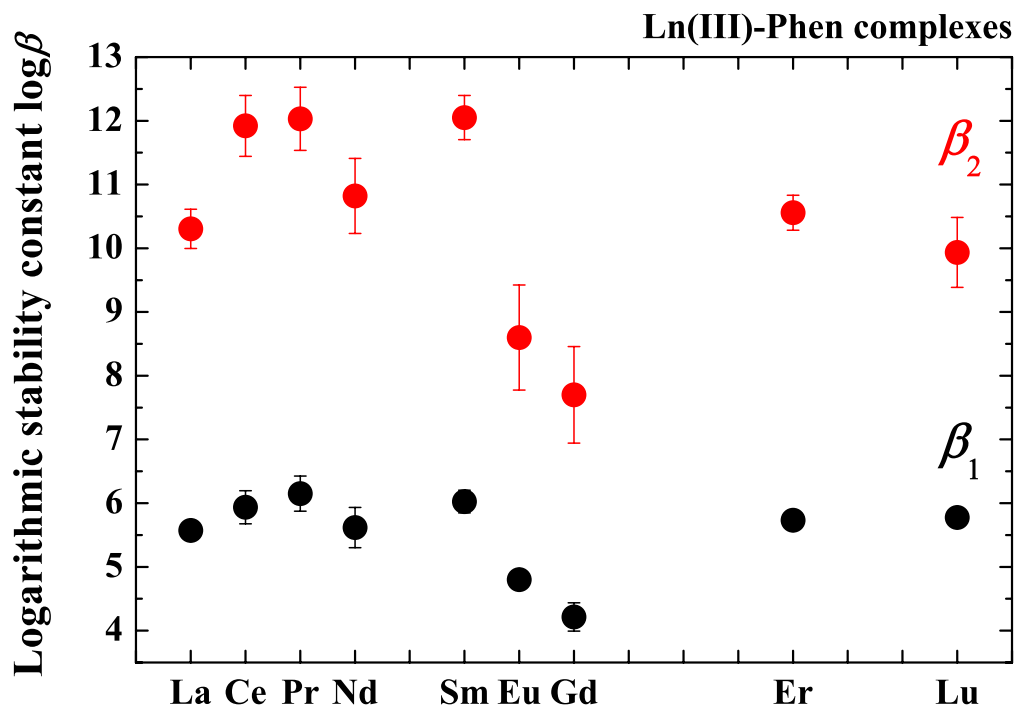
Figure 5-19. Stability constants (β_1 and β_2) of Ln(III)-1,10-phenanthroline complexes in methanol at 293 K.

In addition to the above-mentioned Phen complexes, the stability constants of An(III)/Ln(III)-TPEN (N,N,N',N'-tetrakis(2-pyridylmethyl)ethylenediamine, see **Fig. 5-21**) complexes have been studied by several researchers [131, 132]. The reported stability constants are summarized in **Table 5-8**. The stability of Ln(III)-TPEN complexes increases with an increase of atomic number and the K_1 for Lu is two order of magnitude larger than that for La. This suggests that the stability of Ln(III)-TPEN ($\approx$ Ln(III)-Py) bonding depends mainly on the electron density of the cations: The electron density of heavier Ln is higher than that of lighter Ln due to the lanthanoid contractions. On the other hand, Am-TPEN complex exhibited two order larger K_1 than the complex of Sm that has similar ionic radii to Am, indicating that An(III) form stronger complexes with pyridine type ligands than the homologous Ln(III). However, the K_1 of Lu-TPEN complex is similar to that of Am-TPEN complex. This means that the affinity of TPEN for heavier Ln is almost the same to that for middle An(III) such

as Am or Cm.

Table 5-8. Stability constants ($K_1 = \beta_1$) of An(III)/Ln(III)-TPEN complexes in aqueous solutions.

| | $\log K_1$ (= $\log \beta_1$) | |
	ref. [131] at r.m. in H_2O?	ref. [132] at 298 K in 0.1M $NaClO_4$ solution
La	3.9	3.52
Pr	4.8	
Sm		4.70
Eu	5.7	
Ho	5.7	
Tm	5.5	
Lu	6.2	
Am		6.69

5.4.2   Structure of Trivalent An/Ln-Py Complexes

The larger affinity of soft donor ligands for An(III) over Ln(III) may reflect the structure of their complexes. That is, it may bring the difference in the coordination distance or coordination number. To probe this structural difference of the complexes, the synthesis of Ln(III)-Py complexes has been attempted in various conditions. However, as mentioned in the former section, the stability of Ln(III)-Py complexes is considerably low and, in addition, the directivity of the complexes was probably so poor that we could not obtain even the precipitate. In fact, no Ln(III)-Py complex has been reported yet so far.

Instead of pure Py complexes, the structural comparison between An(III)- and Ln(III)-soft donor ligand complexes was made by the reported complexes. Fortunately, the An(III)/Ln(III) complexes with soft donor ligands have extensively been investigated by many researchers in recent years due to the interest of their application to the An(III)-Ln(III) separation. The chemical structures of the ligands summarized in this section are illustrated in **Figs. 5-20** and **5-21**.

1,10-Phenanthroline
(Phen)

2,2'-Bipyridyl
(Bpy)

2,2':6',2''-Terpyridine
(Tpy)
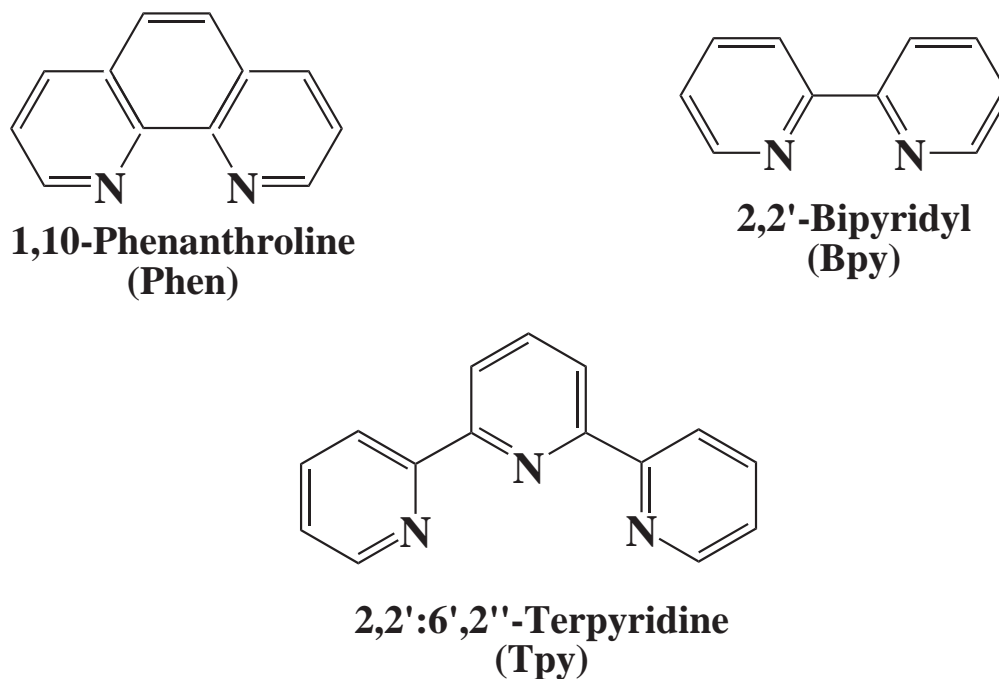
Figure 5-20. Chemical structures of pyridine type ligands.

Tris[(2-pyridyl)methyl]amine
(TPA)

6-Methyl-2-(2-pyridyl)
benzimidazole
(BIZ)

Tetrakis(2-pyridyl-methyl)-
1,2-ethylenediamine
(TPEN)

2,6-Di(5,6-dipropyl-1,2,4-triazin-3-yl)pyridine
(DPTP)

Dithiophosphinic acid

R = Chlorophenyl- : DCPDTP
R = 2,4,4-Trimethylpentyl : Cyanex 301
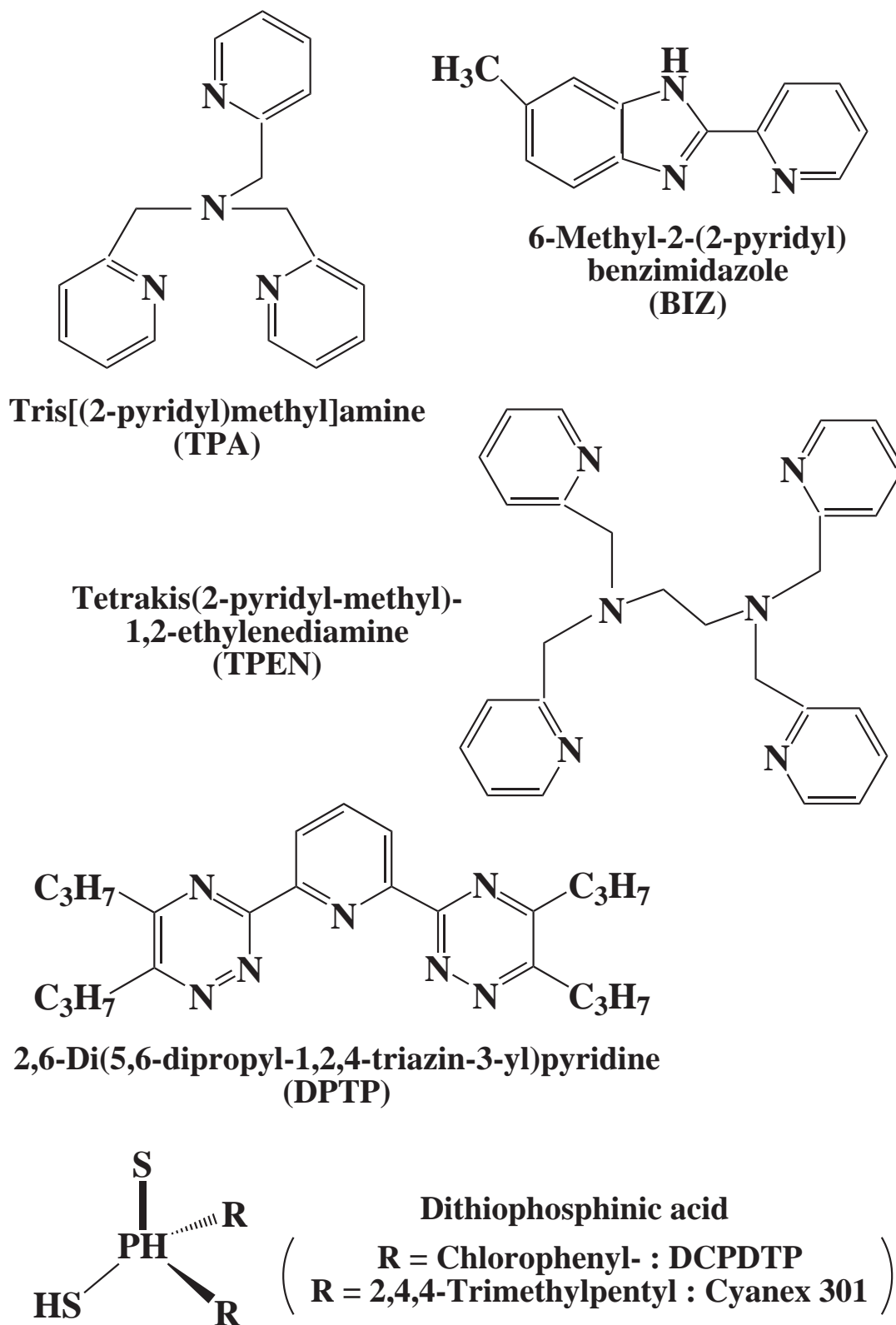
Figure 5-21. Chemical structures of pyridine type and sulfur donor type ligands.

X-ray crystallography is the most common and powerful technique to characterize the structure of complexes. This technique requires macro-amount ($\sim$mg) of single crystal samples for the structural determination by XRD. Unfortunately, it is practically impossible to prepare macro-amount of Am or Cm sample and, due to this reason, no crystallographic data of An(III)-pyridine ligand complex have been obtained at the moment except for the U(III) complex with Bpy [133]. However, the structures of several An(III)-soft donor ligand (pyridine and sulfur) complexes have recently been determined in solution by XAFS spectroscopy and compared with those of the homologous Ln(III) [134–137]. Those results are summarized in **Table 5-9**. It seems that the metal-donor atom (N or S) bond distances are indistinguishable for all N and S donor ligands, whereas these soft donor ligands surely have greater selectivity for An(III) over Ln(III) in the practical separation process as mentioned in the next section. This phenomenon is probably interpreted as the contribution of $6d$-orbitals: the An(III) over $_{95}$Am furnish mainly their $6d$-orbitals to make the bonding with soft donor ligands, while other lighter An under $_{94}$Pu use their $5f$-orbitals. The $6d$-orbitals are relatively rigid and, in consequence, they produce less structural difference [48, 138, 139]. On the other hand, the $5f$-orbitals are more flexible, bringing a slightly shorter M-L bond distance [133, 140, 141]. Although no significant structural difference has been observed between An(III)- and Ln(III)-soft donor ligand complexes, An(III) must form more stable bonding with soft donor ligands than Ln(III).

Tables 5-10 and **5-11** summarize the structural parameters (*CN* and the bond distance between metal and the nitrogen of pyridine ligands) for several An(III)/Ln(III)-pyridine type ligand complexes (single crystals). The M-N distance decreases with an increase in atomic number for all of the ligands in Ln(III) series and it simply reflects the lanthanoid contraction. This means that the M-N bonding becomes stronger as proceeding the atomic number for Ln(III) series, corresponding to the tendency of the stability constants described in the previous section. It should also be noted that the M-N distance is independent of the type of ligand and it is almost constant for the same element. This indicates that the affinity of pyridine groups is almost constant for all of the ligands if the steric hindrance is not considered.

Table 5-9. Structural comparison of An(III)- and Ln(III)-soft donor complexes in solution.

	Ligand	Donor atom	M-N or M-S / Å	Ref.
Nd	BIZ	N	2.57	[134]
Am			2.56	
Ce	DPTP	N	2.62	[135]
Sm			2.58	
Eu			2.56	
Cm			2.57	
Nd	Cyanex 301	S	2.83-2.85	[136]
Sm			2.79-2.80	
Cm			2.79-2.83	
Eu	DCPDTP	S	2.96	[137]
Cm			2.92-2.96	

Table 5-10.   Structural parameters (*CN* and Metal-N(pyridine) distances) of Ln(III) nitrate-pyridine ligand complexes.

	Phen			Bpy			Tpy		
	CN	M-N / Å	Ref.	*CN*	M-N / Å	Ref.	*CN*	M-N / Å	Ref.
Y							1	2.48-2.50	[153]
La	2	2.65-2.70	[149, 152]	2	2.66	[148, 152]	1	2.65-2.68	[150]
							1	2.63-2.69	[153]
Gd							1	2.52-2.56	[153]
Tb							1	2.50-2.52	[153]
Lu	2	2.46-2.48	[152]	2	2.46-2.47	[152]	1	2.47	[153]

	TPEN		
	CN	M-N / Å	Ref.
La	1	2.70-2.73	[151]
Tb	1	2.60-2.66	[151]

Table 5-11.   Structural parameters (*CN* and Metal-N(pyridine) distances) of An(III)/Ln(III) chloride-pyridine ligand complexes. (∗ Iodide)

	Phen			Bpy			Tpy			
	CN	M-N / Å	Ref.	*CN*	M-N / Å	Ref.	*CN*	M-N / Å	Ref.	
Y	2	2.50-2.54	[144]				1	2.5-2.55	[142]	Y
	1	2.48-2.50	[143]							
La	3	2.75-2.77	[144]	2	2.70-2.79	[144, 147]	1	2.66-2.69	[142]	La
	2	2.72-2.75	[144]							
Ce				2	2.64-2.70	[133]∗	1	2.64-2.66	[142]	Ce
Pr				2	2.63-2.70	[144]				Pr
Nd				2	2.60-2.67	[144]	1	2.61-2.62	[142]	Nd
Sm				2	2.61-2.65	[144]	1	2.57-2.58	[142]	Sm
Eu	2	2.63-2.64	[144]	2	2.54-2.63	[144]	1	2.54-2.56	[142]	Eu
Gd							1	2.54	[142]	Gd
Tb							1	2.51-2.52	[142]	Tb
Dy	2	2.52-2.55	[144]				1	2.50-2.51	[142]	Dy
Ho	1	2.50	[143]				1	2.49-2.50	[142]	Ho
Er	2	2.50-2.53	[144]	2	2.51-2.60	[144]	1	2.47-2.50	[142]	Er
Yb							1	2.45-2.46	[142]	Yb
Lu	2	2.48	[144]							Lu
	1	2.45	[143]							
U(III)				2	2.61-6.70	[133]∗				U(III)

	TPA			TPEN		
	CN	M-N / Å	Ref.	*CN*	M-N / Å	Ref.
Nd	1	2.60-2.7	[146]			
Sm				1	2.57-2.69	[145]
Eu	1	2.56-2.61	[146]			
Tb	1	2.51-2.57	[146]			
Lu	1	2.49-2.56	[146]			

5.5 Results and Discussion III
Adsorption and Separation Mechanisms

In order to elucidate the adsorption and separation mechanisms by the tertiary pyridine resin, the information about the chemical species adsorbed in the resin is essential. In the present study, the chemical species of Ln adsorbed in the resin were determined by XAFS.

5.5.1 HCl system

Figure 5-22 shows k^3-weighted EXAFS spectra of Nd K-edge in water, a conc. HCl / MeOH mixed solution (5 / 5 (vol/vol)), pyridine resin, and that of hydrated $NdCl_3$ compound (a pellet with boron nitrate), and their corresponding FTs. The solvent composition of the solution phase of the resin sample was identical with that of the conc. HCl / MeOH mixed solution sample (*i.e.* the solvent composition was 50 vol%-conc. HCl / 50 vol%-MeOH). In the k^3-weighted EXAFS spectra, the conc. HCl / MeOH mixed solution sample and the resin sample showed smaller attenuation of EXAFS oscillation at higher k-range ($11\sim$ $Å^{-1}$) compared with the water sample, suggesting that they had more than two shells in their primary spheres. On the other hand, the FTs indicated that the four samples gave their first peaks (corresponding to O (H_2O) shell) at the same position. A clear second peak observed in the hydrated $NdCl_3$ sample was attributed to Cl shell. The conc. HCl / MeOH mixed solution sample and the resin sample also gave small second peaks at the same position, indicating that there was a slight contribution of Cl shell in these EXAFS spectra. Additionally, it should be noted that the pyridine resin sample had a small but definitely distinguishable third peak at the asterisked ($\star$) point. These observations were also confirmed in the La and Ce K-edge EXAFS spectra given in **Figs. V-9** and **10** in Appendix V). Unfortunately, the EXAFS measurements for heavier Ln (Sm-Lu) were impossible due to their lower K_d for the pyridine resin in the present HCl / MeOH mixed solution.

There are two possible models assumed for fitting the EXAFS spectra of the pyridine resin samples, that is, the chloride complex ($NdCl_m \cdot nH_2O$) and the pyridine complex ($Nd(Py)_l\, Cl_m \cdot nH_2O$). If the pyridine resin works as an anion exchanger, Ln cations should form anionic chloride complexes to be adsorbed in the resin. On the
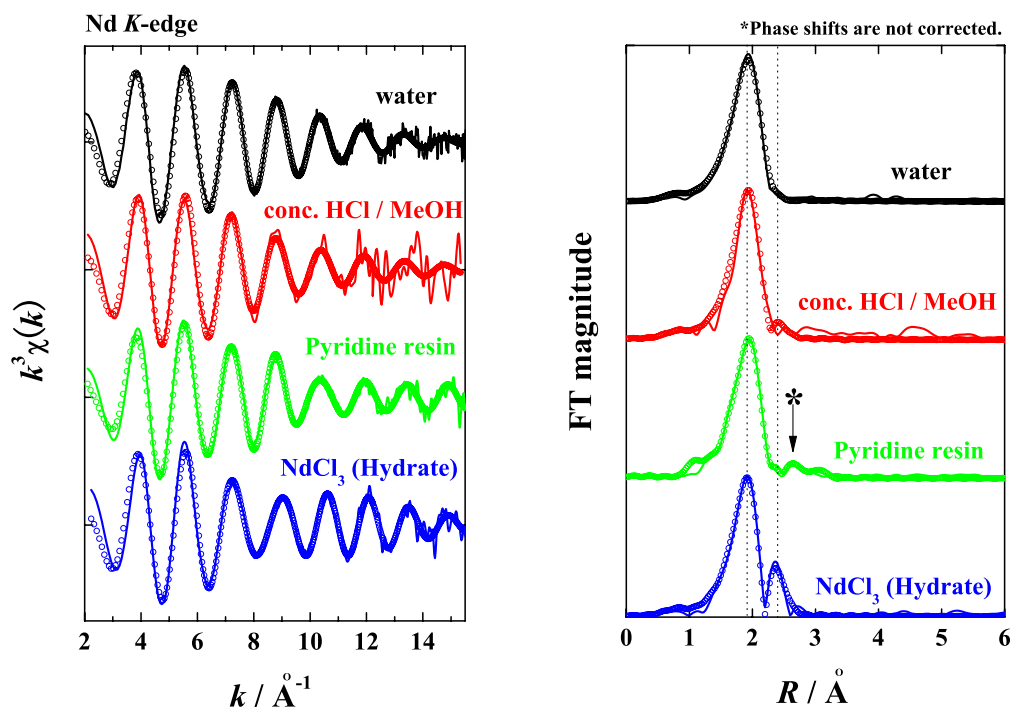
Figure 5-22. k^3-weighted EXAFS spectra of Nd K-edge for various chloride samples (left) and their corresponding Fourier transforms (right). (solid lines: experimental data, ○: curve fitting results, conc. HCl / MeOH = 5 / 5 (vol/vol), the composition of the solution phase of the resin sample was identical with that of the conc. HCl / MeOH solution sample.)

other hand, if the pyridine groups of the resin directly interact with the cations, the contribution of N (and C, according to circumstances) should appear in the EXAFS spectra. To identify the more reliable model, the EXAFS spectra of the pyridine resin samples were fitted by these two different models individually. The fitting results for the Nd sample are shown in **Fig. 5-23**.

In the k-range, it appears that the spectrum was well-fitted by both models and no considerable difference was found. However, a clear difference was observed in their FTs: the pyridine complex model (corresponding to the fitting by O, N, C, and Cl shells) brought a good curve fit even for the third peak, while the chloride complex model (corresponding to the fitting by O and Cl shells) could not trace the third peak.
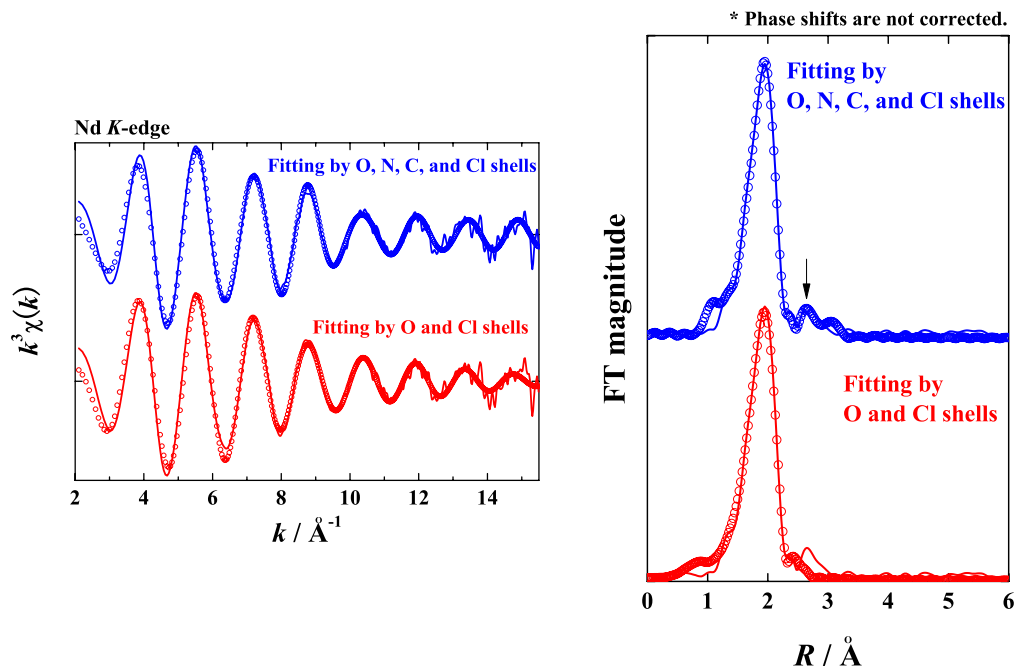
Figure 5-23. Curve fittings of the Nd *K*-edge EXAFS spectra of pyridine resin sample by two different models.

Therefore, we can conclude that the pyridine complex model is more reliable for the curve fitting of the pyridine resin samples. **Fig. 5-24** shows the contribution of each shell on the Fourier transformed Nd *K*-edge EXAFS spectra of the pyridine resin sample.

Table 5-12 summarizes the structural parameters obtained from the curve fitting. In the conc. HCl / MeOH solution system, the lighter Ln cations are surrounded by $\sim$9 water molecules and $\sim$1 Cl$^-$ ion in the solution phase. On the other hand, the hydration number decreases when the cations are adsorbed in the pyridine resin and the coordination of Py (N and C shells) appears instead. The obtained parameters suggest that at least one pyridine group directly interacts with the cations. However, considering the fact that the resin samples still retain considerable volume of the "*bulk*" solution inside their porous structures (**Fig. 5-25**) and, in consequence, the collected EXAFS spectra include not only the information of the adsorbed species
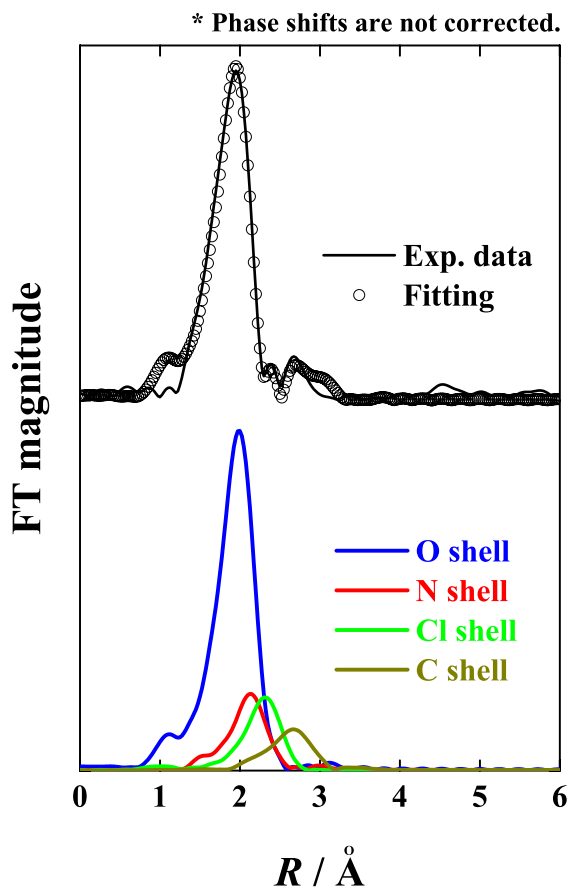
Figure 5-24. Contribution of O, N, C, and Cl shells on the Fourier transformed Nd K-edge EXAFS of pyridine resin sample.

but also the information of the "*bulk*" species ($\approx$ the chemical species in the solution phase), probably more than 1 pyridine interacts with the cations in the resin-solution interface. The actual Py coordination numbers evaluated from the distribution coefficients are 1.38, 1.69, and 0.94 for La, Ce, and Nd, respectively. The M-C distances obtained from the curve fitting are in good agreement with the theoretical distances calculated from the M-N distances using the Pythagorean theorem as shown in **Fig. 5-26**. This supports the validity of the pyridine complex model. The structural parameters for hydrated LnCl$_3$ samples gave good agreement with the results by XRD [118, 119], assuring the accuracy of the fittings for O and Cl shells.
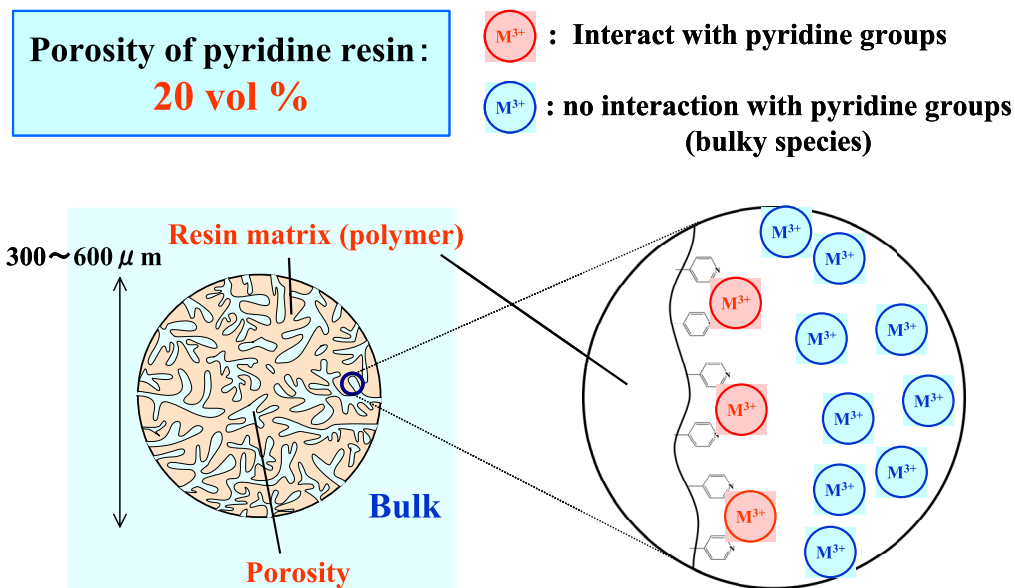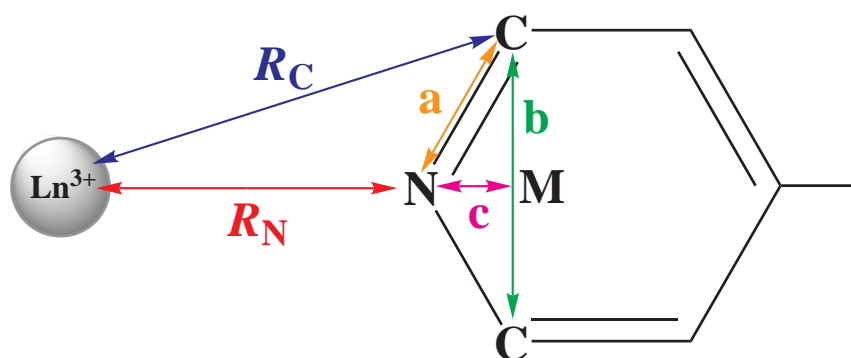
Figure 5-25. Schematic of the chemical environment in resin phase.

$$\angle\, NMC = 90°\ ,\ \angle\, CNM = 60°$$

$$a : b/2 : c = 2 : \sqrt{3} : 1,\quad (R_N + c)^2 + (b/2)^2 = R_C{}^2$$

$$a = 1.34\ \text{Å}\,,\ b = 2.30\ \text{Å}$$

Figure 5-26. Calculation of Ln-C distance from Ln-N distance using the Pythagorean theorem.

Table 5-12. EXAFS structural parameters of La, Ce, and Nd for various chloride samples. (Error: $R \pm 0.01$ Å, $N \pm 5\%$)

Element	Shell	water R / Å	N	conc. HCl / MeOH 5 / 5 (vol/vol) R / Å	N	Pyridine resin (conc. HCl / MeOH) R / Å	N	LnCl$_3$ (Hydrate) R / Å	N
La	O (H$_2$O) or N (Py)	2.55	9.5	2.55	7.9	2.53	8.2	2.54	8.0
	Cl			2.88	1.6	2.84	1.7	2.91	2.2
	C (Py)					3.50	2.2		
Ce	O (H$_2$O) or N (Py)	2.52	9.2	2.51	7.6	2.51	7.6	2.52	8.0
	Cl			2.78	1.4	2.82	1.9	2.89	2.2
	C (Py)					3.43	2.7		
Nd	O (H$_2$O) or N (Py)	2.48	9.3	2.48	8.0	2.48	8.0	2.45	8.0
	Cl			2.78	1.0	2.77	1.0	2.79	2.0
	C (Py)					3.40	1.5		

As mentioned above, the EXAFS measurements proved the direct interaction of pyridine groups with Ln cations in the resin phase. Hence it follows that the adsorption of An(III) and Ln(III) ions by the pyridine resin is "coordinative", not "anion exchange", and the observed separability of the pyridine resin for An(III) and Ln(III) must be attributed to the larger affinity of pyridine groups for An(III) over Ln(III) probably due to the stronger covalency in An bonding with soft donor ligands. The pyridine groups of the resin must overcome the strong hydration of An(III) and Ln(III) cations in order to interact directly with the cations. This means that the strength of hydration is an important factor in the adsorbability and separability of the pyridine resin. The present EXAFS measurements indicate that the hydration of Ln(III) ions is weakened in the resin phase probably due to the hydrophobicity of resin matrix. Furthermore, adding alcohol in solvent also promotes the dehydration by reducing a_w in solvent. As described in **5.1.1**, the hydration of An(III) and Ln(III) become stronger as an increase of atomic number and the hydration of An(III) is weaker than the homologous Ln(III). This is consistent with the observed separation results as

shown in **Fig. 4-18**. In addition, the adsorbed species are accompanied by some Cl^- ions to stabilize them in the resin phase. This chloride complexation enhances the separability for An(III) and Ln(III), as described in **5.1.3**.

Assuming that the pyridine groups directly interact with the cations, the protonation of pyridine groups inhibits this interaction between the pyridine groups and the metal cations. As described in **2.5**, the protonation of pyridine groups is quite strong and, thus, almost all of the pyridine groups of the resin are considered to be influenced by the protonation. Considering these facts, it appears to be difficult for An and Ln cations to interact directly with the pyridine groups in the present HCl solution system. However, as explained later with **Fig. 5-29**, the interaction between Ln(III) (An(III)) ions and pyridine seems to be as strong as that between H^+ and pyridine. Hence, the adsorption of An(III) and Ln(III) ions by the pyridine resin is considered to be in competition with the strong protonation of pyridine groups.

It has been mentioned in **5.1.1** that the hydration of An(III) and Ln(III) ions is very strong and their primary spheres are occupied by water molecules in aqueous chloride solutions even if alcohol is added to the solutions. However, this strong hydration will be relaxed in the resin phase due to the hydrophobic property of the resin matrix and, as a result, the pyridine groups of the resin can interact with the cations. In fact, several studies have suggested that the dehydration of cations occurs in organic resins [114–116, 154, 155]. Moreover, this dehydration in the resin phase is probably enhanced by the addition of alcohol in solvent owing to a decrease in water activity (a_w) [114–116], promoting the adsorbability of the pyridine resin. Adding alcohol in solvent also promotes the adsorbability of the resin by restraining of the protonation of pyridine groups, which hinders the interaction between the pyridine groups and the cations (**Fig. 2-16**). On the other hand, an increase of $X_{alcohol}$ in solvent reduces the concentration of Cl^- in solvent. As mentioned above, Cl^- plays an important role in the adsorbability and separability of the pyridine resin and, therefore, the decrease of [Cl^-] in solvent should lower both K_d and SF, as shown in **Fig. 4-20**. Furthermore, it is well-known that alcohols can dissolve organic compounds more easily than water. This means that alcohol molecules solvate an organic compound of pyridine more strongly than water. The solvation of pyridine groups by alcohol molecules surely obstructs the interaction between the pyridine groups and the cation and, hence, adding excessive alcohol in solvent causes a decrease in K_d. It should also be noted that the solubility of organic compounds in alcohol depends on the type of alcohol, meaning that the degree of the solvation

of pyridine groups also depends on the type of alcohol. The different adsorbability shown in **Figs. 4**-**4** and **4**-**23** probably reflects this different solvation ability of alcohols. The combination of these various phenomena must result in the observed irregular variations in K_d and *SF* (**Fig. 4**-**2**).

The interaction between the pyridine groups and the cations is hindered by the protonation and, thus, lowering the proton concentration ($[H^+]$) in solvent should strengthen the interaction. In this sense, H^+ is just a negative factor in the adsorbablity of the pyridine resin and, in fact, the adsorbability (K_d) of pyridine resin increases with a decrease of $[H^+]$, as shown in **Fig. 4**-**19**. However, to the contrary, An(III) and Ln(III) ions (especially An(III)) are adsorbed in the resin so strongly in the absence of H^+ (*e.g.* **Fig. 4**-**16**) that it is inappropriate to employ the non-acidic chloride solution for the separation of An(III) and Ln(III). In this point of view, H^+ functions as an eluent in the practical separation process and, consequently, a moderate concentration of H^+ is required for the efficient separation by the pyridine resin.

The unexpected chromatographic behavior of La is still open for discussion. **Fig. 5**-**27** gives the plot of the K_d of An(III) and Ln(III) in "conc. HCl / MeOH = 7 / 3" against their M-OH$_2$ distances in the same solvent. The M-OH$_2$ distances for Ln(III) were determined by XAFS in the present study. The values for Am and Cm are replaced by those in water [8]. The M-OH$_2$ distances for Ln(III) gradually decrease as increasing atomic number and, thus, the K_d of La still deviates from the decreasing relationship of other Ln in this plot. One of the possible interpretations of this La deviation is the contribution of $4f$-orbitals in Ln-Py bonding: $4f$-orbitals of Ln(III) ions has been considered to have almost no contribution in their bonding. However, a relatively recent study by Depaoli and his co-workers has demonstrated the possibility of weak but definite covalent interaction between the $4f$-orbitals of Eu(III) and N-donor ligand [156]. Assuming that the $4f$-orbitals of Ln(III) ions participate in Ln-N bonding, the interaction between La(III) ion and pyridine groups will become weaker than those for homologous Ln(III) ions (*i.e.* Ce(III)) since La(III) ion has no electron in its $4f$-orbitals. The same hypothesis can be applied to An(III) series. That is, the smaller K_d of Ac probably reflects the lack of electron in its $5f$-orbitals. As mentioned in the previous section, the contribution of $5f$-orbitals in An bonding is far larger than that of $4f$-orbitals in Ln bonding, meaning that Ac(III) ion forms far weaker bonding with pyridine groups than other An(III). This is consistent with the far smaller K_d of Ac(III) compared with other An(III), as shown in **Fig. 4**-**18**.

∗ Theoretical parameters ($F_j(k)$, $\delta_j(k)$, and λ) for the curve fitting of O, N, C, and Cl shells were calculated from the crystal structures of Ln chloride-Bpy complex [143] using FEFF code. (see **Fig. V-18** in Appendix V)
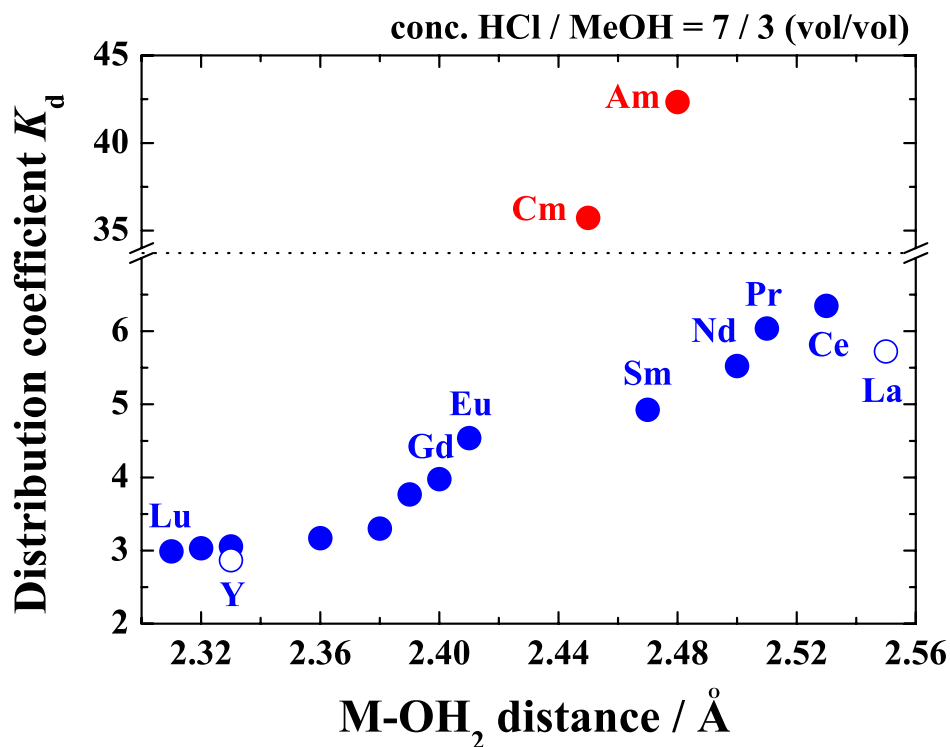

Figure 5-27. Variation of distribution coefficients of An(III) and Ln(III) in a conc. HCl / MeOH mixed solution at 293 K as a function of their M-OH$_2$ distances in the same solvent. (Solvent: conc. HCl / MeOH = 7 / 3 (vol/vol))

5.5.2 LiCl system

Although the direct interaction of pyridine groups has been proved in the HCl solution system, the contribution of pyridine groups on the observed EXAFS spectra was small and not so obvious. This is mainly due to the low K_d of Ln(III) in HCl solutions. Therefore, the XAFS measurements in a non-acidic chloride solution of LiCl solution is expected to give a clearer evidence of the contribution of pyridine groups since the K_d of Ln(III) in LiCl solutions is considerably larger than those in HCl so-

lutions (**Fig. 4-19**) and, thus, the interaction between the pyridine groups and the cations does not suffer from the protonation. In addition, the adsorption and separation behavior of Ln(III) (and probably An(III)) in the LiCl solution system was found to be different from that in the HCl solution system. This means that the adsorption and separation mechanisms in the LiCl solution system may be somewhat different from those in the HCl solution system. In order to clarify these issues, further XAFS measurements were performed in non-acidic LiCl solutions.

Figure 5-28 shows the EXAFS spectra ($k^3\chi(k)$ and FTs) collected in an aqueous LiCl solution system. The aqueous LiCl solution used for XAFS measurements was prepared by mixing an aqueous LiCl solution (11.7 mol-LiCl/dm^3) with MeOH. The mixing ratio was 5 / 5 (vol/vol). The spectrum in the aqueous LiCl / MeOH mixed solution gave almost the same oscillation pattern as that in water in k-space, while the spectrum in the pyridine resin displayed a slightly different frequency in higher k-range (10∼ Å). This spectral difference between the solution sample and the resin sample became clear for their corresponding FTs: The FT for the resin sample exhibited a shoulder at 2.2∼2.3 Å (corresponding to Cl shell) and, additionally, a small but distinguishable peak appeared at 2.8∼2.9 Å (corresponding to C (Py) shell).

The structural parameters obtained from the curve fitting are given in **Table 5-13**. The obtained parameters are almost the same to those for the conc. HCl / MeOH mixed solution system, indicating that the local environment of Nd ions for the aqueous LiCl / MeOH mixed solution system is almost identical with that in the conc. HCl / MeOH mixed solution system both in the solution phase and in the resin phase: the cations are slightly dehydrated and the Cl$^-$ complexation occurs instead in the solution phase, while the cations are surrounded by water molecules, pyridine groups, and Cl$^-$ ions in the resin phase. It should be noted that the coordination number of pyridine groups (*i.e.* N_N and N_C) in the present LiCl solution is slightly larger than that in the former conc. HCl solution. This can be interpreted as a result of the decrease of protonation of pyridine groups in the LiCl solution. That is, the cations can form more long-lasting bonding with pyridine groups in a non-acidic solution of LiCl solution than in an acidic solution of HCl solution due to the absence of protonation, bringing larger K_d in the aqueous LiCl solutions.

Table 5-13. EXAFS structural parameters of Nd for different aqueous LiCl / MeOH mixed solution samples. (Error: $R \pm 0.01$ Å, $N \pm 5\%$)

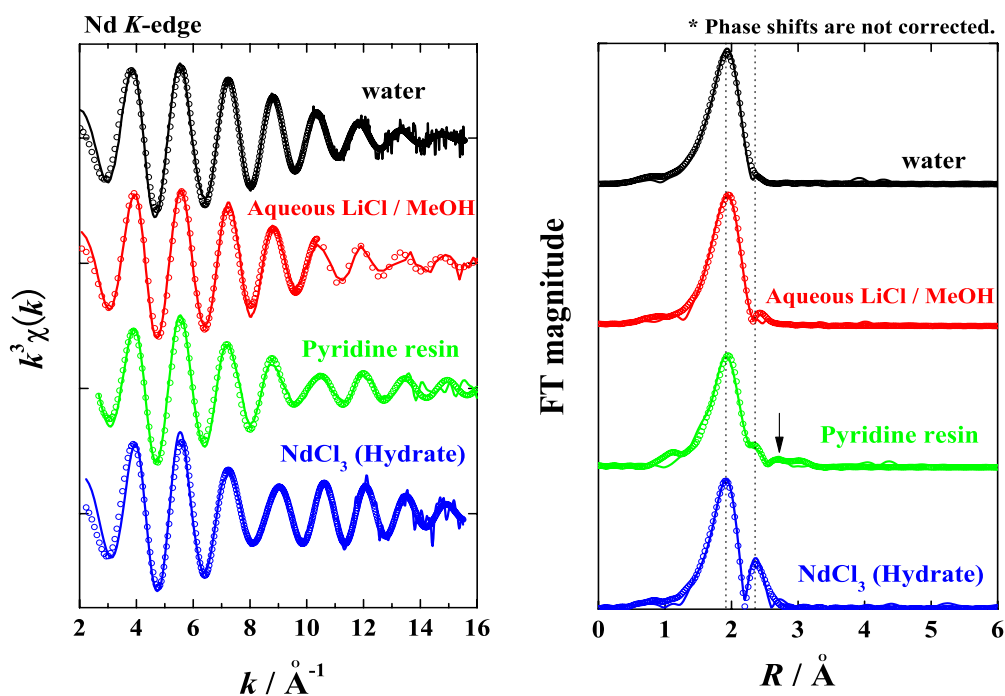| Element	Shell	water		11.7 M-LiCl / MeOH 5 / 5 (vol/vol)		Pyridine resin (from aqueous LiCl / MeOH)		NdCl$_3$ (Hydrate)	
		R / Å	N	R / Å	N	R / Å	N	R / Å	N
Nd	O (H$_2$O) or N (Py)	2.48	9.3	2.49	8.0	2.48	7.8	2.45	8.0
	Cl			2.77	1.0	2.78	1.2	2.79	2.0
	C (Py)					3.41	2.3		

Figure 5-28. k^3-weighted EXAFS spectra of Nd K-edge for aqueous LiCl / MeOH mixed solution samples (left) and their corresponding Fourier transforms (right). (solid lines: experimental data, ○: curve fitting results, Solvent: aqueous LiCl solution (11.7 mol-LiCl/dm^3) / MeOH = 5 / 5 (vol/vol), the composition of the solution phase of the resin sample was identical with that of the aqueous LiCl / MeOH solution sample.)

Unfortunately, the XAFS measurements have not given a clear evidence of stronger adsorbability of the pyridine resin even in a non-acidic chloride solution. In order to thrash out this issue, the local environment of pyridine was investigated in various solvent conditions by measuring the $\pi \rightarrow \pi*$ transition of pyridine. The results are shown in **Fig. 5-29**. The absorption spectrum in water + 0.1 mol-La/dm^3 was almost identical with that in water, implying that La(III) ions hardly form some complex with pyridine in water. The similar phenomenon was observed for a MeOH solution system, although the slightly increasing molar absorbance in MeOH + 0.1 mol-La/dm^3 indicated that La(III) ions can make some complex with pyridine in MeOH to a certain degree. The spectrum in conc. HCl displayed much higher molar absorbance due to the protonation of pyridine. The notable fact is that the absorption spectra in an aqueous LiCl solution system was different from those in water system. That is, the spectrum in an aqueous LiCl solution ([LiCl] = 11.7 mol/dm^3) exhibited larger molar absorbance than those in water system. This is probably caused by the coordination of Li$^+$ ions to pyridine. Additionally, the molar absorbance drastically increased when a 0.1 mol/dm^3 of La(III) ions were added to the aqueous LiCl solution. This increasing absorbance can be interpreted as a result of the interaction between pyridine and La(III) ions, suggesting that pyridine can coordinate to Ln(III) ions more easily in the aqueous LiCl solution than in pure water, MeOH, or HCl solution. The water activity (a_w) in the present aqueous LiCl / MeOH mixture is far lower than that in pure water due to the presence of alcohol and electrolytes (LiCl) with high concentration (see **Fig. 5-4**). This loosens the tight hydration of Ln(III) ions. Furthermore, the absence of protons in solvent surely promotes the direct interaction between the cations and pyridine. From these spectral results, the interaction with pyridine groups is expected to become stronger as the following order: Ln(III) ions in water > Ln(III) ions in alcohol > Li$^+$ ions > Ln(III) ions in aqueous LiCl solution > protons (H$^+$). These results support the observed larger K_d of Ln(III) (and An(III)) ions in aqueous LiCl solutions.
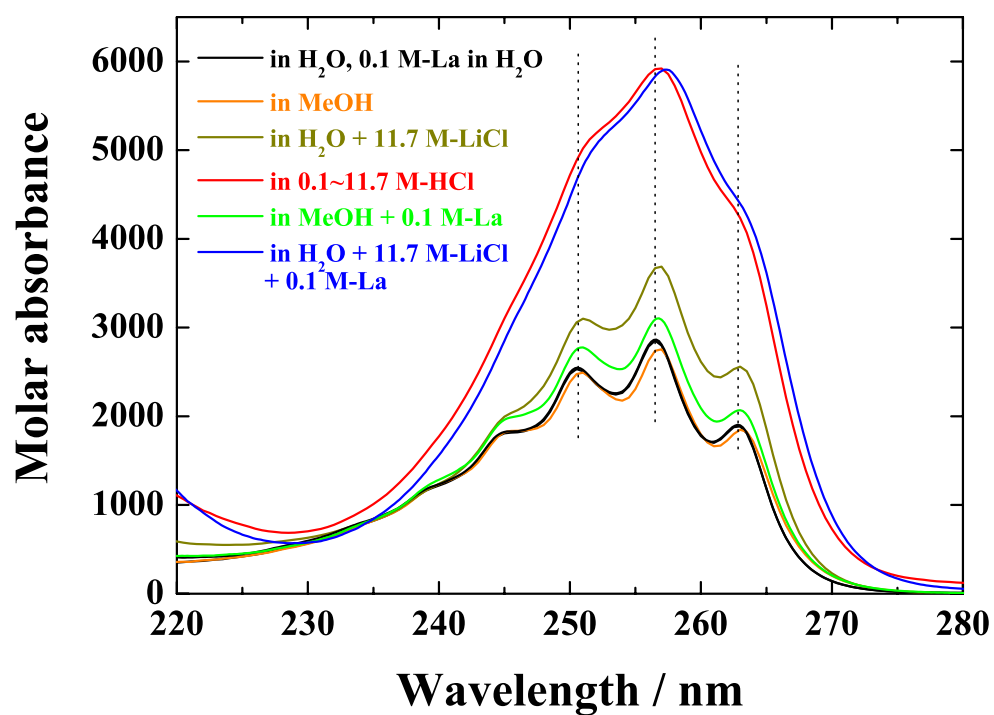
Figure 5-29. Variation of UV-visible absorption spectra of the $\pi \rightarrow \pi*$ transition of pyridine in different chemical environments.

In order to acquire a clearer evidence of the direct interaction of pyridine groups to the Ln cations by XAFS, we need to weaken the hydration of the cations. Then, a methanolic LiCl solution (*i.e.* LiCl was dissolved in pure methanol (99.8∼%-purity)) was employed to prepare samples. The concentration of LiCl was adjusted to 5.0 mol/dm^3. The XAFS measurements were performed for solution, pyridine resin, and Dowex 1X8 samples.

Figure 5-30 gives the k^3-weighted EXAFS spectra of Nd K-edge and their corresponding FTs. The results for La and Ce K-edges are also given in **Figs. V-13** and **V-14** in Appendix V. The k^3-weighted EXAFS spectrum in the methanolic LiCl solution exhibited different oscillation pattern over ∼7 Å^{-1} compared with that in water. The oscillation pattern of the resin samples (both pyridine resin and Dowex 1X8 samples) were similar to that of the methanolic LiCl solution sample, but the amplitude of their oscillations were larger than that of the solution sample. On the other hand, the FTs indicated that the resin samples (pyridine resin and Dowex 1X8) had larger first peaks than the water sample and their peak positions were longer than that of the water sample. The FT of the methanolic LiCl solution sample appeared to be the mixture of the FT of the water sample and those of the resin samples.

The structural parameters obtained from the curve fitting are listed in **Table 5-14**. Unfortunately, no clear proof of the interaction of the pyridine groups and the cations was obtained even in this solution system, whereas the hydration of Ln(III) ions obviously became weak in the methanolic LiCl solution and the chloride complexation is promoted instead. However, it does not mean that the contribution of pyridine groups is still weak, but it means that the contribution of chloride ions becomes too strong. The size of chloride atoms are considerably larger than those of other C, N, and O atoms, bringing 2∼5 times larger back scattering amplitude of chloride atoms compared with those of C, N, and O atoms [80]. Therefore, the increase of the contribution of chloride atoms makes the contribution of other lighter atoms indistinctive. Additionally, the "bulky" solution inside the porosity of the resin also has a great influence on the reduction of the EXAFS signals from C, N, and O atoms (**Fig. 5-25**). Considering the spectral evidence shown in **Fig. 5-29** and the fact that the cations are strongly adsorbed in the pyridine resin in the absence of H$^+$, the direct interaction of pyridine groups seems to be the most reliable interpretation for the observed strong adsorption in non-acidic LiCl solutions.
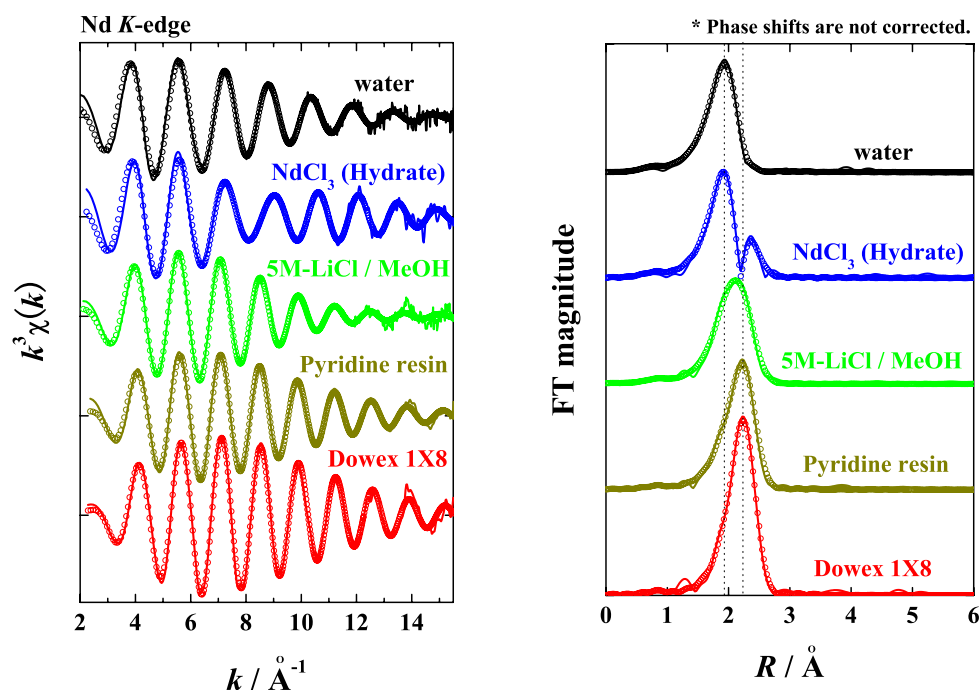
Figure 5-30. k^3-weighted EXAFS spectra of Nd K-edge for various chloride samples (left) and their corresponding Fourier transforms (right). (solid lines: experimental data, ○: curve fitting results, the composition of the solution phase of the resin sample was identical with that of the 5M-LiCl / MeOH solution sample.)

Table 5-14. EXAFS structural parameters of La, Ce, and Nd for different methanolic LiCl samples. (Error: $R \pm 0.01$ Å, $N \pm 5\%$)

Element	Shell	water		LiCl / MeOH [LiCl] = 5.0 mol/dm^3		Pyridine resin (from LiCl / MeOH)		Dowex 1X8 (from LiCl / MeOH)	
		R / Å	N	R / Å	N	R / Å	N	R / Å	N
La	O (H$_2$O)	2.55	9.5	2.55	4.9	2.53	2.8	2.55	1.3
	Cl			2.83	3.9	2.83	4.5	2.82	7.0
Ce	O (H$_2$O)	2.52	9.2	2.53	4.6	2.50	0.6	2.52	0.1
	Cl			2.78	4.1	2.77	6.3	2.77	6.8
Nd	O (H$_2$O)	2.48	9.3	2.51	5.5	2.49	1.1	2.47	0.6
	Cl			2.75	4.5	2.74	6.1	2.73	7.2

Although the clear evidence of the direct interaction of pyridine groups has not been obtained, it should be noted that the dehydration of the cations is promoted when the cations are adsorbed in the resin. The Ln(III) ions are still hydrated by 4~5 water (and probably methanol) molecules in the methanolic LiCl solution. However, these hydrated water molecules are detached when the cations penetrate the resin phase and, as a result, the chloride complexation is enhanced in the resin phase. These results imply that hydrated species are not favorable in the resin phase probably due to the hydrophobicity of resin matrix. The presence of Cl$^-$ in solution enhances the dehydration of cations by forming chloride complexes, improving the adsorbability. In fact, the K_d of Ln(III) are very small in pure methanol solvent (**Fig. IV-15** in Appendix IV), in which Ln(III) ions are still hydrated (**Table 5-7**), while the K_d increase as [LiCl] increases as shown in **Fig. 5-31**. Additionally, the Ln(III) ions can form anionic chloride complexes in the present methanolic LiCl solution and, in consequence, they are also adsorbed in an anion exchange resin.
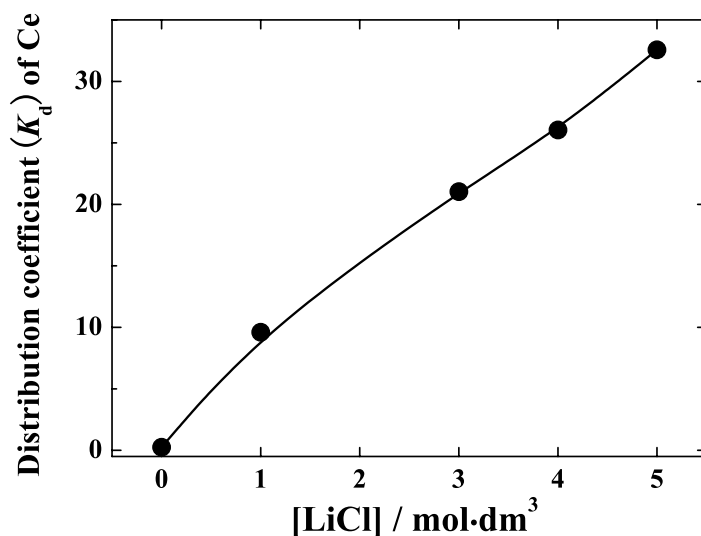

Figure 5-31. [LiCl] dependence of distribution coefficients of Ce in methanolic LiCl solutions at 288 K. (Purity of methanol: 99.8~%)

The degree of dehydration and chloride complexation in the resin phase depends on the type of cations: Ce(III) ion detaches most of its hydrated water molecules in the resin phase and it is probably adsorbed as a non-hydrated chloride complex

([CeCl$_n$]$^{(3-n)-}$), while La(III) ion still holds 2~3 water molecules even in the resin phase. This difference surely affects the adsorbability of these cations.

Interestingly, Ln(III) ions are dehydrated more strongly in the anion exchange resin of Dowex 1X8 than in the pyridine resin. **Fig. 5-32** shows the contribution of O and Cl shells on each Fourier transformed Nd K-edge EXAFS spectrum. The contribution of Cl shell is almost indistinguishable on the spectrum of Dowex 1X8, while small but apparent contribution of Cl shell is observed on the spectrum of the pyridine resin. These results indicate that the chemical environment formed in Dowex 1X8 (quaternary ammonium type anion exchange resin) is more hydrophobic than that formed in the pyridine resin.
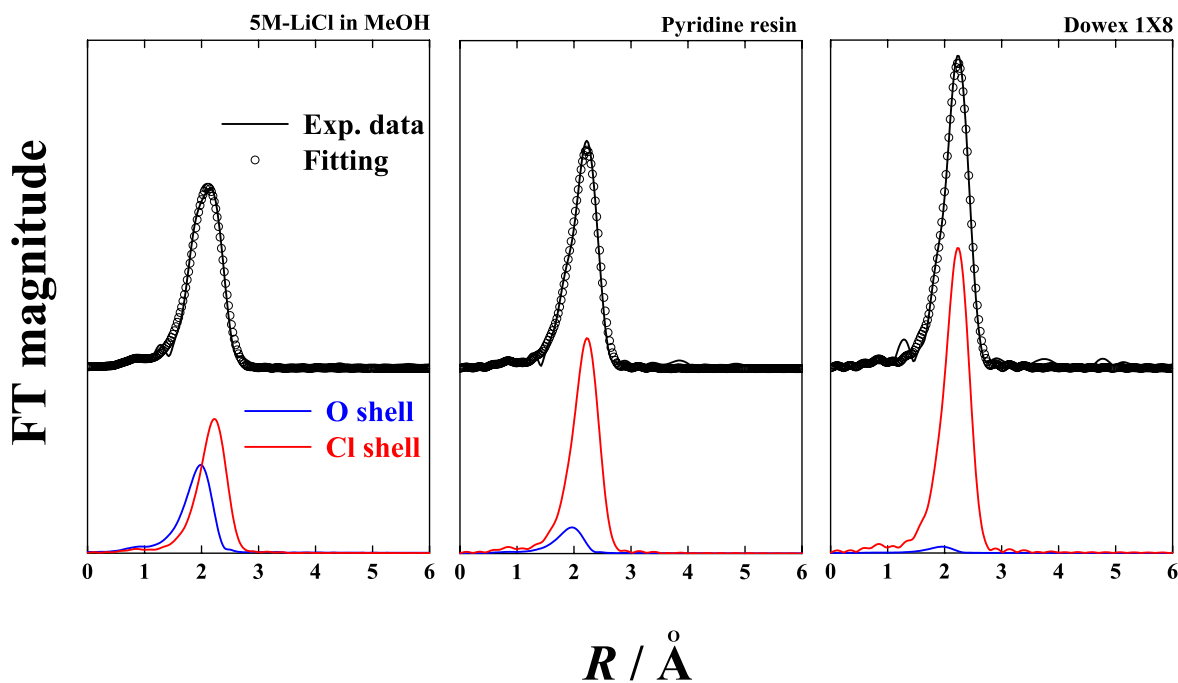

Figure 5-32.   Contribution of O and Cl shells on the Fourier transformed Nd K-edge EXAFS of different methanolic LiCl solution samples.   (Phase shifts are not corrected.)

5.5.3   HNO$_3$ system

As demonstrated in chapter 4, the adsorption and separation properties of the tertiary pyridine resin in the nitrate (HNO$_3$ and LiNO$_3$) solution system is quite different from those in the chloride solution system. That is, the K_d of An(III) and Ln(III) simply depend on their ionic radii in the nitrate system, while An(III) exhibit far larger K_d than Ln(III) in the chloride system. Furthermore, the individual separation of Am and Cm can be achieved in the nitrate system, while it seems difficult to apply the chloride system to the individual separation of An(III) and Ln(III). These differences in adsorption and separation behavior must be originated in the different adsorption mechanism in the two different solvent systems. Then, further XAFS measurements were carried out in the HNO$_3$ solution system in order to compare the adsorption mechanism in the nitrate solution system with that in the chloride solution system and to elucidate the origin of the different adsorption and separation behavior.

Figures 5-33 shows the Nd K-edge and Sm L_{III}-edge EXAFS spectra ($k^3\chi(k)$ and FTs) in a conc. HNO$_3$ / MeOH mixed solution and its corresponding pyridine resin sample. The results of Er L_{III}-edge are also given in **Fig. V-15**. The measured three Ln(III) showed complicated oscillation patterns in k-range both for their solution and resin samples. Their corresponding FTs displayed a clear evidence of MS by NO$_3$ ions at 3.5~4.0 Å, indicating that NO$_3^-$ ions still form inner-sphere complexes with Ln(III) ions even in the resin phase.

Table 5-15 summarizes the structural parameters obtained from the curve fitting. The notable thing is that the adsorption of Nd(III) ions in the pyridine resin is accompanied by the dehydration followed by the nitrate complexation, forming an anionic complex of [Nd(NO$_3$)$_4 \cdot n$H$_2$O]$^-$. in the resin phase. On the other hand, the adsorption of Sm(III) ions is also accompanied by the dehydration, but it does not involve further nitrate complexation. In consequence, Sm(III) ions keep the same cationic complexes with NO$_3^-$ ions (*i.e.* [Sm(NO$_3$)$_2 \cdot n$H$_2$O]$^+$) even in the resin phase, even though the atomic number (*i.e.* ionic radius) of Sm is close to that of Nd. Er(III) ions also exhibit no structural change. The comparison of FTs given in **Fig. 5-34** clearly demonstrates the difference of these structural change of Nd and Sm between the solution phase and the resin phase. Besides, no distinguishable contribution of Py coordination was observed for all the measured spectra.
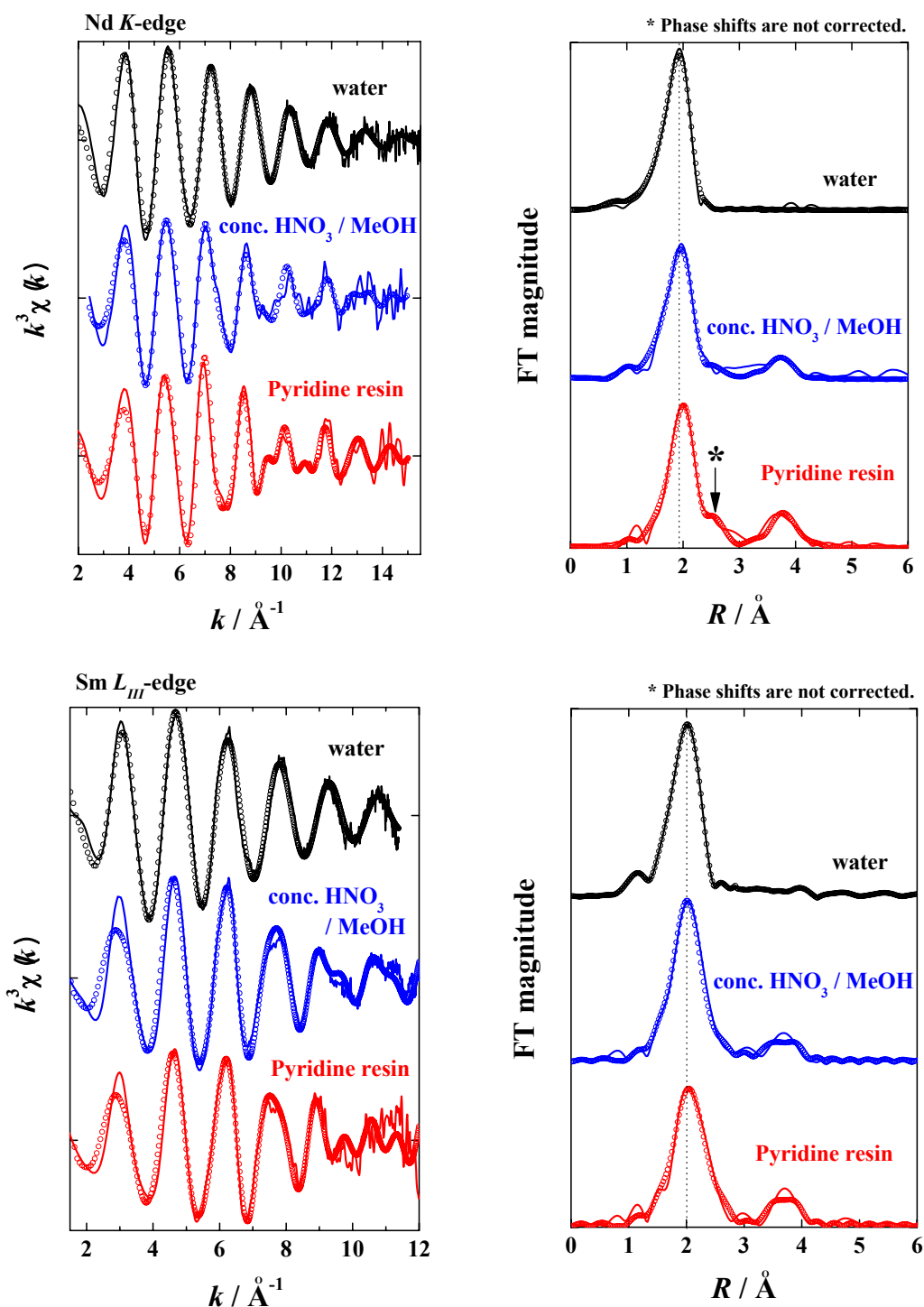
Figure 5-33. k^3-weighted EXAFS spectra of Nd K-edge and Sm L_{III}-edge in a HNO_3 / MeOH mixed solution system (left) and their corresponding Fourier transforms (right). (solid lines: experimental data, ○: curve fitting results, Solvent: conc. HNO_3 / MeOH = 5 / 5 (vol/vol))

Table 5-15. EXAFS structural parameters of Nd, Sm, and Er in a HNO_3 / MeOH mixed solution system. (Error: $R \pm 0.01$ Å, $N \pm 5\%$)

Element	Edge	Shell	water		conc. HNO_3 / MeOH 5 / 5 (vol/vol)		Pyridine resin (from conc. HNO_3 / MeOH)	
			R / Å	N	R / Å	N	R / Å	N
Nd	K	O (H_2O)	2.48	9.3	2.49	5.0	2.48	1.0
		O (O_2NO)			2.57	4.0	2.57	8.0
		N (NO_3)			3.02	2.0	3.02	4.0
		MS (NO_3)			4.19	2.0	4.27	4.0
Sm	L_{III}	O (H_2O)	2.46	9.4	2.44	5.0	2.44	4.8
		O (O_2NO)			2.52	4.0	2.52	4.0
		N (NO_3)			2.99	2.0	2.98	2.0
		MS (NO_3)			4.22	2.0	4.21	2.0
Er	L_{III}	O (H_2O)	2.35	8.2	2.34	4.3	2.34	4.0
		O (O_2NO)			2.43	4.1	2.43	4.0
		N (NO_3)			2.91	2.1	2.91	2.0
		MS (NO_3)			4.09	2.1	4.09	2.0

The obtained structural parameters suggest that Ln(III) ions form some nitrate complexes in the pyridine resin and there seems to be no contribution of Py on the adsorption of the cations in the resin in HNO_3 / MeOH mixed solutions. Considering these facts, the adsorption mechanism of the pyridine resin in alcoholic HNO_3 solutions is expected to be "anion-exchange", not "coordinative". That is, the cations are adsorbed in the resin as anionic nitrate complexes like $[Nd(NO_3)_4 \cdot nH_2O]^-$ by the protonated (*i.e.* positively-charged) pyridine groups. Assuming that the adsorption mechanism in the HNO_3 solution system is "anion-exchange", the cationic complexes of Ln(III) ions, such as $[Sm(NO_3)_2 \cdot nH_2O]^+$, are suppose not to be adsorbed in the resin. As a matter of fact, the adsorbability of Ln(III) drastically changes between Nd and Sm in the practical chromatographic process (*e.g.* **Fig. 3-3**), supporting the validity of the above 'anion-exchange" hypothesis. The chromatographic behavior of Ln(III) by an anion exchange resin (**Fig. 3-12**) can also be interpreted in the same hypothesis, emphasizing the hypothesis.

The hypothesis of "anion-exchange" also gives a good explanation for the observed clear individual separation between Am and Cm in HNO_3 / MeOH mixed solutions (**Figs. 3-20~22**). As shown in **Fig. 5-35**, the M-OH_2 distances Am and Cm in

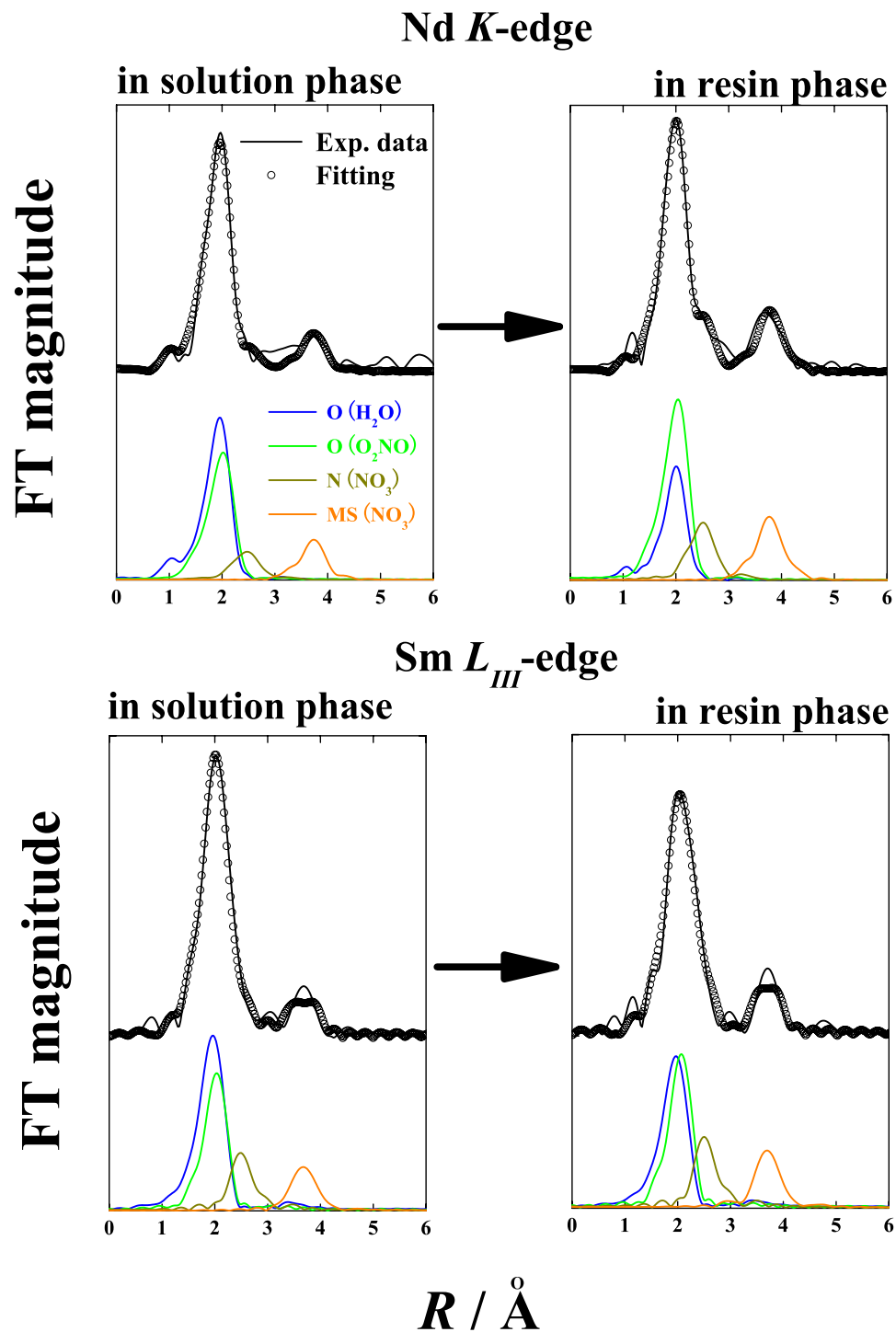**Figure 5-34.** Contribution of O(H$_2$O), O(O$_2$NO), N, and O(ONO$_2$) shells on the Fourier transformed Nd K-edge and Sm L_{III}-edge EXAFS in a HNO$_3$ / MeOH mixed solution system. (Phase shifts are not corrected.)

aqueous solution are close to those of Nd and Sm, suggesting a great possibility that there is also a difference in the nitrate complexation in the resin phase between Am and Cm. That is, Am(III) ions form anionic complexes with NO_3^- ions (*i.e.* $[Am(NO_3)_4 \cdot nH_2O]^-$) in the resin phase and they are adsorbed in the protonated pyridine resin, while Cm(III) ions hold their cationic complexes ($[Cm(NO_3)_2 \cdot nH_2O]^+$) even in the resin phase and, consequently, they are not adsorbed in the resin so strongly. The difference in the nitrate complexation between Am(III) and Cm(III) ions is expected to be very sensitive to the composition of the solvent (*i.e.* $[HNO_3]$ and $X_{alcohol}$) since the sizes of Am(III) and Cm(III) ions are probably the boundary line that decides the manner of the nitrate complexation in the resin phase. The same explanation can be applied to the observed chromatographic behavior of Am and Cm by a quaternary pyridinium type anion exchange resin (**Fig. 3-22**).
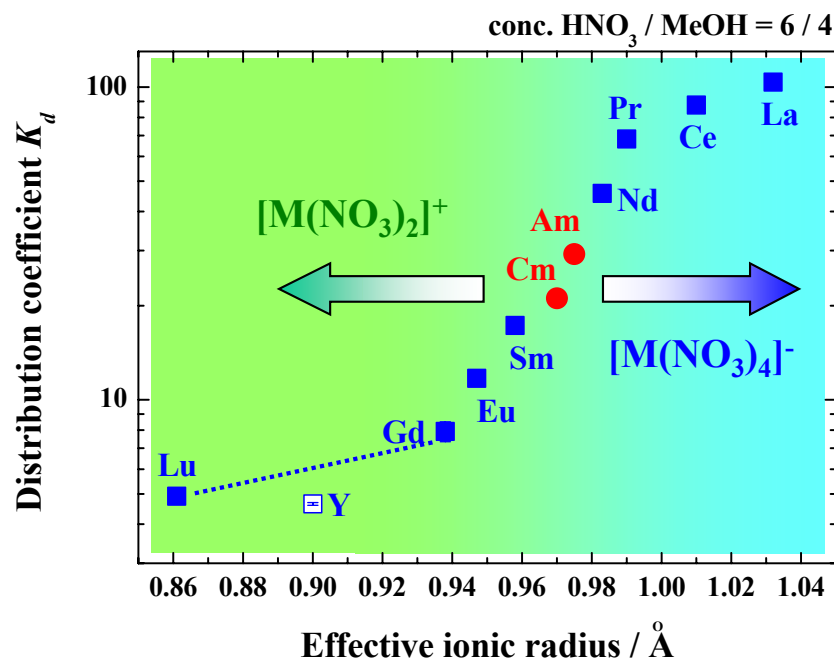

Figure 5-35. Variation of distribution coefficients of An(III) and Ln(III) in a conc. HNO_3 / MeOH mixed solution at 298 K as a function of their M-OH$_2$ distances in the same solvent. (Solvent: conc. HNO_3 / MeOH = 5 / 5 (vol/vol), Effective ionic radii: [9])

Although no data could be obtained concerning a non-acidic nitrate solution of $LiNO_3$ solution, the adsorption mechanism in this solution system is likely to be "coordinative", not "anion exchange". As mentioned before, the pyridine groups of the resin are hardly protonated in a non-acidic solution. Besides, An(III) and Ln(III) ions can form less hydrophilic species in the nitrate solution system due to the coordination of NO_3^- ions in their primary sphere. Assuming that the adsorption of the cations in $LiNO_3$ solution is "coordinative", this solution system also has a potential for the intergroup separation of An(III) and Ln(III). Unfortunately, no data has been available concerning the adsorption and separation behavior of An(III) and Ln(III) mixture in this solution system at the moment. However, the non-acidic nitrate solution system is supposed to be less effective for the intergroup separation of An(III) and Ln(III) than the chloride solution system because there is no synergic effect, as observed in the chloride solution system, on distinguishing the stronger covalency in An-bonding and, furthermore, NO_3^- ions coordinate to the cations with bidentate mode so strongly that they may cause undesirable steric hindrance to the interaction between the cations and pyridine groups.

5.6 Improvement of Partitioning System for More Effective Separation of Trivalent An and Ln

Table 5-16 summarizes the adsorption and separation mechanisms by a tertiary pyridine resin in various solvent systems. On the basis of these proposed mechanisms, further discussion is made for improving the partitioning system using the tertiary pyridine resin.

Basically, the chloride solution systems are appropriate for the intergroup separation of An(III) and Ln(III), while the nitrate solution systems should be employed for the individual separation of An(III) and Ln(III). As demonstrated in chapter 3, a sufficient intergroup separation of An(III) and Ln(III) has been obtained in alcoholic HCl solutions. Thus, the problem for the intergroup separation is not the separability, but the acidity of the solvent used. Using HCl for solvent gives rise to an acidic corrosion of equipment. However, the other side of the coin is that a considerable high concentration of Cl^- is required in order to reduce a_w and to form some hydrophobic

Table 5-16. Adsorption and separation mechanisms by a tertiary pyridine resin in different solvent systems.

Solvent system	Adsorption	Adsorbability	Separability	
			Intergroup	Intragroup
HCl	Coordinative	Appropriate	○	△
LiCl	Coordinative	Strong	△	△
HNO_3	Anion exchange	Appropriate-Strong	×	○
$LiNO_3$	Coordinative	Appropriate-Strong	○ ?	○ ?

chloride complexes in the resin phase. Moreover, a moderate concentration of H^+ is indispensable for a smooth elution in chromatography. Taking these factors into consideration, a ternary system of HCl-LiCl-alcohol should be the best solvent system for the intergroup separation of An(III) and Ln(III) by the pyridine resin: the $[H^+]$ can be optimized by changing the mixing ratio of HCl and LiCl, and the hydration of cations in the resin phase is restrained by adding alcohol in solvent. For the alcohols to be added, larger and branched alcohols are probably appropriate in order to minimize the solvation of pyridine groups by alcohol molecules. Adding nonpolar liquids, such as benzene or carbon tetrachloride, in the solvent may also be effective for improving the adsorbability and separability since they can reduce a_w without solvating the cations and pyridine groups.

On the other hand, the nitrate solution systems have a great potential for several specific individual separations, such as the separation of Am and Cm. However, the tertiary pyridine resin is not necessarily the best resin for the individual separations because the tertiary pyridine resin probably works as an anion exchanger in HNO_3 solutions and other anion exchange resins also give sufficient individual separations, although the tertiary pyridine resin might display another unique separability for An(III) and Ln(III) in non-acidic nitrate solutions. Considering the facts that the tertiary pyridine resin is effective only in acidic solutions and its adsorption capacity is lower than those of other strongly basic anion exchange resins, the tertiary pyridine resin is by no means the best selection for the individual separation. Using a strongly basic anion exchange resin with non-acidic nitrate solution seems to be the mildest and the most effective way to separate some specific An(III) and Ln(III).

5.7 Summary

The adsorption and separation properties of a tertiary pyridine resin for An(III) and Ln(III) were discussed in detail from the point of view of solution and complexation chemistry. An(III) and Ln(III) ions are strongly hydrated by 8-9 water molecules in aqueous solution and their hydration becomes stronger as an increase of atomic number. The hydration of An(III) is slightly weaker than that of Ln(III). In chloride solutions, the cations basically form outer-sphere complexes with Cl^- ions and, consequently, their primary sphere is still occupied by water molecules. NO_3^- ions coordinate to the primary sphere of the cations in nitrate solutions, forming inner-sphere complexes. Adding alcohols in aqueous solutions changes the properties and structure of solvent and it surely influences the properties and structure of solvent, whereas the hydration and anion complexation structures of the cations is hardly affected by the addition of alcohol in the solution phase.

On the other hand, the chemical environment in the resin phase is quite different from that in the solution phase. An(III) and Ln(III) ions are dehydrated when they are adsorbed in the resin and, as a result, anion complexation is enhanced in the resin phase probably due to the hydrophobicity of resin matrix. These dehydration and promoted anion complexation occur not only in the tertiary pyridine resin, but also in other anion exchange resins. The tertiary pyridine resin can function both as a coordinative extractant and as an anion exchanger. That is, the tertiary pyridine resin works as a coordinative extractant in HCl and LiCl solutions and the adsorption in these solutions is caused by the direct interaction of pyridine groups, while the adsorption in HNO_3 solution is attributed to the anion exchange interaction between the protonated (*i.e.* positively-charged) pyridine groups and the negatively-charged nitrate complexes of An(III) and Ln(III) ions. The observed different adsorption and separation properties of the tertiary pyridine resin in chloride solutions and nitrate solutions is due to this difference in adsorption mechanism. The larger adsorbability of the pyridine resin for An(III) ions in the chloride solution system originates in the synergic effect of the pyridine interaction and chloride complexation: both pyridine and chloride ions are classified as "soft donors" and the affinity of these soft donors for An(III) is larger than that for Ln(III). On the other hand, the separability of the pyridine resin (and other anion exchange resins) for An(III) and Ln(III) ions in the nitrate solution system is simply governed by the coordination number of NO_3^- ions of the cations. That is, the cations which can form a negatively-charged nitrate

complex ($[M^{3+}(NO_3)_4 \cdot nH_2O]^-$) in the resin phase are adsorbed in the resins more strongly than other cations which can not form the anionic complex.

References

[1] A. Habenschuss, F. H. Spedding, *J. Chem. Phys.*, **70**, 2797 (1979).

[2] A. Habenschuss, F. H. Spedding, ibid., **70**, 3758 (1979).

[3] A. H. Narten, R. L. Hahn, *J. Phys. Chem.*, **87**, 3193 (1983).

[4] B. K. Annis, R. L. Hahn, A. H. Narten, *J. Chem. Phys.*, **82**, 2086 (1985).

[5] C. Cossy, A. C. Barnes, J. E. Enderby, ibid., **90**, 3254 (1989).

[6] L. Helm, A. E. Merbach, *Eur. J. Solid State Inorg. Chem.*, **28**, 245 (1991).

[7] T. Yamaguchi, M. Nomura, H. Wakita, H. Ohtaki, *J. Chem. Phys.*, **89**, 5153 (1988).

[8] P. G. Allen, J. J. Bucher, D. K. Shuh, N. M. Edelstein, I. Craig, *Inorg. Chem.*, **39**, 595 (2000).

[9] R. D. Shannon, *Acta Cryst.*, **A32**, 751 (1976).

[10] G. R. Choppin, *Radiochim. Acta*, **32**, 43 (1983).

[11] H. Kanno, J. Hiraishi, *J. Phys. Chem.*, **86**, 1488 (1982).

[12] F. H. Spedding, M. J. Pikal, B. O. Ayers, ibid., **70**, 2440 (1966).

[13] F. H. Spedding, V. W. Saeger, K. A. Gray, P. K. Boneau, M. A. Brown, C. W. DeKock, J. L. Baker, L. E. Shiers, H. O. Weber, A. Habenschuss, *J. Chem. Eng. Data*, **20**, 72 (1975).

[14] E. N. Rizkalla, G. R. Choppin, *J. Alloys Compd.*, **180**, 325 (1992).

[15] F. David, *J. Less-Comm. Met.*, **121**, 27 (1986).

[16] C. Cossy, L. Helm, A. E. Merbach, *Inorg. Chem.*, **27**, 1973 (1988).

[17] C. Cossy, L. Helm, A. E. Merbach, ibid., **28**, 2699 (1989).

[18] D. F. Peppard, G. W. Mason, I. Hucher, *J. Inorg. Nucl. Chem.*, **24**, 881 (1962).

[19] G. R. Choppin, P. J. Unrein, ibid., **25**, 387 (1963).

[20] B. M. L. Bansal, S. K. Patil, H. D. Sharma, ibid., **26**, 993 (1964).

[21] T. Sekine, ibid., **26**, 1463 (1964).

[22] T. Sekine, *Acta Chem. Scand.*, **19**, 1435 (1965).

[23] L. S. Smith, Jr., D. L. Wertz, *J. Am. Chem. Soc.*, **97**, 2365 (1975).

[24] M. L. Steele, D. L. Wertz, ibid., **98**, 4424 (1976).

[25] M. L. Steele, D. L. Wertz, *Inorg. Chem.*, **16**, 1225 (1977).

[26] G. Johansson, H. Yokoyama, ibid., **29**, 2460 (1990).

[27] G. R. Choppin, W. F. Strazik, ibid., **4**, 1250 (1965).

[28] G. R. Choppin, D. E. Henrie, K. Buijs, ibid., **5**, 1743 (1966).

[29] N. A. Coward, R. W. Kiser, *J. Phys. Chem.*, **70**, 213 (1966).

[30] I. Abrahamer, Y. Marcus, *J. Inorg. Nucl. Chem.*, **30**, 1563 (1968).

[31] M. Shiloh, M. Givon, Y. Marcus, ibid., **31**, 1807 (1969).

[32] J. Knoeck, *Anal. Chem.*, **41**, 2069 (1969).

[33] A. S. C. Cheung, D. E. Irish, *J. Inorg. Nucl. Chem.*, **43**, 1383 (1981).

[34] H. Kanno, J. Hiraishi, *J. Phys. Chem.*, **88**, 2787 (1984).

[35] K. Nakamura, K. Kawamura, *Bull. Chem. Soc. Jpn.*, **44**, 330 (1971).

[36] J. Reidler, H. B. Silber, *J. Chem. Soc. Chem. Comm.*, 354 (1973).

[37] J. Reuben, *J. Phys. Chem.*, **79**, 2154 (1975).

[38] T. Yaita, D. Ito, S. Tachimori, ibid., **102**, 3886 (1998).

[39] R. Garnsey, D. W. Ebdon, *J. Am. Chem. Soc.*, **91**, 50 (1969).

[40] J.-C. G. Bünzli, J.-R. Yersin, *Inorg. Chem.*, **18**, 605 (1979).

[41] H. Yokoyama, G. Johansson, *Acta. Chem. Scand.*, **44**, 567 (1990).

[42] P. G. Allen, D. K. Veirs, S. D. Conradson, C. A. Smith, S. F. Marsh, *Inorg. Chem.*, **35**, 2841 (1996).

[43] T. Yaita, H. Narita, S. Suzuki, S. Tachimori, H. Motohashi, H. Shiwaku, *J. Radioanal. Nucl. Chem.*, **239**, 371 (1999).

[44] Y. Marcus, "Introduction to Liquid State Chemistry", John Wiley & Sons, London (1977).

[45] M. E. Guendouzi, A. Dinane, A. Mounir, *J. Chem. Thermodynamics*, **33**, 1059 (2001).

[46] W. Davis, Jr., H. J. De Bruin, *J. Inorg. Nucl. Chem.*, **26**, 1069 (1964).

[47] Y. Zhu, J. Chen, R. Jiao, *Solv. Extr. Ion Exch.*, **14**, 61 (1996).

[48] M. Miguirditchian, D. Guillaneux, D. Guillamont, P. Moisy, C. Madic, M. P. Jensen, K. L. Nash, *Inorg. Chem.*, **44**, 1404 (2005).

[49] G. R. Choppin, Q. Liu, J. C. Sullivan, *Inorg. Chem.*, **24**, 3968 (1985).

[50] G. R. Choppin, E. N. Rizkalla, J. C. Sullivan, ibid., **26**, 2318 (1987).

[51] G. R. Choppin, *J. Alloys Compd.*, **223**, 174 (1995).

[52] G. R. Choppin, ibid., **344**, 55 (2002).

[53] D. D. Ensor, G. D. Jarvinen, B. F. Smith, *Solv. Extr. Ion Exch.*, **6**, 439 (1988).

[54] Z. Kolarik, U. Mülllich, F. Gassner, ibid., **17**, 23 (1999).

[55] M. Watanabe, R. Mirvaliev, S. Tachimori, K. Takeshita, Y. Nakano, K. Morikawa, R. Mori, *Chem. Lett.*, **31**, 1230 (2002).

[56] Z. Kolarik, U. Mülllich, *Solv. Extr. Ion Exch.*, **15**, 361 (1997).

[57] P.-Y. Cordier, C. Hill, P. Baron, C. Madic, M. J. Hudson, J. O. Liljenzin, *J. Alloys Compd.*, **271**-**273**, 738 (1998).

[58] K. Street, Jr., G. T. Seaborg, *J. Am. Chem. Soc.*, **72**, 2790 (1950).

[59] R. M. Diamond, K. Street, Jr., G. T. Seaborg, ibid., **76**, 1461 (1954).

[60] G. R. Choppin, A. Chatham-Strode, *J. Inorg. Nucl. Chem.*, **15**, 377 (1960).

[61] S. Usuda, N. Shinohara, H. Yoshikawa, *J. Radioanal. Nucl. Chem., Art.*, **109**, 353 (1987).

[62] S. Usuda, ibid., **123**, 619 (1988).

[63] T. Sato, ibid., **139**, 79 (1990).

[64] S. Usuda, ibid., **111**, 477 (1987).

[65] R. J. Morrow, *Talanta*, **13**, 1265 (1966).

[66] Y. Marcus, *J. Inorg. Nucl. Chem.*, **28**, 209 (1966).

[67] S. Usuda, *J. Radioanal. Nucl. Chem., Art.*, **111**, 399 (1987).

[68] W. Kraak, W. A. van der Heijden, *J. Inorg. Nucl. Chem.*, **28**, 221 (1966).

[69] J. P. Surls, Jr., G. R. Choppin, ibid., **4**, 42 (1957).

[70] J. S. Coleman, L. B. Asprey, R. C. Chisholm, ibid., **31**, 1167 (1969).

[71] E. K. Hulet, R. G. Gutmacher, M. S. Coops, ibid., **17**, 350 (1961).

[72] D. E. Sayers, F. W. Lytle, E. A. Stern, *Adv. X-ray Anal.*, **13**, 248 (1970).

[73] D. E. Sayers, E. A. Stern, F. W. Lytle, *Phys. Rev. Lett.*, **27**, 1204 (1971).

[74] F. W. Lytle, D. E. Sayers, E. A. Stern, *Phys. Rev. B*, **11**, 4825 (1975).

[75] H. Fricke, *Phys. Rev.*, **16**, 202 (1920).

[76] G. Hertz, *Z. Phys.*, **3**, 19 (1920).

[77] A. E. Lindh, ibid., **6**, 303 (1921).

[78] D. Coster, ibid., **25**, 83 (1924).

[79] A. E. Lindh, ibid., **31**, 210 (1925).

[80] B. K. Teo, "EXAFS: Basic Principles and Data Analysis", Springer-Verlag, Berlin (1986).

[81] D. C. Koningsberger and R. Prins Eds., "X-ray Absorption: Principles, Applications, Techniques of EXAFS, SEXAFS and XANES", John Wiley & Sons, New York (1988).

[82] P. A. Lee, P. H. Citrin, P. Eisenberger, B. M. Kincaid, *Rev. Mod. Phys.*, **53**, 769 (1981).

[83] J. E. Enderby, D. M. North, P. A. Egelstaff, *Philos. Mag.*, **14**, 961 (1966).

[84] P. Fuoss, P. Eisenberger, W. K. Warburton, A. Bienenstock, *Phys. Rev. Lett.*, **46**, 1537 (1981).

[85] A. L. Ankudinov, B. Ravel, J. J. Rehr, S. D. Conradson, *Phys. Rev. B*, **58**, 7565 (1998).

[86] J. J. Rehr, R. C. Albers, *Rev. Mod. Phys.*, **72**, 621 (2000).

[87] T. Ressler, *J. Synchrotron Rad.*, **5**, 118 (1998).

[88] http://www.spring8.or.jp/e/general_info/overview/

[89] J. A. Solera, J. García, M. G. Proietti, *Phys. Rev. B*, **51**, 2678 (1995).

[90] H. Shiwaku, T. Yaita, Y. Okamoto, S. Suzuki, T. Harami, S. Inoue, T. Kudo, T. Tanida, "XAFS Measurement of Lanthanides and Actinides on BL11XU at SPring-8", *3rd Workshop on Speciation, Techniques, and Facilities for Radioactive Materials at Synchrotron Light Sources (Actinide-XAS-2004)*, Sep. 2004, Berkeley, USA.

[91] A. Krolzig, G. Materlik, M. Swars, J. Zegenhagen, *Nucl. Inst. Meth. Phys. Res.*, **219**, 430 (1984).

[92] R. W. Alkire, G. Rosenbaum, G. Evans, *J. Synchrotron Rad.*, **7**, 61 (2000).

[93]   ,   ,   ,   ,   ,   ,   ,   , **16**, 39 (2003).

[94] G. Åkerlöf, *J. Am. Chem. Soc.*, **54**, 4125 (1932).

[95] R. G. Pearson, *J. Am. Chem. Soc.*, **85**, 3533 (1963).

[96] R. G. Pearson, "Chemical Hardness", Wiley-VCH, Weinheim (1997).

[97] M. Ageno, C. Frontali, *Proc. Nat. Acad. Sci. USA*, **57**, 856 (1967).

[98] M. Matsumoto, N. Nishi, T. Furusawa, M. Saita, T. Takamuku, M. Yamagami, T. Yamaguchi, *Bull. Chem. Soc. Jpn.*, **68**, 1775 (1995).

[99] N. Nishi, S. Takahashi, M. Matsumoto, A. Tanaka, K. Muraya, T. Takamuku, T. Yamaguchi, *J. Phys. Chem.*, **99**, 432 (1995).

[100] T. Takamuku, T. Yamaguchi, M. Asato, M. Matsumoto, N. Nishi, *Z. Naturforsch.*, **55a**, 513 (2000).

[101] K. Nishikawa, H. Hayashi, T. Iijima, *J. Phys. Chem.*, **93**, 6559 (1989).

[102] H. Hayashi, K. Nishikawa, T. Iijima, ibid., **94**, 8334 (1990).

[103] K. Nishikawa, T. Iijima, ibid., **97**, 10824 (1993).

[104] R. Ludwig, *Chem. Phys.*, **195**, 329 (1995).

[105] Y. G. Wu, M. Tabata, T. Takamuku, *Talanta*, **54**, 69 (2001).

[106] S. Mashimo, S. Kuwabara, S. Yagihara, K. Higasi, *J. Chem. Phys.*, **90**, 3292 (1989).

[107] S. Mashimo, T. Umehara, H. Redlin, ibid., **95**, 6257 (1991).

[108] T. Takei, C. Amano, Y. Nishimoto, Y. Sugitani, *Anal. Sci.*, **13**, 1043 (1997).

[109] G. Hefter, Y. Marcus, W. E. Waghorne, *Chem. Rev.*, **102**, 2773 (2002).

[110] J. Reidler, H. B. Silber, *J. Inorg. Nucl. Chem.*, **36**, 175 (1974).

[111] J. Reidler, H. B. Silber, *J. Phys. Chem.*, **78**, 424 (1974).

[112] H. Suganuma, M. Arisaka, I. Satoh, T. Omori, G. R. Choppin, *Radiochim. Acta*, **83**, 153 (1998).

[113] T. Kimura, R. Nagaishi, Y. Kato, Z. Yoshida, *J. Alloys. Compd.*, **323**-**324**, 164 (2001).

[114] M. Arisaka, T. Kimura, H. Suganuma, Z. Yoshida, *Radiochim. Acta*, **89**, 593 (2001).

[115] M. Arisaka, T. Kimura, H. Suganuma, Z. Yoshida, ibid., **90**, 193 (2002).

[116] M. Arisaka, T. Kimura, H. Suganuma, Z. Yoshida, *J. Radioanal. Nucl. Chem.*, **255**, 385 (2003).

[117] A. Habenschuss, F. H. Spedding, *Cryst. Struct. Comm.*, **7**, 535 (1978).

[118] A. Habenschuss, F. H. Spedding, ibid, **8**, 511 (1979).

[119] A. Habenschuss, F. H. Spedding, ibid., **9**, 71 (1980).

[120] A. Habenschuss, F. H. Spedding, ibid., **9**, 157 (1980).

[121] G. E. Toogood, C. Chieh, *Can. J. Chem.*, **53**, 831 (1975).

[122] D. J. Rogers, N. J. Taylor, G. E. Toogood, *Acta Cryst.*, **C39**, 939 (1983).

[123] B. Eriksson, L. O. Larsson, L. Niinistö, J. Valkonen, *Inorg. Chem.*, **19**, 1207 (1980).

[124] N. Milinski, B. Ribár, M. Satarić, *Cryst. Struct. Comm.*, **9**, 473 (1980).

[125] C. Musikas, G. le Marois, R. Fitoussi, C. Guillerdier, "Actinide Separations", ACS Symposium Series, Vol. 117 (J.D. Navratil, W.W. Shulz Ed.), American Chemical Society, Washington, D. C., pp. 131 (1980).

[126] P. Pyykkö, L. J. Laakkonen, K. Tatsumi, *Inorg. Chem.*, **28**, 1801 (1989).

[127] K. Tatsumi, R. Hoffman, ibid., **19**, 2656 (1990).

[128] B. E. Bursten, L. F. Rhodes, R. J. Strittmatter, *J. Am. Chem. Soc.*, **111**, 2758 (1989).

[129] W. B. Lewis, J. A. Jackson, J. F. Lemons, H. Taube, *J. Chem. Phys.*, **36**, 694 (1962).

[130] D. F. Peppard, G. W. Mason, S. Lewey, *J, Inorg. Nucl. Chem.*, **31**, 2271 (1969).

[131] M. Yashiro, A. Ishikubo, T. Takarada, M. Komiyama, *Chem. Lett.*, 665 (1995).

[132] M. P. Jensen, L. R. Morss, J. V. Beitz, D. D. Ensor, *J. Alloys. Compd.*, **303-304**, 137 (2000).

[133] C. Rivière, M. Nierlich, M. Ephritikhine, C. Madic, *Inorg. Chem.*, **40**, 4428 (2001).

[134] T. Yaita, S. Tachimori, N. M. Edelstein, J. J. Bucher, L. Rao, D. K. Shuh, P. G. Allen, *J. Synchrotron Rad.*, **8**, 663 (2001).

[135] M. A. Denecke, A. Rossberg, P. J. Panak, M. Weigl, B. Shimmelpfennig, A. Geist, *Inorg. Chem.*, **44**, 8418 (2005).

[136] M. P. Jensen, A. H. Bond, *J. Am. Chem. Soc.*, **124**, 9870 (2002).

[137] M. Weigl, M. A. Denecke, P. J. Panak, A. Geist, K. Gompper, *Dalton Trans.*, **7**, 1281 (2005).

[138] M. Miguirditchian, D. Guillaneux, D. Guillamont, P. Moisy, C. Madic, M. P. Jensen, K. L. Nash,"Thermodynamic study of the complexation of actinide(III) and lanthanide(III) cations by ADTPZ, a tridentate N-donor ligand", *24th Rare Earth Research Conference*, June 2005, Colorado, USA.

[139] T. Yaita, Private communication, Kansai Photon Science Institute, Japan Atomic Energy Agency (2005).

[140] M. Mazzanti, R. Wietzke, J. Pécaut, J.-M. Latour, P. Maldivi, M. Remy, *Inorg. Chem.*, **41**, 2389 (2002).

[141] T. Mehdoui, J.-C. Berthet, P. Thuéry, M. Ephritikhine, *Chem. Comm.*, **22**, 2860 (2005).

[142] C. J. Kepert, L. Weimin, B. W. Skelton, A. H. White, *Aust. J. Chem.*, **47**, 365 (1994).

[143] L. I. Semenova, B. W. Skelton, A. H. White, ibid., **52**, 551 (1999).

[144] L. I. Semenova, A. H. White, ibid., **52**, 571 (1999).

[145] H.-Y. Jin, M. Akiba, K. Umakoshi, Y. Sasaki, K. Kubota, *Acta Cryst.*, **C53**, 60 (1997).

[146] R. Wietzke, M. Mazzanti, J.-M. Latour, J. Pécaut, P.-Y. Cordier, C. Madic, *Inorg. Chem.*, **37**, 6690 (1998).

[147] D. R. van Staveren, G. A. van Albada, J. G. Haasnoot, H. Kooijman, A. M. M. Lanfredi, P. J. Nieuwenhuizen, A. L. Spek, F. Ugozzoli, T. Weyhermüller, J. Reedijk, *Inorg. Chim. Acta*, **315**, 163 (2001).

[148] A. R. Al-Karaghouli, J. S. Wood, *Inorg. Chem.*, **11**, 2293 (1972).

[149] M. Fréchette, I. R. Butler, R. Hynes, C. Detellier, ibid., **31**, 1650 (1992).

[150] M. Fréchette, C. Bensimon, ibid., **34**, 3520 (1995).

[151] L. R. Morss, R. D. Rogers, *Inorg. Chim. Acta*, **255**, 193 (1997).

[152] D. L. Kepert, L. I. Semenova, A. N. Sobolev, A. H. White, *Aust. J. Chem.*, **49**, 1005 (1996).

[153] L. I. Semenova, A. H. White, ibid., **52**, 507 (1999).

[154] P. G. Allen, J. J. Bucher, D. K. Shuh, N. M. Edelstein, T. Reich, *Inorg. Chem.*, **36**, 4676 (1997).

[155] T. Kimura, Y. Kato, H. Takeishi, G. R. Choppin, *J. Alloys Compd.*, **271**-**273**, 719 (1998).

[156] G. Depaoli, U. Russo, G. Valle, F. Grandjean, A. F. Williams, G. J. Long, *J. Am. Chem. Soc.*, **116**, 5999 (1994).

6   Application of the Partitioning Technique Using Tertiary Pyridine Resin to Innovative Reprocessing

6.1   Concept of Innovative Reprocessing System Using Tertiary Pyridine Resin

For the moment, an urgent requirement for performing the partitioning and trans-mutation strategy is the isolation of Am and Cm from HLW. It has been demonstrated in chapters 3 and 4 that a complete intergroup separation between An(III) and Ln(III) is attained by using a tertiary pyridine resin with alcoholic HCl solutions and, fur-thermore, individual separations between Am and Cm, and between specific Ln(III) are possible by using anion exchange resins including the tertiary pyridine resin in combination with alcoholic HNO_3 solutions. Therefore, the present separation tech-nique using the tertiary pyridine resin is sufficiently applicable for the partitioning of HLW by selecting appropriate solvent systems.

In addition to the application to the partitioning of HLW, the present separation system using the tertiary pyridine resin also has a potential for the application to the reprocessing of spent fuels. That is, it has previously been reported by Nogami [1] and Nur [2] that the tertiary pyridine resin can separate U and Pu from several FPs in methanolic HCl solutions. Therefore, by uniting these previous information to the present partitioning concept, a novel and innovative reprocessing system is proposed as shown in **Fig. 6-1**.

The first step is performed in a dilute HCl solution to recover several FPs includ-ing platinum metals from HLW or spent fuels. The resultant solution from the first step is then treated in a HCl solution having high Cl concentration and is divided into three groups: Ln and FPs, An(III), and other non-trivalent An (*i.e.* fissile actinides of U, Np, and Pu) groups. The FPs and Ln separated in the first and second steps are recycled or sent to the geological disposal. The separation of An is also achieved
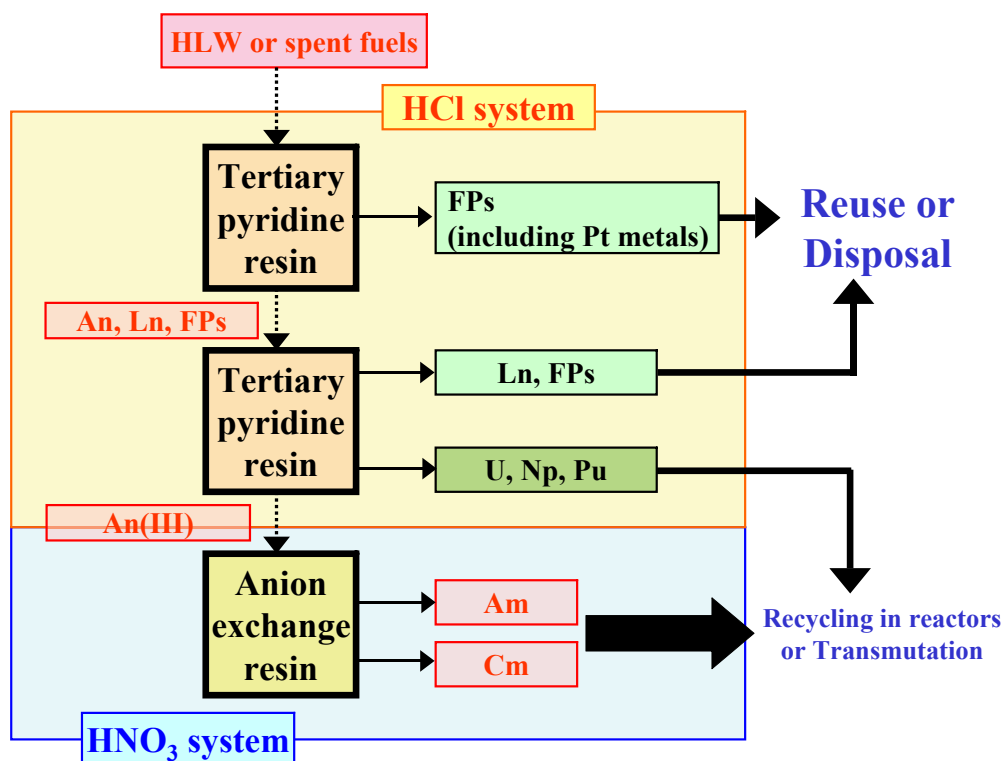

Figure 6-1. Flowchart of the overall HLW partitioning process using a tertiary pyridine resin.

in this step. The separation of An(III) from U and Pu is not so difficult owing to the large difference in their adsorbability for the pyridine resin. At this moment, no investigation has been done concerning the separation of An(III) and Np. However, the separation of Np from An(III) will be achieved relatively easily by optimizing solvent composition since Np forms NpO_2^+ ions whose hydration and complexation properties are different from those of An(III) ions. The isolated A(III) are separated individually in the last step operated in a HNO_3 solution system. Both the tertiary pyridine resin and typical anion exchange resins are applicable for the stationary phase of the last step. The separated Am and Cm are then transmuted by accelerators or FBRs to reduce (or extinguish) their radioactivity. The advantages of this novel reprocessing process are as follows:

- The recovery of fissile An and the isolation of An(III) can be achieved by just three steps.

- No special and expensive reagent is required.

- The wastes generated from the process is expected to become smaller than those from the existing reprocessing process using solvent extraction.

- Separating reagents (*i.e.* resins) are recyclable.

In fact, the practicability of this reprocessing concept has recently been proved by Koyama and his co-workers [3, 4] as summarized in the following several sections.

6.2   Practical Partitioning Experiments Using Irradiated Mixed Oxide Fuels

In order to evaluate the practicability of the present separation system using the tertiary pyridine resin for practical partitioning processes and to confirm the behavior of FPs in the partitioning process, practical separation experiments using real irradiated mixed oxide (MOX) fuels were carried out by Koyama and his co-workers.

6.2.1   Experimental

Materials   The MOX fuel sample employed in this study was prepared by irradiating an uranium-plutonium mixed oxide fuel composed of 80 wt% uranium (18 wt% ^{235}U enriched) and 20 wt% pulutonium in the experimental fast-breeder reactor JOYO, Japan Nuclear Cycle Development Institute (JNC)-Oharai (Core arrangement: MK-II) for 1019 days followed by 1560 days cooling. It was found from γ-ray and α-ray measurements that the irradiated sample contained Ru, Sb, Cs, Ce, Eu, U, Np, Pu, Am, and Cm. Further detailed information about the irradiated sample has been reported by Koyama [3, 4].

Procedure   A flowchart of the partitioning experiments is given in **Fig. 6-2**. The irradiated MOX fuel sample was first dissolved in a 8 mol/dm^3-HNO$_3$ solution (**Original solution**) and dried to identify its elemental composition by α- and γ-ray spectrometry. The γ-ray spectrum of the irradiated sample is shown in **Fig. VI-1** in Appendix VI. Then the sample was dissolved in a 3.0 cm^3 of dilute HCl solution (0.5 mol-HCl/dm^3) and the resultant solution (**1st feed solution**) was introduced into a plastic column (1 cm-$\phi \times$ 15 cm), in which 1 cm-$\phi \times$ 10 cm of polymer type tertiary
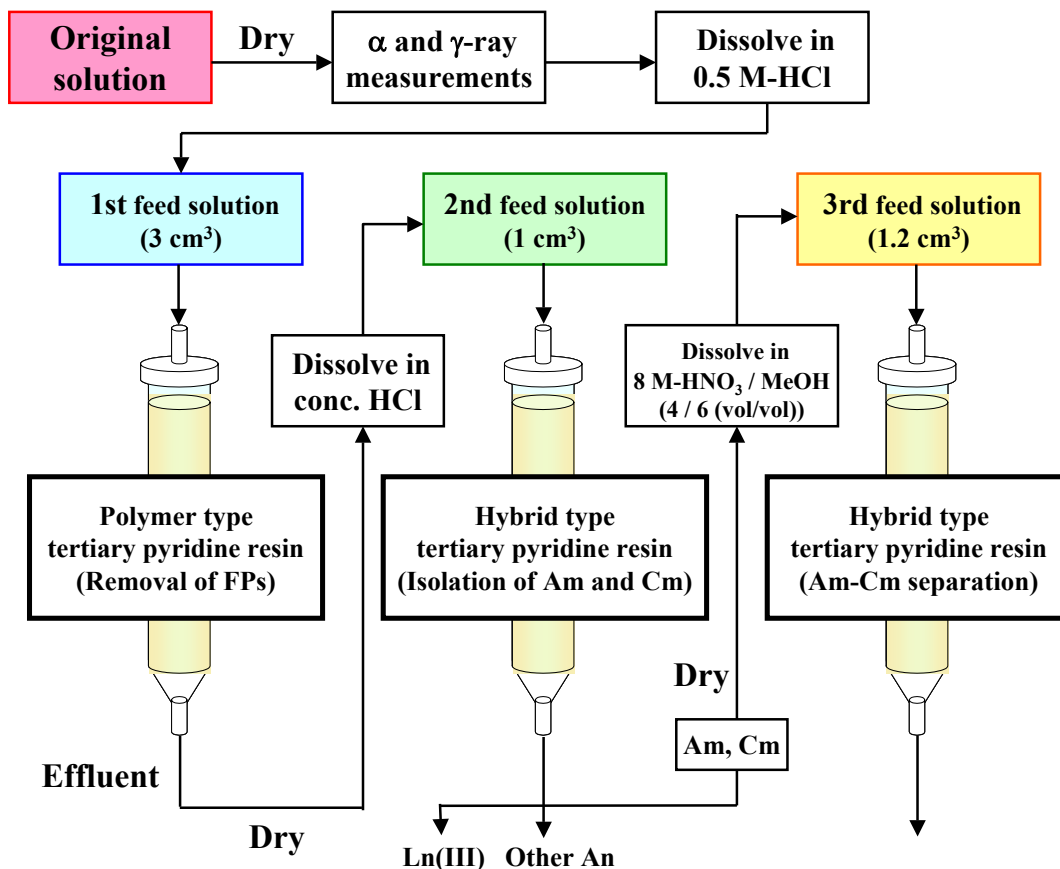
Figure 6-2. Flowchart of partitioning experiments using irradiated MOX fuels.

pyridine resin (crosslinkage: 10 wt%, porosity: 40∼50 vol%, particle size: ∼100 μm) was packed, to remove FPs from the solution. The effluent from the first resin column was collected, dried, and dissolved again in a 1.0 cm^3 of conc. HCl solution (**2nd feed solution**). The solution was then introduced into a Si-based type tertiary pyridine resin column (the sizes of plastic column and resin bed were the same as those of the polymer type resin column) to separate An(III) from other non-trivalent An, Ln(III), and some FPs. The crosslinkage and porosity of the Si-based resin were 10 wt% and 60∼65 vol%, respectively. The fractions containing Am and Cm were then collected together, dried, and dissolved in a 1.2 cm^3 of methanolic HNO$_3$ solution (8 mol/dm^3-HNO$_3$ solution / MeOH = 4 / 6 (vol/vol), **3rd feed solution**) in order to change the solvent system from HCl to HNO$_3$. The resultant solution was developed in a Si-based type tertiary pyridine resin column to attain the individual separation of Am and Cm. The sizes of plastic column and resin bed, and the

properties of the resin were equal to those of the second resin column. In the last partitioning process, the eluent was changed from the methanolic HNO_3 solution to a dilute HNO_3 solution (0.5 mol-HNO_3/dm^3) so that the latter elution of Am became quick. The nuclides in each effluent were basically detected by γ-ray spectrometry. α-ray spectrometry was also employed for more precise determination of Am and Cm in the third partitioning process. In the second partitioning process, the elution chromatogram was first drawn by radioactivity measurements using an ion chamber. Then the γ-ray measurements were carried out for the fractions around each elution peak to identify the elemental composition. The resin columns were preconditioned with appropriate solvents before use. All the experiments were performed in the hot cell at the Alpha-Gamma Facility (AGF), JNC-Oharai.

6.2.2 Results

First Partitioning Process: Removal of FPs   It is desirable that FPs are separated from An and Ln(III) as much as possible before the following An(III) partitioning processes. It is well known that pyridine forms strong complexes with some transition metals. This means that the tertiary pyridine resin may also be applicable for removing some metallic FPs from HLW. Therefore, in the present study, the pretreatment of the irradiated sample solution was performed by using the tertiary pyridine resin with a dilute HCl solution to confirm the adsorption behavior of FPs.

    Table 6-**1** gives the material balance of the nuclides in each step of the 1st partitioning process. The values were calculated from the radioactivity of each nuclide (see **Fig. VI**-**2** in Appendix VI). It is clear that An(III), Ln(III), and Cs passed through the resin column, while Ru and Sb were strongly adsorbed in the resin and non of them were eluted from the column. These Ru and Sb were hardly desorbed from the column even by washing with water and 1 mol/dm^3-NaOH solution, indicating that their adsorption in the pyridine resin was considerably strong. High concentration of acidic solution might be effective for the desorption of these nuclides. It should be noted that Cs, which is one of the significant target nuclides for the transmutation [5], can also be separated from other FPs in the present separation system. This makes the partitioning process for the transmutation simpler.

Table 6-1. Material balance in the first partitioning process using a tertiary pyridine resin in 0.5 mol/dm^3-HCl solution. (NaOH: 1.0 mol/dm^3)

		^{106}Ru	^{125}Sb	^{137}Cs	^{144}Ce	^{155}Eu	^{241}Am
Feed solution		100.00	100.00	100.00	100.00	100.00	100.00
Effluent		-	-	99.57	99.75	99.78	99.59
Washing by water	Resin	63.66	28.05	< 0.01	0.02	0.01	0.14
	Effluent	5.14	17.00	0.42	0.23	0.21	0.21
Washing by NaOH	Resin	31.20	50.88	< 0.01	-	-	0.05
	Effluent	-	4.08	< 0.01	-	< 0.01	< 0.01

Second Partitioning Process: Separation of An(III) In the first partitioning process, FPs of Ru and Sb were separated from the irradiated fuel sample. Then, the second partitioning process aims at isolating the An(III) of Am and Cm from the sample for the following individual separation process. The effluent from the first resin column contained Cs, Ln(III) (Ce and Eu), U, Np, Pu, and An(III) (Am and Cm). This means that the second partitioning process must include the inter-group separation of An(III) and Ln(III). Therefore, the second process was performed in a HCl solution system. A conc. HCl was employed for eluent so that the elution of nuclides becomes faster than that in alcoholic conc. HCl solution.

The elution behavior of nuclides was first confirmed by monitoring the radioactivity of effluent using an ion chamber. The obtained chromatogram is shown in the upper graph of **Fig. 6-3**. Three elution peaks were observed at around 5, 20, and 65 cm^3-effluent volume. Then the elemental compositions of these elution peaks were determined by α- and γ-ray spectrometry, revealing that the first elution peak was composed of Cs and Ln(III) (Ce and Eu) and the second and third peaks contained An(III) (Am and Cm) and Pu, respectively (the lower graph of **Fig. 6-3**). Unfortunately, the radioactivity of U and Np nuclides was so weak that it was difficult to identify these nuclides in the effluent.
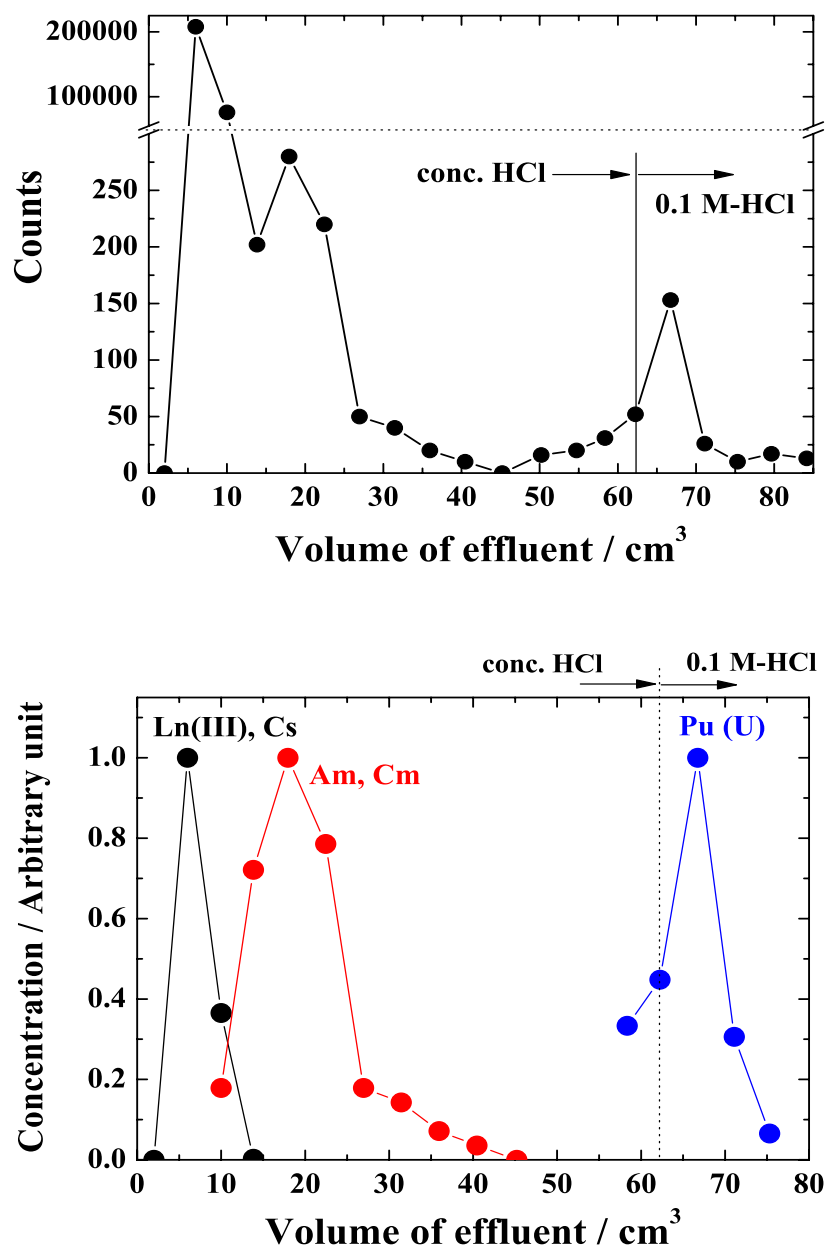
Figure 6-3.   Variation of radioactivity on the elution chromatography of 2nd feed sample by a tertiary pyridine resin (upper) and its identified chromatogram (lower). (Temperature: room temperature, Flow rate: 7.0 cm^3/h (~28.7 cm^3-effluent) and 26.0 cm^3/h (28.7~ cm^3-effluent))

It has been suggested in chapter 5 that the tertiary pyridine resin functions as "co-ordinative" extractant in the HCl solution system. This means that the adsorbability of ions for the pyridine resin (*i.e.* the affinity of ions for pyridine groups) depends on the surface charge density of the ions. It is well-known that the surface charge density of An ions decrease in the following order: $An^{4+} > AnO_2^{2+} \gg An^{3+} > AnO_2^{+}$. Pu probably formed Pu^{4+} ions in the present conc. HCl solution since it adsorbed in the pyridine resin far strongly than An(III) ions. U is expected to form UO_2^{2+} ions in the present solution system and, thus, its adsorption in the pyridine resin is supposed to be stronger than that of An(III). Consequently, it seems appropriate to consider that U were eluted from the column together with Pu. On the other hand, Np probably forms NpO_2^{+} and, therefore, its adsorption will be similar to that of An(III). In fact, a small but distinguishable amount of ^{239}Np was detected in the γ-ray spectra for the fractions around the second peak containing An(III) (*e.g.* **Fig. VI-3** in Appendix VI). However, the amount of Np in the fractions around the second peak was far smaller than those of Am and Cm and, accordingly, it is negligible in the following third partitioning process.

To sum up the results, the elution order (= adsorbability) of An, Ln(III), and Cs in the HCl solution system was as follows:

$$Ln(III) \approx Cs < An(III) \approx Np \ll Pu \ (U).$$

This suggests the potential of the present separation system using the tertiary pyridine resin with HCl solutions for the separation of An(III) from other non-trivalent An.

Third Partitioning Process: Individual Separation of An(III) The Am and Cm in **2nd feed solution** were isolated from other nuclides for the most part in the second partitioning process. Then the individual separation of these Am and Cm was carried out in the third partitioning process using a methanolic HNO_3 solution.

Fig. 6-4 shows a result of chromatographic separation of Am and Cm in "8 mol/dm³-HNO_3 / MeOH = 4 / 6" solvent. The elution curve of Am was clearly separated from that of Cm. In order to evaluate the separation efficiency between Am and Cm in the present process, further α spectra measurements were carried out for the fractions around the Cm elution peak (α**1** in **Fig. 6-4**), the border between the elution peaks (α**2**), and around the Am elution peak (α**3**). The obtained spectra are given in **Fig. VI-4**, Appendix VI. No significant contamination of Am was observed in

the fractions of the Cm elution area and, on the other hand, no contamination of Cm was observed in the fractions of the Am elution area. Additionally, the fractions at the border of these two elution curves contained far smaller amount of Am and Cm than those around the elution peaks, indicating that the individual separation of Am and Cm was completed with considerably high efficiency in the present process.

Table 6-2 summarizes the efficiency of the present partitioning processes. FPs of Ru and Sb were completely removed from the irradiated MOX fuel sample in the first step. Then, the isolation of An(III) from the rest FPs including Cs and Ln(III) and from other non-trivalent An was attained in the next second step. The isolated An(III) contained no significant amount of Cs and Ln(III), satisfying the required DF (decontamination factor) values for the transmutation process [6]. The isolated Am and Cm were separated individually and high-purity Am and Cm products were obtained in the last step. The Am recovery rate of the whole partitioning process was over 95% and there is still room for improvement.
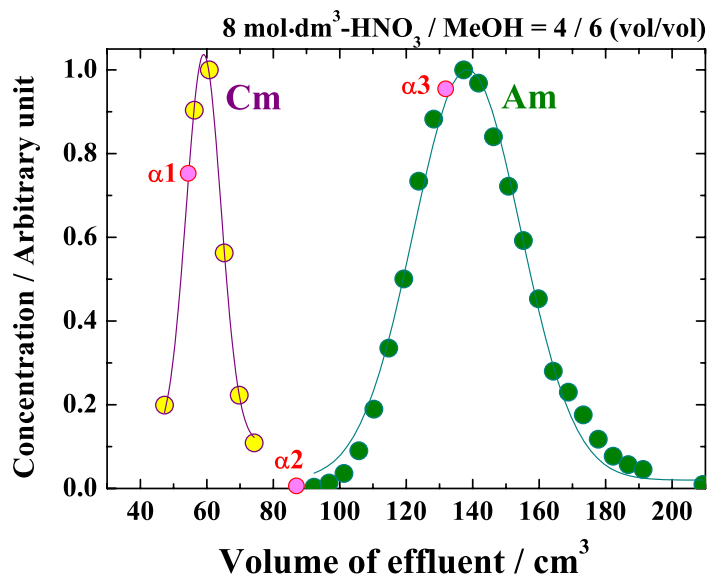

Figure 6-4. Elution chromatogram of Am and Cm by a tertiary pyridine resin in a methanolic HNO$_3$ solution. (Temperature: room temperature, Flow rate: 80 cm^3/h, Solvent: 8 mol/dm^3-HNO$_3$ / MeOH = 4 / 6 (vol/vol)

Table 6-2. Evaluation of An(III)-partitioning efficiency in the present partitioning system using a tertiary pyridine resin.

First step	Removal rate	Ru	100%
		Sb	100%
Second step	Decontamination factor for Am (DF: activity / activity)	Cs	3.9×10^4
		Eu	1.0×10^5
		Requirement [6]	$1 \sim 2 \times 10^3$
Third step	Separation factor (α)	Am/Cm	2.2×10^3
	Purity of Am product	Ln(Ce+Eu)/Am	< 0.3 ppm
		Cm/Am	< 1.0 ppm
		FPs(Ru+Sb+Cs)/Am	< 1.8 ppm
	Purity of Cm product	Am/Cm	7.8×10^3 ppm
Total	Recovery rate of Am		< 95%

6.3   Future Subjects

In order to establish this overall partitioning process, the following issues should be solved for the future:

- Desorption and recovery of the FPs adsorbed in the pyridine resin.

- Separation of Ln(III) from other FPs.

- Separation of U, Np, and Pu.

The existing separation technique such as solvent extraction might give some solution to these issues.

In addition to these issues, the chromatographic separation method has a disadvantage of less treatment capacity compared with the solvent extraction method. Therefore, when we try to substitute the chromatographic partitioning system developed in this study for the present reprocessing system using solvent extraction, first of all, we need to consider the treatment capacity of the system. One possible solution to this issue may be to use of precipitant, such as NCP [7, 8] to recover U.

Uranium is the most massive component in spent fuels and, if U can be preliminary removed from spent fuels, not so large treatment capacity is required for the following partitioning process.

6.4 Summary

A novel and innovative reprocessing concept has been proposed on the basis of the results obtained in this study and the previously reported information. The practicability of this reprocessing concept has proved by the practical partitioning experiments using irradiated mixed oxide fuels. That is, it has been demonstrated in these experiments that Am and Cm are isolated from the irradiated fuel sample with high purity via three partitioning steps, and that other nuclides are divided into three groups: FPs including platinum metals, FPs and Ln, and non-trivalent An. Furthermore, each partitioning process has provided sufficient decontamination factors (DF) and purity for the transmutation process.

References

[1] M. Nogami, Doctor Thesis, Department of Nuclear Engineering, Tokyo Institute of Technology, Tokyo (1996).

[2] Rifaid M. Nur, Doctor Thesis, Department of Nuclear Engineering, Tokyo Institute of Technology, Tokyo (1999).

[3] S. Koyama, A. Hanami, Y. Sawado, M. Sato, K. Otake, T. Suzuki, M. Ozawa, K. Tanaka, JNC report, TN9400 (2005).

[4] S. Koyama, Doctor Thesis, Department of Quantum Science and Energy Engineering, Tohoku University (2006).

[5] S. Chwaszczewski, B. Slowiński, *Appl. Energy*, **75**, 87 (2003).

[6] H. Bokelund, C. Apostolidis and J.-P. Glatz, *J. Nucl. Mater.*, **166**, 181 (1989).

[7] T. R. Varga, M. Sato, Zs. Fazekas, M. Harada, Y. Ikeda, H. Tomiyasu, *Inorg. Chem. Comm.*, **3**, 637 (2000).

[8] M. Harada, T. R. Varga, M. Sato, Zs. Fazekas, H. Tomiyasu, Y. Ikeda, "International Conference on Back-End of the Fuel Cycle, Global'2001", Paris, France, Sept. 2001.

7   Conclusions

This study has aimed to develop a novel separation technique using a tertiary pyridine resin for the partitioning of trivalent actinoids (An(III)) and lanthanoids (Ln(III)). In order to attain this purpose, various investigations have been carried out from different viewpoints. The conclusions obtained from the results are summarized as follows:

Synthesis and properties of tertiary pyridine resin

Two different types of tertiary pyridine resin have been synthesized in this study, that is, polymer type pyridine resin and Si-based type pyridine resin. The former resin is synthesized by the simple copolymerization reaction of 4-vinylpyridine and m/p-divinyl benzene, while the latter resin is prepared by embedding the polymer pyridine resin in highly porous silica beads. The polymer pyridine resin has larger adsorption capacity than the Si-based resin. On the other hand, the Si-based resin has a great advantage on the use of chromatography, bringing smooth elution and clear and well-defined elution chromatograms.

The synthesized pyridine resins have displayed high resistance both for α- and γ-ray irradiation. This high radiation resistance is one of the most important properties of the pyridine resin considering its practical use in high radiation-dose condition. The resins are hardly deteriorated by conc. HCl solution and, thus, their adsorptivity and separability are long-lasting in high [HCl] solutions. However, they are partly decomposed in HNO$_3$ solutions, although they still work enough after the decomposition.

In acidic solutions, the pyridine groups of the resin are protonated for the most part. Adding alcohol in solvent weakens the protonation, while the type of alcohol has almost no effect on restraining the protonation.

Adsorption and separation properties of tertiary pyridine resin for trivalent An and Ln in nitrate solution system

The adsorbability and separability of the pyridine resin in the nitrate solution system are governed by the concentration of electrolytes. In HNO$_3$ solutions, the K_d of An(III) and Ln(III) and their α show convex variations with an increase of [HNO$_3$]

and they become maximum at around 8 mol/dm^3-HNO$_3$. On the other hand, the K_d and α simply increase with an increase of $X_{alcohol}$, although the type of alcohol has almost no influence on this encouraging effect in the nitrate solution system.

In chromatographic process in HNO$_3$ solutions, An(III) and Ln(III) are eluted from the tertiary pyridine resin column just in the reverse order of their ionic radii and no intergroup separation was observed between An(III) and Ln(III) in the nitrate solution system, while there is a difference in K_d between Am and Cm for An(III) series, and between Nd and Sm for Ln(III) series, bringing clear individual separations between Am and Cm and between Nd and Sm.

The elution behavior of Ln(III) in a non-acidic nitrate solution of LiNO$_3$ solution is similar to that in acidic HNO$_3$ solution, although the K_d in LiNO$_3$ solution are larger than those in HNO$_3$ solution.

In the nitrate solution system, the chromatographic behavior of An(III) and Ln(III) by the pyridine resin is similar to that by anion exchange resins. That is, the individual separation of Am/Cm and Nd/Sm are also achieved by employing anion exchange resins with nitrate solutions.

Adsorption and separation properties of tertiary pyridine resin for trivalent An and Ln in chloride solution system

The adsorbability (K_d) and separability ($SF = \alpha$) of the tertiary pyridine resin also depend the concentration of electrolytes in the chloride solution system. In this solution system, they are governed by the concentration of protons (H$^+$), chloride ions (Cl$^-$), and other electrolytes such as lithium ions (Li$^+$). Lowering [H$^+$] in solvent enhances both K_d and α, while these two values decrease with a decrease of [Cl$^-$]. Adding alcohol in aqueous chloride solutions encourages the adsorbability and separability of the pyridine resin. Among the tested six monohydric alcohols, 2-propanol has been the most effective alcohol. On the other hand, the dihydric alcohol of ethylene glycol has displayed no encouraging effect.

In the chloride solution system, An(III) are adsorbed in the pyridine resin far strongly than Ln(III), enabling a complete intergroup separation between An(III) and Ln(III) by chromatography. This chromatographic behavior of An(III) and Ln(III) in chloride solutions is completely different from that in nitrate solutions. However, it is difficult to apply this chloride solution system to the individual separation of

An(III) and Ln(III). The α between An(III) and Ln(III) increase with increasing the volume fraction of alcohol in solvent ($X_{alcohol}$), although the α and K_d gradually decrease in higher $X_{alcohol}$ region ($\sim$70 vol%). The separability of the pyridine resin in approximately pure alcohol solvent ($X_{alcohol} \geq 95\%$) is quite different from that in aqueous soluion. The adsorption and separation behavior of An(III) and Ln(III) by the pyridine resin depends on the acidity of solvent. That is, the K_d of the cations in non-acidic chloride solutions are far larger than those in acidic chloride solutions. Furthermore, the lanthanoid pattern of K_d in non-acidic solutions is quite different from that in acidic solutions: the K_d of the Ln(III) except La gradually decrease with an increase in atomic number in acidic chloride solutions, while the K_d of Ln(III) in non-acidic chloride solutions exhibit a clear and unique tetrad effect.

The adsorbability and separability of the pyridine resin for An(III) and Ln(III) in the HCl solution system are almost independent of the flow rate, but they slightly depend on the temperature.

The chromatographic behavior of An(III) and Ln(III) by the tertiary pyridine resin is quite different from that by anion exchange resins in the chloride solution system. That is, anion exchange resins hardly adsorb An(III) and Ln(III) in alcoholic chloride solutions and, in consequence, no intergroup separation is achieved.

Adsorption and separation mechanisms of tertiary pyridine resin

Hydration and anion complexation: The hydration of An(III) and Ln(III) becomes tighter with an increase of atomic number for each series. The hydration of An(III) is slightly weaker than that of the homologous Ln(III). The chloride complexation of An(III) and Ln(III) ions is basically very weak and it becomes weaker as increasing atomic number for each series. The chloride complexation of An(III) ions is slightly stronger than that of Ln(III) ions. On the other hand, nitrate ions form far stronger complexes with An(III) and Ln(III) ions and the stability of these nitrate complexes are almost the same. Chloride ions form outer-sphere complexes with An(III) and Ln(III) ions due to their weak complexation ability, while nitrate ions form tight inner-sphere complexes with bidentate mode.

Water-alcohol binary solution system: Adding alcohol in aqueous solution surely changes the properties of solvent, such as dielectric constants or association structure of solvent molecules. However, the hydration and anion complexation structures of An(III) and Ln(III) ions in their primary spheres are almost independent of the presence of alcohol in solvent at least in the solution phase.

Complexation property of pyridine type ligands: Soft donor type ligands, such as pyridine, have larger affinity for An(III) ions over Ln(III) ions due to the presence of slightly greater covalency in An-bonding. This brings the larger selectivity of soft donor type extractants for An(III) over Ln(III) in the solvent extraction process, whereas there is almost no structural difference between An(III)-soft donor ligand complexes and the homologous Ln(III) complexes.

Adsorption and separation mechanisms: An(III) and Ln(III) ions undergo some structural change of their hydration and anion complexation when they are adsorbed in organic resins. That is, they are partly dehydrated in the organic resin phase probably due to the hydrophobicity of resin matrix and, as a result, the anion complexation is enhanced in the resin phase. Additionally, coordinative ligands can also interact directly with the cations in the resin phase owing to the weakened hydration of the cations.

In HCl solutions, a tertiary pyridine resin can work both as a coordinative extractant and as an anion exchanger. However, An(III) and Ln(III) ions hardly form anionic complexes with chloride ions to be adsorbed by anion exchange resins even in the resin phase. On the other hand, the pyridine groups of the tertiary pyridine resin can directly interact with the cations in the resin phase as competing with the protonation of pyridine groups. Furthermore, the chloride complexation of the cations must be important in order to stabilize the cations in the hydrophobic resin phase. Therefore, the remarkable selectivity of the pyridine resin for An(III) over Ln(III) in HCl solutions is concluded as a result of the synergic effect of the preferential coordination of pyridine groups (soft donor) for An(III) and the slightly stronger chloride complexation of An(III). This synergic effect is enhanced in non-acidic chloride solutions since the pyridine groups scarcely suffer from the protonation, increasing the adsorbability of the resin.

On the other hand, the tertiary pyridine resin functions as an anion exchanger in HNO_3 solutions and it adsorbs anionic nitrate complexes of An(III) and Ln(III) ions in the resin phase. An(III) and Ln(III) ions basically form cationic complexes with two nitrate ions ($[M(NO_3)_2 \cdot nH_2O]^+$) in HNO_3 solutions, while lighter An(III) and Ln(III) ions tend to form anionic nitrate complexes ($[M(NO_3)_4 \cdot nH_2O]^-$) in the resin phase to be adsorbed by anion exchange resins. For An(III) series, Am(III) ions can form the anionic nitrate complex in the resin phase and they are strongly adsorbed both in the tertiary pyridine resin and in typical anion exchange resins in HNO_3 solutions. However, Cm(III) ions hardly form the anionic nitrate complex and, consequently, the

adsorption of Cm by the pyridine resin or anion exchange resins is weaker than that of Am. This brings a clear individual separation between Am and Cm by the pyridine resin and anion exchange resins in the HNO_3 solution system. The same interpretation is applied to the observed clear individual separation between Nd and Sm for Ln(III) series. The anion exchange interaction between the cations and the pyridine resin (or anion exchange resins) possesses no selectivity for An(III) and Ln(III). Therefore, the K_d of An(III) and Ln(III) in HNO_3 solutions just depend on their ionic radii.

Optimization and improvement of separating conditions: Considering the adsorption and separation mechanisms of the pyridine resin, an efficient intergroup separation between An(III) and Ln(III) using chloride solutions requires high Cl^- concentration and moderate H^+ concentration. On the other hand, a moderate concentration of NO_3^- is necessary for the individual separation of Am and Cm not only by the tertiary pyridine resin, but also by typical anion exchange resins. In order to encourage the dehydration and anion complexation of the cations and the direct interaction of pyridine groups to the cations in the resin phase, longer-chain alcohols seem to be better. Adding non-polar solvents in solvent might also be effective to improve the adsorbability and separability of the tertiary pyridine resin and other anion exchange resins.

Practicability of the present separation technique using tertiary pyridine resin

The practical partitioning experiments using irradiated mixed oxide fuels has proved that the present separation technique using the tertiary pyridine resin is sufficiently practicable for the partitioning of HLW. The isolation of Am and Cm is achieved with high purity and high decontamination factors by just three partitioning steps employing the tertiary pyridine resin and an anion exchange resin.

To sum up these conclusions, this study reaches the comprehensive conclusion that a tertiary pyridine resin is a very powerful solid extractant for the separation of An(III) and Ln(III) and it has a great potential for applying to the practical partitioning process for the transmutation of HLW. In order to establish the overall partitioning system employing the pyridine resin, further investigation is expected on the further optimization of solvent and the improvement of functional sites.

-Acknowledgement-

Raul Boue Gutierrez

Philippe Rapold Nicolas Vierge Bessiron Vincent Celine Yohan

2006 3 24

Research Achievements

Publications

1 <u>Atsushi Ikeda</u>, Tatsuya Suzuki, Masao Aida, Kouhei Ohtake, Yasuhiko Fujii, Keisuke Itoh, Mitsuo Hara, Toshiaki Mitsugashira, "Effect of f-electron configurations on the adsorption of trivalent f-elements on tertiary pyridine resin in hydrochloric acid/alcohol mixed solvents", *J. Alloys Compd.*, **374** (1-2), 245-248 (2004).

2 <u>Atsushi Ikeda</u>, Tatsuya Suzuki, Masao Aida, Yasuhiko Fujii, Keisuke Itoh, Toshiaki Mitsugashira, Mitsuo Hara, Masaki Ozawa, "Effect of alcohols on elution chromatography of trivalent actinides and lanthanides using tertiary pyridine resin with hydrochloric acid-alcohol mixed solvents", *J. Chromatog. A*, **1041** (1-2), 195-200 (2004).

3 <u>Atsushi Ikeda</u>, Tatsuya Suzuki, Masao Aida, Kouhei Otake, Yasuhiko Fujii, Keisuke Itoh, Toshiaki Mitsugashira, Mitsuo Hara, Masaki Ozawa, "Chromatographic separation of trivalent actinides by using tertiary pyridine resin with methanolic nitric acid solutions", *J. Nucl. Sci. Technol.*, **41** (9), 915-918 (2004).

4 <u>Atsushi Ikeda</u>, Tatsuya Suzuki, Masao Aida, Yasuhiko Fujii, Toshiaki Mitsugashira, Mitsuo Hara, Masaki Ozawa, "Chromatographic separation of trivalent actinides and rare earth elements by using pyridine type resin", *J. Radioanal. Nucl. Chem.*, **263** (3), 605-611 (2005).

5 Tatsuya Suzuki, Keisuke Itoh, <u>Atsushi Ikeda</u>, Masao Aida, Masaki Ozawa, Yasuhiko Fujii, "Separation of rare earth elements by tertiary pyridine type resin", *J. Alloys Compd.*, **408-412**, 1013-1016 (2005).

6 <u>Atsushi Ikeda</u>, Keisuke Itoh, Tatsuya Suzuki, Masao Aida, Yasuhiko Fujii, Toshiaki Mitsugashira, Mitsuo Hara, Masaki Ozawa, "Effect of counter-anions on the adsorption of trivalent actinides and lanthanides on tertiary pyridine resin in alcoholic chloride and nitrate solutions", *J. Alloys Compd.*, **408-412**, 1052-1055 (2005).

7 <u>Atsushi Ikeda</u>, Tatsuya Suzuki, Masao Aida, Yasuhiko Fujii, Toshiaki Mitsugashira, Mitsuo Hara, Masaki Ozawa, "A novel chromatographic separation technique using tertiary pyridine resin for the partitioning of trivalent actinides and lanthanides", *Prog. Nucl. Energy*, **47** (1-4), 454-461 (2005).

8 <u>Atsushi Ikeda</u>, Tsuyoshi Yaita, Hideaki Shiwaku, Tatsuya Suzuki, Yasuhiko Fujii, "XAFS analysis on the adsorption of trivalent f-elements in tertiary pyridine resin", *to be submitted.*

9 <u>Atsushi Ikeda</u>, Tsuyoshi Yaita, Hideaki Shiwaku, Shinichi Suzuki, Tatsuya Suzuki, Yasuhiko Fujii, "Solvation and anion complexation of lanthanide cations in mineral acid / alcohol binary solvent systems", *to be submitted.*

<u>Presentation at International Conferences</u>

1 "Chromatographic separation of trivalent actinides and rare earth elements by using tertiary pyridine type resin", *6th International Conference on Methods and Applications of Radioanalytical Chemistry (MARC VI)*, Hawaii, USA, Apr. 2003 (Oral).

2 "Effect of f-electron configurations on the adsorption of trivalent f-elements on tertiary pyridine resin in hydrochloric acid / alcohol mixed solvents", *5th International Conference on f-elements (ICFE'5)*, Geneva, Switzerland, Aug. 2003 (Oral).

3 "XAFS analysis of lanthanide species adsorbed in pyridine resin", *3rd Workshop on Speciation, Techniques, and Facilities for Radioactive Materials at Synchrotron Light Sources (An-XAS-2004)*, Berkeley CA, USA, Sep. 2004 (Poster).

4 "A novel chromatographic separation technique using tertiary pyridine resin for the partitioning of trivalent actinides from lanthanides", *The 1st COE-INES International Symposium*, Tokyo, Japan, Nov. 2004 (Oral).

5 "Effect of counter-anions on the adsorption of trivalent actinides and lanthanides on tertiary pyridine resin in alcoholic chloride and nitrate solutions", *Rare Earths '04*, Nara, Japan, Nov. 2004 (Poster).

Research Proposals

1   14
    XAFS   -
                    2002P015

2   16
    XAFS   ·   /
                                    2004G279

3   17   K   XAFS
                    (La-Nd)   H17-3-n

Appendix I
-Equipment and Beamlines-

Spectroscopic Equipment

FT-IR Spectrometer

Figure I-1. JASCO Fourier transform infrared spectrometer FT/IR-410.

UV-Visible Spectrophotometer

Figure I-2. JASCO UV-Visible spectrophotometer V-560 (JAERI-Tokai).

ICP-Mass Spectrometer

 Figure I-3. Seiko Instruments Inc. ICP-Mass spectrometer SPQ9200 (JAERI-Tokai).

ICP-Atomic Emission Spectrometer

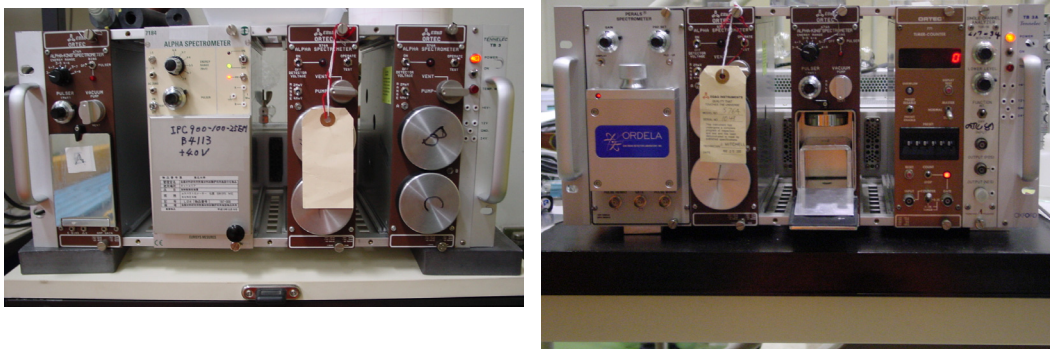Figure I-4. PerkinElmer Inc. ICP-Atomic emission spectrometer OPTIMA-3000.

α-ray Spectrometer

Figure I-5.   Eurisys Mesures IPC500-100-21EM (left) and Canberra Industries PG900-27AM (right) α-ray Spectrometers (IMR, Tohoku University).

γ-ray Spectrometer

Figure I-6. Eurisys Mesures coaxial n-type germanium detector EGC 20-195-R (IMR, Tohoku University).

Beamlines for XAFS measurements

Table I-1. Synchrotrons and beamlines for XAFS measurements.

Synchrotron	Ring parameters	Beamline	Light source	Monochromator	Exp. Mode	Detector for I_0 (Gas)	Detector for I (Gas)	Target
Photon Factory-KEK	350~400 mA*¹ ~2.5 GeV	BL-7C		Si(111)	Transmission	IC (N_2)	IC ($50N_2/50Ar$)	La, Pr, Gd, Yb - L_{III} edge
		BL-12C	Bending magnet	Si(111)	Transmission	IC ($50N_2/50Ar$)	IC (Ar)	Y - K edge
						IC (He/N_2, N_2)	IC (N_2, N_2/Ar)	Ce, Nd, Er - L_{III} edge
		BL-27B		Si(111)	Transmission	IC (N_2)	IC ($50N_2/50Ar$)	La~Lu - L_{III} edge
					Fluorescence	IC (N_2)	7-unit SSD*⁴ (-)	
SPring-8	99 mA*² - 8 GeV	BL11XU	Undulator	Si(311)	Transmission	IC (N_2)	IC ($50N_2/50Ar$)	La~Nd - K edge

*¹ at multi-bunch mode, *² at top-up mode, *³ IC: Ion Chamber, *⁴ SSD: Solid-State Detector

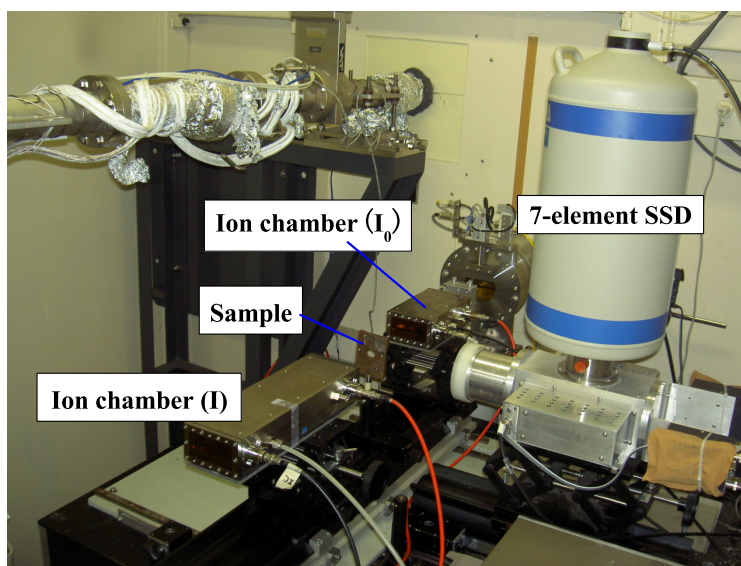## Beamline BL-27B (Photon Factory, KEK)

Figure I-7. Detection system for XAFS measurements (transmission and fluorescence modes) at BL-27B.
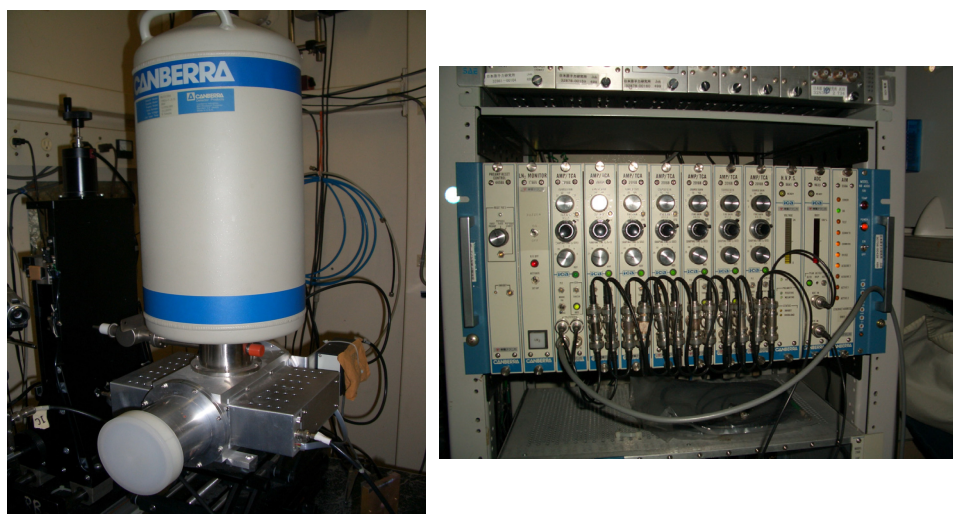
Figure I-8. 7-element solid state detector for fluorescence mode XAFS measurements (left) and its amplifiers (right).

Beamline BL11XU (JAEA Quantum Dynamics Beamline at SPring-8)
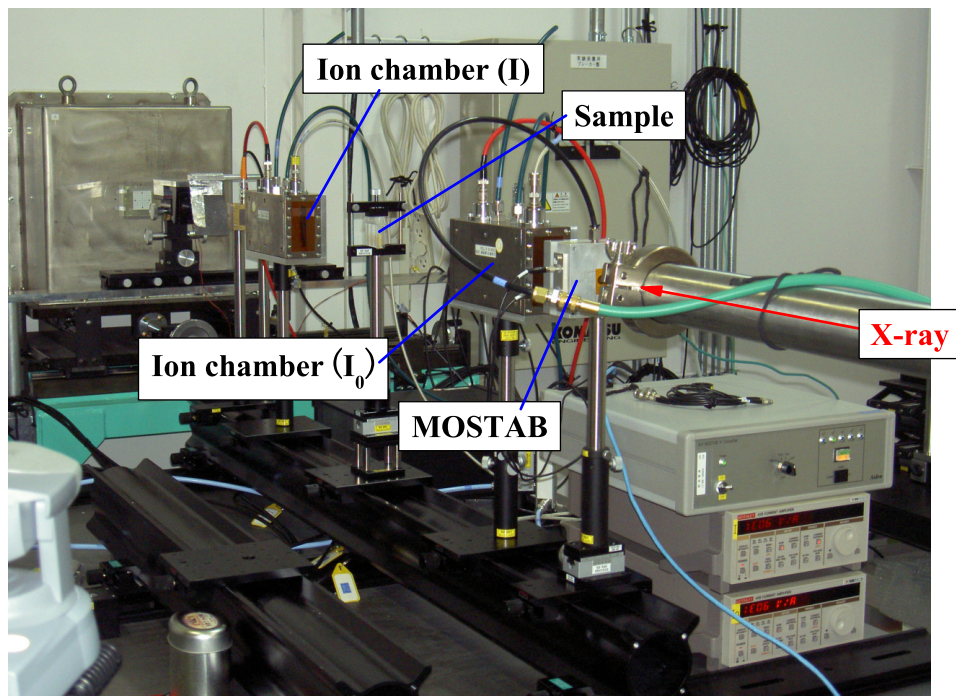
Figure I-9. Detection system for XAFS measurements (transmission mode) at BL11XU.
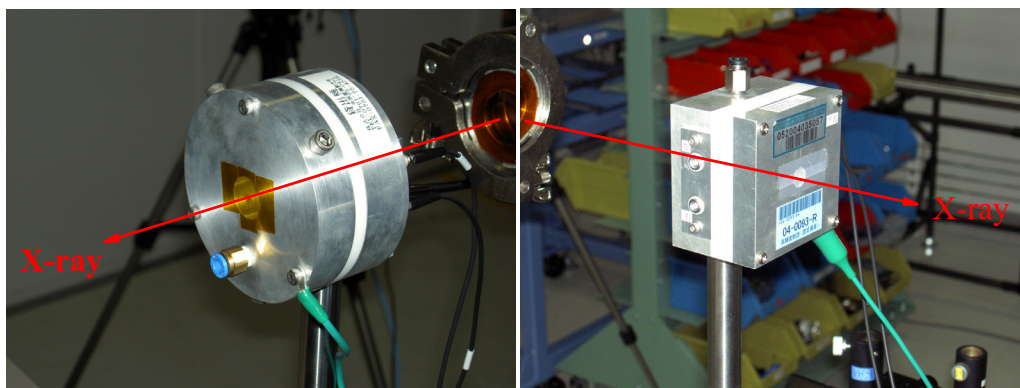
Figure I-10. Monochromator stabilization unit at BL11XU.

Appendix II

-Synthesis and Properties of Tertiary Pyridine Resin-

Figure II-1. Experimental apparatus for suspension copolymerization of polymer pyridine resin.

Figure II-2. Experimental apparatus for synthesis of Si-based pyridine resin.

Figure II-3. Photo of polymer pyridine resin.

Figure II-4. FT-IR spectra of polymer pyridine resin before and after soaking in conc. HCl.

Figure II-5. FT-IR spectra of polymer pyridine resin before and after soaking in conc. HNO$_3$.
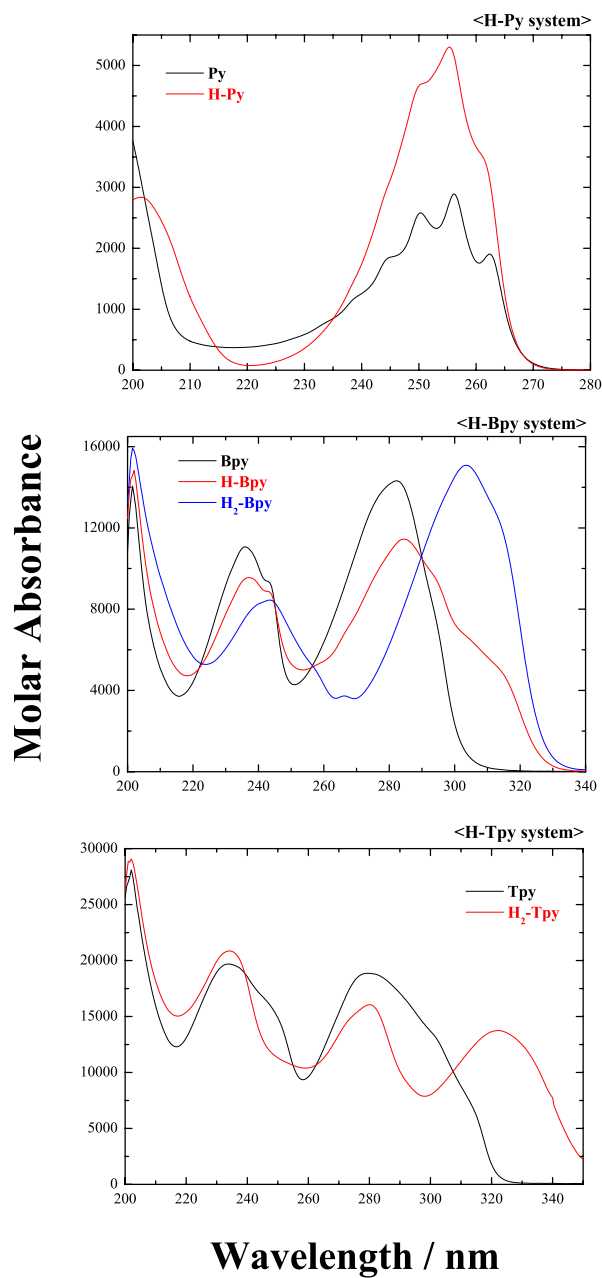
Figure II-6. Molar absorbances of the chemical species of pyridine derivatives in ethanol (Calculated by HYPERQUAD).

Table II-1. Physical and chemical parameters of water and alcohols.

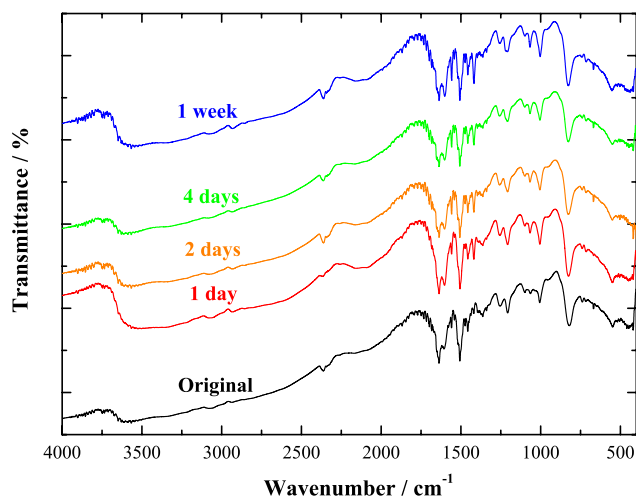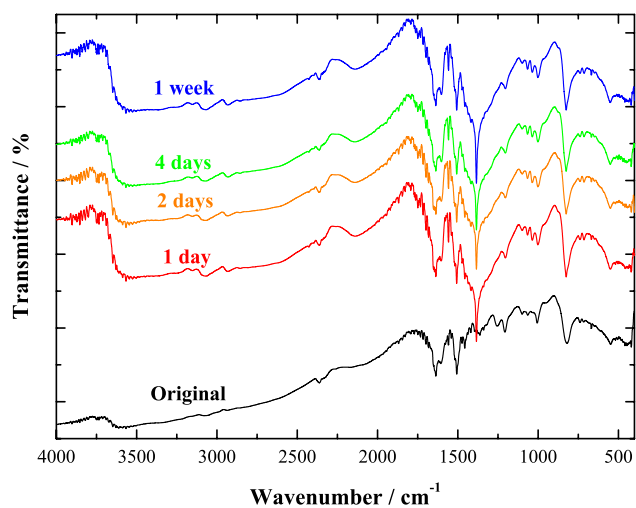|	M. W.	Specific gravity (g/cm^3) [1]	Viscosity (cPa·s) [2]	Dipole moment (D)	DEC [3]	pK_s [4]	logK_a(HCl) [5]
water	18.02	0.9982	1.00	1.94	78.3	14.0	3.7
MeOH	32.04	0.7913	0.594	1.66	33.1	16.7	-1.1
EtOH	46.07	0.7893	1.17	1.68	23.8	19.7	-1.9
1-PrOH	60.09	0.8036	2.26	1.66	22.2	19.4	-
2-PrOH	60.09	0.7863	2.43	1.68	18.3	20.6	-3.1
1-BtOH	74.12	0.8097	2.95	1.68	17.1	-	-
2-BtOH	74.12	0.8069	4.21	-	15.5	-	-
1,2-EtGly	62.07	1.1155	10.4	2.2	37.7	15.8	-

[1] at 293 K, [2] at 293 K, [3] DEC: Dielectric constant at 298 K

[4] HS + HS ⇔ H$_2$S$^+$ + S$^-$, K_s = a$_{H2S+}$·a$_{S-}$ / a$_{HS}^2$, G. Fonrrodona, C. Ràfols, E. Bosch, M. Rosés, *Anal. Chim. Acta*, **335**, 291 (1996).

[5] HCl ⇔ H$^+$ + Cl-, K_a(HCl) = a$_{H+}$·a$_{Cl-}$ / a$_{HCl}$, 電気化学便覧 (第5版), 電気化学会編, 丸善, 2000.
Specific gravity, Viscosity, Dipole moment, DEC; 溶剤ハンドブック, 浅原照三 他, 講談社, 1991.

Appendix III

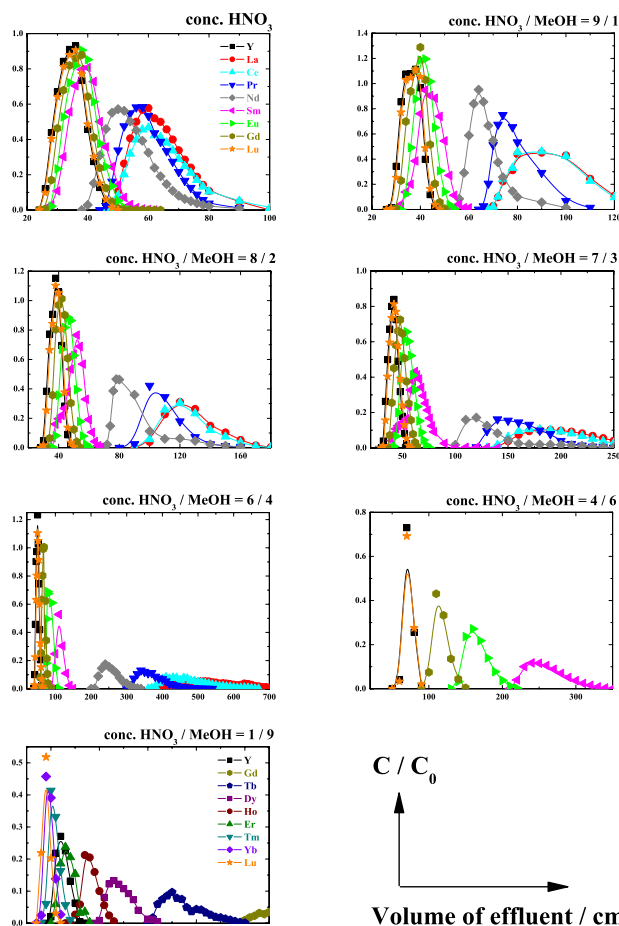## -Adsorption and Separation Behavior of Trivalent *f*-Elements in Nitrate Solution System-

Figure III-1. Elution chromatograms of Y and Ln(III) by tertiary pyridine resin in different conc. HNO_3 / MeOH mixed solutions at 298 K. (Flow rate: 100 cm^3/h, Resin column: 1 cm-ϕ × 50 cm, C: concentration in effluent, C_0: concentration in feed solution)

Table III-1. Distribution coefficients of Y and Ln(III) and their separation factors by tertiary pyridine resin in conc. HNO_3 / MeOH mixed solutions at 298 K. ((Flow rate: 100 cm^3/h, Resin column: 1 cm-$\phi \times$ 50 cm, Error: $K_d \leq \pm$ 5%, $\alpha \leq \pm$ 3%)

| | K_d | | | | | | |
| | conc. HNO_3 / MeOH (vol/vol) = | | | | | | |
Element	10 / 0	9 / 1	8 / 2	7 / 3	6 / 4	4 / 6	1 / 9
Y	1.61	1.65	2.10	2.80	4.58	8.97	19.09
La	6.64	12.52	19.36	33.26	100.16		
Ce	6.64	12.52	18.56	31.15	83.81		
Pr	5.94	9.57	15.69	23.69	65.05		
Nd	4.62	7.51	10.49	18.31	45.90		
Sm	2.39	3.38	5.15	7.36	17.01	44.00	
Eu	2.21	2.89	3.90	5.22	10.68	26.60	
Gd	1.90	2.52	2.80	4.21	7.90	17.67	
Tb							66.16
Dy							41.61
Ho							30.72
Er							21.36
Tm							15.63
Yb							13.86
Lu	1.61	1.65	2.31	2.95	4.97	8.97	12.74

| | Separation factor (α) | | | | | |
| | conc. HNO_3 / MeOH (vol/vol) = | | | | | |
	10 / 0	9 / 1	8 / 2	7 / 3	6 / 4	4 / 6
Ce / Eu	3.01	4.34	4.76	5.97	7.85	
Ce / Lu	4.13	7.59	8.04	10.57	16.87	
Eu / Lu	1.37	1.75	1.69	1.77	2.15	2.97
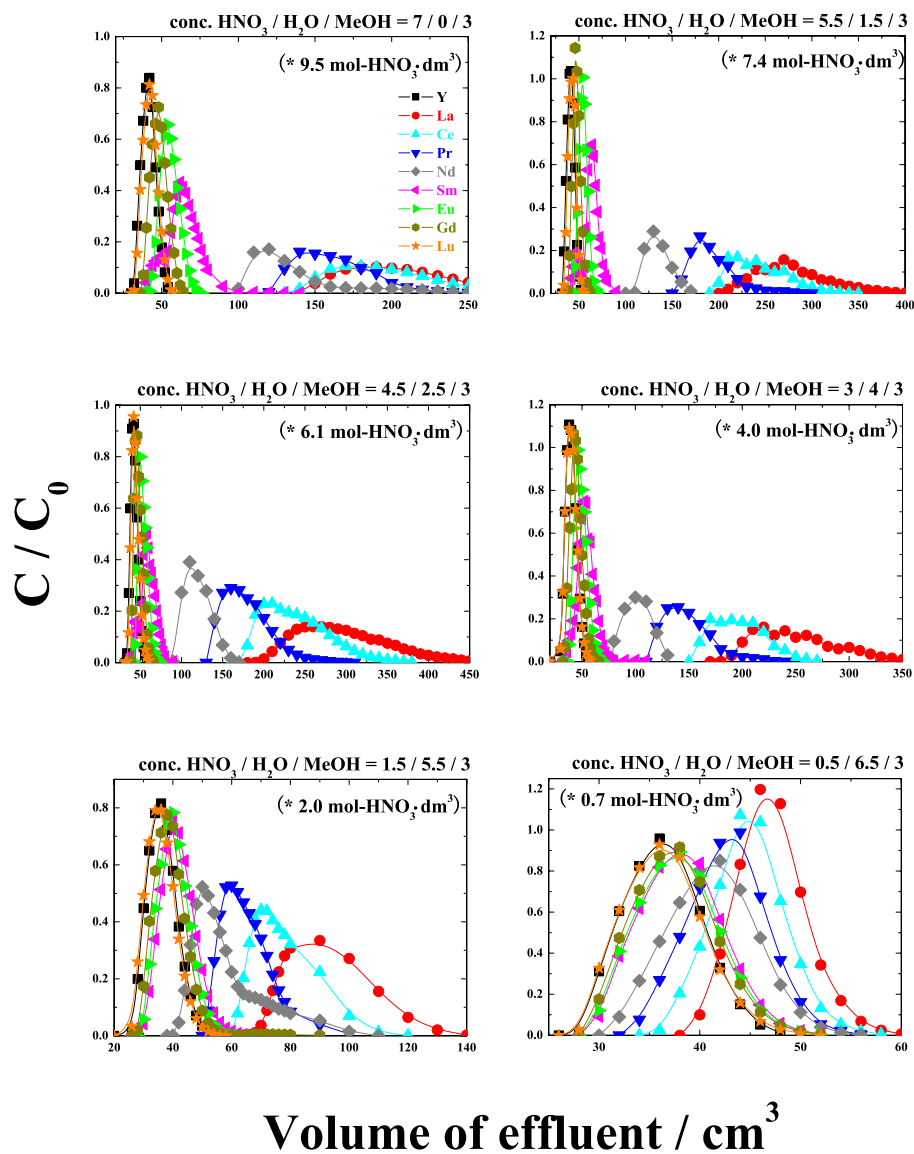
Figure III-2. Elution chromatograms of Y and Ln(III) by tertiary pyridine resin in different HNO_3 / MeOH mixed solutions at 298 K. (Flow rate: 100 cm^3/h, Resin column: 1 cm-ϕ × 50 cm, Solvent: 70 vol%-HNO_3 / 30 vol%-MeOH)

Table III-2. Distribution coefficients of Y and Ln(III) and their separation factors by tertiary pyridine resin in HNO_3 / MeOH mixed solutions at 298 K. ((Flow rate: 100 cm^3/h, Resin column: 1 cm-$\phi \times$ 50 cm, Solvent: 70 vol%-HNO_3 / 30 vol%-MeOH, Error: $K_d \leq \pm$ 5%, $\alpha \leq \pm$ 3%)

	K_d					
	H_2O / MeOH (vol/vol) = 7 / 3					
	[HNO_3] in mixed solution / mol·dm^3					
Element	9.45	7.43	6.08	4.05	2.03	0.68
Y	2.80	2.78	2.82	2.35	1.65	1.88
La	33.26	48.97	48.41	42.39	12.04	3.96
Ce	31.15	40.23	36.97	32.97	8.91	3.59
Pr	23.69	31.65	27.51	22.68	6.62	3.22
Nd	18.31	21.15	17.30	15.15	4.66	2.89
Sm	7.36	7.30	6.10	5.22	2.70	2.21
Eu	5.22	5.40	4.70	3.92	2.47	2.12
Gd	4.21	3.84	3.65	3.30	2.23	2.10
Lu	2.95	2.99	3.03	2.39	1.51	1.84

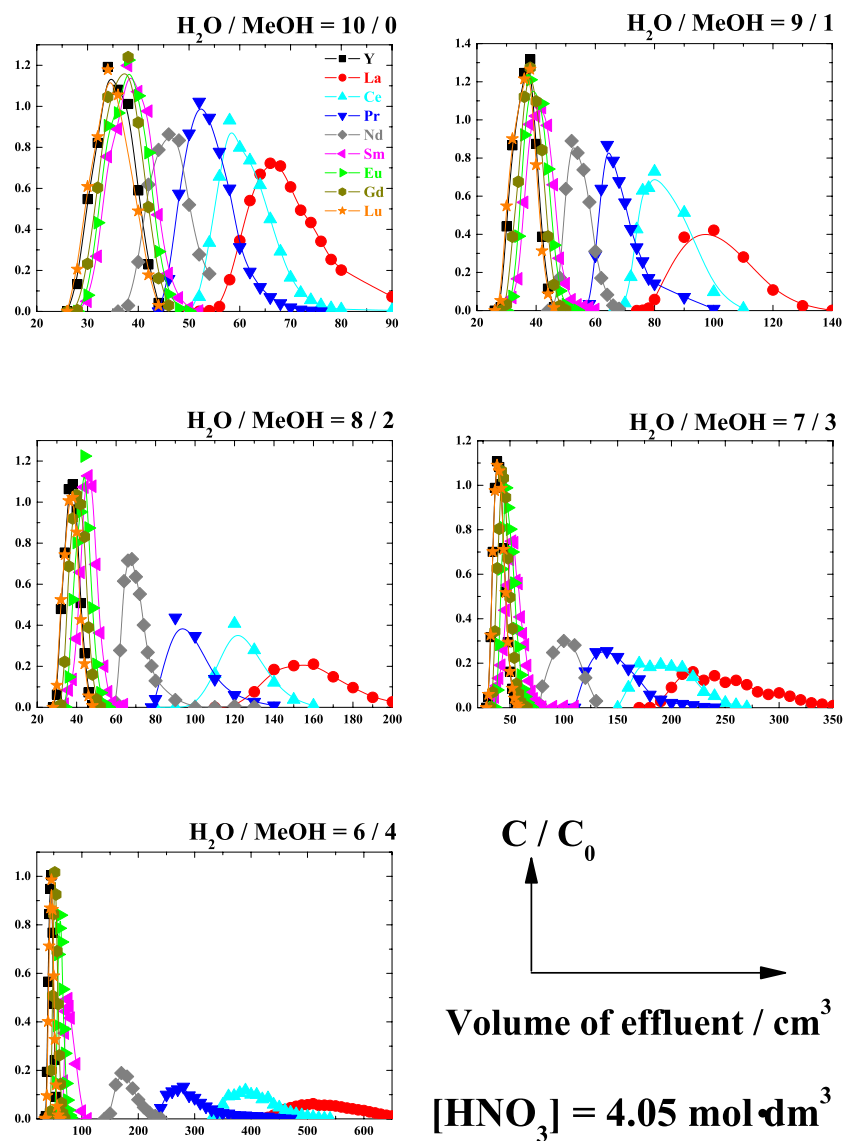| | Separation factor (α) | | | | | |
| | H_2O / MeOH (vol/vol) = 7 / 3 | | | | | |
| | [HNO_3] in mixed solution / mol·dm^3 | | | | | |
	9.45	7.43	6.08	4.05	2.03	0.68
Ce / Eu	5.97	7.45	7.86	8.42	3.60	1.69
Ce / Lu	10.57	13.46	12.20	13.78	5.92	1.96
Eu / Lu	1.77	1.81	1.55	1.64	1.64	1.16

Figure III-3. Elution chromatograms of Y and Ln(III) by tertiary pyridine resin in different HNO_3 / MeOH mixed solutions at 298 K. (Flow rate: 100 cm^3/h, Resin column: 1 cm-ϕ × 50 cm, Solvent: [HNO_3] = 4.05 mol/dm_3)

Table III-3. Distribution coefficients of Y and Ln(III) and their separation factors by tertiary pyridine resin in HNO_3 / MeOH mixed solutions at 298 K. (Flow rate: 100 cm^3/h, Resin column: 1 cm-ϕ × 50 cm, Solvent: $[HNO_3]$ = 4.05 mol/dm_3, Error: K_d $\leq \pm$ 4%, $\alpha \leq \pm$ 3%)

	K_d				
	$[HNO_3]$ = 4.05 mol·dm^3				
	Volume fraction of methanol (X_{MeOH}, %))				
Element	0	10	20	30	40
Y	1.51	2.02	2.06	2.35	3.63
La	7.98	14.23	25.75	42.39	99.51
Ce	6.41	10.74	19.40	32.97	74.06
Pr	5.13	7.61	13.63	22.68	50.21
Nd	3.90	5.22	8.12	15.15	30.31
Sm	2.33	2.78	3.84	5.22	9.77
Eu	2.19	2.41	3.40	3.92	6.99
Gd	2.00	2.14	2.68	3.30	5.11
Lu	1.46	1.98	2.02	2.39	3.84

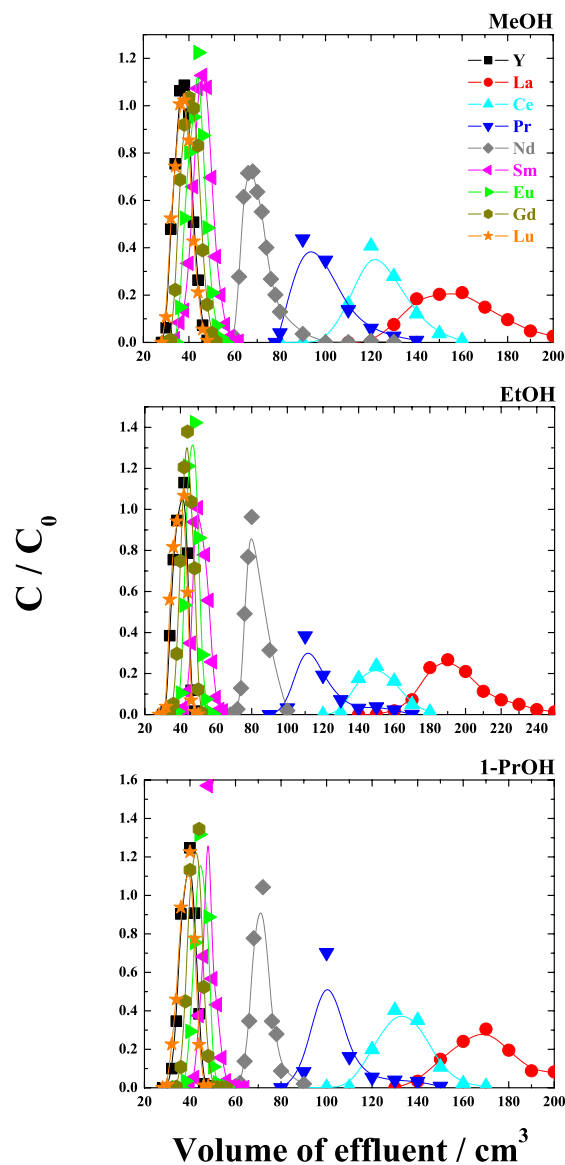| | Separation factor (α) | | | | |
| | $[HNO_3]$ = 4.05 mol·dm^3 | | | | |
| | Volume fraction of methanol (X_{MeOH}, %) | | | | |
	0	10	20	30	40
Ce / Eu	2.93	4.45	5.70	8.42	10.60
Ce / Lu	4.38	5.43	9.60	13.78	19.31
Eu / Lu	1.49	1.22	1.68	1.64	1.82

Figure III-4. Elution chromatograms of Y and Ln(III) by tertiary pyridine resin in different alcoholic HNO_3 solutions at 298 K. (Flow rate: 100 cm^3/h, Resin column: 1 cm-ϕ × 50 cm, Solvent: H_2O / alcohol = 8 / 2 (vol/vol), $[HNO_3]$ = 4.05 mol/dm^3)

Table III-4. Distribution coefficients of Y and Ln(III) and their separation factors by tertiary pyridine resin in different alcoholic HNO_3 solutions at 298 K. (Flow rate: 100 cm^3/h, Resin column: 1 cm-ϕ × 50 cm, Solvent: H_2O / alcohol = 8 / 2 (vol/vol), $[HNO_3]$ = 4.05 mol/dm^3, Error: $K_d \leq \pm$ 5%, $\alpha \leq \pm$ 4%)

Element	K_d H_2O / alcohol = 8 / 2 (vol/vol) $[HNO_3]$ = 4.05 mol·dm^3 Alcohol		
	MeOH	EtOH	1-PrOH
Y	2.06	2.56	2.56
La	25.75	33.40	28.99
Ce	19.40	25.18	21.84
Pr	13.63	17.40	15.09
Nd	8.12	10.80	8.97
Sm	3.84	4.89	4.23
Eu	3.40	3.98	3.65
Gd	2.68	3.30	3.11
Lu	2.02	2.58	2.41

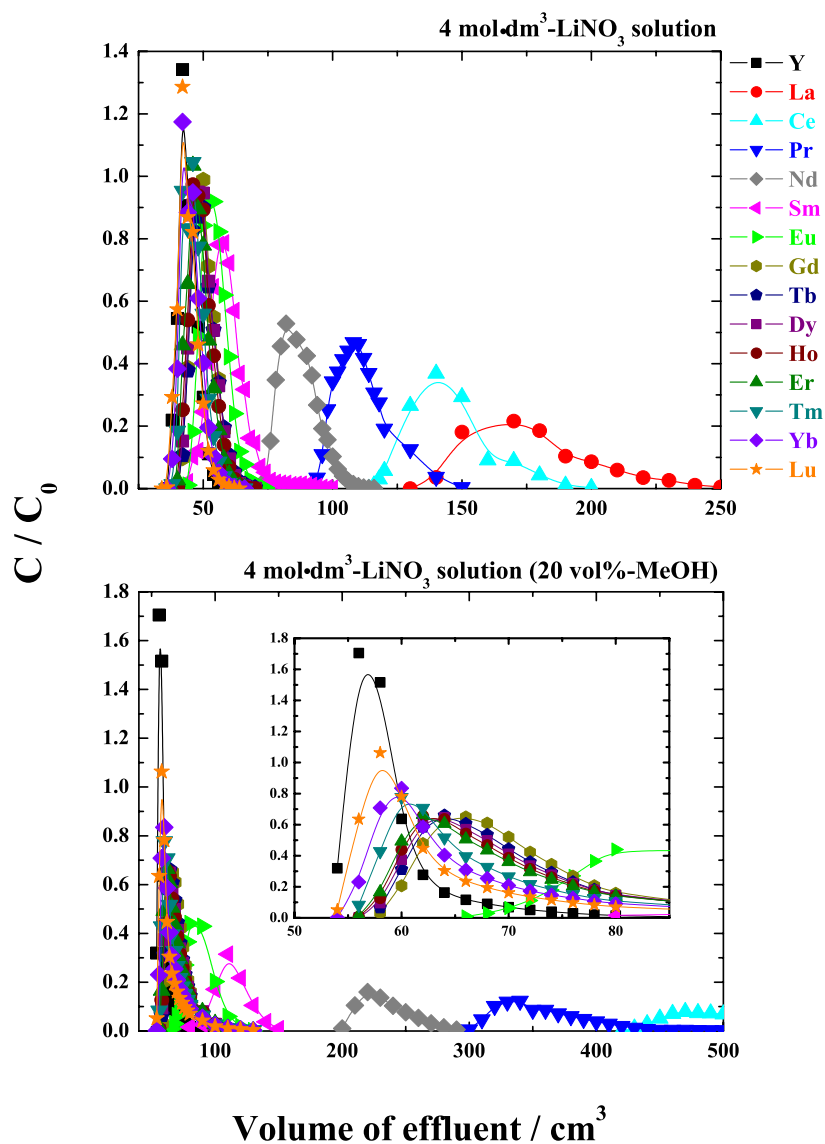|	Separation factor (α) H_2O / alcohol = 8 / 2 (vol/vol) $[HNO_3]$ = 4.05 mol·dm^3 Alcohol		
	MeOH	EtOH	1-PrOH
Ce / Eu	5.70	6.33	5.98
Ce / Lu	9.60	9.77	9.05
Eu / Lu	1.68	1.54	1.51

Figure III-5. Elution chromatograms of Y and Ln(III) by tertiary pyridine resin in LiNO$_3$ solutions at 298 K. (Flow rate: 100 cm^3/h, Resin column: 1 cm-ϕ $\times$ 50 cm, Solvent: [LiNO$_3$] = 4.0 mol/dm^3)

Table III-5. Distribution coefficients of Y and Ln(III) and their separation factors by tertiary pyridine resin in $LiNO_3$ solutions at 298 K. (Flow rate: 100 cm^3/h, Resin column: 1 cm-ϕ × 50 cm, Solvent: Solvent: [$LiNO_3$] = 4.0 mol/dm^3, Error: $K_d \leq \pm$ 5%, $\alpha \leq \pm$ 4%)

| | $\boldsymbol{K}_d$ | |
| | [$LiNO_3$] = 4.0 mol·dm^3 | |
	H_2O	H_2O / MeOH = 8 / 2
Y	3.40	6.06
La	28.37	
Ce	23.32	92.27
Pr	16.39	64.04
Nd	11.57	40.37
Sm	6.16	17.34
Eu	5.24	11.71
Gd	4.35	7.96
Tb	4.31	7.55
Dy	4.25	7.55
Ho	4.25	7.34
Er	4.10	7.22
Tm	3.79	6.89
Yb	3.40	6.64
Lu	3.40	6.33

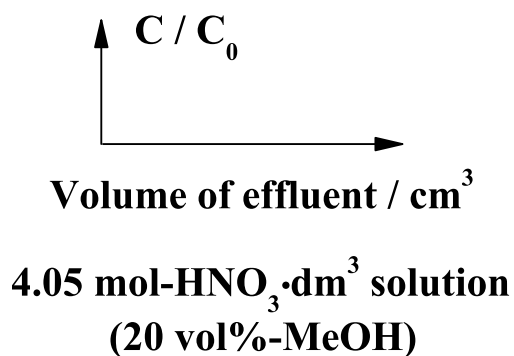| | Separation factor (α) | |
| | [$LiNO_3$] = 4.0 mol·dm^3 | |
Element	H_2O	H_2O / MeOH = 8 / 2
Ce / Eu	4.45	7.88
Ce / Lu	6.85	14.58
Eu / Lu	1.54	1.85

Figure III-6. Elution chromatograms of Y and Ln(III) by tertiary pyridine resin in HNO$_3$ / MeOH mixed solution at different temperatures. (Flow rate: 100 cm^3/h, Resin column: 1 cm-ϕ × 50 cm, Solvent: H$_2$O / MeOH = 8 / 2 (vol/vol), [HNO$_3$] = 4.05 mol/dm^3)

Table III-6. Distribution coefficients of Y and Ln(III) and their separation factors by tertiary pyridine resin in HNO_3 MeOH mixed solution at different temperatures. (Flow rate: 100 cm^3/h, Resin column: 1 cm-$\phi \times$ 50 cm, Solvent: H_2O / MeOH = 8 / 2 (vol/vol), [HNO_3] = 4.05 mol/dm^3, Error: $K_d \leq \pm$ 5%, $\alpha \leq \pm$ 3%)

	$\boldsymbol{K}_d$				
	4.05 mol-$HNO_3 \cdot$dm^3 (20 vol%-MeOH)				
	Temperature / K				
Element	278	288	298	308	323
Y	2.04	2.23	2.06	1.94	1.84
La	45.59	33.15	25.75	21.73	16.56
Ce	28.93	23.79	19.40	17.07	12.56
Pr	19.77	16.62	13.63	11.36	9.61
Nd	10.76	9.40	8.12	8.14	6.85
Sm	4.41	3.98	3.84	3.98	3.61
Eu	3.42	3.44	3.40	3.34	2.80
Gd	2.82	2.99	2.68	2.78	2.29
Lu	2.04	2.14	2.02	2.00	1.84

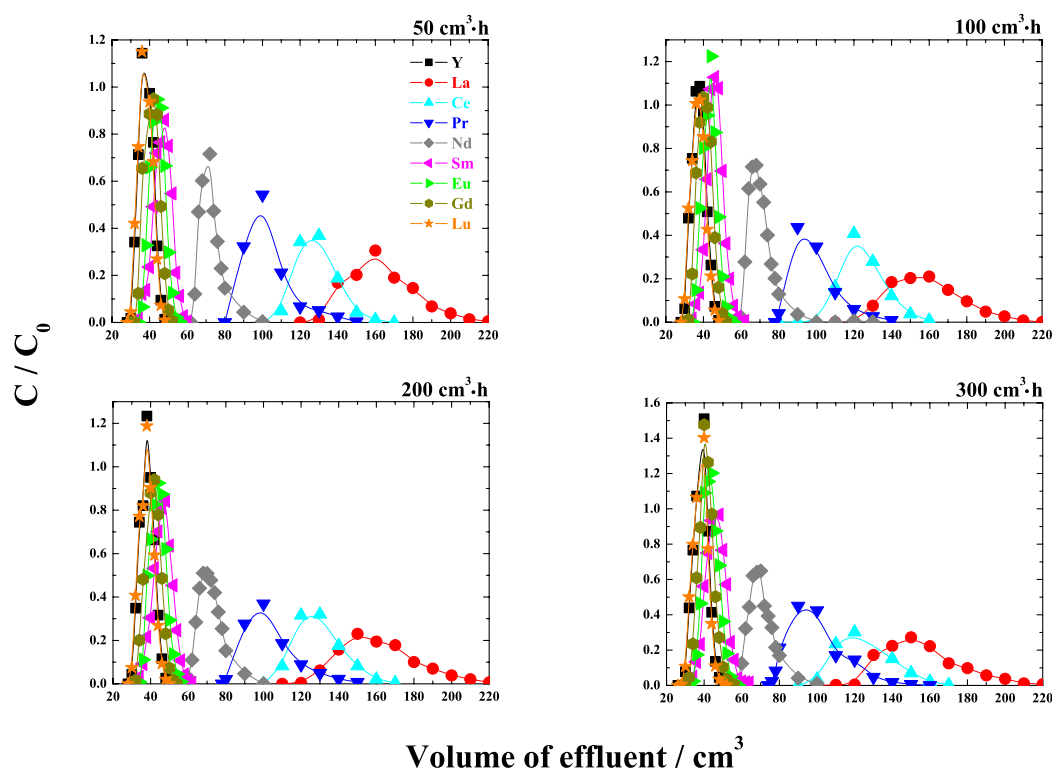| | Separation factor (α) | | | | |
| | 4.05 mol-$HNO_3 \cdot$dm^3 (20 vol%-MeOH) | | | | |
| | Temperature / K | | | | |
	278	288	298	308	323
Ce / Eu	8.45	6.91	5.70	5.11	4.48
Ce / Lu	14.17	11.10	9.60	8.54	6.84
Eu / Lu	1.68	1.61	1.68	1.67	1.53

Figure III-7. Elution chromatograms of Y and Ln(III) by tertiary pyridine resin in HNO$_3$ / MeOH mixed solution at 298 K with different flow rates. (Resin column: 1 cm-ϕ × 50 cm, Solvent: H$_2$O / MeOH = 8 / 2 (vol/vol), [HNO$_3$] = 4.05 mol/dm^3)

Table III-7. Distribution coefficients of Y and Ln(III) and their separation factors by tertiary pyridine resin in HNO_3 MeOH mixed solution at 298 K with different flow rates. (Resin column: 1 cm-ϕ × 50 cm, Solvent: Solvent: Solvent: H_2O / MeOH = 8 / 2 (vol/vol), $[HNO_3]$ = 4.05 mol/dm^3, Error: $K_d \leq \pm$ 4%, $\alpha \leq \pm$ 3%)

	$\boldsymbol{K}_d$			
	4.05 mol-HNO$_3$·dm^3 (20 vol%-MeOH)			
	Flow rate / cm^3/h			
Element	50	100	200	300
Y	2.04	2.06	2.06	2.25
La	27.11	25.75	26.43	25.24
Ce	20.37	19.40	20.16	19.96
Pr	14.68	13.63	14.37	13.86
Nd	8.89	8.12	8.72	8.37
Sm	4.10	3.84	4.06	3.84
Eu	3.48	3.40	3.42	3.07
Gd	3.01	2.68	2.87	2.78
Lu	2.04	2.02	2.06	2.25

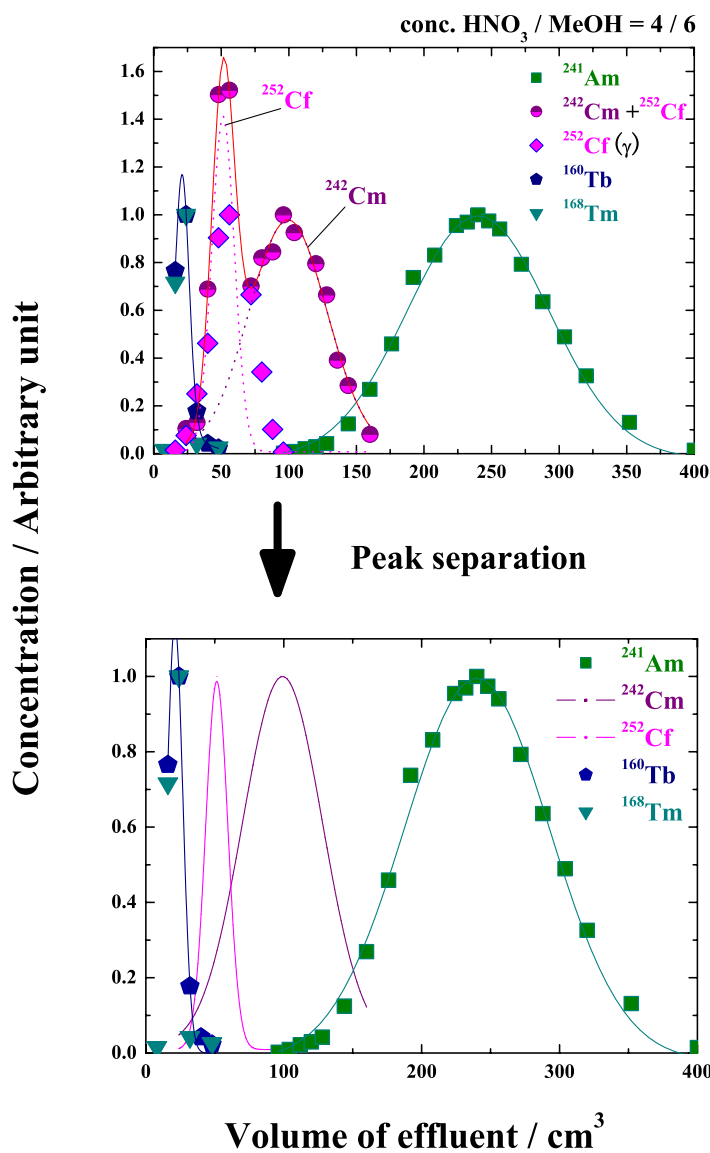| | Separation factor (α) | | | |
| | 4.05 mol-HNO$_3$·dm^3 (20 vol%-MeOH) | | | |
| | Flow rate / cm^3/h | | | |
	50	100	200	300
Ce / Eu	5.85	5.70	5.89	6.50
Ce / Lu	9.98	9.60	9.78	8.88
Eu / Lu	1.71	1.68	1.66	1.37

Figure III-8. Elution chromatogram of An(III) and Ln(III) by tertiary pyridine resin in conc. HNO_3 / MeOH mixed solution at 293 K. (Flow rate: 100 cm^3/h, Resin column: 1 cm-ϕ × 10 cm, Solvent: conc. HNO_3 / MeOH = 4 / 6 (vol/vol))
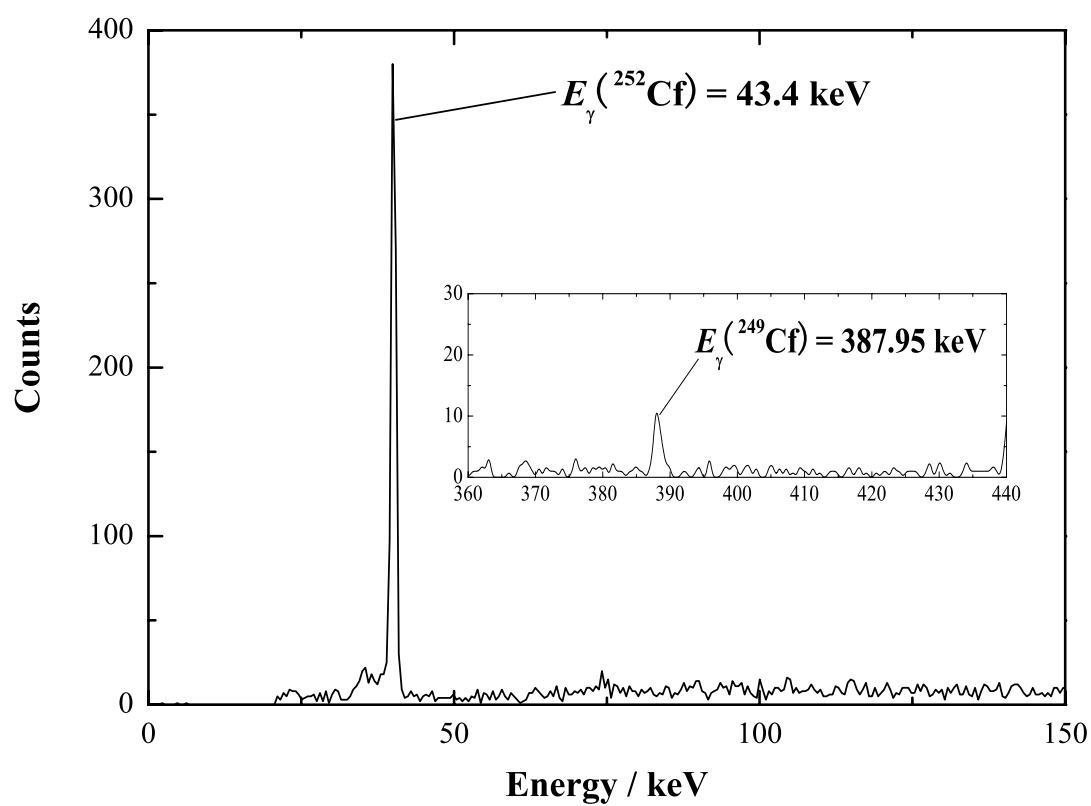
Figure III-9. γ-ray spectrum of Cf

Table III-8. Distribution coefficients of An(III) and Ln(III) and separation factors between Am and Cm by tertiary pyridine resin in conc. HNO_3 MeOH mixed solutions at 293 K. (Flow rate: 100 cm^3/h, Resin column: 1 cm-$\phi \times$ 10 cm, Error: $K_d \leq \pm$ 0.5, $\alpha \leq \pm$ 0.3)

Element	$\boldsymbol{K}_d$ conc. HNO_3 / MeOH $\boldsymbol{X}_{MeOH}$			
	0	30	40	60
Am	9.98	21.62	65.64	250.16
Cm	6.82	15.60	24.28	99.81
Cf				48.40
Ce	19.71	63.82	214.22	
Nd	13.24	34.32	110.86	
Tb		5.02		10.87

	Separation factor (α) conc. HNO_3 / MeOH $\boldsymbol{X}_{MeOH}$			
	0	30	40	60
Am / Cm	1.46	1.39	2.70	2.51

Figure III-10. Elution chromatograms of Am and Cm by tertiary pyridine resin in different HNO$_3$ / MeOH mixed solutions at 293 K. (Flow rate: 100 cm^3/h, Resin column: 1 cm-ϕ × 10 cm, Solvent: X_{MeOH} = 60%)

Table III-9. Distribution coefficients of Am and Cm and their separation factors by tertiary pyridine resin in different HNO_3 MeOH mixed solutions at 293 K. (Flow rate: 100 cm^3/h, Resin column: 1 cm-$\phi \times$ 10 cm, Solvent: X_{MeOH} = 60%, Error: $K_d \leq \pm$ 0.5, $\alpha \leq \pm$ 0.3)

	K_d				
	H$_2$O / MeOH = 4 / 6 (vol/vol)				
	[HNO$_3$] in mixed solution / mol·dm^3				
Element	5.40	4.05	3.38	2.70	2.03
Am	250.16	279.71	229.84	170.05	115.19
Cm	99.81	115.78	67.19	61.07	46.10

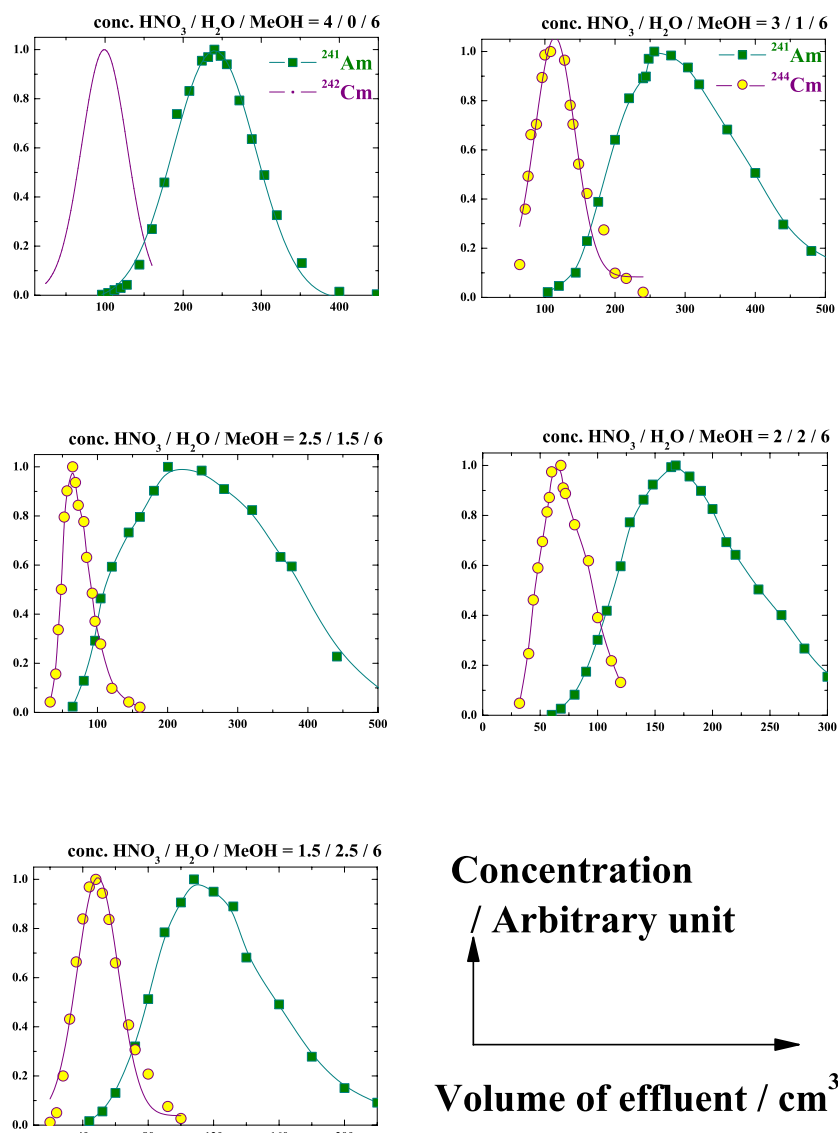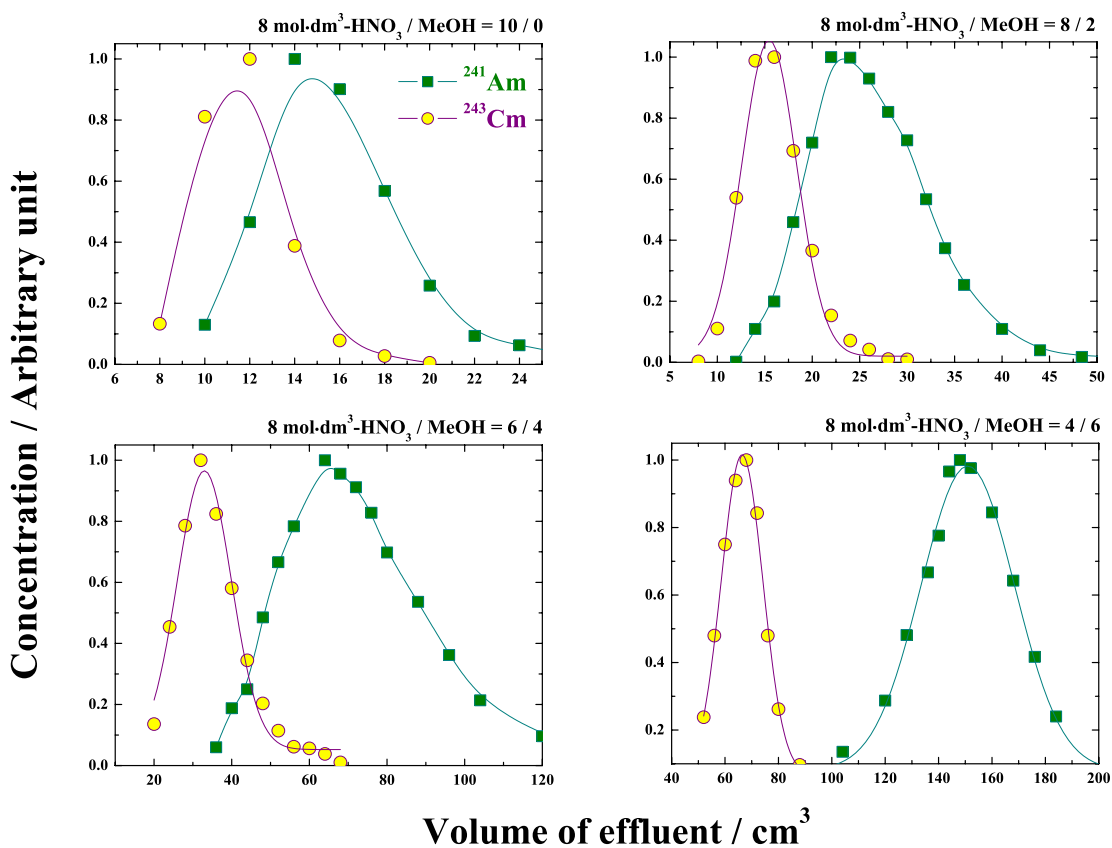| | Separation factor (α) | | | | |
| | H$_2$O / MeOH = 4 / 6 (vol/vol) | | | | |
| | [HNO$_3$] in mixed solution / mol·dm^3 | | | | |
	5.40	4.05	3.38	2.70	2.03
Am / Cm	2.51	2.42	3.42	2.78	2.50

Figure III-11. Elution chromatograms of Am and Cm by tertiary pyridine resin in 8.0 mol-HNO$_3$·dm^3 / MeOH mixed solutions at 293 K. (Flow rate: 100 cm^3/h, Resin column: 1 cm-ϕ × 10 cm)

Table III-10. Distribution coefficients of Am and Cm and their separation factors by tertiary pyridine resin in 8.0 mol-HNO$_3$·dm^3 / MeOH mixed solutions at 293 K. (Flow rate: 100 cm^3/h, Resin column: 1 cm-ϕ × 10 cm, Error: $K_d \leq \pm$ 0.5, $\alpha \leq \pm$ 0.4)

	K_d			
	8 mol-HNO$_3$·dm^3 / MeOH mixed solution			
	X_{MeOH}			
Element	0	20	40	60
Am	9.24	19.33	63.38	154.91
Cm	5.69	10.02	28.73	64.47

	Separation factor (α)			
	8 mol-HNO$_3$·dm^3 / MeOH mixed solution			
	X_{MeOH}			
	0	20	40	60
Am / Cm	1.62	1.93	2.21	2.40

Table III-11. Distribution coefficients of Am and Cm and their separation factor by tertiary pyridine resin in a 1.0 mol-HNO$_3$·dm^3 / MeOH mixed solution at 293 K. (Flow rate: 100 cm^3/h, Resin column: 1 cm-ϕ × 10 cm, Solvent: 1.0 mol-HNO$_3$·dm^3 / MeOH = 2 / 8 (vol/vol), [HNO$_3$] = 0.2 mol·dm^3, Error: $K_d \leq \pm$ 0.3, $\alpha \leq \pm$ 0.2)

K_d	Am	92.25
	Cm	36.30
α(Am/Cm)		2.54

Table III-12. Distribution coefficients of An(III) and Ln(III) and separation factors between Am and Cm by quaternary pyridine resin in conc. HNO_3 / MeOH mixed solutions at 293 K. (Flow rate: 100 cm^3/h, Resin column: 1 cm-ϕ × 10 cm, Error: $K_d \leq \pm 0.4$, $\alpha \leq \pm 0.2$)

Element	K_d conc. HNO_3 / MeOH X_{MeOH}	
	30	60
Am	35.49	482.25
Cm	16.15	181.03
Ce	125.99	
Nd	61.65	
Tm	5.35	

	Separation factor (α) conc. HNO_3 / MeOH X_{MeOH}	
	30	60
Am / Cm	2.20	2.66

Appendix IV

-Adsorption and Separation Behavior of Trivalent f-Elements in Chloride Solution System-
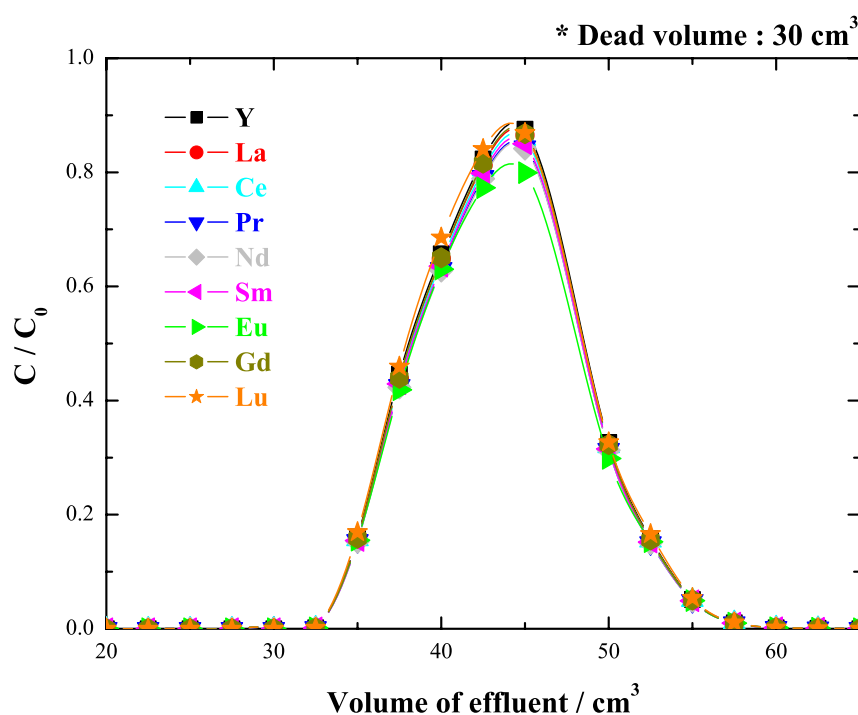
Figure IV-1. Elution chromatogram of Y and Ln(III) by silica beads in HCl/MeOH mixed solution at 298 K. (Silica beads column: 1 cm-$\phi \times$ 50 cm, Solvent: 70 vol%-conc. HCl / 30 vol%-MeOH, C: concentration in effluent, C_0: concentration in feed sample, The same chromatogram was obtained in a HNO_3 / MeOH mixed solution.)
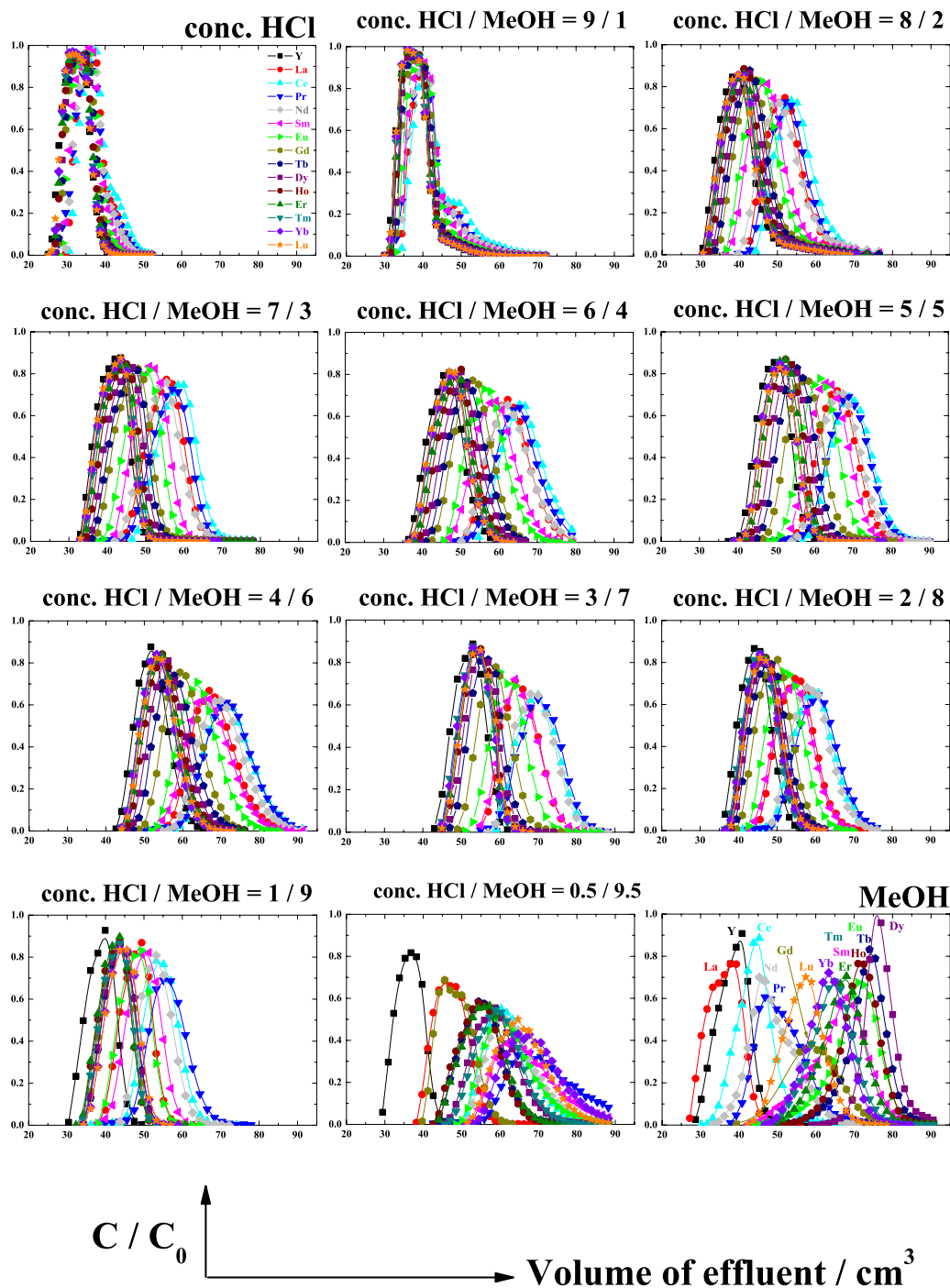
Figure IV-2. Elution chromatograms of Y and Ln(III) by tertiary pyridine resin in conc. HCl / MeOH mixed solutions at 293 K. (Flow rate: 50 cm^3/h, Resin column: 1 cm-$\phi \times$ 51 cm)

Table IV-1. Distribution coefficients of Y and Ln(III) and their separation factors by tertiary pyridine resin in conc. HCl / MeOH mixed solutions at 293 K. (Flow rate: 50 cm^3/h, Resin column: 1 cm-$\phi \times$ 51 cm, Error: $K_d \leq \pm$ 0.05, $\alpha \leq \pm$ 0.1)

Element	K_d conc. HCl / MeOH (vol/vol) =											
	10 / 0	9 / 1	8 / 2	7 / 3	6 / 4	5 / 5	4 / 6	3 / 7	2 / 8	1 / 9	0.5 / 9.5	0 / 10
Y	1.00	1.99	2.37	2.87	3.84	4.51	5.03	5.07	3.46	2.35	1.97	2.74
La	1.76	2.65	4.92	5.72	7.23	7.94	8.29	7.80	5.66	4.25	3.96	1.84
Ce	1.89	2.72	5.48	6.35	7.93	8.70	9.11	8.72	6.60	5.56	6.81	3.51
Pr	1.67	2.54	5.17	6.04	7.66	8.56	9.14	8.88	6.78	5.91	8.18	4.06
Nd	1.70	2.58	4.74	5.52	7.18	8.11	8.72	8.55	6.41	5.27	6.79	3.69
Sm	1.56	2.52	4.03	4.92	6.45	7.48	8.04	7.71	5.53	4.65	7.41	8.41
Eu	1.45	2.44	3.75	4.54	6.02	6.98	7.51	7.15	5.08	4.17	6.65	9.13
Gd	1.31	2.31	3.27	3.98	5.30	6.18	6.69	6.41	4.49	3.26	4.67	6.66
Tb	1.26	2.25	3.14	3.77	4.99	5.74	6.19	5.95	4.19	3.34	5.66	9.61
Dy	1.20	2.18	2.97	3.54	4.69	5.43	5.88	5.75	4.02	3.32	6.38	10.02
Ho	1.13	2.11	2.77	3.30	4.41	5.14	5.63	5.57	3.88	3.10	5.55	9.13
Er	1.08	2.06	2.65	3.17	4.25	4.97	5.49	5.48	3.82	3.08	5.96	8.41
Tm	1.05	2.02	2.57	3.06	4.10	4.82	5.34	5.37	3.75	3.17	6.56	7.79
Yb	1.03	2.00	2.55	3.03	4.07	4.80	5.36	5.42	3.83	3.47	8.11	7.42
Lu	1.01	1.99	2.49	2.99	4.05	4.82	5.44	5.53	3.94	3.48	7.76	6.25

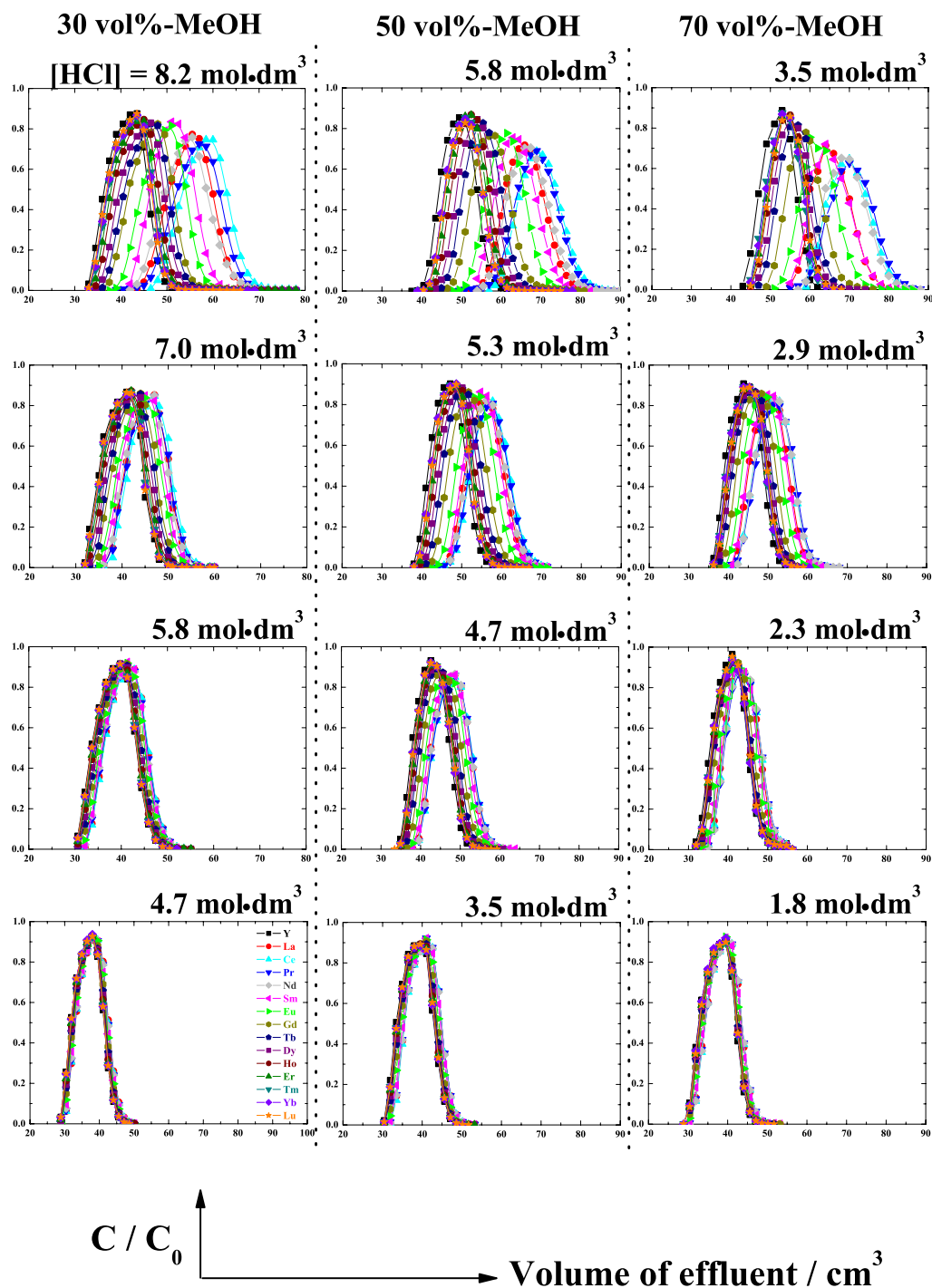|	Separation factor (α) conc. HCl / MeOH (vol/vol) =											
	10 / 0	9 / 1	8 / 2	7 / 3	6 / 4	5 / 5	4 / 6	3 / 7	2 / 8	1 / 9	0.5 / 9.5	0 / 10
Ce / Eu	1.30	1.11	1.46	1.40	1.32	1.25	1.21	1.22	1.30	1.33	1.02	0.38
Ce / Lu	1.87	1.37	2.20	2.12	1.96	1.80	1.68	1.58	1.68	1.60	0.88	0.56
Eu / Lu	1.44	1.23	1.50	1.52	1.49	1.45	1.38	1.29	1.29	1.20	0.86	1.46

Figure IV-3. Elution chromatograms of Y and Ln(III) by tertiary pyridine resin in HCl / MeOH mixed solutions at 293 K. (Flow rate: 50 cm^3/h, Resin column: 1 cm-ϕ × 51 cm)

Table IV-2. Distribution coefficients of Y and Ln(III) and their separation factors by tertiary pyridine resin in HCl / MeOH mixed solutions at 293 K. (Flow rate: 50 cm^3/h, Resin column: 1 cm-$\phi \times$ 51 cm, Error: $K_d \leq \pm$ 0.05, $\alpha \leq \pm$ 0.1)

	K_d											
	30 vol%-MeOH				50 vol%-MeOH				70 vol%-MeOH			
	[HCl] / mol/dm^3				[HCl] / mol/dm^3				[HCl] / mol/dm^3			
Element	8.19	7.02	5.85	4.68	5.85	5.27	4.68	3.51	3.51	2.93	2.34	1.76
Y	2.87	2.59	2.30	1.93	4.51	3.96	3.15	2.26	5.07	3.43	2.68	2.10
La	5.72	3.72	2.83	2.20	7.94	5.86	4.19	2.67	7.80	4.71	3.29	2.39
Ce	6.35	3.84	2.84	2.19	8.70	6.13	4.26	2.68	8.72	4.93	3.33	2.41
Pr	6.04	3.74	2.80	2.18	8.56	6.08	4.25	2.66	8.88	5.00	3.36	2.41
Nd	5.52	3.64	2.77	2.17	8.11	5.93	4.20	2.66	8.55	4.94	3.36	2.41
Sm	4.92	3.50	2.75	2.13	7.48	5.71	4.06	2.59	7.71	4.64	3.19	2.33
Eu	4.54	3.39	2.68	2.10	6.98	5.40	3.92	2.52	7.15	4.37	3.08	2.26
Gd	3.98	3.16	2.59	2.06	6.18	4.97	3.70	2.44	6.41	4.06	2.96	2.21
Tb	3.77	3.04	2.52	2.02	5.74	4.68	3.53	2.39	5.95	3.84	2.85	2.17
Dy	3.54	2.92	2.46	2.00	5.43	4.49	3.44	2.36	5.75	3.74	2.81	2.15
Ho	3.30	2.81	2.41	1.98	5.14	4.33	3.35	2.33	5.57	3.66	2.78	2.14
Er	3.17	2.74	2.38	1.96	4.97	4.23	3.31	2.32	5.48	3.61	2.76	2.13
Tm	3.06	2.67	2.34	1.95	4.82	4.12	3.25	2.30	5.37	3.55	2.73	2.12
Yb	3.03	2.64	2.33	1.94	4.80	4.11	3.23	2.30	5.42	3.56	2.74	2.12
Lu	2.99	2.63	2.32	1.94	4.82	4.14	3.25	2.30	5.53	3.62	2.76	2.13

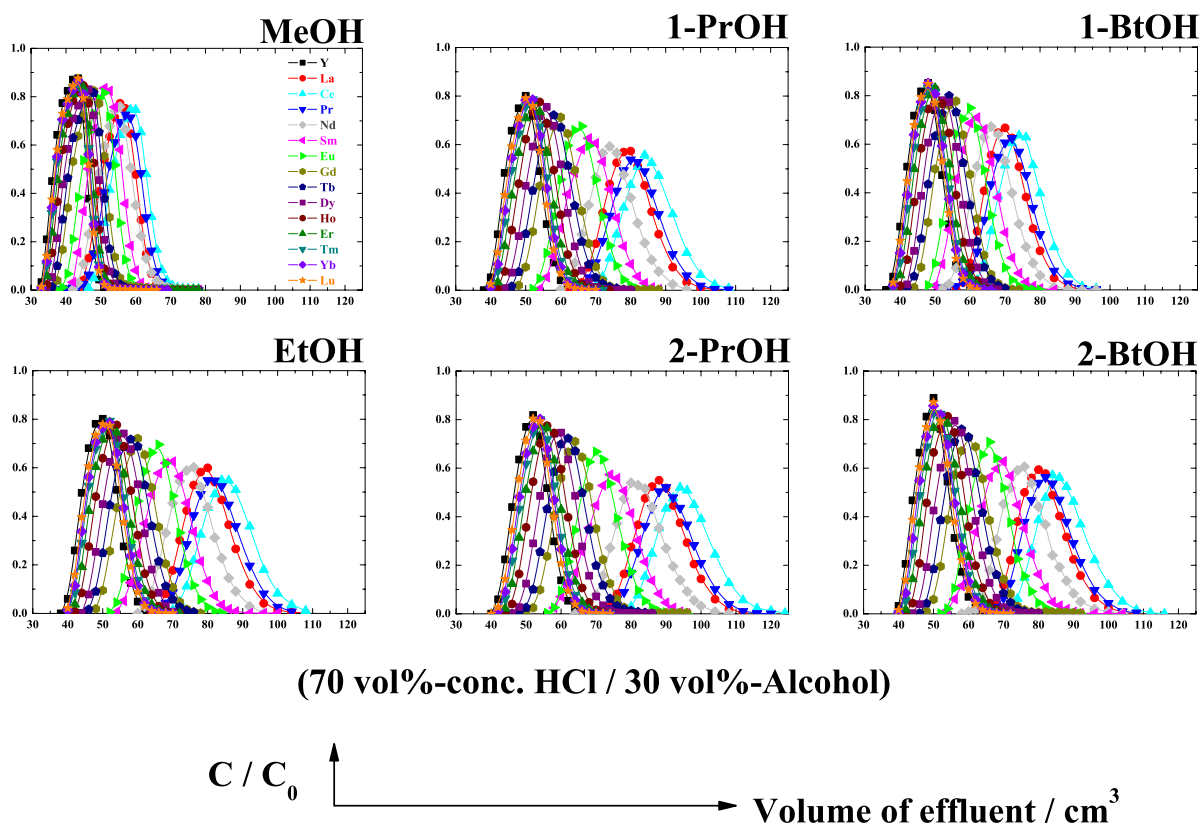|	Separation factor (α)											
	30 vol%-MeOH				50 vol%-MeOH				70 vol%-MeOH			
	[HCl] / mol/dm^3				[HCl] / mol/dm^3				[HCl] / mol/dm^3			
	8.19	7.02	5.85	4.68	5.85	5.27	4.68	3.51	3.51	2.93	2.34	1.76
Ce / Eu	1.40	1.13	1.06	1.04	1.25	1.13	1.09	1.06	1.22	1.13	1.08	1.07
Ce / Lu	2.12	1.46	1.22	1.13	1.80	1.48	1.31	1.16	1.58	1.36	1.21	1.13
Eu / Lu	1.52	1.29	1.15	1.09	1.45	1.31	1.20	1.10	1.29	1.21	1.11	1.06

Figure IV-4. Elution chromatograms of Y and Ln(III) by tertiary pyridine resin in different conc. HCl / alcohol mixed solutions at 293 K. (Flow rate: 50 cm^3/h, Resin column: 1 cm-$\phi \times$ 51 cm, Solvent: 70 vol%-conc. HCl / 30 vol%-alcohol)

Table IV-3. Distribution coefficients of Y and Ln(III) and their separation factors by tertiary pyridine resin in different conc. HCl / alcohol mixed solutions at 293 K. (Flow rate: 50 cm^3/h, Resin column: 1 cm-$\phi \times$ 51 cm, Solvent: 70 vol%-conc. HCl / 30 vol%-alcohol, Error: $K_d \leq \pm$ 0.05, $\alpha \leq \pm$ 0.1)

| | $\mathbf{K}_d$ | | | | | |
| | 70 vol%-conc. HCl / 30 vol%-Alcohol | | | | | |
Element	MeOH	EtOH	1-PrOH	2-PrOH	1-BtOH	2-BtOH
Y	2.87	4.50	4.51	4.96	4.05	4.56
La	5.72	10.78	10.68	12.55	8.78	10.98
Ce	6.35	11.98	11.85	13.92	9.66	12.13
Pr	6.04	11.22	11.08	12.97	9.08	11.34
Nd	5.52	9.83	9.71	11.28	8.05	9.94
Sm	4.92	8.54	8.45	9.72	7.09	8.64
Eu	4.54	7.41	7.78	8.88	6.58	7.93
Gd	3.98	6.66	6.63	7.51	5.70	6.76
Tb	3.77	6.25	6.26	7.06	5.43	6.38
Dy	3.54	5.80	5.81	6.52	5.08	5.91
Ho	3.30	5.34	5.36	5.97	4.72	5.43
Er	3.17	5.06	5.07	5.63	4.49	5.13
Tm	3.06	4.87	4.87	5.40	4.32	4.92
Yb	3.03	4.79	4.78	5.29	4.24	4.82
Lu	2.99	4.68	4.66	5.15	4.15	4.69

| | Separation factor (α) | | | | | |
| | 70 vol%-conc. HCl / 30 vol%-Alcohol | | | | | |
	MeOH	EtOH	1-PrOH	2-PrOH	1-BtOH	2-BtOH
Ce / Eu	1.40	1.62	1.52	1.57	1.47	1.53
Ce / Lu	2.12	2.56	2.54	2.70	2.33	2.58
Eu / Lu	1.52	1.58	1.67	1.72	1.59	1.69

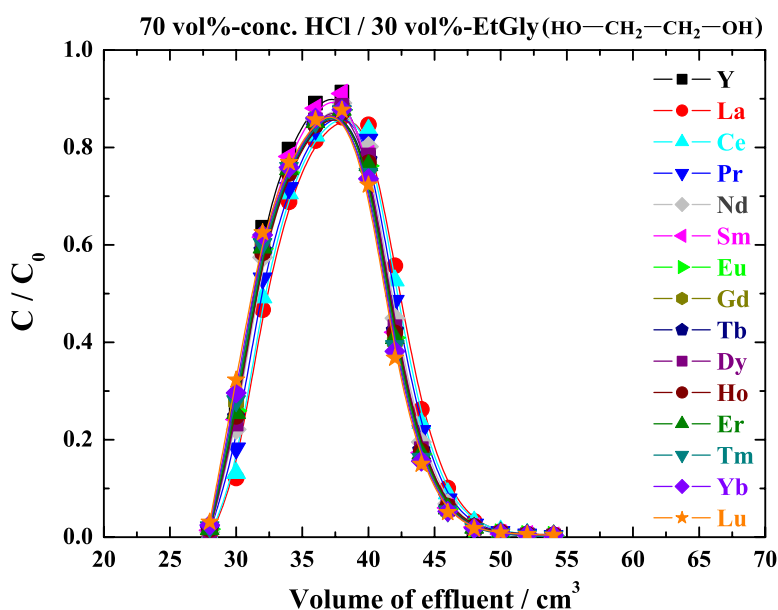**70 vol%-conc. HCl / 30 vol%-EtGly** (HO—CH$_2$—CH$_2$—OH)

Figure IV-5. Elution chromatogram of Y and Ln(III) by tertiary pyridine resin in conc. HCl / ethylene glycol mixed solution at 293 K. (Flow rate: 50 cm^3/h, Resin column: 1 cm-ϕ × 51 cm, Solvent: 70 vol%-conc. HCl / 30 vol%-EtGly)

Table IV-4. Distribution coefficients of Y and Ln(III) and their separation factors by tertiary pyridine resin in LiCl / MeOH mixed solution at 293 K. (Flow rate: 50 cm^3/h, Resin column: 1 cm-ϕ × 50 cm, Solvent: 70 vol%-11.7 mol·dm^3-LiCl / 30 vol%-MeOH, Error: $\alpha \leq \pm$ 0.1)

| Element | Kd | Separation factor |
|---|---|---|---|---|---|---|---|---|---|---|---|---|---|---|
| | | M / La | M / Ce | M / Pr | M / Nd | M / Sm | M / Eu | M / Gd | M / Tb | M / Dy | M / Er | M / Tm | M / Yb | M / Lu |
| Y | 3.20 | 0.95 | 0.70 | 0.64 | 0.68 | 0.62 | 0.61 | 0.74 | 0.66 | 0.59 | 0.56 | 0.48 | 0.39 | 0.39 |
| La | 3.37 | | 0.74 | 0.68 | 0.72 | 0.65 | 0.64 | 0.78 | 0.70 | 0.62 | 0.59 | 0.50 | 0.41 | 0.41 |
| Ce | 4.58 | 1.36 | | 0.92 | 0.98 | 0.88 | 0.88 | 1.06 | 0.95 | 0.84 | 0.80 | 0.69 | 0.56 | 0.56 |
| Pr | 4.97 | 1.48 | 1.09 | | 1.06 | 0.96 | 0.95 | 1.15 | 1.03 | 0.91 | 0.86 | 0.74 | 0.61 | 0.61 |
| Nd | 4.69 | 1.39 | 1.02 | 0.94 | | 0.90 | 0.90 | 1.09 | 0.97 | 0.86 | 0.82 | 0.70 | 0.58 | 0.58 |
| Sm | 5.19 | 1.54 | 1.13 | 1.05 | 1.11 | | 0.99 | 1.20 | 1.08 | 0.95 | 0.90 | 0.78 | 0.64 | 0.64 |
| Eu | 5.22 | 1.55 | 1.14 | 1.05 | 1.11 | 1.01 | | 1.21 | 1.08 | 0.96 | 0.91 | 0.78 | 0.64 | 0.64 |
| Gd | 4.32 | 1.28 | 0.94 | 0.87 | 0.92 | 0.83 | 0.83 | | 0.89 | 0.79 | 0.75 | 0.65 | 0.53 | 0.53 |
| Tb | 4.83 | 1.43 | 1.05 | 0.97 | 1.03 | 0.93 | 0.92 | 1.12 | | 0.89 | 0.84 | 0.72 | 0.59 | 0.59 |
| Dy | 5.46 | 1.62 | 1.19 | 1.10 | 1.16 | 1.05 | 1.04 | 1.26 | 1.13 | | 0.95 | 0.82 | 0.67 | 0.67 |
| Er | 5.75 | 1.71 | 1.26 | 1.16 | 1.23 | 1.11 | 1.10 | 1.33 | 1.19 | 1.05 | | 0.86 | 0.71 | 0.71 |
| Tm | 6.68 | 1.98 | 1.46 | 1.34 | 1.42 | 1.29 | 1.28 | 1.55 | 1.38 | 1.22 | 1.16 | | 0.82 | 0.82 |
| Yb | 8.13 | 2.41 | 1.77 | 1.64 | 1.73 | 1.56 | 1.56 | 1.88 | 1.68 | 1.49 | 1.41 | 1.22 | | 1.00 |
| Lu | 8.14 | 2.42 | 1.78 | 1.64 | 1.74 | 1.57 | 1.56 | 1.88 | 1.69 | 1.49 | 1.42 | 1.22 | 1.00 | |
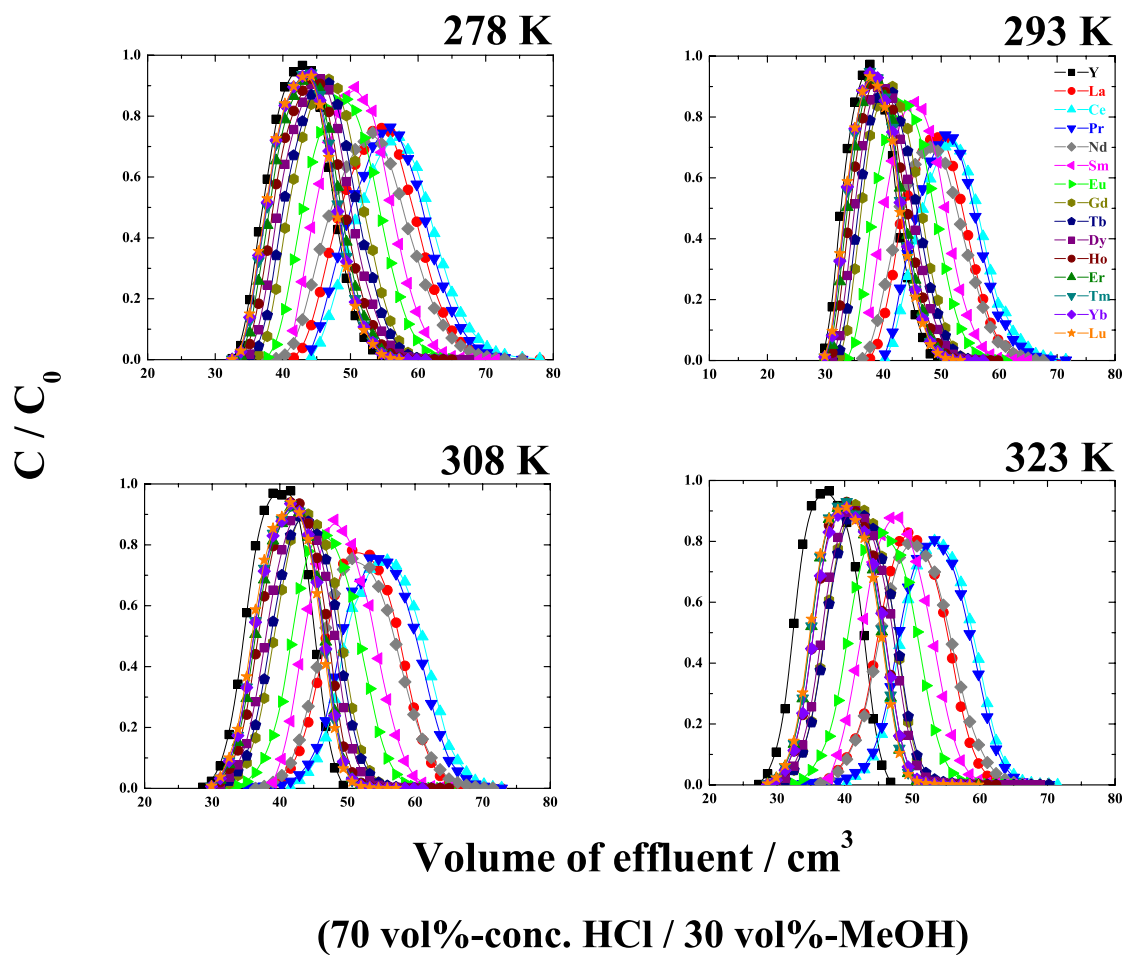
Figure IV-6. Elution chromatograms of Y and Ln(III) by tertiary pyridine resin in conc. HCl / MeOH mixed solution at different temperatures. (Flow rate: 50 cm^3/h, Resin column: 1 cm-ϕ × 50 cm, Solvent: 70 vol%-conc. HCl / 30 vol%-MeOH)

Table IV-5. Distribution coefficients of Y and Ln(III) and their separation factors by tertiary pyridine resin in conc. HCl / MeOH mixed solution at different temperatures. (Flow rate: 50 cm^3/h, Resin column: 1 cm-ϕ × 50 cm, Solvent: 70 vol%-conc. HCl / 30 vol%-MeOH, Error: $K_d \leq \pm$ 0.05, $\alpha \leq \pm$ 0.1)

| | K_d | | | |
| | Temperature / K | | | |
Element	278	293	308	323
Y	1.28	0.74	0.84	0.72
La	2.60	2.01	2.17	2.14
Ce	2.88	2.32	2.54	2.56
Pr	2.76	2.23	2.45	2.51
Nd	2.44	1.92	2.13	2.19
Sm	2.20	1.63	1.80	1.87
Eu	1.99	1.42	1.57	1.63
Gd	1.75	1.16	1.28	1.25
Tb	1.65	1.10	1.23	1.26
Dy	1.55	1.01	1.16	1.20
Ho	1.46	0.92	1.05	1.07
Er	1.39	0.86	1.00	1.02
Tm	1.35	0.83	0.98	1.02
Yb	1.33	0.82	0.98	1.06
Lu	1.32	0.80	0.96	1.01

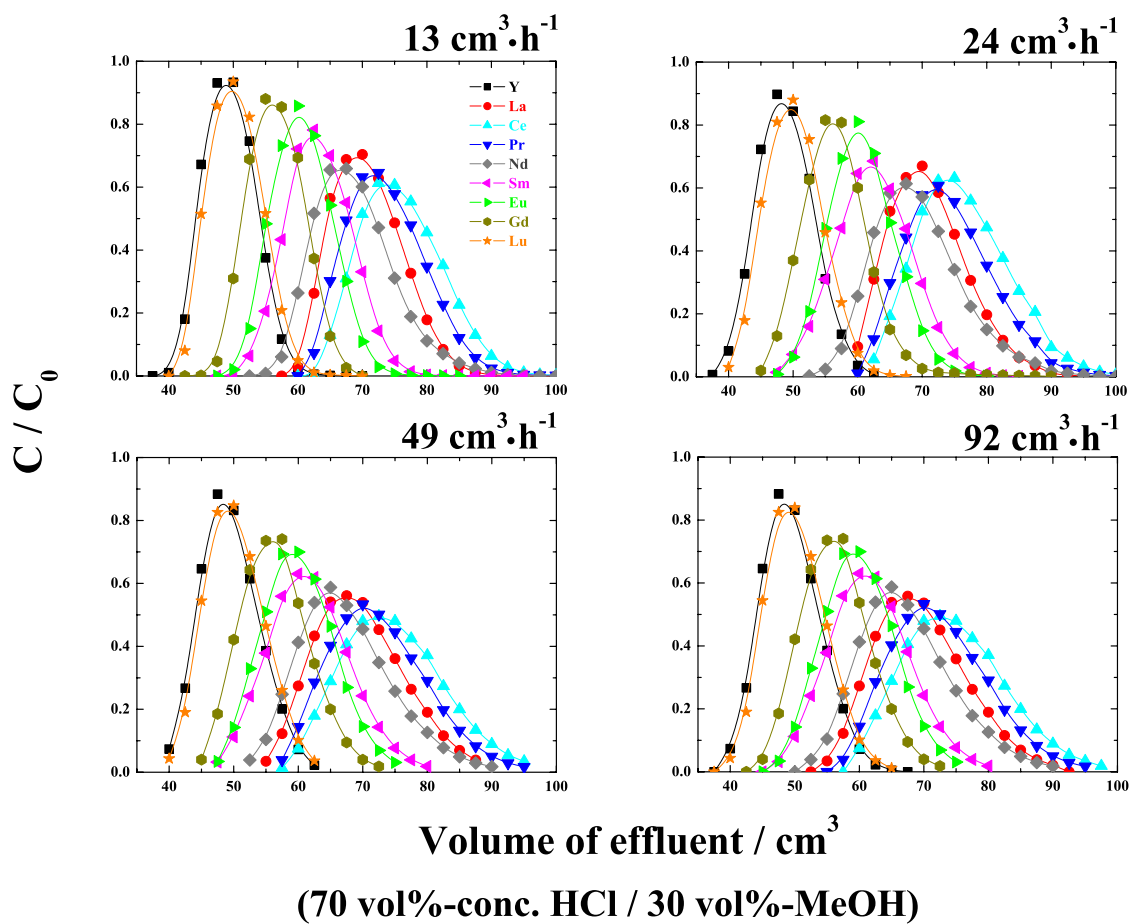| | Separation factor (α) | | | |
| | Temperature / K | | | |
Element	278	293	308	323
Ce / Eu	1.44	1.64	1.61	1.57
Ce / Lu	2.18	2.89	2.65	2.54
Eu / Lu	1.51	1.76	1.64	1.62

Figure IV-7. Elution chromatograms of Y and Ln(III) by tertiary pyridine resin in conc. HCl / MeOH mixed solution at 298 K with different flow rates. (Resin column: 1 cm-ϕ $\times$ 50 cm, Solvent: 70 vol%-conc. HCl / 30 vol%-MeOH)

Table IV-6. Distribution coefficients of Y and Ln(III) and their separation factors by tertiary pyridine resin in conc. HCl / MeOH mixed solution at 298 K with different flow rates. (Resin column: 1 cm-ϕ × 50 cm, Solvent: 70 vol%-conc. HCl / 30 vol%-MeOH, Error: $K_d \leq \pm 0.05$, $\alpha \leq \pm 0.1$)

| | K_d | | | |
| | Flow rate / cm^3/h | | | |
	13	24	49	92
Y	3.93	3.80	3.88	3.89
La	8.36	8.33	8.01	8.04
Ce	9.44	9.47	9.13	9.13
Pr	8.94	9.03	8.62	8.64
Nd	7.85	7.96	7.52	7.53
Sm	6.86	6.72	6.48	6.49
Eu	6.31	6.29	6.15	6.15
Gd	5.46	5.41	5.36	5.36
Lu	4.12	4.10	4.05	4.05

| | Separation factor (α) | | | |
| | Flow rate / cm^3/h | | | |
	13	24	49	92
Ce / Eu	1.50	1.50	1.49	1.49
Ce / Lu	2.29	2.31	2.25	2.25
Eu / Lu	1.53	1.53	1.52	1.52

Table IV-7. Distribution coefficients of Y and Ln(III) by DMAA resin in conc. HCl / MeOH mixed solution at 298 K. (Flow rate: 50 cm^3/h, Resin column: 1 cm-ϕ× 50 cm, Solvent: 70 vol%-conc. HCl / 30 vol%-MeOH, Error: $K_d \leq \pm 0.05$)

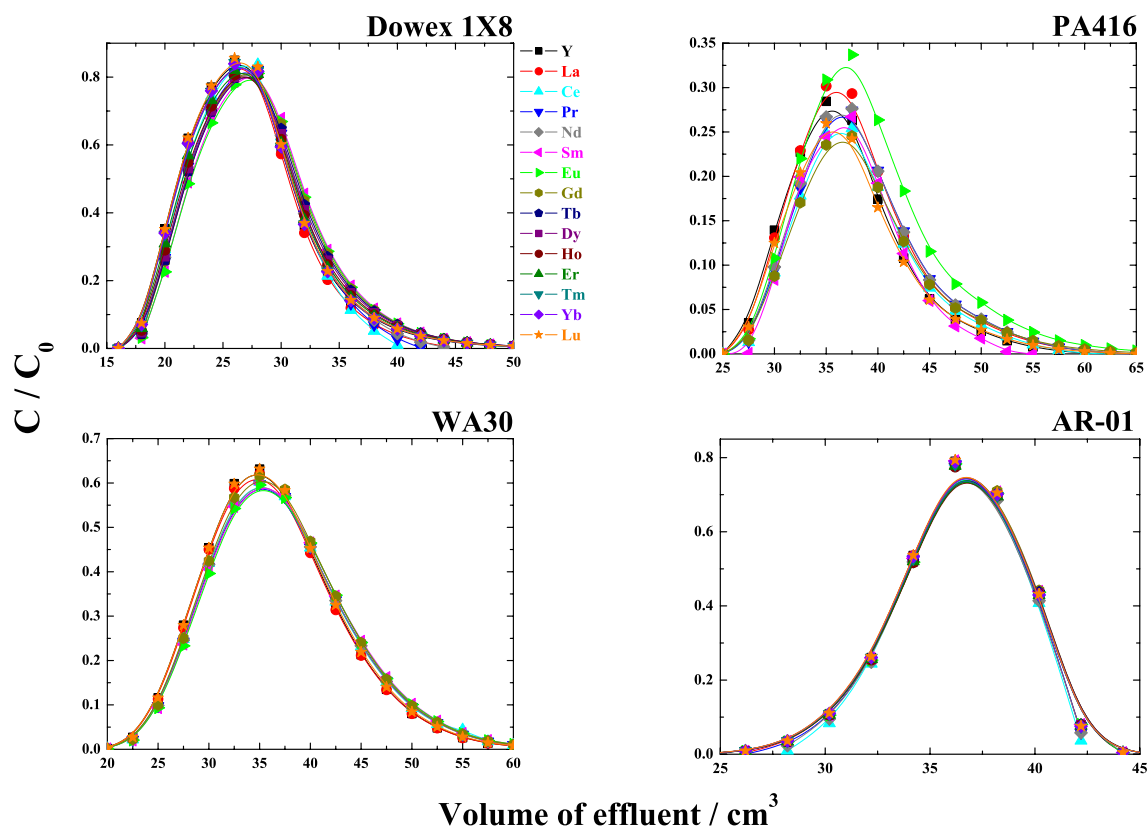| Element	Y	La	Ce	Pr	Nd	Sm	Eu	Gd	Tb	Dy	Ho	Er	Tm	Yb	Lu
Kd	3.66	5.86	8.23	8.64	7.96	8.17	7.82	6.49	5.81	5.18	4.33	3.83	3.44	3.35	3.13

Figure IV-8. Elution chromatograms of Y and Ln(III) by different anion exchange resins in conc. HCl / MeOH mixed solution at 298 K. (Flow rate: 50 cm^3/h, Resin column: 1 cm-$\phi \times$ 50 cm, Solvent: 70 vol%-conc. HCl / 30 vol%-MeOH)
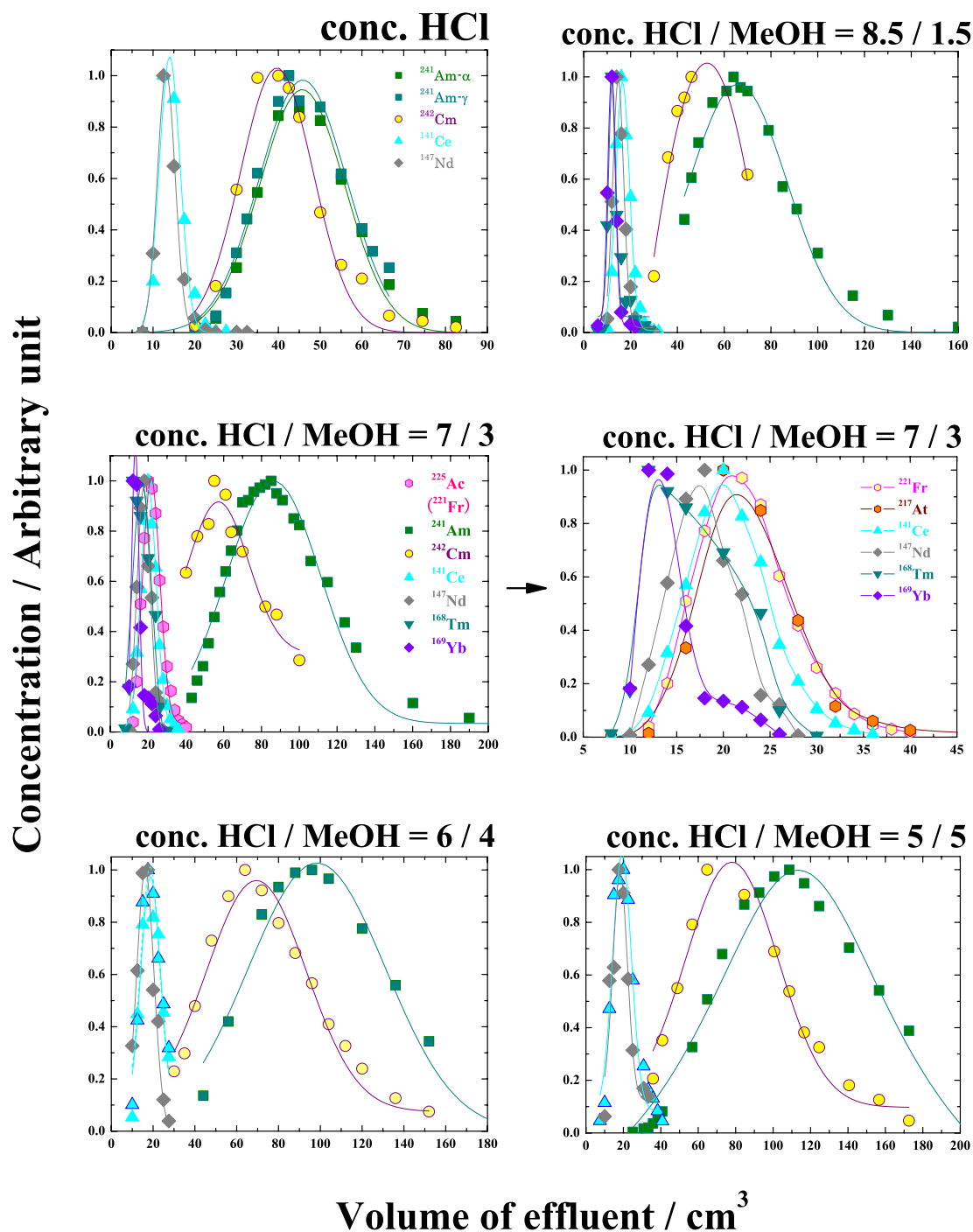
Figure IV-9. Elution chromatograms of An(III) and Ln(III) by tertiary pyridine resin in different conc. HCl / MeOH mixed solutions at 293 K. (Flow rate: 100 cm^3/h, Resin column: 1 cm-ϕ × 10 cm)
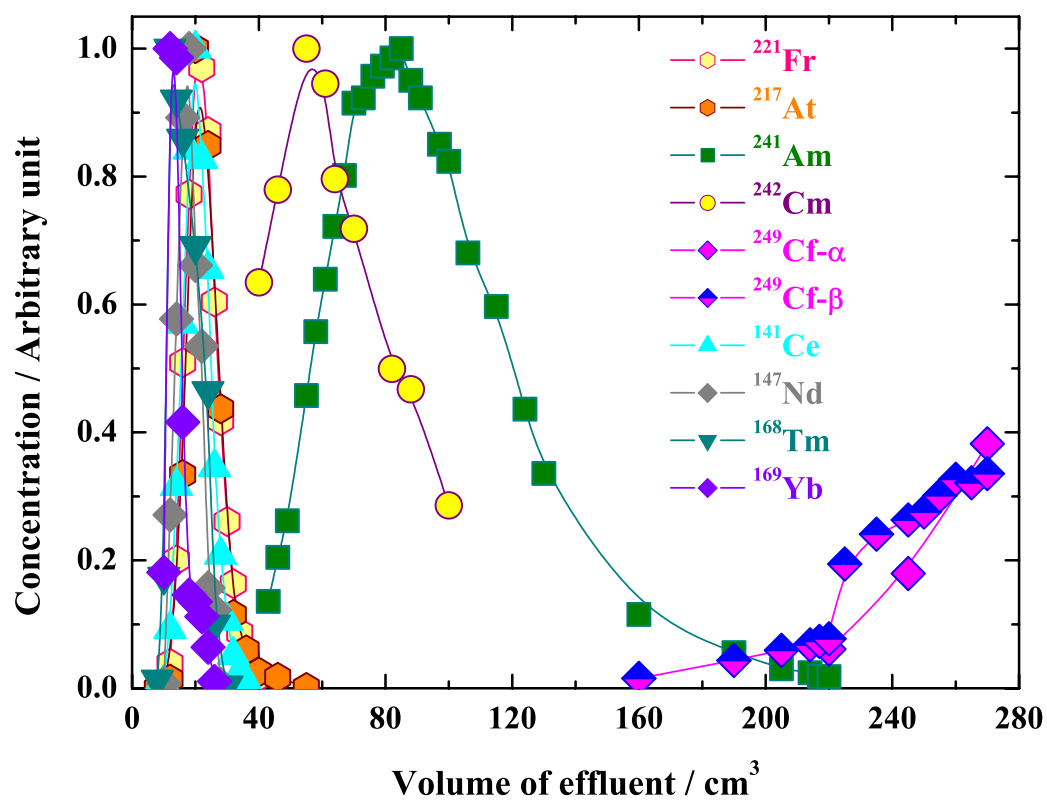
Figure IV-10. Elution chromatogram of An(III) and Ln(III) by tertiary pyridine resin in 70 vol%-conc. HCl / 30 vol%-MeOH mixed solution at 293 K. (Flow rate: 100 cm^3/h, Resin column: 1 cm-$\phi \times$ 10 cm)
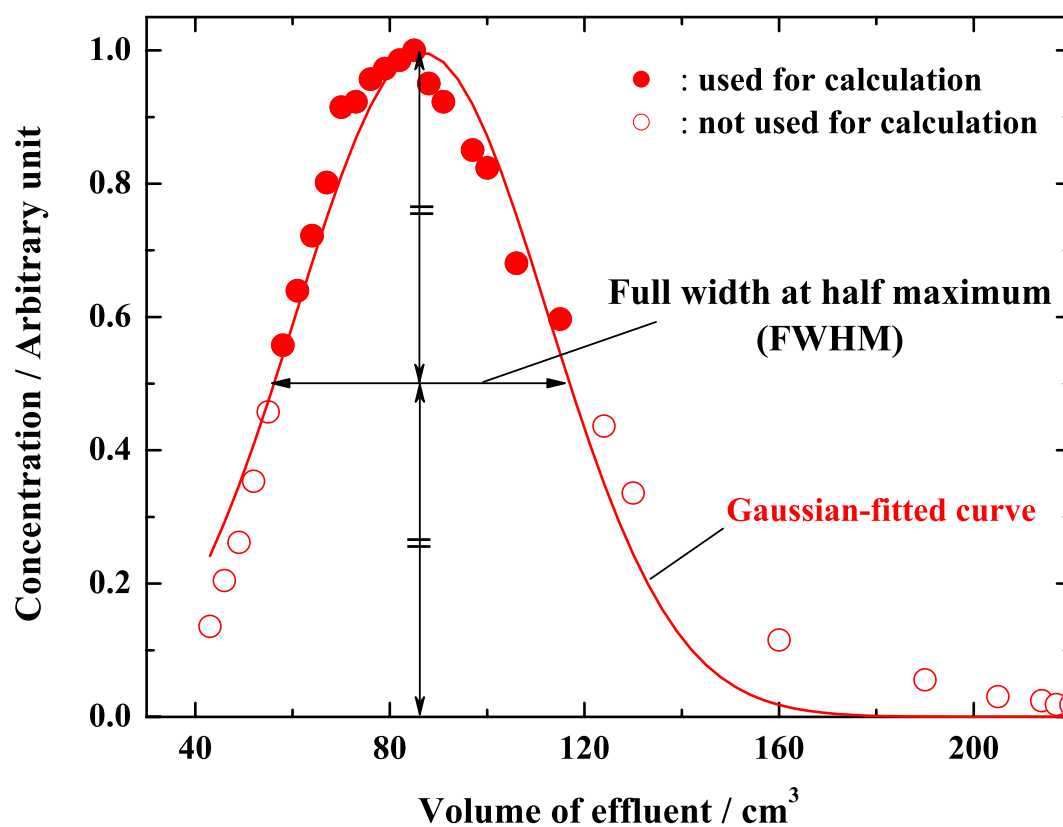
Figure IV-11. Gaussian curve fitting for tail-broadened elution curves. (Elution curve: Am(III) in tertiary pyridine resin - 70 vol%-conc. HCl / 30 vol%-MeOH mixed solution system.)

Table IV-8. Distribution coefficients of An(III) and Ln(III) and their separation factors by tertiary pyridine resin in different conc. HCl / MeOH mixed solutions at 293 K. (Flow rate: 100 cm^3/h, Resin column: 1 cm-$\phi \times$ 10 cm, Error: K_d(An) $\leq \pm$ 1.5, K_d(Ln) $\leq \pm$ 0.05, $\alpha^{Am}_{Ce} \leq \pm$ 0.5, $\alpha^{Am}_{Cm} \leq \pm$ 0.1)

| | $\boldsymbol{K}_d$ | | | | |
| | conc. HCl / MeOH (vol/vol) = | | | | |
Element	10 / 0	8.5 / 1.5	7 / 3	6 / 4	5 / 5
Ce	8.43	11.18	15.14	13.47	14.09
Nd	7.54	9.21	12.32	10.84	13.00
Tm		6.45	11.30		
Yb		6.14	7.61		
Ac			16.62		
Am	42.34	64.01	94.63	99.77	113.71
Cm	35.73	49.80	69.32	67.51	76.85

| | Separation factor (α) | | | | |
| | conc. HCl / MeOH (vol/vol) = | | | | |
	10 / 0	8.5 / 1.5	7 / 3	6 / 4	5 / 5
Am / Ce	5.03	5.73	6.25	7.40	8.07
Am / Cm	1.19	1.29	1.37	1.48	1.48

Table IV-9. Distribution coefficients of An(III) and Ln(III) and their separation factors by tertiary pyridine resin in different HCl / MeOH mixed solutions at 293 K. (Flow rate: 100 cm^3/h, Resin column: 1 cm-$\phi \times$ 10 cm, Error: K_d(An) $\leq \pm$ 1.5, K_d(Ln), $\leq \pm$ 0.05, $\alpha^{Am}{}_{Ce} \leq \pm$ 0.5, $\alpha^{Am}{}_{Cm} \leq \pm$ 0.1)

	$\boldsymbol{K}_d$			
	[HCl] / mol·dm^3			
	30 vol%-MeOH		40 vol%-MeOH	
Element	8.19	7.02	7.02	5.85
Ce	15.14	5.18	13.47	5.16
Nd	12.32	4.35	10.84	4.96
Am	94.63	17.81	99.77	14.83
Cm	69.32	13.57	67.51	11.45

	Separation factor (α)			
	[HCl] / mol·dm^3			
	30 vol%-MeOH		40 vol%-MeOH	
	8.19	7.02	7.02	5.85
Am / Ce	6.25	3.44	7.40	2.87
Am / Cm	1.37	1.31	1.48	1.29
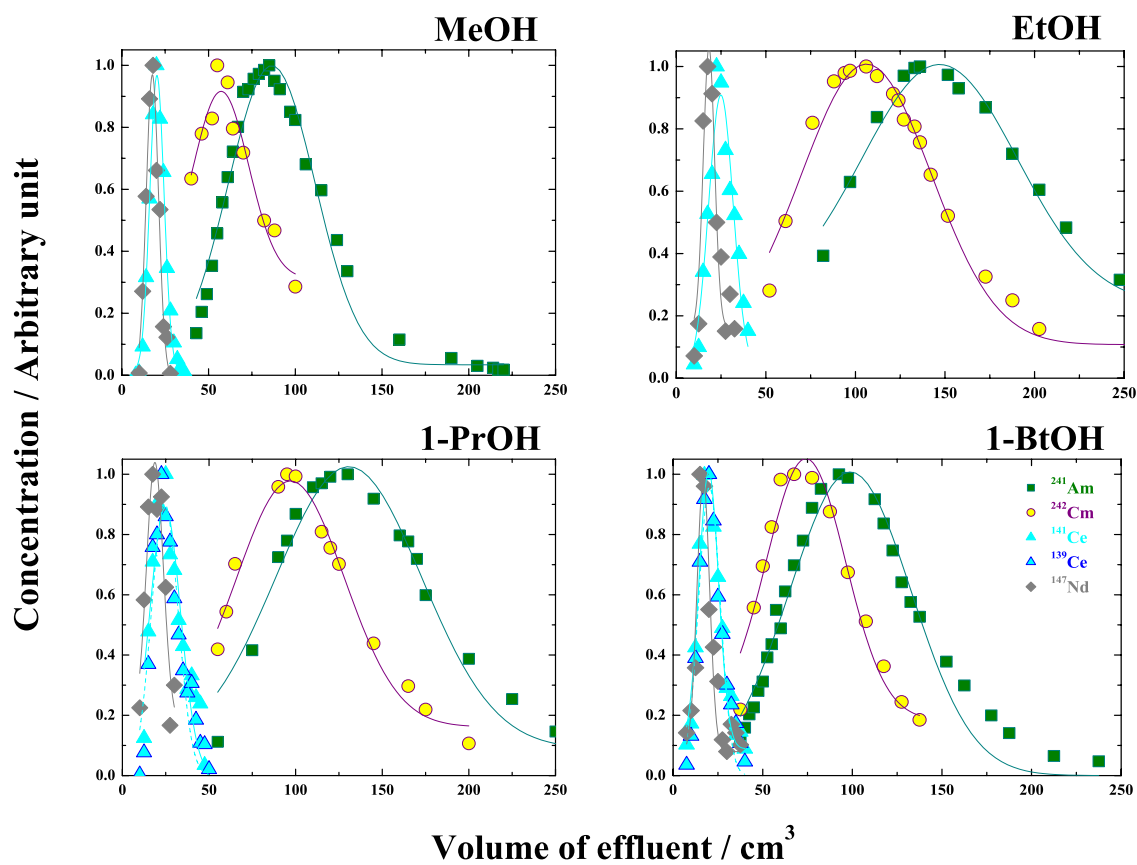
Figure IV-12. Elution chromatograms of An(III) and Ln(III) by tertiary pyridine resin in conc. HCl / alcohol mixed solutions at 293 K. (Flow rate: 100 cm^3/h, Resin column: 1 cm-$\phi \times$ 10 cm, Solvent: 70 vol%-conc. HCl / 30 vol%-alcohol)

Table IV-10. Distribution coefficients of An(III) and Ln(III) and their separation factors by tertiary pyridine resin in different conc. HCl / alcohol mixed solutions at 293 K. (Flow rate: 100 cm^3/h, Resin column: 1 cm-ϕ × 10 cm, Solvent: 70 vol%-conc. HCl / 30 vol%-alcohol, Error: K_d(An) $\leq$ ± 1.5, K_d(Ln), $\leq$ ± 0.05, α^{Am}_{Ce} $\leq$ ± 0.5, α^{Am}_{Cm} $\leq$ ± 0.1)

| | K_d | | | |
| | 70 vol%-conc. HCl / 30 vol%-alcohol | | | |
Element	methanol	ethanol	1-propanol	1-butanol
Ce	15.14	20.13	19.16	14.95
Nd	12.32	12.98	13.60	11.35
Am	94.63	150.67	133.33	98.65
Cm	69.32	106.99	97.28	72.86

| | Separation factor (α) | | | |
| | 70 vol%-conc. HCl / 30 vol%-alcohol | | | |
	methanol	ethanol	1-propanol	1-butanol
Am / Ce	6.25	7.49	6.96	6.60
Am / Cm	1.37	1.41	1.37	1.35

Table IV-11. Distribution coefficients of An(III) and Ln(III) and their separation factors by quaternary pyridine resin in conc. HCl / MeOH mixed solutions at 293 K. (Flow rate: 100 cm^3/h, Resin column: 1 cm-ϕ × 10 cm, Solvent: 70 vol%-conc. HCl / 30 vol%-alcohol, Error: K_d(An) $\leq$ ± 0.16, K_d(Ln), $\leq$ ± 0.02, α^{Am}_{Ln} $\leq$ ± 0.2, α^{Am}_{Cm} $\leq$ ± 0.05)

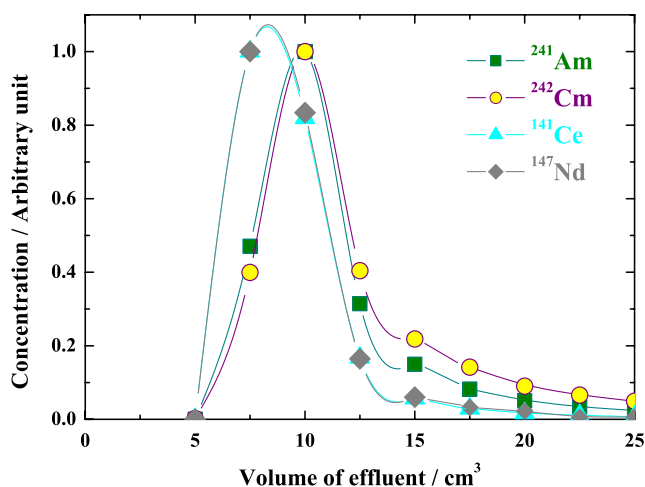|	Ce	Nd	Tm	Yb	Am	Cm
K_d	2.89	2.91	0.97	1.02	7.11	5.61
α^{Am}_{M}	2.46	2.45	7.31	7.00		1.27

Figure IV-13. Elution chromatogram of An(III) and Ln(III) by quaternary ammonium type anion exchange resin (Dowex 1X8) in conc. HCl / MeOH mixed solution at 293 K. (Flow rate: 100 cm^3/h, Resin column: 1 cm-ϕ × 10 cm, Solvent: 70 vol%-conc. HCl / 30 vol%-MeOH)
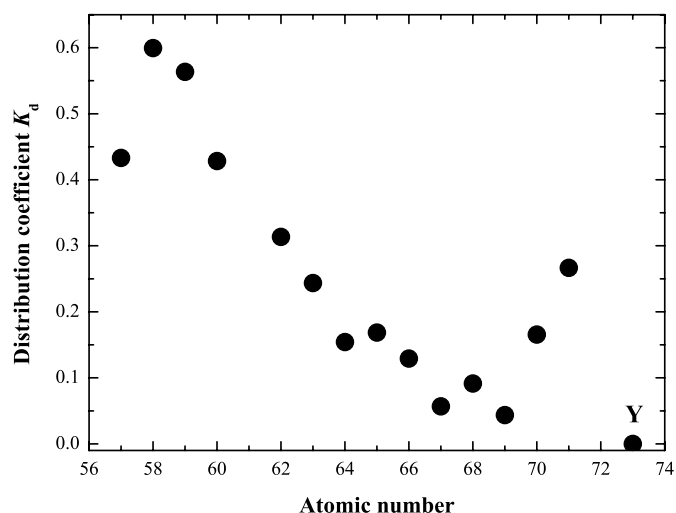

Figure IV-14. Distribution coefficients of Y and Ln(III) for tertiary pyridine resin in conc. HCl at 288 K. The error bars are smaller than the plotted points.
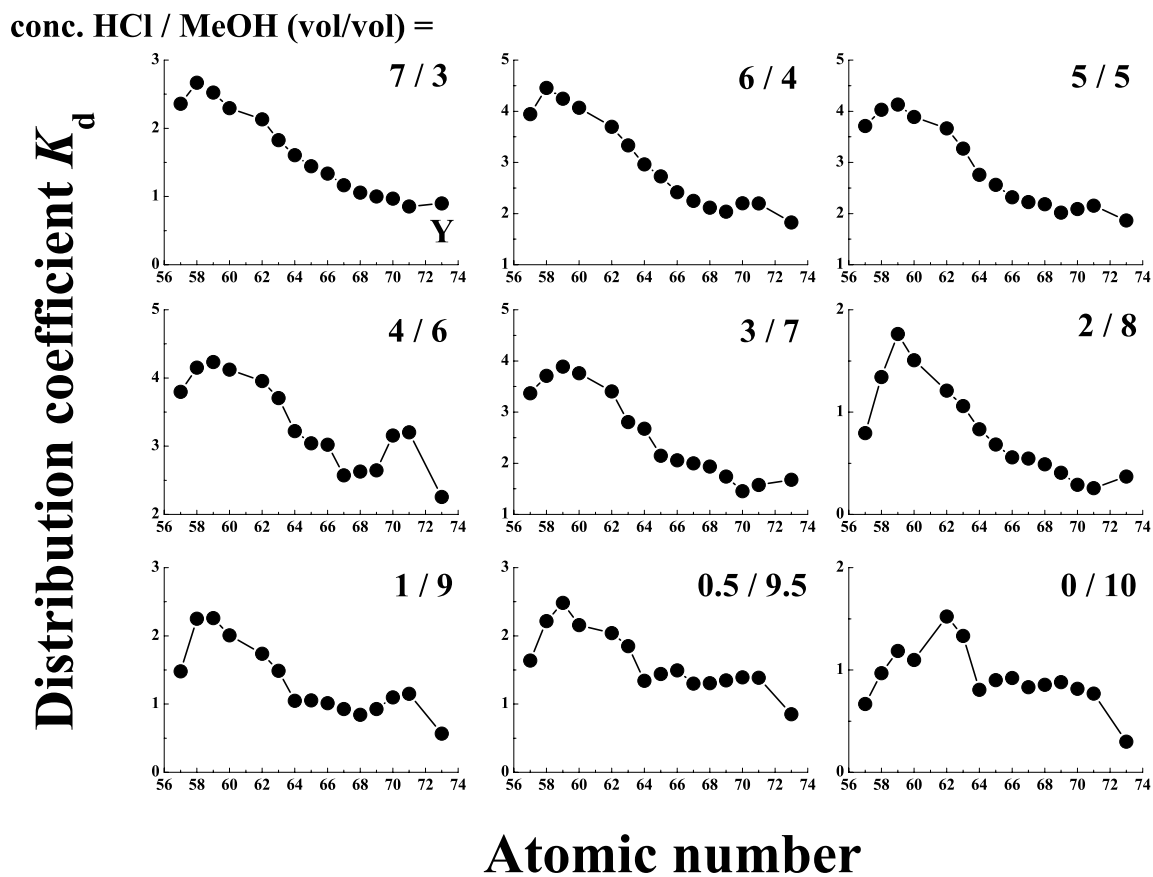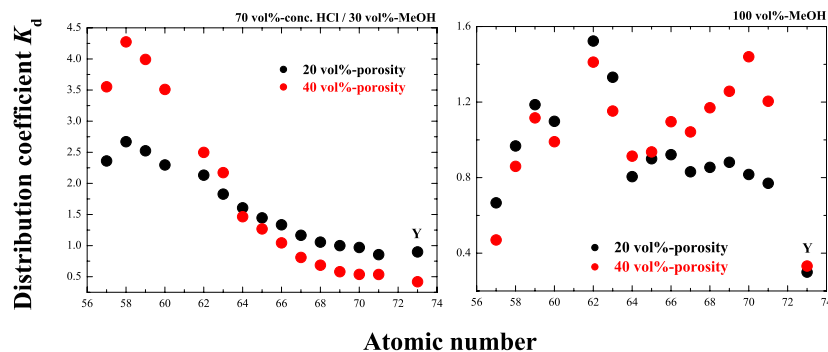
conc. HCl / MeOH (vol/vol) =

Figure IV-15. Distribution coefficients of Y and Ln(III) for tertiary pyridine resin in different conc. HCl / MeOH mixed solutions at 288 K. The error bars are smaller than the plotted points.

Figure IV-16. Effect of porosity on the distribution coefficients of Y and Ln(III) for tertiary pyridine resin in conc. HCl / methanol mixed solutions at 288 K. The error bars are smaller than the plotted points.
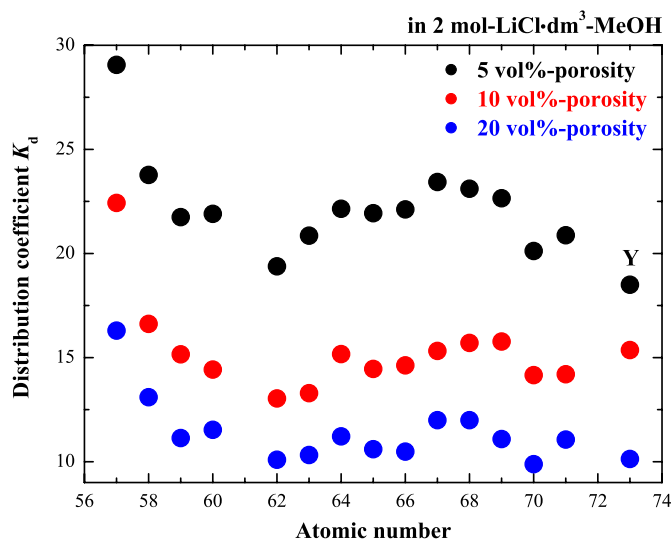

Figure IV-17. Effect of porosity on the distribution coefficients of Y and Ln(III) for tertiary pyridine resin in methanolic LiCl solution at 288 K. The error bars are smaller than the plotted points.

Appendix V

-Adsorption and Separation Mechanisms-

Table V-1. EXAFS structural parameters of Y and Ln(III) in water. (S_0^2 = 0.9, Error: $R \pm 0.01$ Å, $N \pm 5\%$)

Element	Edge	Shell	R / Å	N	σ^2 / Å^2	ΔE_0 / eV	FT range	Fitting residual	
								k-space	R-space
La	K	O (H_2O)	2.55	9.5	0.0077	0.46	2-15	21.52	8.65
Ce	K	O (H_2O)	2.52	9.2	0.0073	-2.94	2-15	21.90	11.91
	L_{III}	O (H_2O)	2.53	9.5	0.0085	4.31	1.5-10.5	24.18	9.25
Pr	L_{III}	O (H_2O)	2.51	9.4	0.0085	3.80	1.5-10	23.25	8.10
Nd	K	O (H_2O)	2.48	9.3	0.0079	-3.96	2-15.5	27.29	13.21
	L_{III}	O (H_2O)	2.49	9.6	0.0084	3.30	1.5-11	23.15	9.30
Sm	L_{III}	O (H_2O)	2.46	9.4	0.0083	4.38	1.5-11.5	21.90	4.01
Eu	L_{III}	O (H_2O)	2.42	9.0	0.0052	5.05	1.5-10.5	27.11	3.91
Gd	L_{III}	O (H_2O)	2.41	8.4	0.0066	4.50	1.5-13	23.14	3.91
Tb	L_{III}	O (H_2O)	2.38	8.4	0.0070	4.36	1.5-11	22.39	5.23
Dy	L_{III}	O (H_2O)	2.36	8.6	0.0067	2.19	1.5-13.5	27.53	8.48
Ho	L_{III}	O (H_2O)	2.36	8.3	0.0060	4.26	1.5-12.5	23.99	4.37
Er	L_{III}	O (H_2O)	2.35	8.2	0.0060	3.21	1.5-14	22.87	6.16
Tm	L_{III}	O (H_2O)	2.34	8.0	0.0061	2.65	1.5-15	20.47	1.83
Yb	L_{III}	O (H_2O)	2.32	8.2	0.0064	4.52	1.5-14.5	22.11	4.43
Lu	L_{III}	O (H_2O)	2.32	8.2	0.0064	7.29	2.5-15.5	18.25	4.94
Y	K	O (H_2O)	2.33	8.3	0.0055	-1.02	1.8-16	16.39	6.28

Table V-2. EXAFS structural parameters of Y and Ln(III) in conc. HCl / MeOH mixed solution. (Solvent: conc. HCl / MeOH = 7 / 3 (vol/vol), S_0^2 = 0.9, Error: $R \pm 0.01$ Å, $N \pm 5\%$)

Element	Edge	Shell	R / Å	N	σ^2 / Å^2	ΔE_0 / eV	FT range	Fitting residual k-space	R-space
La	K	O (H_2O)	2.55	7.9	0.0079	0.42	2-12.5	42.19	6.28
		Cl	2.88	1.6	0.0085				
Ce	L_{III}	O (H_2O)	2.53	8.1	0.0083	4.21	1.5-10	27.89	17.81
		Cl	2.85	1.2	0.0079				
Pr	L_{III}	O (H_2O)	2.51	8.4	0.0079	4.20	1.5-10	28.45	8.90
		Cl	2.86	0.9	0.0081				
Nd	L_{III}	O (H_2O)	2.50	7.8	0.0080	1.50	15-11.5	20.83	4.38
		Cl	2.78	1.2	0.0041				
Sm	L_{III}	O (H_2O)	2.46	8.6	0.0070	6.67	1.5-11.5	41.85	5.41
Eu	L_{III}	O (H_2O)	2.42	8.7	0.0078	5.61	1.5-10.5	48.40	12.11
Gd	L_{III}	O (H_2O)	2.40	8.3	0.0071	4.13	1.5-13	42.36	7.88
Tb	L_{III}	O (H_2O)	2.39	8.6	0.0076	3.83	1.5-13	34.14	7.11
Dy	L_{III}	O (H_2O)	2.36	8.3	0.0072	0.85	1.5-13	45.70	15.46
Ho	L_{III}	O (H_2O)	2.35	8.5	0.0067	2.42	1.5-12.8	34.11	5.72
Er	L_{III}	O (H_2O)	2.35	8.0	0.0056	1.01	1.5-14	34.95	7.62
		Cl	2.72	0.6	0.0064				
Tm	L_{III}	O (H_2O)							
Yb	L_{III}	O (H_2O)	2.33	8.0	0.0063	4.25	1.5-11.5	25.55	4.91
Lu	L_{III}	O (H_2O)	2.31	7.7	0.0053	4.82	1.5-11	21.67	6.56
Y	K	O (H_2O)	2.33	8.2	0.0058	-0.73	1.8-13.5	16.94	6.72

Table V-3. EXAFS structural parameters of Nd L_{III}-edge in conc. HCl / MeOH mixed solutions. (Solvent: conc. HCl / MeOH (vol/vol), S_0^2 = 0.9, Error: $R \pm 0.01$ Å, $N \pm 5\%$)

Solvent	Shell	R / Å	N	σ^2 / Å^2	ΔE_0 / eV	FT range	Fitting residual	
							k-space	R-space
water	O (H_2O)	2.49	9.6	0.0084	3.30	1.5-11	23.15	9.30
HCl / MeOH 7 / 3	O (H_2O)	2.50	7.8	0.0080	1.50	15-11.5	20.83	4.38
	Cl	2.78	1.2	0.0041				
5 / 5	O (H_2O)	2.48	8.0	0.0045	4.27	1.5-11	20.93	5.33
	Cl	2.83	1.0	0.0003				
3 / 7	O (H_2O)	2.49	8.0	0.0063	4.24	15-11.5	33.07	3.08
	Cl	2.80	1.0	0.0056				
2 / 8	O (H_2O)	2.49	8.0	0.0052	4.76	1.5-11	27.60	5.91
	Cl	2.80	1.0	0.0026				
1 / 9	O (H_2O)	2.49	8.0	0.0056	4.18	15-11.5	31.75	5.34
	Cl	2.81	1.0	0.0060				
MeOH	O (H_2O)	2.48	6.2	0.0063	4.50	1.5-11	29.58	13.27
	O (MeOH)	2.54	3.3	0.0100				
	C (MeOH)	3.01	3.3	0.0061				
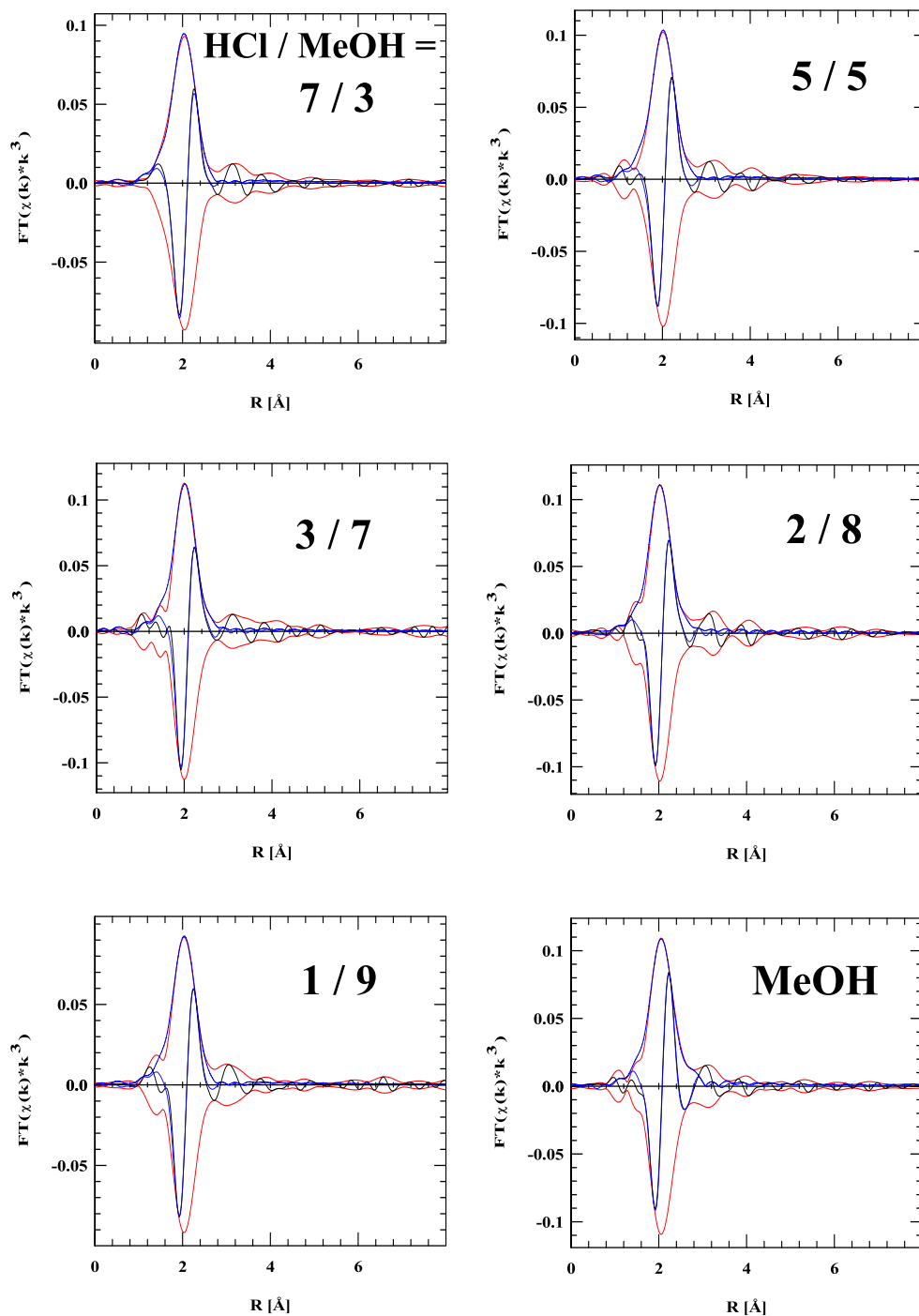
Figure V-1. Fourier transforms (magnitude: red lines, imaginary part: black lines) of the EXAFS of Nd L_{III}-edge in conc. HCl / MeOH mixed solutions. (Solvent: conc. HCl / MeOH (vol/vol), blue line: corresponding curve fitting results)

Table V-4. EXAFS structural parameters of Er L_{III}-edge in conc. HCl / MeOH mixed solutions and in alcohols. (Solvent: conc. HCl / MeOH (vol/vol), S_0^2 = 0.9, Error: $R \pm$ 0.01 Å, $N \pm$ 5%)

| Solvent	Shell	R / Å	N	σ^2 / Å^2	ΔE_0 / eV	FT range	Fitting residual k-space	R-space
water	O (H_2O)	2.35	8.2	0.0060	3.21	1.5-14	22.87	6.16
HCl / MeOH 7 / 3	O (H_2O)	2.35	8.0	0.0056	1.01	1.5-14	34.95	7.62
	Cl	2.72	0.6	0.0064				
5 / 5	O (H_2O)	2.36	8.5	0.0067	2.73	1.5-14.5	35.95	10.22
	Cl	2.75	0.4	0.0059				
3 / 7	O (H_2O)	2.36	8.0	0.0060	3.27	1.5-14.5	31.19	3.70
	Cl	2.74	0.5	0.0032				
2 / 8	O (H_2O)	2.35	8.3	0.0063	2.52	1.5-14.5	25.54	4.70
	Cl	2.73	0.5	0.0050				
1 / 9	O (H_2O)	2.35	8.1	0.0067	3.90	1.5-14.5	24.45	3.66
	O (MeOH)	2.47	0.6	0.0065				
	C (MeOH)	2.97	0.6	0.0044				
MeOH	O (H_2O)	2.33	4.4	0.0030	5.73	1.5-14.5	29.32	9.78
	O (MeOH)	2.45	3.1	0.0009				
	C (MeOH)	2.85	3.1	0.0083				
EtOH	O (H_2O)	2.33	4.4	0.0035	5.58	1.5-13	22.03	9.87
	O (EtOH)	2.44	3.1	0.0011				
	C (EtOH)	2.84	3.1	0.0073				
1-PrOH	O (H_2O)	2.33	4.4	0.0037	5.78	1.5-14	30.6	6.77
	O (PrOH)	2.45	3.1	0.0017				
	C (PrOH)	2.85	3.1	0.0094				
2-PrOH	O (H_2O)	2.33	4.2	0.0038	6.94	1.5-14	39.4	5.17
	O (PrOH)	2.44	3.0	0.0018				
	C (PrOH)	2.87	3.0	0.0072				
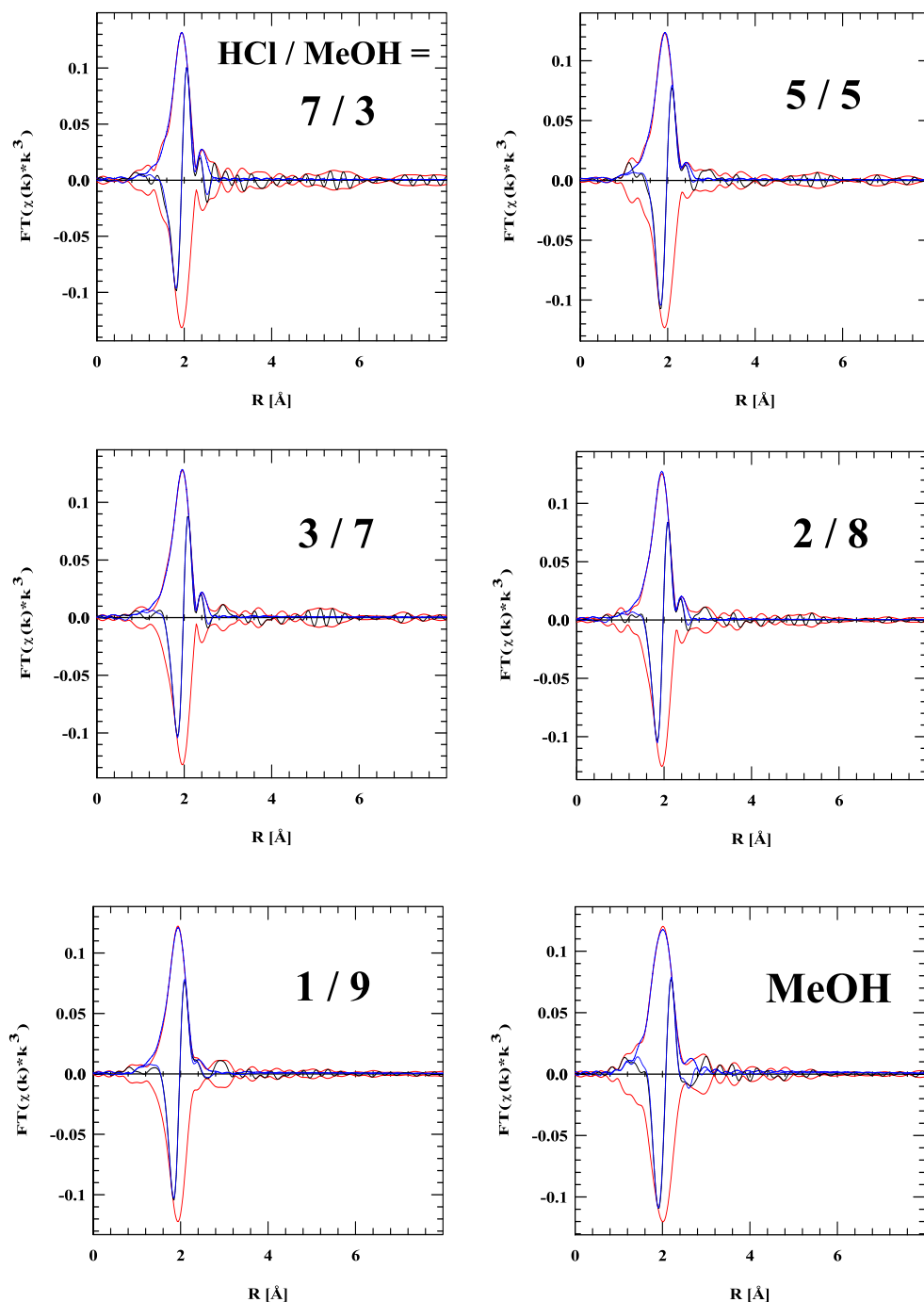
Figure V-2. (1) Fourier transforms (magnitude: red lines, imaginary part: black lines) of the EXAFS of Er L_{III}-edge in conc. HCl / MeOH mixed solutions. (Solvent: conc. HCl / MeOH (vol/vol), blue line: corresponding curve fitting results)
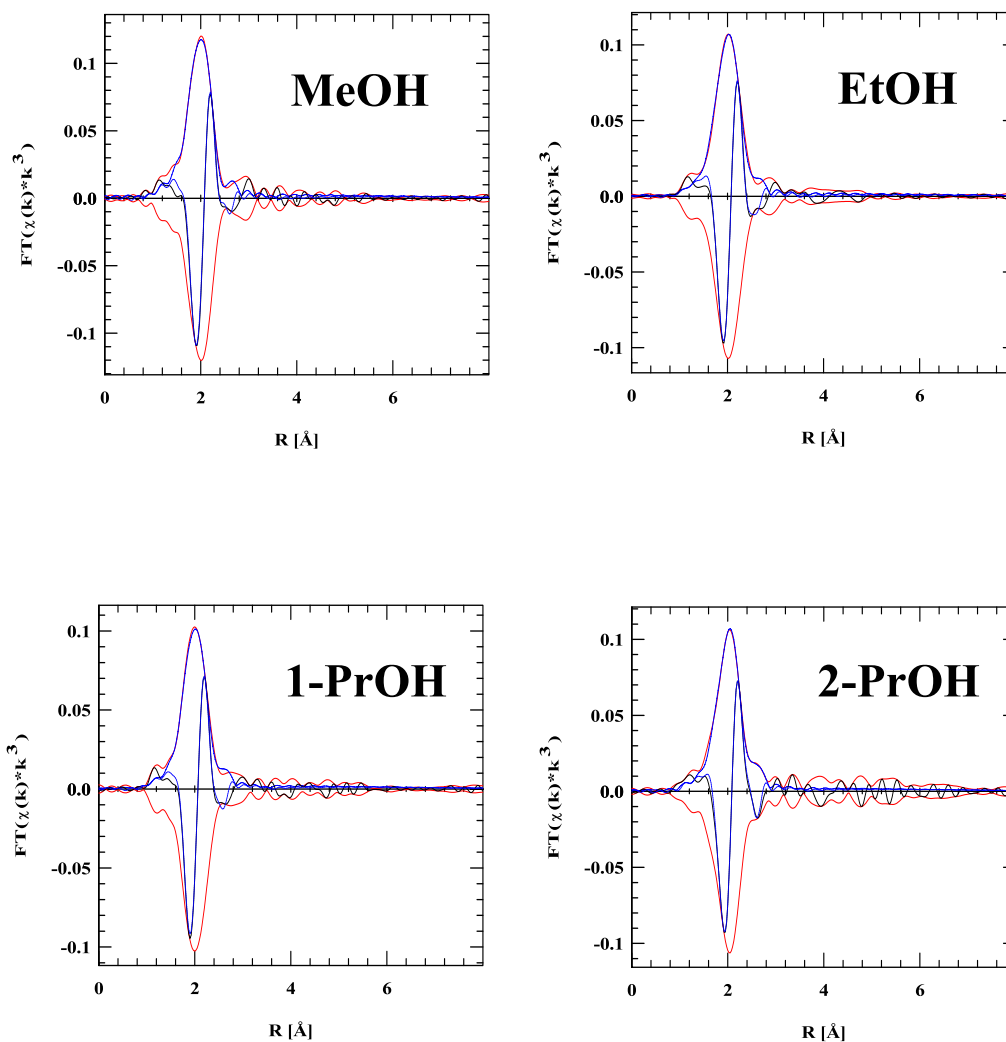
Figure V-2. (2) Fourier transforms (magnitude: red lines, imaginary part: black lines) of the EXAFS of Er L_{III}-edge in different alcohols. (blue line: corresponding curve fitting results)

Table V-5. EXAFS structural parameters of Y and Ln(III) in conc. HNO_3 / MeOH mixed solution. (Solvent: conc. HNO_3 / MeOH = 5 / 5 (vol/vol), S_0^2 = 0.9, Error: $R \pm$ 0.01 Å, $N \pm 5\%$)

Element	Edge	Shell	R / Å	N	σ^2 / Å^2	ΔE_0 / eV	FT range	Residual (R-space)
La	K	O (H_2O)	2.55	5.0	0.0059	5.68	2-12.5	10.48
		O (NO_3)	2.66	4.0	0.0040			
		N (NO_3)	3.45	2.0	0.0066			
Ce	L_{III}	O (H_2O)	2.52	4.6	0.0041	7.22	1.5-10.5	13.53
		O (NO_3)	2.60	4.4	0.0080			
		N (NO_3)	3.10	2.2	0.0003			
Pr	L_{III}	O (H_2O)	2.51	4.9	0.0055	9.30	1.5-11	16.74
		O (NO_3)	2.59	4.1	0.0071			
		N (NO_3)	3.11	2.1	0.0013			
Nd	K	O (H_2O)	2.49	5.0	0.0063	2.49	2-15.5	13.86
		O (NO_3)	2.57	4.0	0.0081			
		N (NO_3)	3.03	2.0	0.0061			
Sm	L_{III}	O (H_2O)	2.44	5.0	0.0052	8.24	1.5-12	12.51
		O (NO_3)	2.52	4.0	0.0069			
		N (NO_3)	2.99	2.0	0.0022			
Eu	L_{III}	O (H_2O)	2.41	5.3	0.0058	8.68	1.5-12.5	14.93
		O (NO_3)	2.50	3.9	0.0067			
		N (NO_3)	2.95	2.0	0.0012			
Gd	L_{III}	O (H_2O)	2.39	5.0	0.0061	8.85	1.5-13	9.90
		O (NO_3)	2.48	4.1	0.0049			
		N (NO_3)	2.98	2.0	0.0057			
Tb	L_{III}	O (H_2O)	2.38	5.0	0.0066	8.60	1.5-13	12.60
		O (NO_3)	2.47	4.2	0.0072			
		N (NO_3)	2.96	2.1	0.0073			
Dy	L_{III}	O (H_2O)	2.36	5.1	0.0044	7.96	1.5-14	14.76
		O (NO_3)	2.48	4.1	0.0049			
		N (NO_3)	2.93	2.1	0.0062			
Ho	L_{III}	O (H_2O)	2.34	4.1	0.0051	6.51	1.5-13.5	9.90
		O (NO_3)	2.42	4.1	0.0050			
		N (NO_3)	2.90	2.1	0.0058			

Element	Edge	Shell	R / Å	N	σ^2 / Å^2	ΔE_0 / eV	FT range	Residual (R-space)
Er	L_{III}	O (H_2O)	2.34	4.3	0.0045	6.95	1.5-14	10.92
		O (NO_3)	2.43	4.1	0.0059			
		N (NO_3)	2.91	2.1	0.0024			
Tm	L_{III}	O (H_2O)	2.33	4.1	0.0046	7.99	1.5-12	14.57
		O (NO_3)	2.41	3.9	0.0068			
		N (NO_3)	2.91	1.9	0.0058			
Yb	L_{III}	O (H_2O)	2.31	4.1	0.0048	9.45	1.5-12.5	16.52
		O (NO_3)	2.38	3.9	0.0077			
		N (NO_3)	2.90	2.0	0.0058			
Lu	L_{III}	O (H_2O)	2.29	3.9	0.0028	9.44	1.5-11.5	14.96
		O (NO_3)	2.38	4.1	0.0066			
		N (NO_3)	2.85	2.1	0.0065			
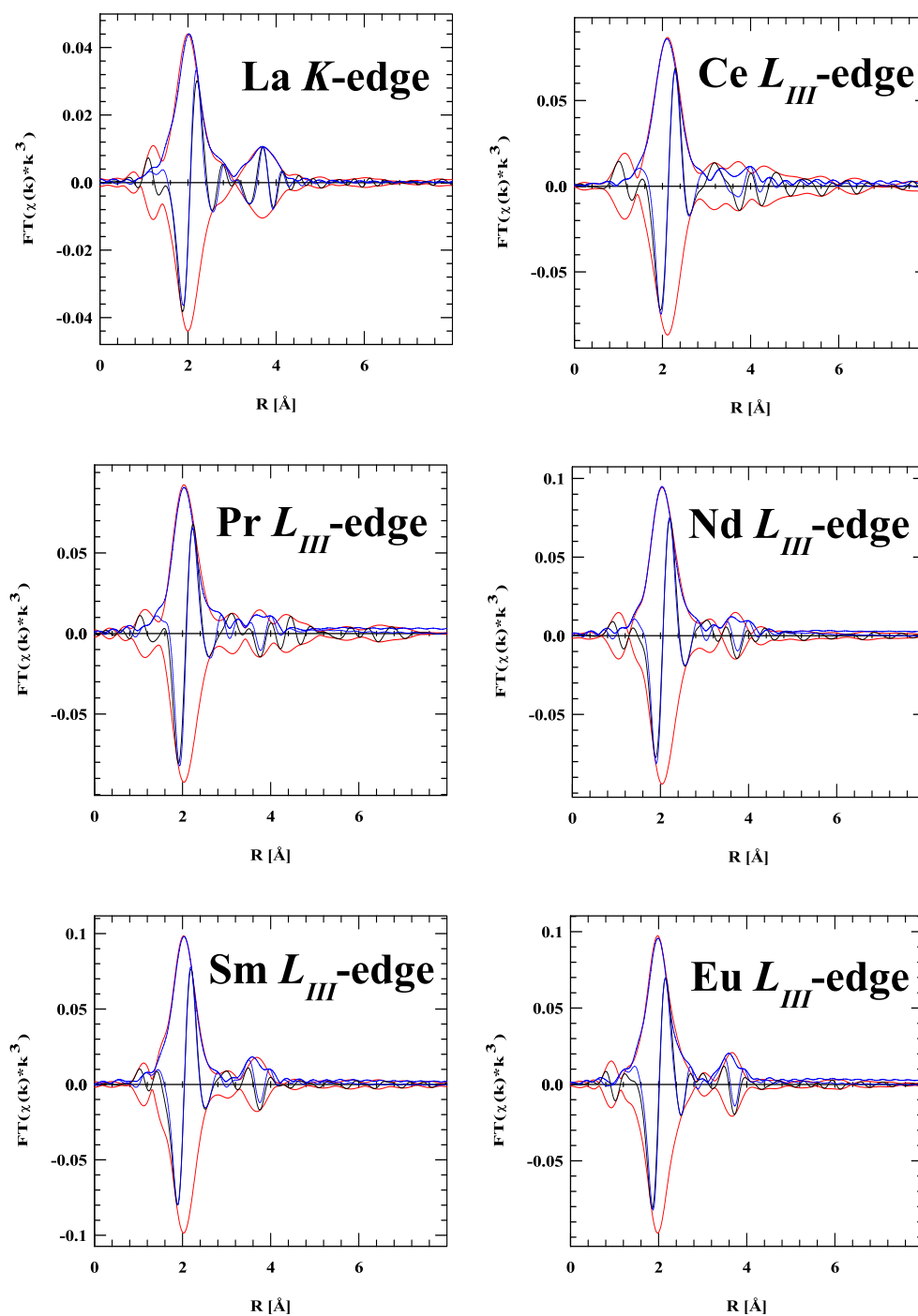
Figure V-3. (1) Fourier transforms (magnitude: red lines, imaginary part: black lines) of the EXAFS of La-Eu in conc. HNO_3 / MeOH mixed solution. (Solvent: conc. HNO_3 / MeOH = 5 / 5 (vol/vol), blue line: corresponding curve fitting results)
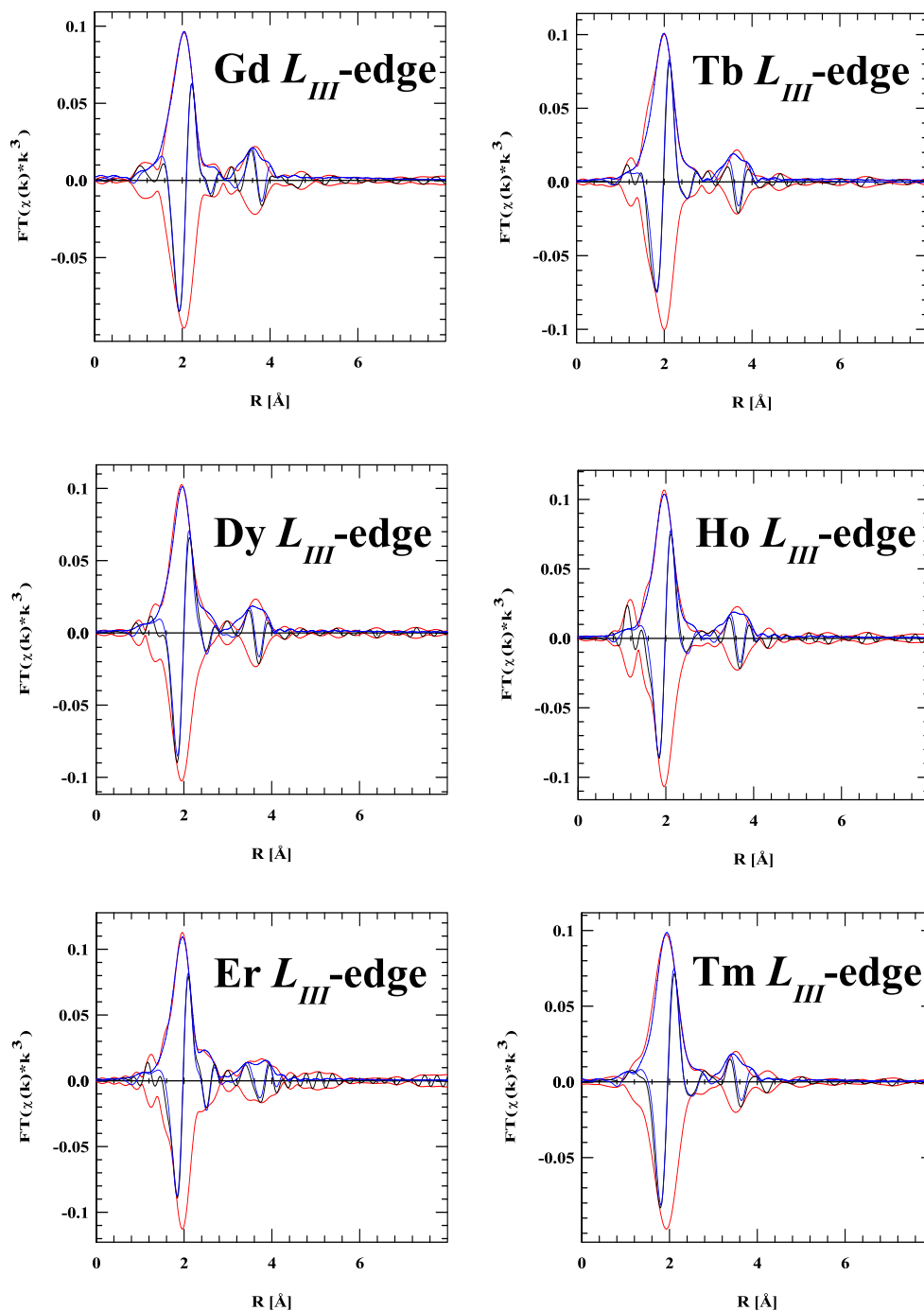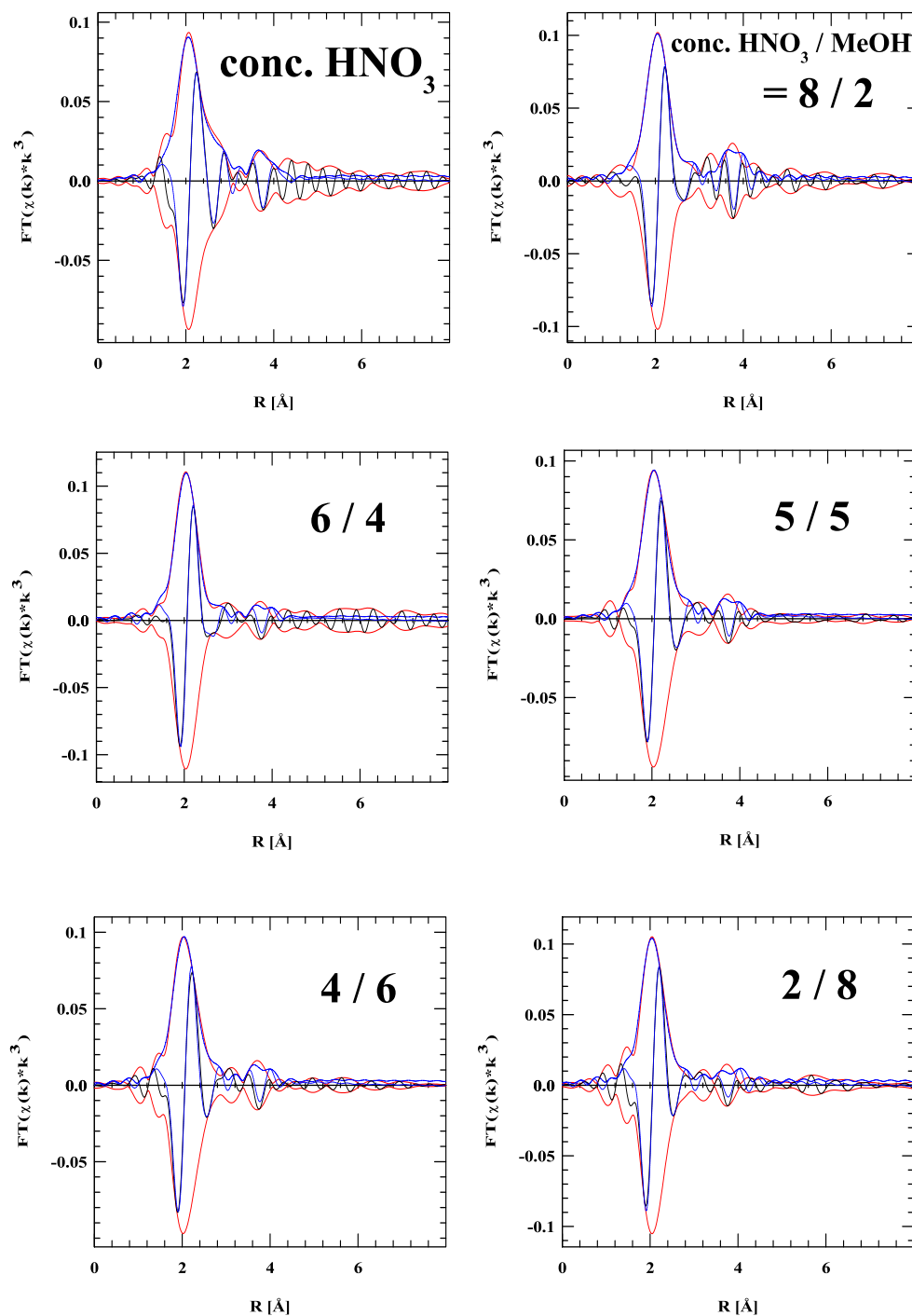
Figure V-3. (2) Fourier transforms (magnitude: red lines, imaginary part: black lines) of the EXAFS of Gd-Tm in conc. HNO_3 / MeOH mixed solution. (Solvent: conc. HNO_3 / MeOH = 5 / 5 (vol/vol), blue line: corresponding curve fitting results)
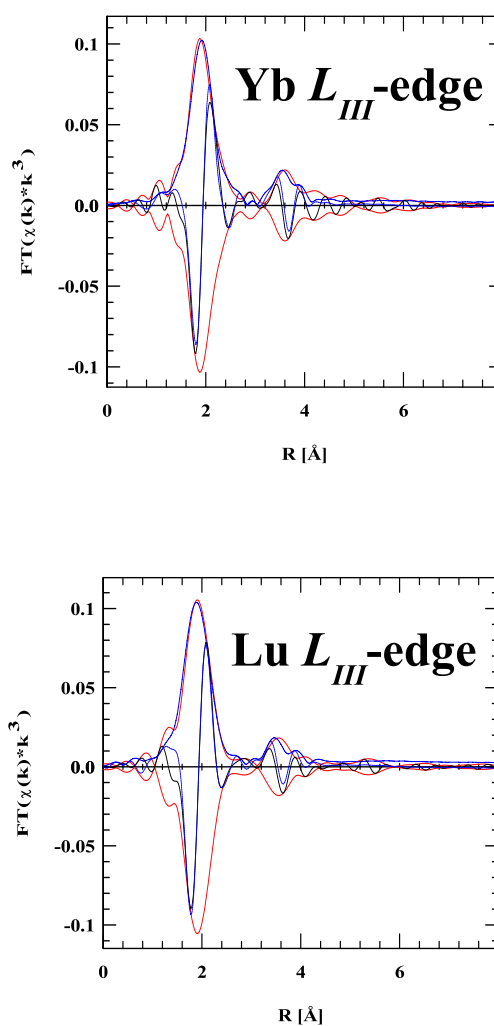
Figure V-3. (3) Fourier transforms (magnitude: red lines, imaginary part: black lines) of the EXAFS of Yb and Lu in conc. HNO_3 / MeOH mixed solution. (Solvent: conc. HNO_3 / MeOH = 5 / 5 (vol/vol), blue line: corresponding curve fitting results)

Table V-6. EXAFS structural parameters of Nd L_{III}-edge in conc. HNO_3 / MeOH mixed solutions. (Solvent: conc. HNO_3 / MeOH (vol/vol), $S_0^2 = 0.9$, Error: $R \pm 0.01$ Å, $N \pm 5\%$)

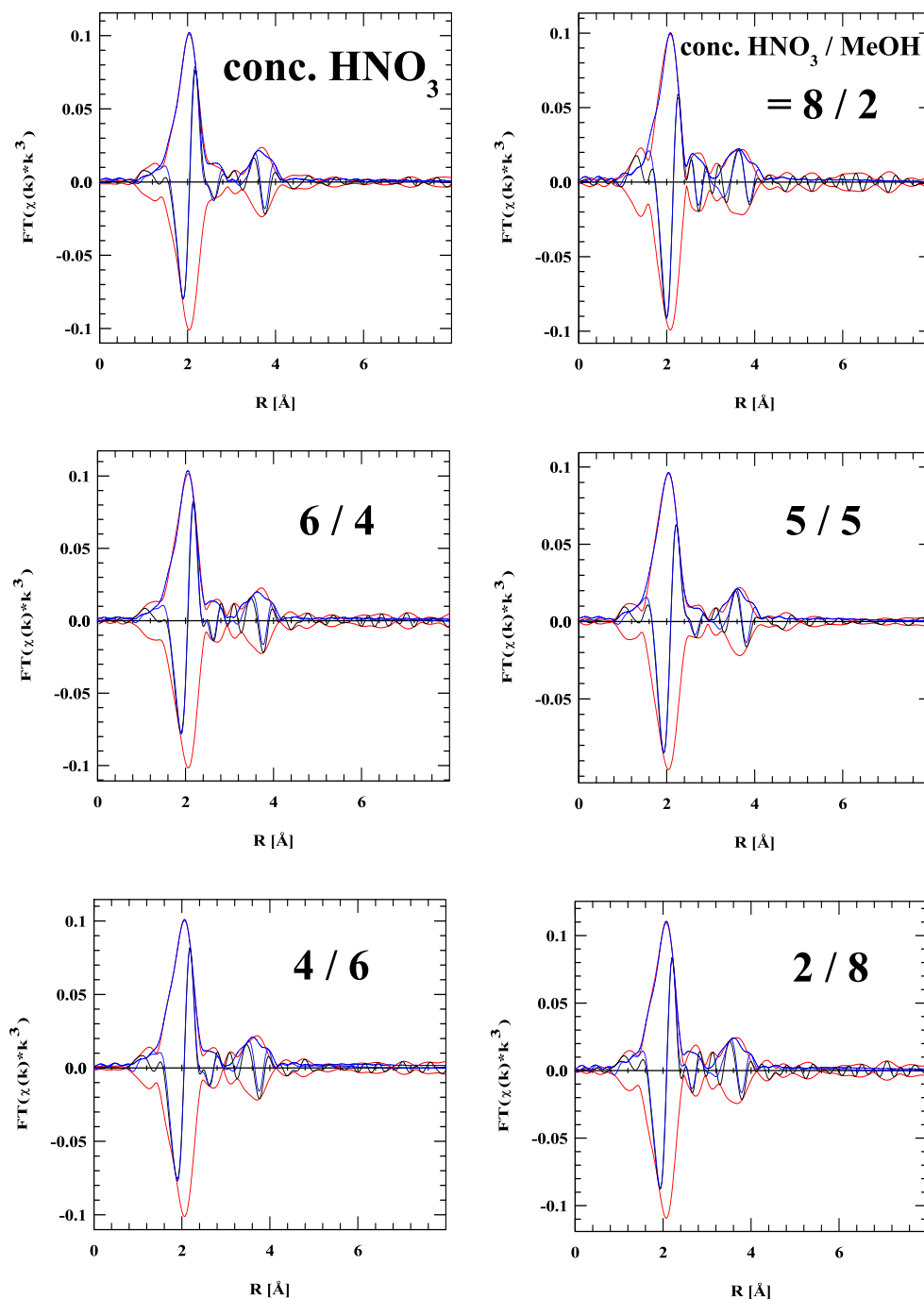| Solvent	Shell	R / Å	N	σ^2 / Å^2	ΔE_0 / eV	FT range	Residual (R-space)
	O (H$_2$O)	2.49	4.6	0.0038			
conc. HNO$_3$	O (NO$_3$)	2.58	4.4	0.0034	8.80	1.5-11.5	11.98
	N (NO$_3$)	3.07	2.2	0.0065			
conc. HNO$_3$	O (H$_2$O)	2.48	4.8	0.0039			
/ MeOH	O (NO$_3$)	2.58	4.2	0.0058	8.45	1.5-11.5	12.08
8 / 2	N (NO3)	3.07	2.1	0.0077			
	O (H$_2$O)	2.49	5.0	0.0053			
6 / 4	O (NO$_3$)	2.57	4.0	0.0080	8.28	1.5-11.5	13.18
	N (NO$_3$)	3.09	2.0	0.0041			
	O (H$_2$O)	2.49	5.0	0.0063			
5 / 5	O (NO$_3$)	2.57	4.0	0.0081	2.49	1.5-11.5	13.12
	N (NO$_3$)	3.03	2.0	0.0061			
	O (H$_2$O)	2.49	4.9	0.0048			
4 / 6	O (NO$_3$)	2.57	4.1	0.0052	9.30	1.5-11.5	14.35
	N (NO$_3$)	3.06	2.0	0.0064			
	O (H$_2$O)	2.49	4.7	0.0001			
2 / 8	O (NO$_3$)	2.57	4.3	0.0036	8.27	1.5-11.5	15.23
	N (NO$_3$)	3.04	2.2	0.0064			

Figure V-4. Fourier transforms (magnitude: red lines, imaginary part: black lines) of the EXAFS of Nd L_{III}-edge in conc. HNO_3 / MeOH mixed solutions. (Solvent: conc. HNO_3 / MeOH (vol/vol), blue line: corresponding curve fitting results)

Table V-7. EXAFS structural parameters of Gd L_{III}-edge in conc. HNO_3 / MeOH mixed solutions. (Solvent: conc. HNO_3 / MeOH (vol/vol), $S_0^2 = 0.9$, Error: $R \pm 0.01$ Å, $N \pm 5\%$)

Solvent	Shell	R / Å	N	σ^2 / Å^2	ΔE_0 / eV	FT range	Residual (R-space)
conc. HNO_3	O (H_2O)	2.40	4.8	0.0072			
	O (NO_3)	2.49	4.0	0.0028	6.00	1.5-13	10.81
	N (NO_3)	2.99	2.0	0.0034			
conc. HNO_3	O (H_2O)	2.40	4.4	0.0080			
/ MeOH	O (NO_3)	2.50	4.0	0.0036	6.65	1.5-13	12.87
8 / 2	N (NO_3)	3.01	2.0	0.0050			
	O (H_2O)	2.40	4.7	0.0068			
6 / 4	O (NO_3)	2.49	4.0	0.0022	6.84	1.5-13	12.21
	N (NO_3)	3.02	2.0	0.0032			
	O (H_2O)	2.39	5.0	0.0061			
5 / 5	O (NO_3)	2.48	4.1	0.0049	8.85	1.5-13	9.90
	N (NO_3)	2.98	2.0	0.0057			
	O (H_2O)	2.40	4.6	0.0069			
4 / 6	O (NO_3)	2.49	4.0	0.0024	6.99	1.5-13	10.84
	N (NO_3)	3.01	2.0	0.0039			
	O (H_2O)	2.40	4.7	0.0066			
2 / 8	O (NO_3)	2.49	4.0	0.0020	7.11	1.5-13	11.87
	N (NO_3)	3.01	2.0	0.0037			

Figure V-5. Fourier transforms (magnitude: red lines, imaginary part: black lines) of the EXAFS of Gd L_{III}-edge in conc. HNO_3 / MeOH mixed solutions. (Solvent: conc. HNO_3 / MeOH (vol/vol), blue line: corresponding curve fitting results)
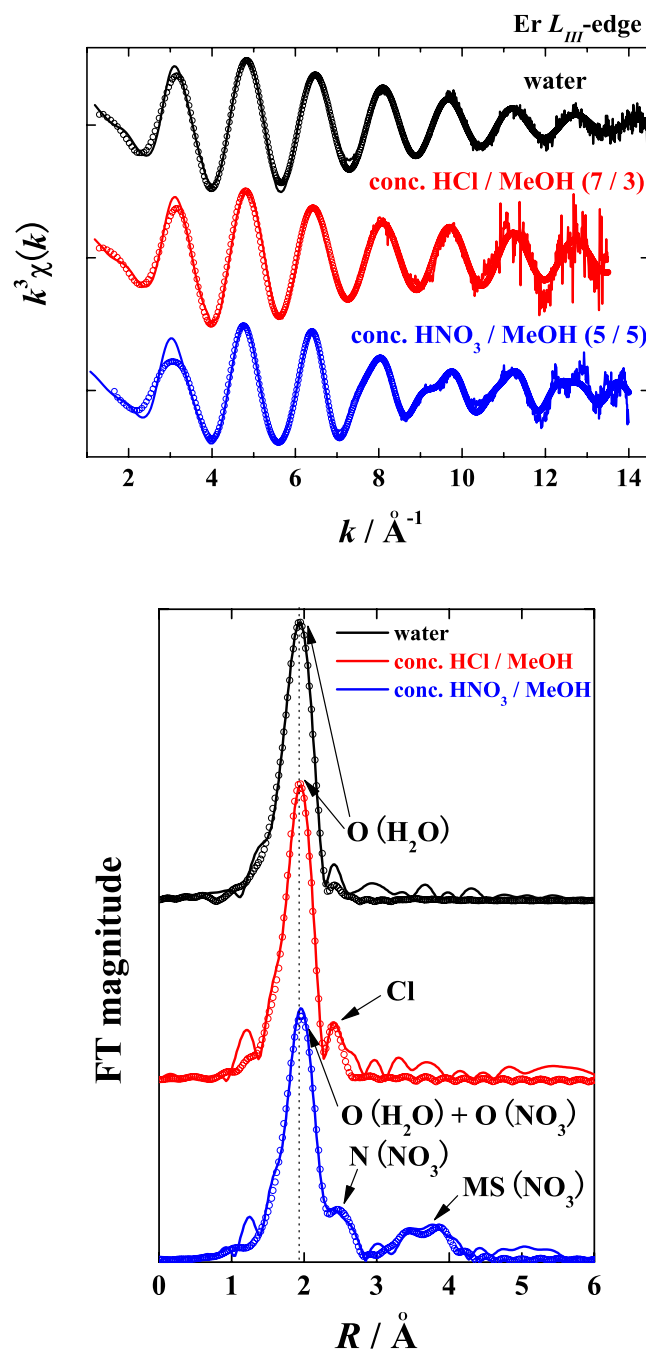
Figure V-6. k^3-weighted EXAFS spectra of Er L_{III}-edge in different solvents (upper) and their corresponding Fourier transforms (lower). (solid line: experimental data, ○: curve fitting results)
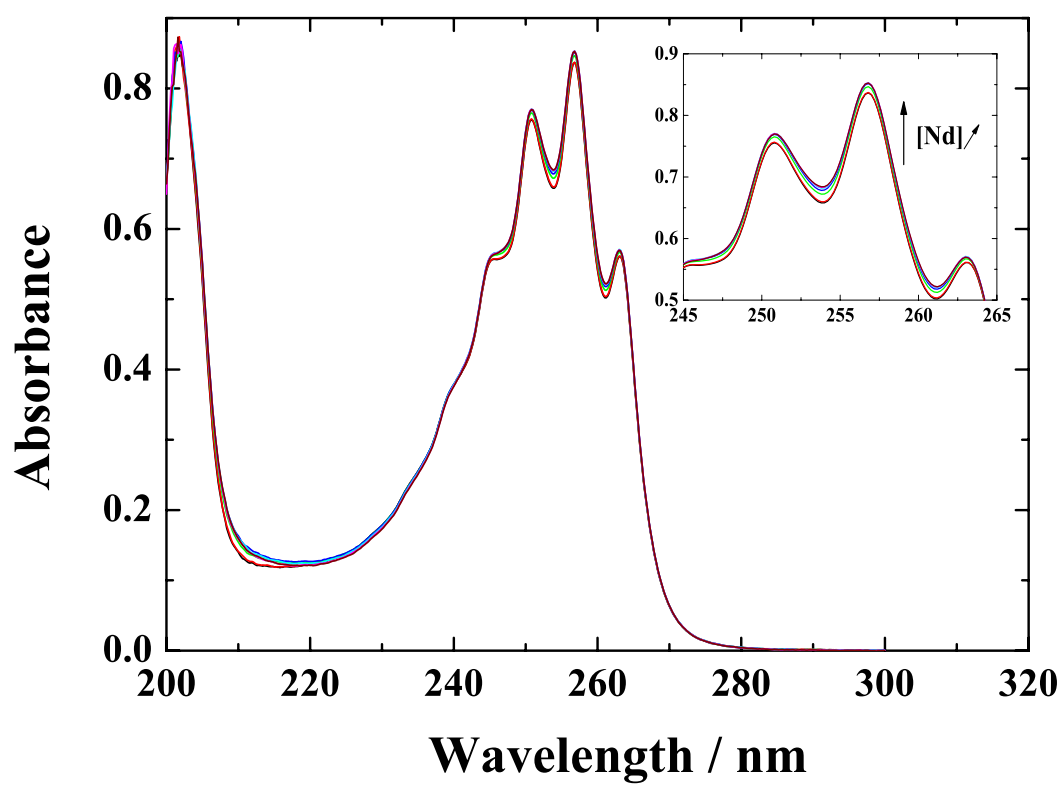
Figure V-7. Spectrophotometric titration data of Nd-pyridine complex in methanol at 293 K.
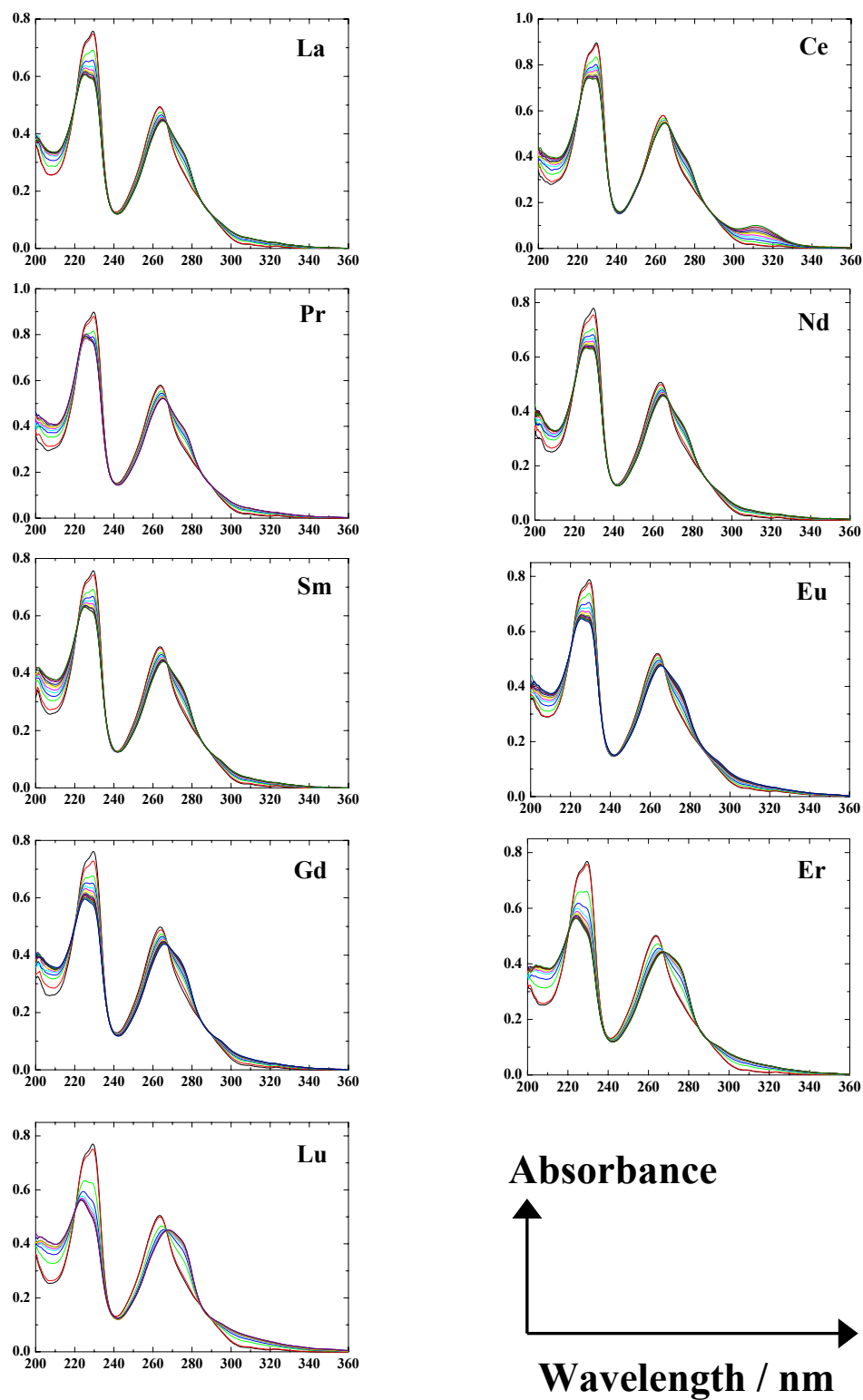
Figure V-8. Spectrophotometric titration data of Ln(III)-1,10-phenanthroline complexes in methanol at 293 K.

Table V-8. Stability constants of Ln(III)-1,10-phenanthroline complexes in methanol at 293 K.

Element	$log\beta_1$	Error ($\pm$)	$log\beta_2$	Error ($\pm$)
La	5.57	0.10	10.31	0.31
Ce	5.94	0.26	11.92	0.48
Pr	6.15	0.28	12.03	0.50
Nd	5.62	0.32	10.82	0.59
Sm	6.02	0.18	12.05	0.35
Eu	4.80	0.13	8.60	0.82
Gd	4.21	0.22	7.70	0.76
Er	5.73	0.10	10.56	0.27
Lu	5.78	0.13	9.94	0.55

$$Ln + L \rightleftharpoons LnL, \quad K_1 = \frac{[LnL]}{[Ln][L]} \tag{1}$$

$$LnL + L \rightleftharpoons LnL_2, \quad K_2 = \frac{[LnL_2]}{[LnL][L]} \tag{2}$$
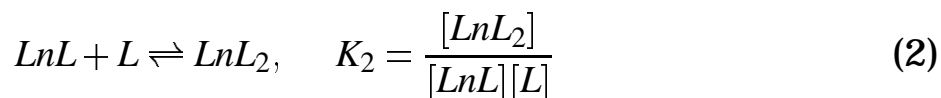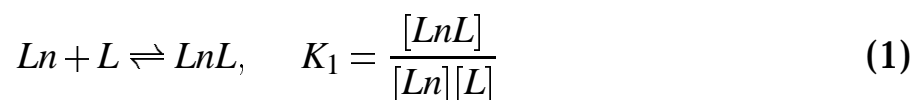
$$\beta_1 = K_1, \quad \beta_2 = K_1 K_2 \tag{3}$$

Table V-9. EXAFS structural parameters of La K-edge for various samples. ($S_0^2 = 0.9$, Error: $R \pm 0.01$ Å, $N \pm 5\%$)

Sample	Shell	R / Å	N	σ^2 / Å^2	ΔE_0 / eV	FT range	Fitting residual (R-range)
water	O (H$_2$O)	2.55	9.5	0.0077	0.46	2-15	6.84
conc. HCl / MeOH	O (H$_2$O)	2.55	7.9	0.0079	0.42	2-13.7	8.55
(5 / 5 (vol/vol))	Cl	2.88	1.6	0.0085			
	O or N	2.53	8.2	0.0067			
Pyridine resin	Cl	2.84	1.7	0.0045	2.21	2-13	14.73
(conc. HCl / MeOH)	C (Py)	3.50	2.2	0.0030			
LiCl in MeOH	O	2.55	4.9	0.0080	0.79	2-15	2.85
[LiCl] = 5 mol/dm^3	Cl	2.83	3.9	0.0085			
Pyridine resin	O	2.53	2.8	0.0083	2.18	2-12.5	8.52
(LiCl in MeOH)	Cl	2.83	4.5	0.0081			
Dowex 1X8	O	2.55	1.3	0.0064	2.38	2-15	4.96
(LiCl in MeOH)	Cl	2.82	7.0	0.0096			
LaCl$_3$ (Hydrate)	O (H$_2$O)	2.54	8.0	0.0075	-1.10	2-15	4.86
	Cl	2.91	2.2	0.0100			

Table V-10. EXAFS structural parameters of Ce K-edge for various samples. ($S_0^2 = 0.9$, Error: $R \pm 0.01$ Å, $N \pm 5\%$)

Sample	Shell	R / Å	N	σ^2 / Å^2	ΔE_0 / eV	FT range	Fitting residual (R-range)
water	O (H$_2$O)	2.52	9.2	0.0073	-2.94	2-15.5	5.77
conc. HCl / MeOH	O (H$_2$O)	2.51	7.6	0.0070	-3.05	2-15.5	10.58
(5 / 5 (vol/vol))	Cl	2.78	1.4	0.0050			
	O or N	2.51	7.6	0.0073			
Pyridine resin	Cl	2.82	1.9	0.0080	1.37	2-13	9.93
(conc. HCl / MeOH)	C (Py)	3.40	2.7	0.0044			
LiCl in MeOH	O	2.53	4.6	0.0090	-1.60	2-14.5	6.24
[LiCl] = 5 mol/dm^3	Cl	2.78	4.1	0.0078			
Pyridine resin	O	2.50	0.6	0.0044	-0.71	2-15.5	3.12
(LiCl in MeOH)	Cl	2.77	6.3	0.0078			
Dowex 1X8	O	2.52	0.1	0.0001	1.90	2-15.5	2.14
(LiCl in MeOH)	Cl	2.77	6.8	0.0085			
CeCl$_3$ (Hydrate)	O (H$_2$O)	2.52	8.0	0.0074	-3.76	2-15.5	4.99
	Cl	2.89	2.2	0.0100			

Table V-11. EXAFS structural parameters of Nd K-edge for various samples. ($S_0^2 =$ 0.9, Error: $R \pm 0.01$ Å, $N \pm 5\%$)

Sample	Shell	R / Å	N	σ^2 / Å^2	ΔE_0 / eV	FT range	Fitting residual (R-range)
water	O (H$_2$O)	2.48	9.3	0.0079	-3.96	2-15.5	11.06
conc. HCl / MeOH	O (H$_2$O)	2.48	8.0	0.0070	-0.35	2-15	6.05
(5 / 5 (vol/vol))	Cl	2.78	1.0	0.0061			
Pyridine resin	O (H$_2$O)	2.48	8.0	0.0071	-3.58	2-15.5	8.85
(conc. HCl / MeOH)	Cl	2.77	1.0	0.0059			
Aqueous LiCl / MeOH	O (H$_2$O)	2.49	8.0	0.0072	-0.53	2-16	7.41
(5 / 5 (vol/vol))	Cl	2.77	1.0	0.0065			
Pyridine resin	O (H$_2$O)	2.48	7.8	0.0080	-3.80	2-16	10.70
(Aqueous LiCl / MeOH)	Cl	2.78	1.2	0.0064			
LiCl in MeOH	O	2.52	5.5	0.0100	-0.54	2-15.5	7.38
[LiCl] = 5 mol/dm^3	Cl	2.75	4.5	0.0090			
Pyridine resin	O	2.49	1.1	0.0086	0.11	2-15.5	6.52
(LiCl in MeOH)	Cl	2.74	6.1	0.0080			
Dowex 1X8	O	2.47	0.6	0.0100	0.99	2-15.5	5.42
(LiCl in MeOH)	Cl	2.73	7.2	0.0070			
NdCl$_3$ (Hydrate)	O (H$_2$O)	2.45	8.0	0.0069	-4.33	2-15.5	6.04
	Cl	2.79	2.0	0.0071			
conc. HNO$_3$ / MeOH	O (H$_2$O)	2.49	5.0	0.0069	2.48	2-15	13.33
	O (O$_2$NO)	2.57	4.0	0.0089			
(5 / 5 (vol/vol))	N (NO$_3$)	3.02	2.0	0.0064			
	MS (NO$_3$)	4.19	2.0	0.0054			
	O (H$_2$O)	2.48	1.0	0.0029	3.92	2-15	12.41
Pyridine resin	O (O$_2$NO)	2.57	8.0	0.0083			
(conc. HNO$_3$ / MeOH)	N (NO$_3$)	3.02	4.0	0.0043			
	MS (NO$_3$)	4.20	4.0	0.0046			

Table V-12. EXAFS structural parameters of Sm L_{III}-edge for various samples. ($S_0^2 = 0.9$, Error: $R \pm 0.01$ Å, $N \pm 5\%$)

Sample	Shell	R / Å	N	σ^2 / Å^2	ΔE_0 / eV	FT range	Fitting residual (R-range)
water	O (H$_2$O)	2.46	9.4	0.0083	4.38	1.5-11.5	4.01
conc. HNO$_3$ / MeOH (5 / 5 (vol/vol))	O (H$_2$O)	2.44	5.0	0.0052	8.24	1.5-12	12.51
	O (O$_2$NO)	2.52	4.0	0.0069			
	N (NO$_3$)	2.99	2.0	0.0022			
	MS (NO$_3$)	4.11	2.1	0.0009			
Pyridine resin (conc. HNO$_3$ / MeOH)	O (H$_2$O)	2.44	4.8	0.0078	6.45	1.5-12	14.46
	O (O$_2$NO)	2.53	4.2	0.0051			
	N (NO$_3$)	2.98	2.1	0.0001			
	MS (NO$_3$)	4.12	2.1	0.0016			

Table V-13. EXAFS structural parameters of Er L_{III}-edge in various samples. ($S_0^2 = 0.9$, Error: $R \pm 0.01$ Å, $N \pm 5\%$)

Sample	Shell	R / Å	N	σ^2 / Å^2	ΔE_0 / eV	FT range	Fitting residual (R-range)
water	O (H$_2$O)	2.35	8.2	0.0060	3.21	1.5-14	6.16
conc. HNO$_3$ / MeOH (5 / 5 (vol/vol))	O (H$_2$O)	2.34	4.3	0.0045	6.95	1.5-14	10.92
	O (O$_2$NO)	2.43	4.1	0.0059			
	N (NO$_3$)	2.91	2.1	0.0024			
	MS (NO$_3$)	4.09	2.0	0.0001			
Pyridine resin (conc. HNO$_3$ / MeOH)	O (H$_2$O)	2.34	4.0	0.0043	7.53	1.5-14	14.97
	O (O$_2$NO)	2.43	4.0	0.0072			
	N (NO$_3$)	2.91	2.0	0.0032			
	MS (NO$_3$)	4.10	2.0	0.0080			
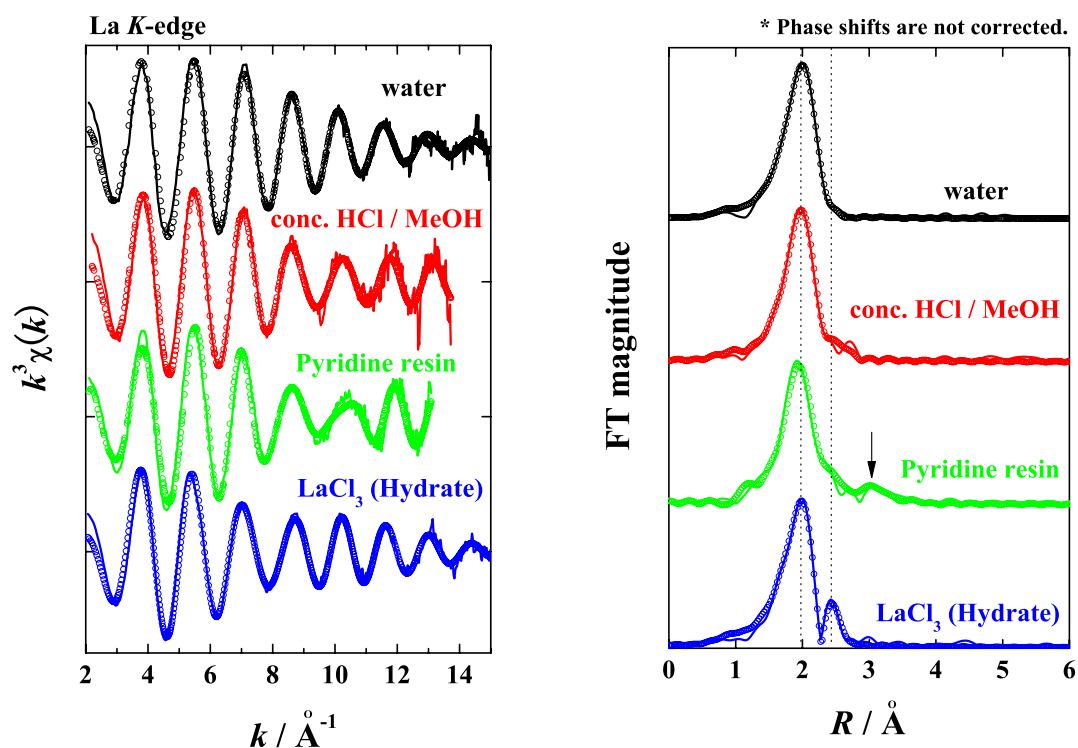
Figure V-9. k^3-weighted EXAFS spectra of La K-edge of different chloride samples (left) and their corresponding Fourier transforms (right). (solid line: experimental data, ○: curve fitting results)
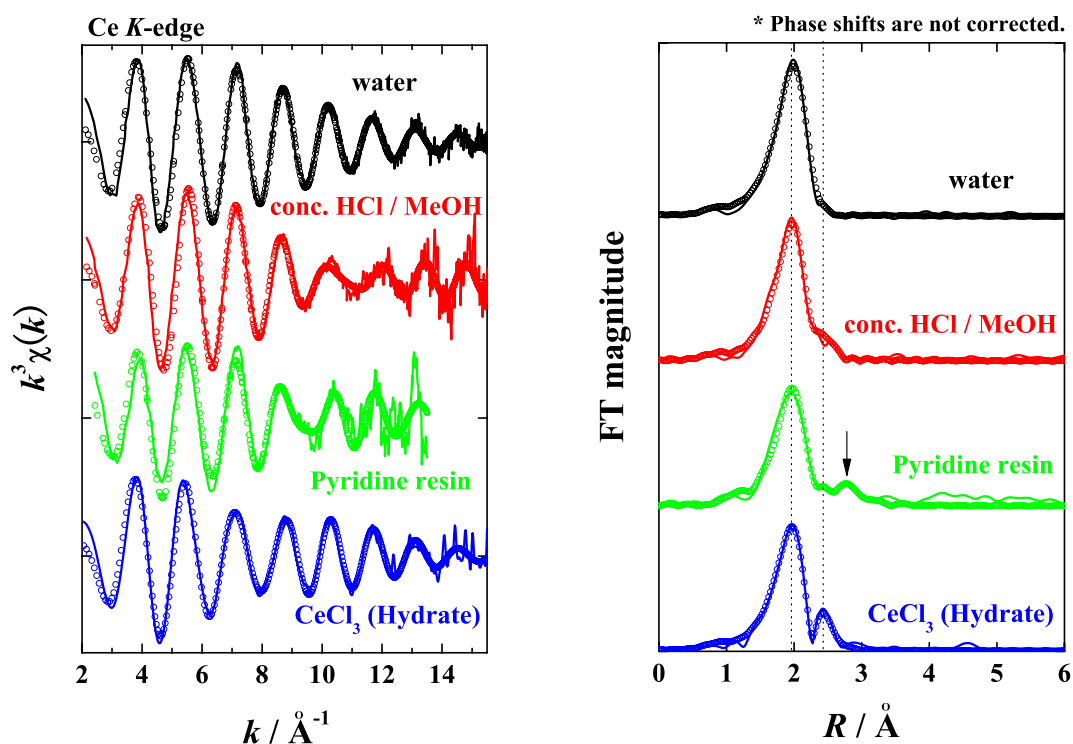
Figure V-10. k^3-weighted EXAFS spectra of Ce K-edge of different chloride samples (left) and their corresponding Fourier transforms (right). (solid line: experimental data, ○: curve fitting results)
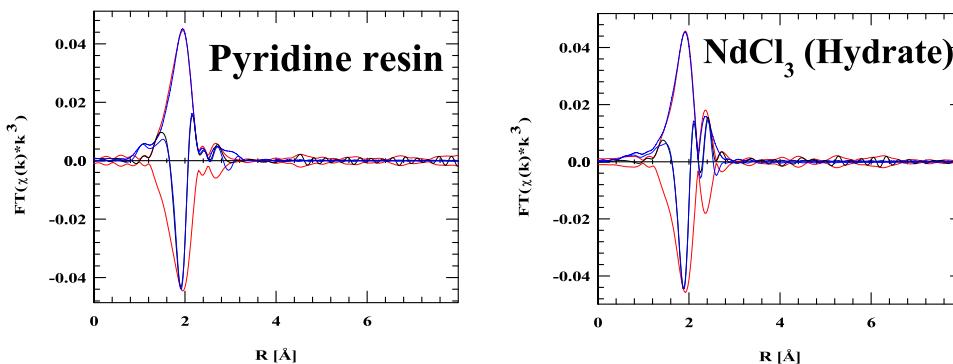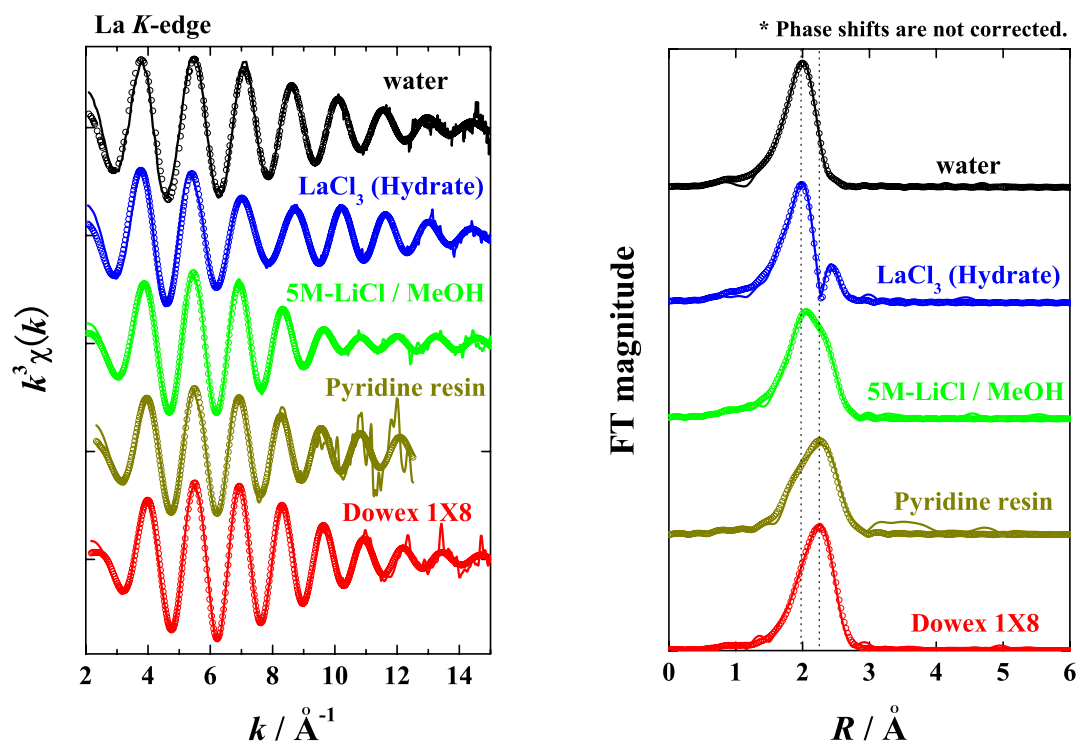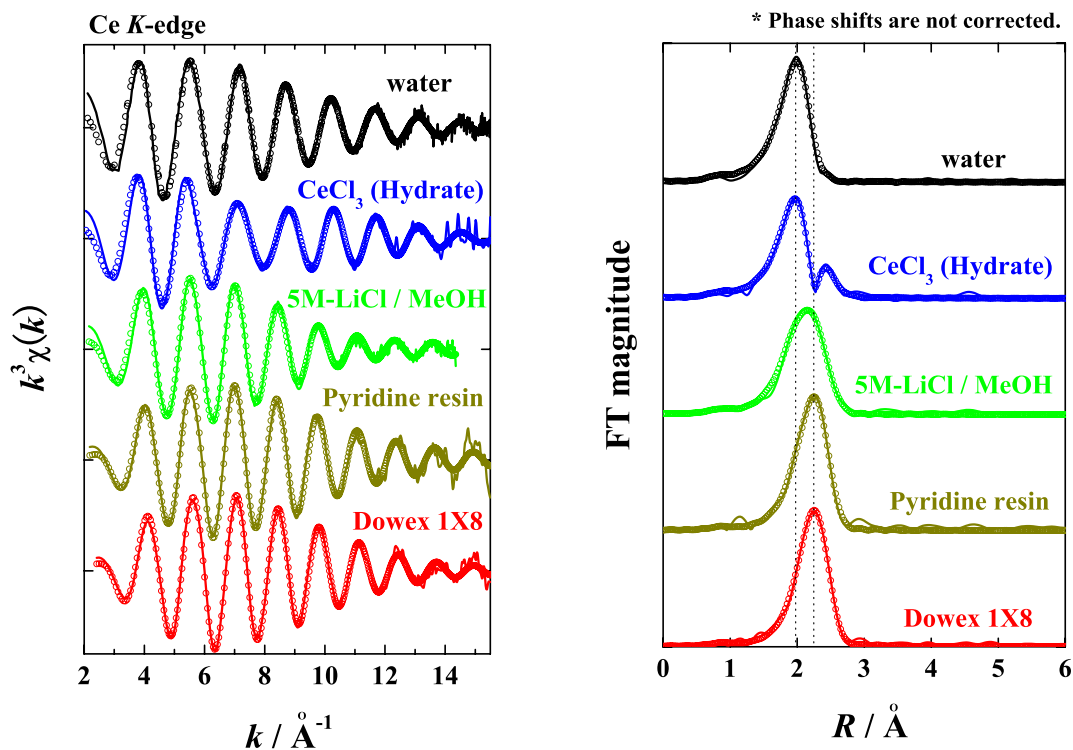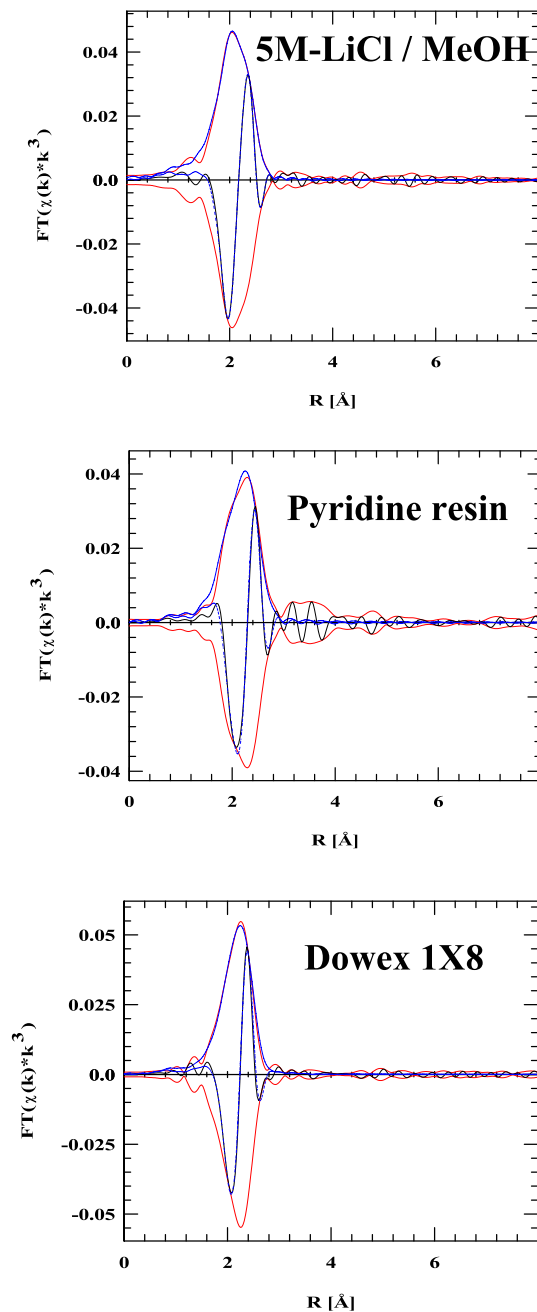
La *K*-edge
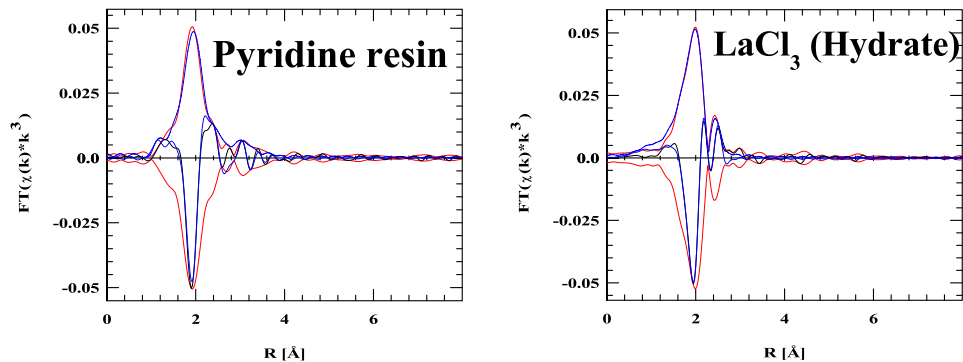
Ce *K*-edge
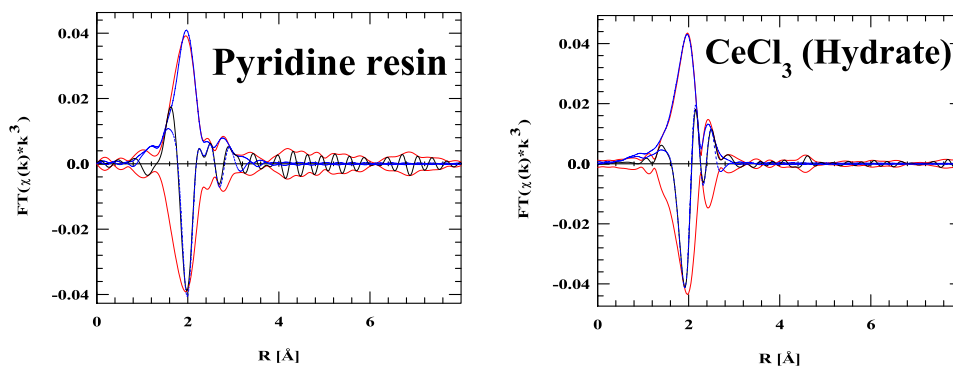
Nd *K*-edge

Figure V-11. Fourier transforms (magnitude: red lines, imaginary part: black lines) of the EXAFS of La, Ce, and Nd *K*-edges of pyridine resin samples (left) and $LnCl_3 \cdot nH_2O$ (right). (blue line: corresponding curve fitting results)
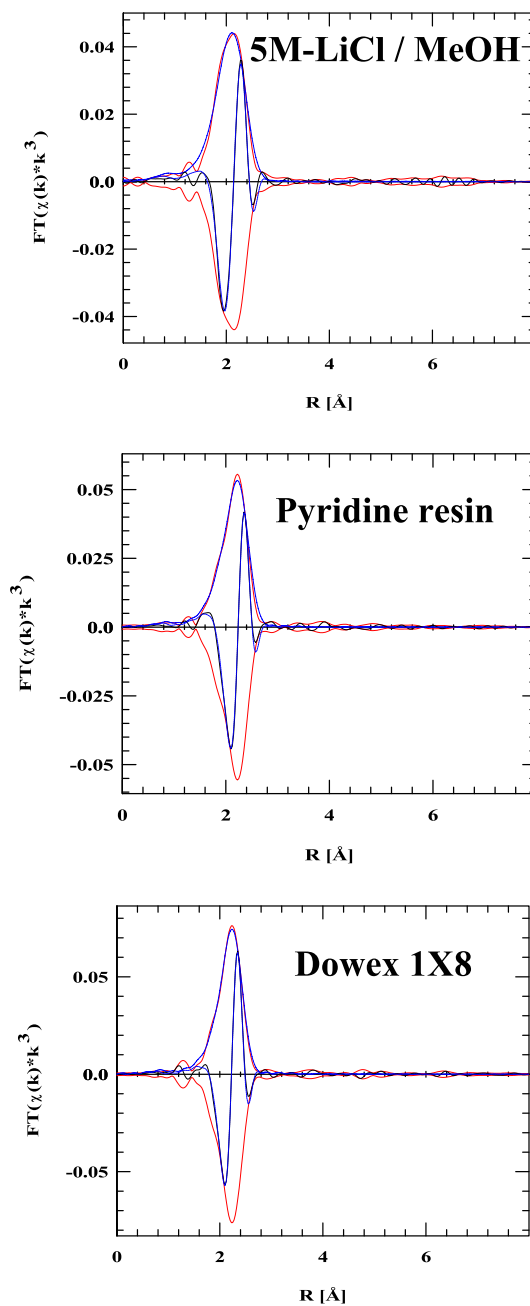
in solution phase

in resin phase
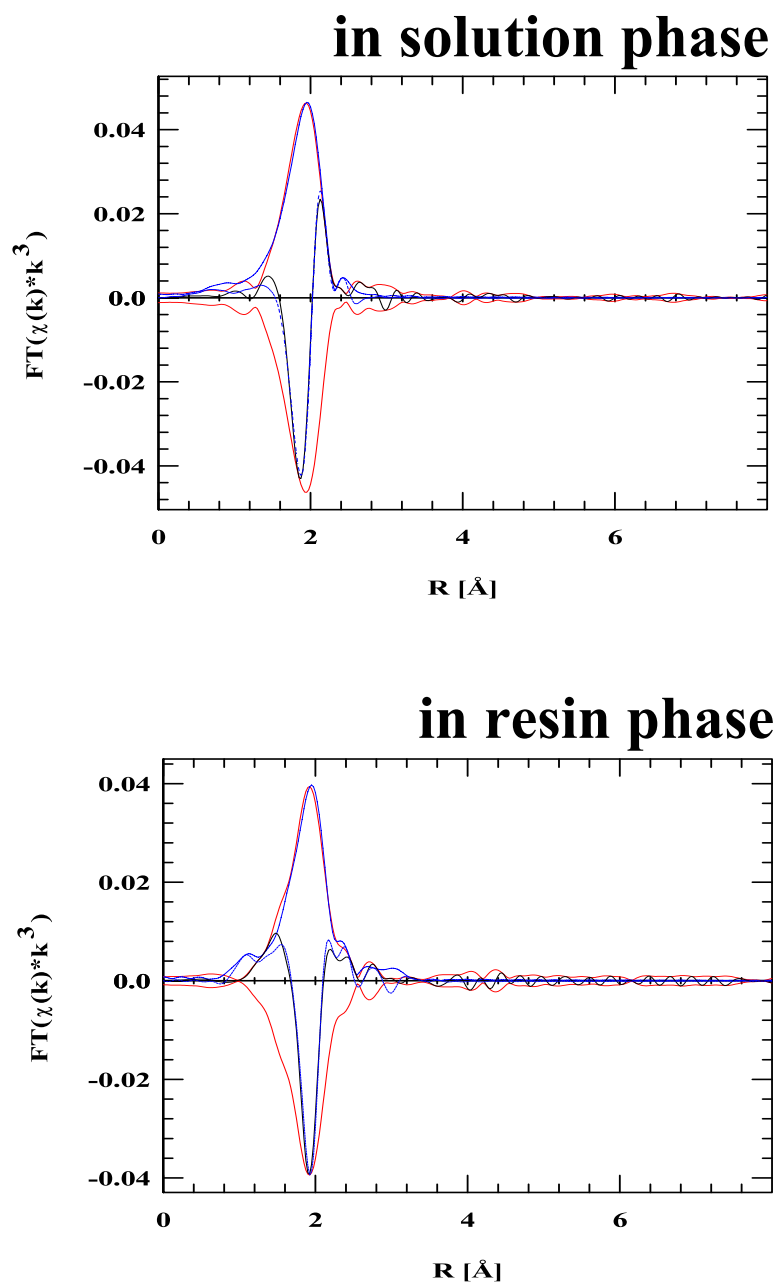
Figure V-12. Fourier transforms (magnitude: red lines, imaginary part: black lines) of the EXAFS of Nd K-edges of aqueous LiCl / MeOH mixed solution samples. (blue line: corresponding curve fitting results, Solvent: 50 vol%-aqueous LiCl solution (11.7 mol-LiCl/dm^3) / 50 vol%-MeOH)
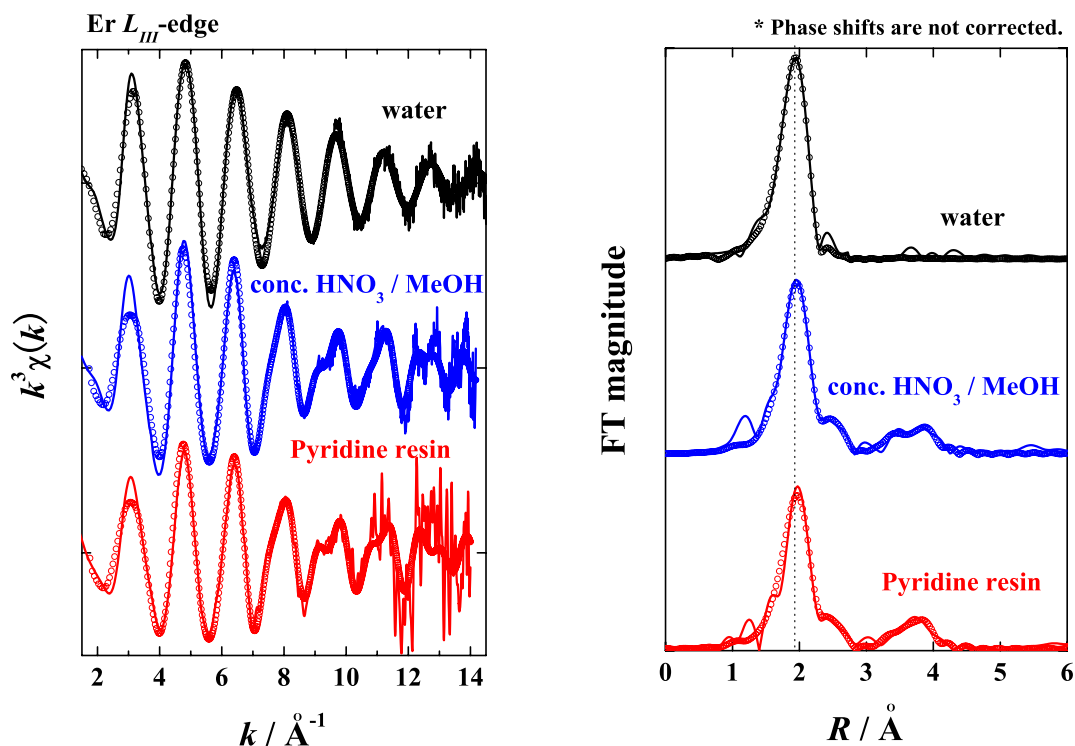
Figure V-13. k^3-weighted EXAFS spectra of La K-edge of different alcoholic chloride samples (left) and their corresponding Fourier transforms (right). (solid line: experimental data, ○: curve fitting results)

Figure V-14. k^3-weighted EXAFS spectra of Ce K-edge of different alcoholic chloride samples (left) and their corresponding Fourier transforms (right). (solid line: experimental data, ○: curve fitting results)

La *K*-edge

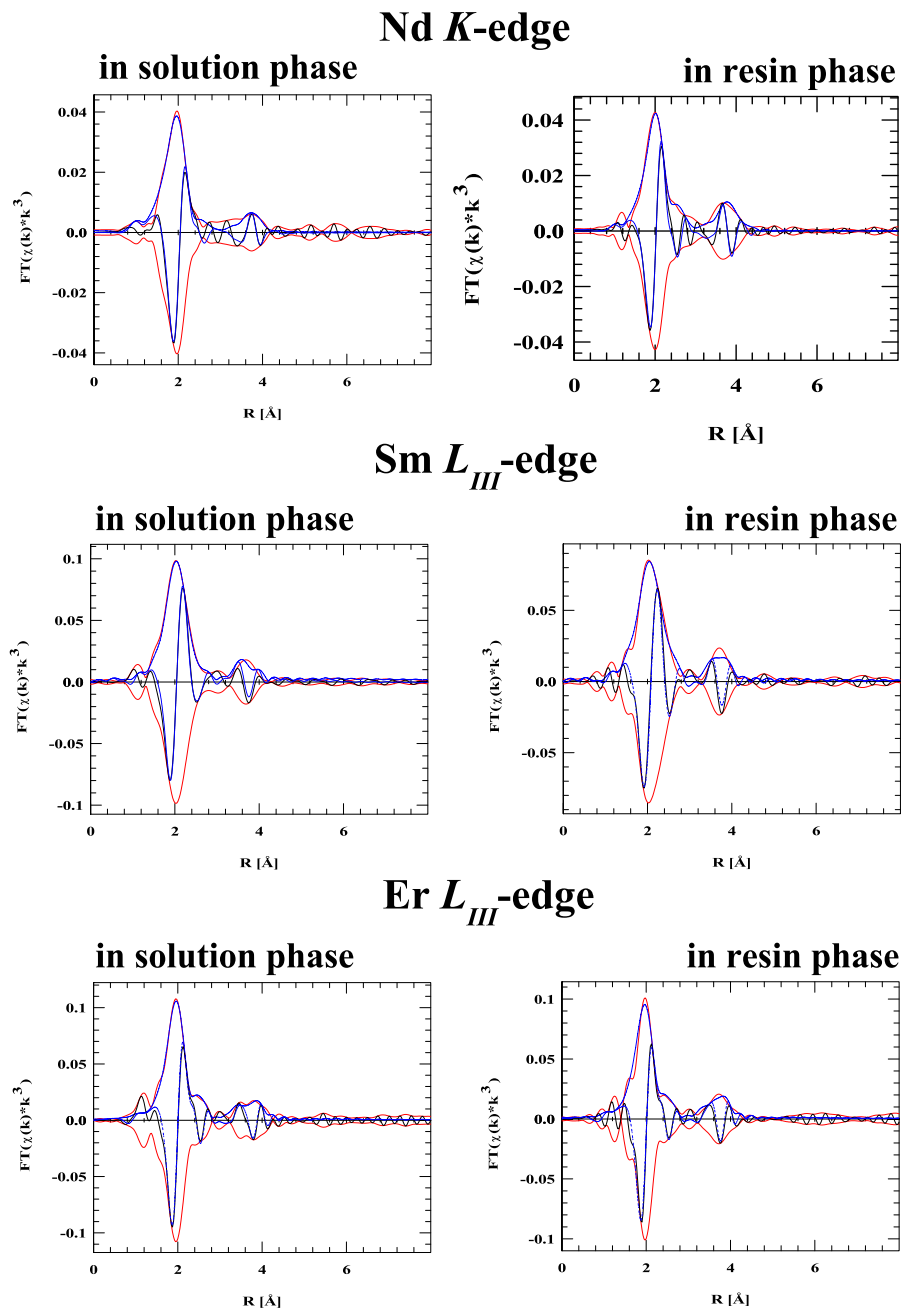Figure V-15. (1) Fourier transforms (magnitude: red lines, imaginary part: black lines) of the EXAFS of La *K*-edge of different alcoholic chloride samples. (blue line: corresponding curve fitting results)

Ce *K*-edge
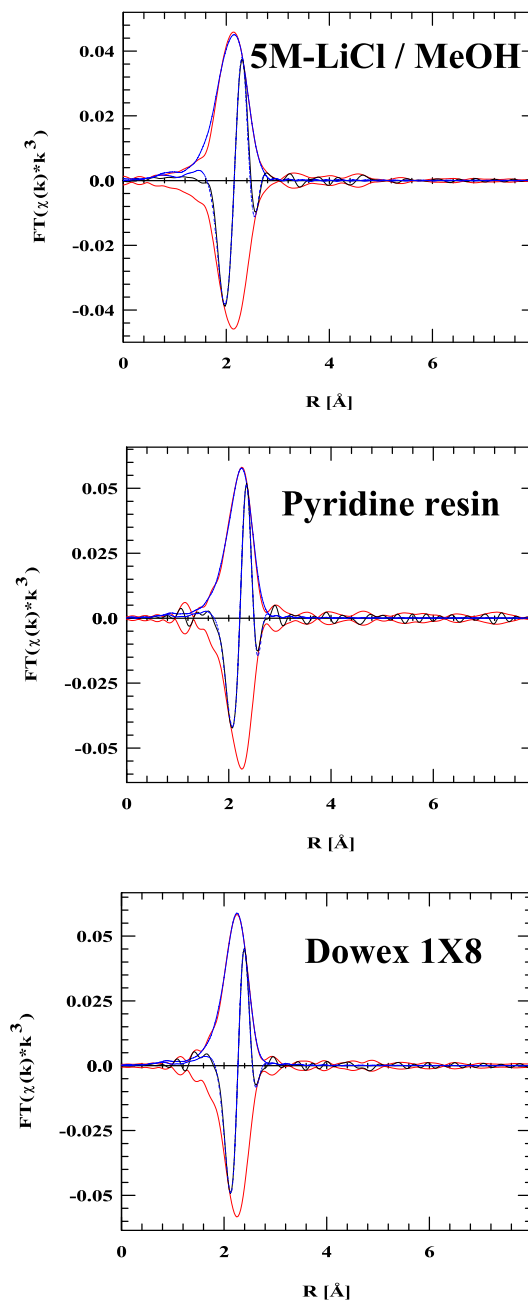
Figure V-15. (2) Fourier transforms (magnitude: red lines, imaginary part: black lines) of the EXAFS of Ce *K*-edge of different alcoholic chloride samples. (blue line: corresponding curve fitting results)

Nd *K*-edge

Figure V-15. (3) Fourier transforms (magnitude: red lines, imaginary part: black lines) of the EXAFS of Nd *K*-edge of different alcoholic chloride samples. (blue line: corresponding curve fitting results)

Figure V-16. k^3-weighted EXAFS spectra of Er L_{III}-edge of different nitrate samples (left) and their corresponding Fourier transforms (right). (solid line: experimental data, ○: curve fitting results)

Figure V-17. Fourier transforms (magnitude: red lines, imaginary part: black lines) of the EXAFS of Nd K-edge and Sm and Er L_{III}-edges in solution phase (left) and in resin phase (right) for conc. HNO_3 / MeOH mixed solution samples. (Solvent: conc. HNO_3 / MeOH = 5 / 5 (vol/vol), blue line: corresponding curve fitting results)
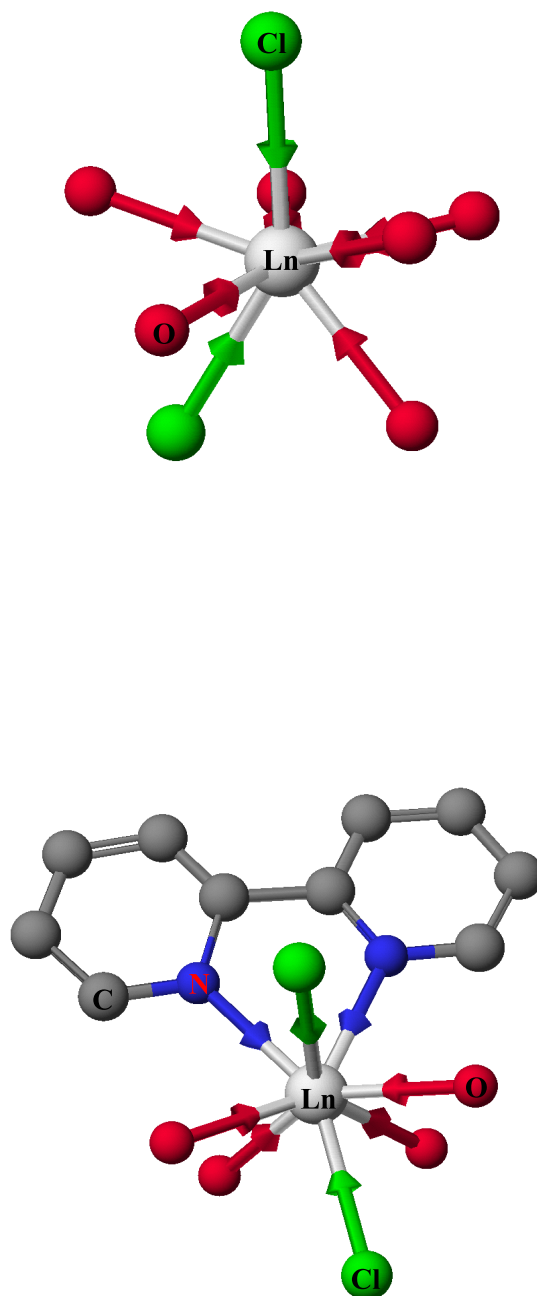
Figure V-18. (1) Crystal structures of hydrated Ln chloride compound (upper) and Ln chloride-Bpy complex (lower) employed for calculating theoretical XAFS parameters.
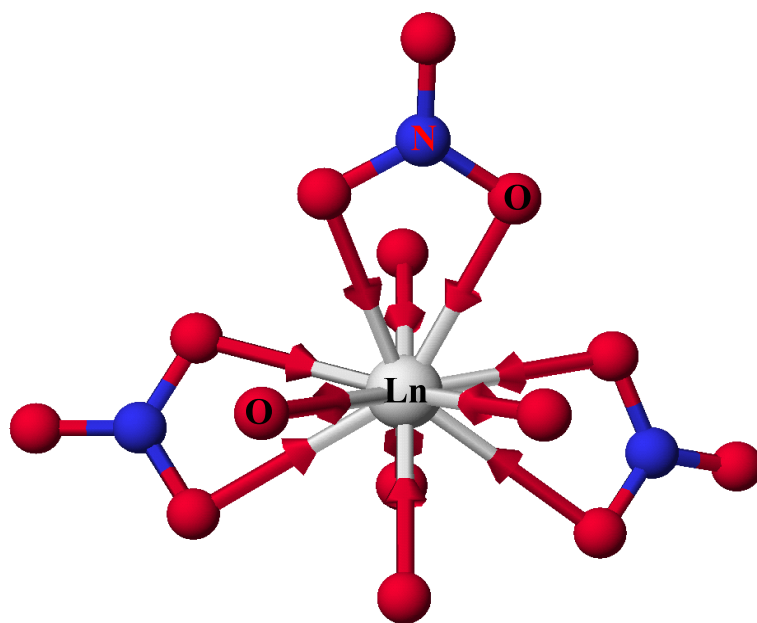
Figure V-18. (2) Crystal structure of hydrated Ln nitrate compound for calculating theoretical XAFS parameters.

Appendix VI

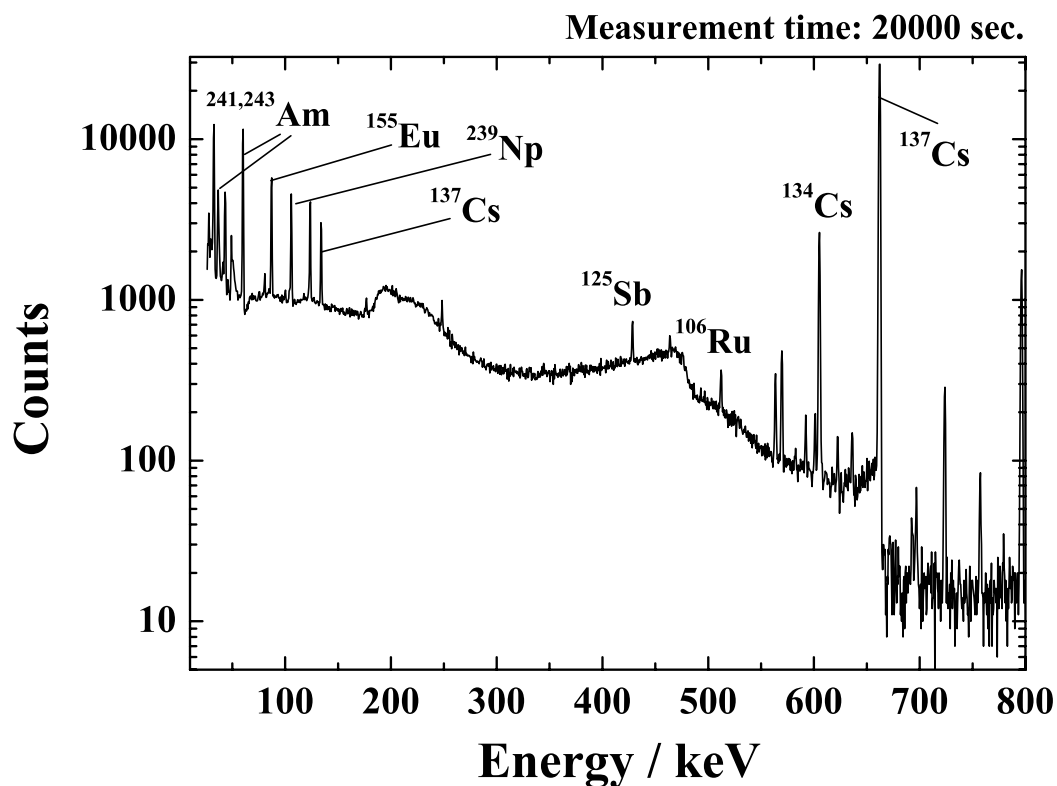## -Practical Partitioning Experiments Using Irradiated Mixed Oxide Fuels-

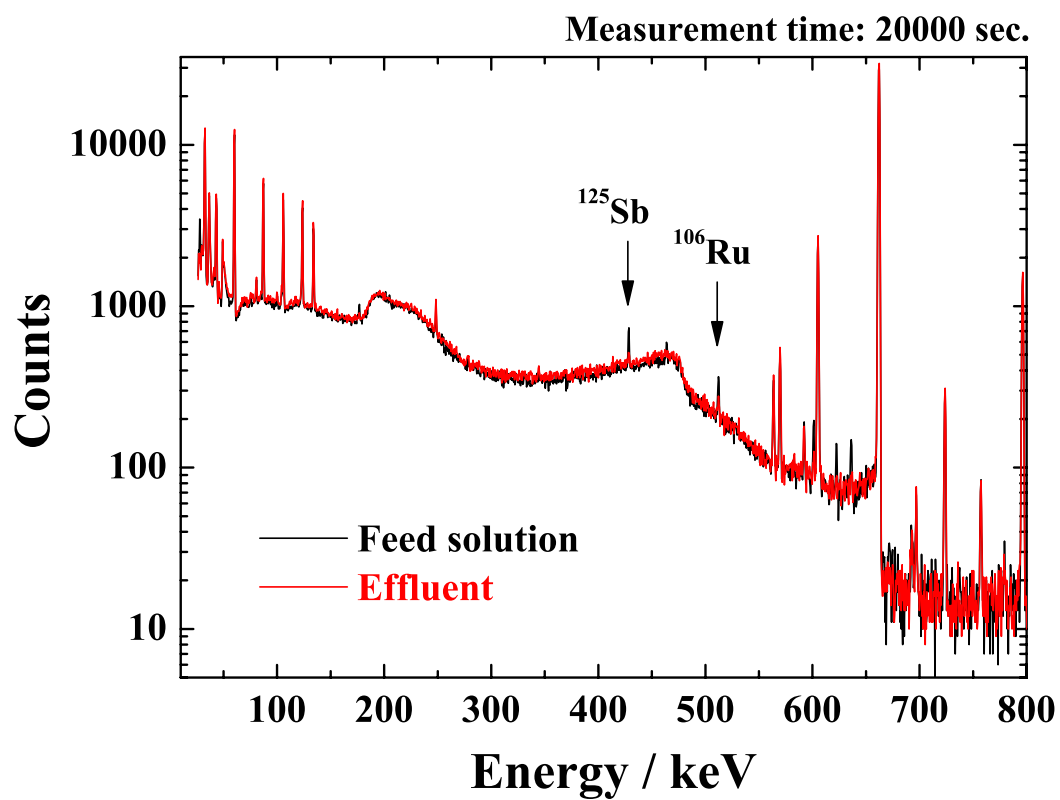Figure VI-1. γ-ray spectrum of the irradiated mixed oxide fuel sample employed in this study.

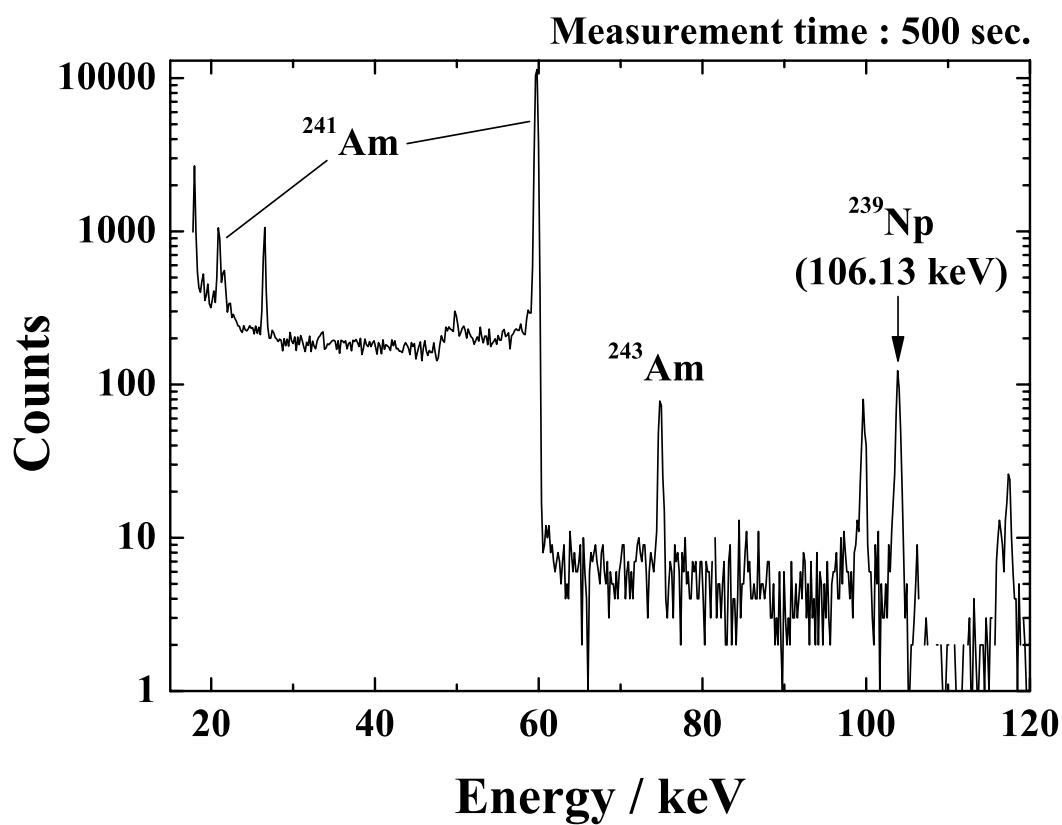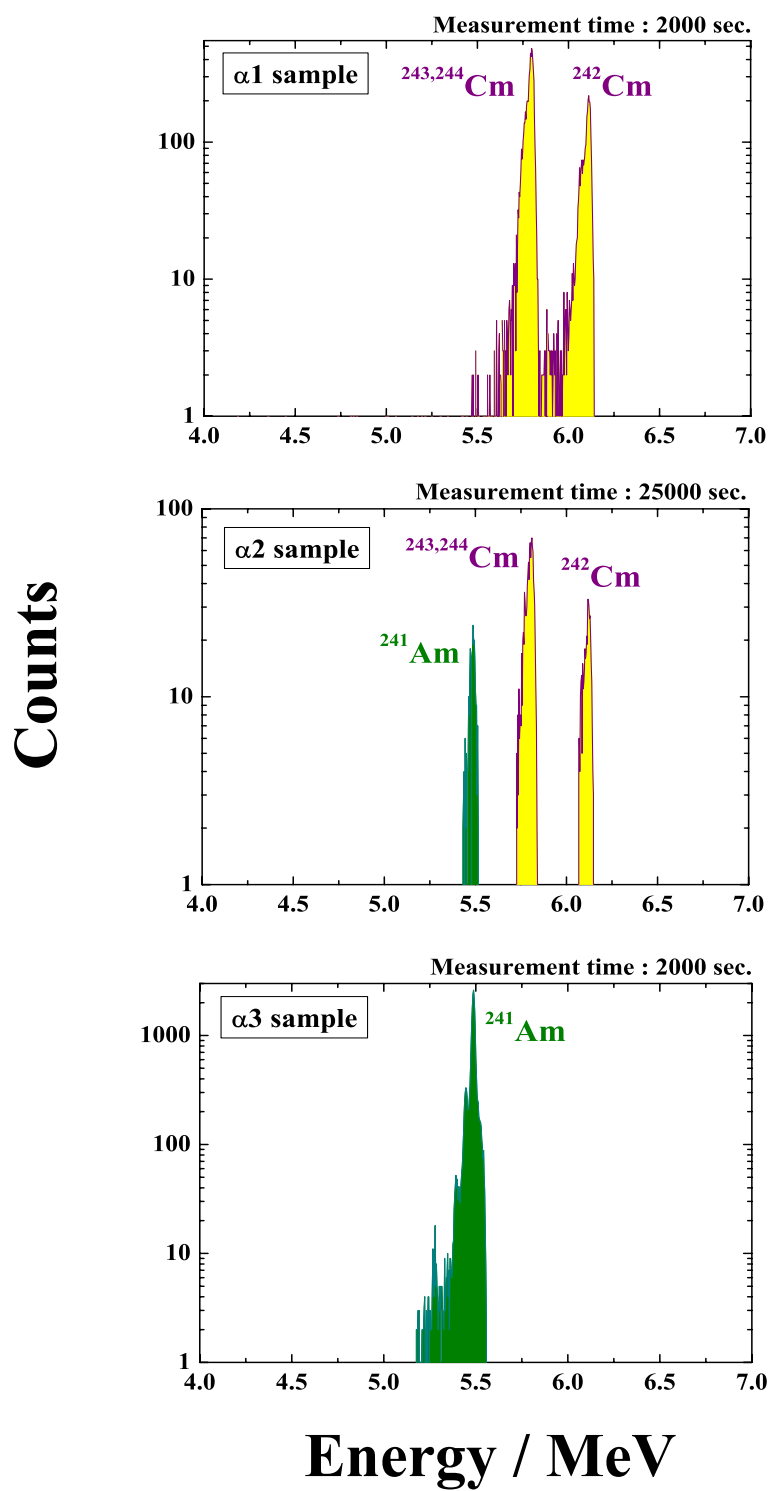Figure VI-2. γ-ray spectra of the feed solution and effluent in the first partitioning process.

Figure VI-3. γ-ray spectrum of the fraction around the second peak in **Fig. 6-2**.

Figure VI-4. α-ray spectra of the fractions in **Fig. 6-3**.